UNIVERSITÀ
degli STUDI
di CATANIA

DIPARTIMENTO DI SCIENZE UMANISTICHE

DOTTORATO DI RICERCA IN SCIENZE PER IL PATRIMONIO
E LA PRODUZIONE CULTURALE

XXXIV Ciclo

MAURA FUGAZZOTTO

Tesi di Dottorato

Functionalized geopolymers for restoration: new materials for brick masonries recovery in Mediterranean archaeological sites

TUTOR
Chiar.ma Prof.ssa Germana Barone
CO-TUTOR
Chiar.mo Prof. Paolo Mazzoleni
Chiar.mo Prof. Giuseppe Cultrone
COORDINATORE
Chiar.mo Prof. Pietro M. Militello

ANNO ACCADEMICO 2020-2021

TABLE OF CONTENTS

List of Figures

List of Tables

Abstract

For the archaeological Cultural Heritage, the most diffused and important material is represented by ceramics; a really vulnerable material when exposed outdoors, thus undergoing extensive damage, like *lacunae* and disintegration, often with subsequent structural consequences in case of monuments. In the current scenario of climatic emergency, the conservation policies became more and more attentive to green practices for environment safeguard, determining more complex requirements for the new restoration products, in respect to the traditional ones. Indeed, they need to be at the same time compatible with the original substrate and reversible, but also as much eco-friendly as possible. This research project aims to develop alkali activated materials (among which geopolymers) suitable for the restoration of brick masonries in Mediterranean archaeological sites, generally exposed to aggressive environmental conditions. Alkali activated materials (AAMs) are a group of innovative eco-friendly products, with promising features in the field of construction and restoration of stone materials. This is due to their chemical, physical and mechanical characteristics (such as the breathability, the high compressive resistance or the durability), together with their high versatility. AAMs are synthesized starting from alumino-silicate powdered precursors (such as clay, ceramic, fly ash, etc.) which, after reacting with an alkaline solution, determine the formation of a durable material, consolidated at low or room temperature, reducing the CO_2 emissions. In order to achieve a chemico-physical as well as chromatic compatibility with the bricks to restore, ceramics have been used in this project as raw material. Furthermore, the use of ceramic waste supplied by local industries promotes also a process of circular economy. By changing and optimizing the chemical and physical parameters of the synthesis, it has been possible to functionalize the products in order to obtain both restoration mortars, to apply *in situ,* and pre-casted bricks and decorative elements for substitutions. Tests of applicability on fragmentary bricks and potsherds coming from different archaeological sites, and a test performed directly on the masonries of the Odéon in Catania, supported the evaluation of the critical issues linked to adhesion properties, aesthetical effects and application procedures, and finally to individuate, among the developed products, whose formulations are the more promising for a possible market introduction.

Sintesi

La ceramica è uno dei materiali archeologici più diffusi ed importanti per il patrimonio archeologico. Pur essendo un materiale molto resistente, essa presenta una elevata vulnerabilità se esposta a condizioni ambientali aggressive, manifestando spesso gravi forme di degrado che possono compromettere l'integrità del reperto o del monumento.

Inoltre, nell'attuale contesto delle emergenze climatiche, il campo della tutela e della conservazione dei Beni Culturali guarda sempre più a politiche e pratiche di restauro ecosostenibili. Ciò determina la necessità di impiegare materiali da restauro che rispondano a requisiti più complessi rispetto ai materiali tradizionali. Oltre ai più comuni requisiti di compatibilità nei confronti del substrato da restaurare, reversibilità e durabilità, i nuovi materiali dovranno essere quanto più possibile ecosostenibili.

Il presente progetto di ricerca ha lo scopo di sviluppare materiali ad attivazione alcalina (tra cui si annoverano i geopolimeri) idonei per il restauro di laterizi di interesse archeologico in area Mediterranea. I materiali ad attivazione alcalina (AAMs) sono dei prodotti innovativi ed ecosostenibili che stanno mostrando promettenti caratteristiche per applicazioni in ambito edile e del restauro di materiali lapidei. Partendo da polveri allumino-silicatiche (ottenute da argilla, ceramica, cenere vulcanica, ecc.), attraverso la miscelazione e la conseguente reazione con una soluzione alcalina, si ottengono a temperatura ambiente o mediante trattamenti termici moderati, materiali consolidati e con ottime proprietà meccaniche e fisiche. Il consolidamento a basse temperature consente un considerevole abbattimento delle emissioni di CO_2 ed anche dei costi di produzione. Inoltre, in questo progetto di ricerca, il reimpiego di scarti ceramici come precursori geopolimerici, ha permesso di coinvolgere lo sviluppo dei materiali da restauro in una piccola economia circolare.

Variando ed ottimizzando i parametri chimici e fisici di sintesi, è stato possibile funzionalizzare i prodotti geopolimerici in modo da ottenere malte da restauro da applicare *in situ* ed anche elementi tridimensionali come mattoni e piastrelle per interventi di sostituzione. Infine, diverse prove di applicabilità delle malte effettuate su frammenti ceramici di interesse archeologico e sulla muratura dell'Odéon di Catania, hanno permesso la valutazione della compatibilità e dell'efficienza del prodotto dal punto di vista dell'adesione, nonché degli aspetti estetici e delle procedure di applicazione. Si è così giunti

all’individuazione tra tutti i materiali sperimentati delle formulazioni più promettenti per un restauro compatibile, efficiente, durevole ed ecosostenibile, nonchè per possibili immissioni nel mondo del mercato.

Introduction and aims

In the present context of dramatic climatic changes, the restoration field has to face new and complex needs in respect to the traditional practices. In addition to the already consolidated and universally recognized requirements of reversibility and compatibility of restoration materials towards the original support, the new restoration products must be sustainable. The improvement and promotion of Cultural Heritage preservation becomes urgent, with the use of restoration materials which do not further affect the environment, already deeply compromised. A new class of inorganic materials gains interest throughout the scientific community, alkali activated materials (among which the subclass of the most famous geopolymers). Easy to prepare, highly performing, consolidating at low or ambient temperature, involving the recycling of natural and industrial wastes, these materials could be considered eco-friendly and suitable for this purpose. Furthermore, they could be functionalized by changing the type and/or proportions of the precursors or by the use of specific additives, being optimized according to the finality of their application. This aspect is of primary importance in order to enhance the intervention efficacy.

In the Cultural Heritage field, the environment acts especially on outdoor monuments and archaeological structures, among which brick masonries are the most abundant and also the most vulnerable. This problem is furthermore boosted in the Mediterranean area where bricks in archaeological sites have to face long exposures to solar radiation, humidity cycles, the action of marine spray if near the sea and biocolonization, causing severe degradation processes; the traditional restoration products are not able to solve efficiently these conservation problems and do not have good durability over time.

Considering the current literature, geopolymers application in the restoration field is completely new and quite unexplored. Thus, this research project aims at experimenting some geopolymeric restoration mortars for ceramic materials of archaeological interest, by including ceramic waste easily retrieved from local industries, promoting its recycling. Furthermore, the comparison between original archaeological samples and the new tested ones will allow the improvement of suitable restoration products, promoting a green restoration, created *ad hoc* for archaeological masonries and being at the same time compatible, efficient, durable and eco-friendly.

The PhD thesis is organized in a first part dedicated to the state of the art on ceramic materials and their conservation issues (Chapter 1), followed by an introduction on alkali activated materials, focusing in particular on geopolymers (Chapter 2). In the same chapter, the current knowledge on their chemistry and structure is reported, with particular regard on those realized starting from ceramic waste, as well as their application on Cultural Heritage. Chapter 3 describes the analytical methods used in order to characterize the raw materials and the geopolymeric products. Chapter 4 describes, instead, the raw materials considered and displays the characterization results acquired on them. The synthesis procedure and parameters are indicated in Chapter 5, which is followed by two chapters dedicated to the characterization of the developed materials (Chapter 6 and Chapter 7). These last two chapters show the results on two large series of geopolymers prepared starting from two different ceramic wastes. These chapters are subdivided into two sections, a first part dedicated to the binder's characterization, the second part dedicated to the synthesis and characterization of the restoration products, namely restoration mortars and pre-casted elements, among which there are geopolymeric bricks. The last chapter (Chapter 8) shows the case-studies after a discussion of the complete compatibility of the new experimented materials with the original archaeological remains which need the restoration intervention. Conclusions focus on final remarks and on ongoing further studies.

Chapter 1

The historical ceramic materials: brick masonries and their conservation issues

1.1 The historical ceramic

The term “ceramic” indicates any material which is cold worked and formed starting from a clayey material and water, then fired generally between 700 and 1300 °C. The characteristics of the final products change according the clay purity, composition, the eventual additives used, the firing temperature and environmental conditions (oxidizing or reducing). In any case, the ceramic product obtained will be a solid brittle material, with physical and mechanical properties analogue to those of natural stone materials (Warren, 1999). Besides brittleness, these materials show poor electrical and thermal conductivity, compressive strength and stability in harsh environments. Being a generalization however it is necessary to take in mind the possibility of exceptions (Barry Carter and Norton Grant, 2007).

The unicity and historical importance of this kind of materials in archaeology is due to the large amount of technological information which they can tell us, regarding the society that had produced and used them. By studying ceramics, it is therefore possible to acquire more information compared to what natural stone artefacts can reveal. For this reason, their conservation and preservation is a point of crucial interest in the field of Cultural Heritage.

Ceramic materials furthermore have been employed since ancient times, changing in shape, technology, use, and so on (Vidale, 2007). They have been used in architecture and for the common domestic use, as well as for transport and storage. The knowledge obtainable from them is huge and one of the most valuable things in understanding past societies and human behaviour.

In the following are summarized the different characteristics which can differentiate the ceramic materials, allowing their classification:

1) Colour (Esbert et al., 1997; Lazzarini and Laurenzi Tabasso, 1986)

The firing environment and the type of the raw material used are the two parameters which determine the final colour of the product once consolidated. In general, oxidizing firing conditions determine a reddish or beige ceramic paste, while a reducing one gives a brown-to-black colour to it. In particular, in oxidizing conditions, haematite is formed (α-Fe_2O_3), giving the reddish colour. The presence of carbonates (i.e. calcite and/or dolomite) will favour the development of yellowish hues. The colour indeed depends strictly also on the chemical composition of the clay, for example kaolinitic clays or poor-iron clays give the typical white appearance of those ceramics known as porcelain.

The presence of organic matter, the use of a plastic clay or a fast firing process instead determines the formation of magnetite ($FeFe_2O_4$) which leads to a dark colour to the final product.

2) Texture/porosity

Porosity, defined as the ratio between the empty space in the material (due to pores and cracks) and the solid volume, is an important parameter that defines the quality of a ceramic material. It indeed directly influences many properties, first of all mechanical strength, compactness, permeability and durability (Fernandes et al., 2010).

Ceramic materials are characterized by a high porosity, between 15 and 40%, but it strictly depends on the kind of product (Esbert et al., 1997). The porosity is mainly function of the constituents of the material and of the fabrication process; generally, the higher is the firing temperature, the higher is the sintering (or vitrification) of the matrix with a resulting formation of a more compact structure. Furthermore, it is possible to assume that the larger the particles size of the used raw material, the larger the pores dimension will be. The porosity then depends also on the presence of organic matter that burns at 200-400 °C leaving imprints or by the amount of calcite grains, which over about 700 °C decomposes into CaO releasing CO_2 (Esbert et al., 1997).

The highest porosity values (30-40%) are generally measured on bricks used in historical buildings (Esbert et al., 1997). This could be attributed both to the ancient production technology and on the decay undergone by the material in masonry over time.

Porosity is one of the main properties that can determine a high or low durability of the material. This is because it represents the path for water and aggressive compounds migration into the material and contributes to characterize the structure of the material itself. Therefore, there is the need to consider not just the total amount of porosity (mainly with regards to the accessible porosity), but also the shape and dimension of the pores.

3) Finishing surface

The ceramic object is generally treated on the external surface; this finishing could have exclusively a decorative function or a specific technical role. The latest is strictly linked to the porous nature of ceramic materials, which, if not highly sintered, are susceptible to water penetration through the open porosity. Thus with the application of a glaze or of other impermeable layers a higher efficiency and durability could be obtained. The finishing process could occur during the first or second firing step, the latter generally at lower temperature.

According to these characteristics, the ceramic materials are classified as follows (Barry Carter and Norton Grant, 2007; Cuomo di Caprio, 2007; Fiori et al., 2003; Lazzarini and Laurenzi Tabasso, 1986):

Terracotta, or earthenware, is the term to indicate the most generic ceramic materials, red coloured and with a porous structure, generally obtained by firing clayey materials at temperatures between 800 and 1200 °C. These could be subdivided again according to their finishing, which could be most frequently an engobe, that means a thin layer of clay applied before the firing on the formed and dried object, and fixed during the firing step together with the ceramic body (engobe terracotta); a *vetrina*, that means a very thin glassy and transparent layer (*terracotta invetriata*); or a layer of smalt (commonly containing SnO_2 – namely cassiterite), opaque, applied in a second firing step (majolica). If the firing conditions of the terracotta were reducing, and the final products assumed a black colour and, if the paste had been purified, the terracotta could be called *bucchero*. Common products made of earthenware are bricks, tiles and vessels (Barry Carter and Norton Grant, 2007).

Apart from the most common terracotta and its subclasses, other types of traditional ceramic materials have to be mentioned, more compact in structure because of a higher firing temperature (over 1200 °C): the gres, (or stoneware), which is a low porosity coloured ceramic material, partially vitrified. It is produced starting from non-carbonate clays. If present, differently from the terracotta, the finishing layer has a decorative function, because the gres is already not permeable to water (Lazzarini and Laurenzi

Tabasso, 1986). Porcelain, instead, is a white vitrified and almost not porous ceramic because of its high compactness. It is obtained by kaolinitic clays and quartz. Also in this case the finishing layer has a decorative function (Lazzarini and Laurenzi Tabasso, 1986).

The last class of ceramic materials is the so called *terraglie*. With white paste, these could be both porous (soft) or compact (hard). These are realized starting from carbonate and low-iron clays or with feldspars as fluxing agents, respectively. Table 1.1 shows a scheme of the ceramic materials' classification.

Class	Porous/compact	Red/white	Finishing surface	Firing temperature
Terracotta	Porous	Red	Not finished	800-1200 °C
Terracotta invetriata	Porous	Red	Vetrina	800-1200 °C
Terracotta ingobbiata	Porous	Red	Engobe	800-1200 °C
Majolica	Porous	Red	Smalt	800-1200 °C
Gres	Compact	Red	Indifferent	>1200°C
Porcelain	Compact	White	Indifferent	>1200°C
Terraglia	Porous/compact	White	Indifferent	>1200°C

Table 1.1 – Ceramic materials' classification scheme.

A brief petrographic summary of ceramics:

From a technological point of view, the ceramic materials are constituted by two main components, one plastic material, namely clay minerals with sizes below 20-30 μm, and the aplastic part, which is composed of various kinds of minerals/rock fragments of larger dimensions and that constitute the structure of the paste. Among the aplastic components, also *cocciopesto* could be used (the so called *chamotte*). The plastic component is the protagonist of the irreversible transformations that occur during firing, while the aplastic one allows to avoid excessive shrinkage during the drying (Cuomo di Caprio, 2007; Hodges, 1989; Maggetti, 1982a). Moreover, organic components could also be present, like straw, that are completely decomposed during firing, leaving their imprints behind as porosity. This further porosity is added to the porous structure due to air bubbles and volume contractions. Once consolidated, the plastic part will constitute the matrix, that means the binder of the final product; while the aplastic elements are defined as tempers, or inclusions (Hodges, 1989; Maggetti, 1982b).

The mineralogical phase transformations occurring during firing could be simplified as follows:

Non carbonate clayey materials under high firing conditions see first the microcline ($KAlSi_3O_8$) collapse and/or its partial transformation into its polymorph orthoclase and then sanidine; when the temperature exceeds 800 °C new mineralogical phases as mullite ($3Al_2O_3*2SiO_2$) and sanidine ($(K,Na)(Si,Al)_2O_8$) are formed to the expenses of the present clay minerals, namely muscovite ($KAl_2(Si_3Al)O_{10}(OH,F)$) and illite ($(K,H_3O)(Al,Mg,Fe)_2(Si,Al)_4O_{10}$), by solid-state replacement. At the same time, in carbonate-rich clays, gehlenite ($Ca_2Al(AlSi)O_7$), wollastonite ($CaSiO_3$), diopside ($CaMgSi_2O_6$) and anorthite ($CaAl_2Si_2O_8$), all calcium (and magnesium) silicates, are formed by means of a diffusion reaction process at the carbonate-silicate interface (Cultrone and Carrillo Rosua, 2020); while gehlenite starts to appear at temperatures up to 800 °C, anorthite and wollastonite/diopside need even higher temperatures, over 1000 °C (Riccardi et al., 1999).

Furthermore, the dynamic of the firing can determine different situations, e.g. it is known that incomplete phase reactions occur, from which derives the coexistence of relict minerals and newly formed phases (Riccardi et al., 1999); or the formation of metastable phases in respect to the stable ones in rapid heating conditions (Cultrone and Carrillo Rosua, 2020).

What about the solid bricks used historically for masonries?

The solid brick is one of the most ancient construction building materials used in the world. It was produced since ancient times, in different areas, according to what was available and required at that time and in that place (Fernandes et al., 2010). For example, it is necessary to mention the adobe, which were mud bricks, shaped and left to dry under the sun, without firing. Many constructions in areas which are not affected by rainfall and humidity are still built in this way (Caneva et al., 2007; Costa et al., 2019; Elert et al., 2019). It is not clear how and when, but in rainier areas fired bricks started to be produced: very different fired bricks typologies are spread all over the world, according to the raw materials combinations and the production parameters. In the Mediterranean area, furthermore, the brick production was always very intense, stimulated by the simultaneous absence of good and easily available natural stones and the abundance of clay soils.

It is easy to understand how different could be the performance of these materials produced over time and over countries. In this PhD thesis we are going to focus on two types of bricks, different one from the other, but both diffused in the Mediterranean regions and dated to the Roman time, a period of flourishing bricks and ceramic production (Bonetto, 2016; Fernandes et al., 2010): first, a red solid brick visibly porous and rough, with millimeter inclusions, and a modern reproduction of a yellowish, very compact and with fine-texture solid brick.

Brick's technical characteristics:

The chemical, physical and mechanical properties of historical bricks cover a wide range of values and a significant variability (Fernandes et al., 2010). It is difficult, if not impossible to summarize the large variety of technical characteristics of such materials over time, also because, generally, to obtain this kind of information, destructive analyses are needed. Furthermore, the current technical data on ancient materials will be influenced by their decay, and it is therefore not representative of its original properties. Thus, we will expose here some technical information about historical bricks obtained by historical treatises of architecture and construction.

Old clay bricks exhibit high porosity values, ranging between 15 and 40% in volume, with water absorption values between 10 and 20% (Esbert et al., 1997; Fernandes et al., 2010).

Regarding the compressive strength, Curioni (1868) reports the compressive strength measured on different types of solid bricks of different quality. These data are reported in Table 1.2 and could be considered as representative of historical bricks.

He mentioned *albasi*, *forti* (hard) and *ferrioli* bricks, which are bricks of not high quality because of firing reasons; in particular, *albasi* are those bricks which have undergone a low firing, thus are easily subjected to crumbling. *Forti* and *ferrioli*, instead, are, respectively, bricks fired just up to the best firing grade and beyond it. *Mezzanelli*, instead, is a term which indicates bricks of a good firing grade (Curioni, 1868; Rizzi, 1914). From Table 1.2 it is possible to notice that the higher is the firing grade, the greater the bricks' resistance. The values range between 30 and 150 Kg/cm^2 (i.e. 3-15 MPa), in accordance with

Campanella (1928), another important historical treatise on building construction, and with Fernandes et al. (2010).

	Compressive strength	
Kind of brick	(Kg/cm^2)	(MPa)
Mud bricks	33	3.3
Albasi bricks	40	4
Mezzanelli bricks	60	6
Hard bricks	70	7
Ferrioli bricks	150	15

Table 1.2 – Summary of the compressive strengths measured on historical bricks by Curioni (1868). In order to make the data comparable with the successive results obtained on the synthetic materials objects of this thesis, the original data reported by Curioni (1868) in Kg/cm^2 are converted in MPa.

1.2 Ceramic and masonry decays

Ceramic materials always undergo the action of environmental factors, even if sometimes they are more durable than natural stones. The effects that artificial materials could show depends on their composition, on the complex systems of integrated external and internal factors, and on the function of the objects themselves, that is how they are used (Cultrone et al., 2000; Fiori et al., 2003; Lazzarini and Laurenzi Tabasso, 1986). The causes of the degradation processes and forms could be grouped in physical (e.g. moisture and thermal variations, water state transitions, vibrations, wind action and so on…), chemical (e.g. acid rains, pollutions and so on…) and biological (e.g. lichens growth, plants infestation and so on…). Beside these natural agents, also anthropic actions could induce considerable damages (Lazzarini and Laurenzi Tabasso, 1986).

The most important degradation phenomena involving ceramic materials are caused by physical factors, particularly by water infiltration and its transport (Charola and Lazzarini, 1986; Fernandes et al., 2010; Franzoni, 2014; Sandrolini and Franzoni, 2006). The presence of water in historical brick masonries, specifically, is one of the most important problems affecting architectural heritage (Franzoni, 2014; Sandrolini and Franzoni, 2006). It can bring soluble salts from the external environment, or solubilize salts already present in the materials, with negative consequences: when the environmental conditions determine water evaporation, salts could crystallize, inside or on the surface. This surely causes an unpleasant feature, but above all a mechanical action on the pores' walls because of volume expansions, with subsequent crack of the bulk materials sometimes leading to complete disaggregation. Water can furthermore determine a direct mechanical action on the ceramic structure because of possible freeze-thaw cycles (even if these are quite uncommon in temperate areas like the Mediterranean regions above all near the coast). Water freezing could determine a volume increase of around 9%. And when the tensile forces in the pore system exceeds the tensile strength in the material, damage will occur (Lisø et al., 2007).

A further negative and widespread problem indirectly determined by water action is the fracturing of ceramic materials when in contact with iron bars which have undergone corrosion process, causing a considerable volume expansion. This effect also highlights another fundamental critical issue in the conservation field, that is combining incompatible materials (Lazzarini and Laurenzi Tabasso, 1986; Rodrigues and Grossi, 2007; Vidale, 2007). Coupling iron bars with ceramic, cement and bricks or other softer materials could determine what already seen; applying cement as bedding mortar on historical brick masonries could determine over time their preferential preservation, to the expenses of bricks (Fig. 1.1), which will be more vulnerable, and so on…

Fig. 1.1 – Decay of bricks at the Odéon, Catania. Example of differential decay of a masonry where cement mortars were applied on softer bricks.

Furthermore, it is noteworthy to consider the possibility that serious damages could be even determined by previous restoration interventions, performed with not suitable materials or practices (Fiori et al., 2003; Grimmer, 1984; Lazzarini and Laurenzi Tabasso, 1986).

In the following lines I'm going to describe the most common conservation issues which can affect ceramic materials that, being employed in masonries, are exposed outdoor.

Water infiltration and damages:

- Efflorescence and sub-florescence

  As defined by ICOMOS and ISCS (2008) efflorescences are whitish, powdery or whisker-like crystals which grow on the surface of a material and generally are not well cohesive. These are made of soluble salts, which according to their solubility tend to migrate throughout the materials (Charola, 2000). When salts crystallize beneath the surface, these crystals take the name of sub-florescence and could determine the detachment of the upper portions because of their volume expansion. Their negative effects are worse when crystallization happens in the internal parts of the materials, creating the so called crypto-efflorescence. Crypto-efflorescences are not visible from outside but could be very dangerous for the integrity of the material (Grimmer, 1984). The most ubiquitous weathering patterns thus determined are powdering and scaling (Charola, 2000). The most common soluble salts forming the efflorescence are chlorites (e.g. halite – NaCl) and sulphates (e.g. thenardite – Na_2SO_4 or epsomite - $MgSO_4*7H_2O$), but it is also possible to find carbonates (e.g. secondary calcite – $CaCO_3$) even if less soluble (ICOMOS and ISCS, 2008).

- Detachment

  Detachment is a general term which includes different kinds of separation of parts of the material, sometimes with loss of solid portions. The kind of detachment typically determined by water action because of presence of soluble salts is blistering, defined by ICOMOS and ISCS (2008) as follows: *separated, air-filled, raised hemispherical elevations on the face of stone resulting from the detachment of an outer stone layer.* The presence of water causing the increase in volume of mineral inclusions, or the development of pressure inside the materials (e.g. corroded iron bars) are in some way acting towards local loss of the stone surface. Bursting is defined as *local loss of stone surface from internal pressure usually manifesting in the form of an irregularly-sided crater* (ICOMOS and ISCS, 2008).

- Disaggregation

  Also known as disintegration, it is the detachment of single grains or aggregates of them (ICOMOS and ISCS, 2008). It consists in a loss of cohesion of the material because of chemical alterations by water or aggressive agents (with partial matrix solubilisation) or also because of wind erosion, which is mechanical. This degradation form has, as main consequence, the increase in total porosity. This, in turn, facilitates further decays.

- Biodeterioration and vegetation growth

  According to the bioreceptivity of the stone material (the aptitude of a material to be colonized by organisms, that varies depending on its structure and chemical composition) and to the climatic conditions (water availability, pH, climatic exposure, nutrient sources, temperature) the intensity of the biological attack is determined. Biocolonization is the responsible of the formation of coloured patinas (the colour depending on the type of microorganisms forming the patina), which, contrary to what generally thought, do not compromise only the aesthetical appearance of the monument/architecture. In fact, the patina especially promotes further damages, as the acidic attack of the substrate with consequent staining and eventual loss of compactness (Caneva et al., 2007; Warscheid and Braams, 2000). The phenomena determined by biocolonization on Cultural Heritage are defined as biodeterioration (Caneva et al., 2007). Nevertheless, because of their silicatic (thus more durable) composition, bricks are not the most vulnerable inorganic materials to this kind of degradation.

  When the conditions are suitable, and mainly when ordinary maintenance practices have not been carried out, shrubs and plants can grow and strongly infest Cultural Heritage, as masonries structures. The irreversible consequence is their roots penetration, which can be strong enough to completely destroy a structure.

Erosion

Loss of original surface, leading to smoothed shapes (ICOMOS and ISCS, 2008). This frequent morphological decay depends for sure on the hardness and compactness of the material exposed, as well as on the importance of the external factors acting on it, first of all the wind action and the anthropic use. The main negative consequence is the complete loss of readability when this decay occurs on decorative elements. Otherwise it could be in some way considered, in normal condition, a slow process, affecting mostly the softer materials (Grimmer, 1984).

Alveolization

Cavities, called alveoles, generally of centimetric dimension, of different shape and sometimes interconnected, are found on the surface of a material (ICOMOS and ISCS, 2008). These cavities are mainly the consequence of salt crystallization (Delgado et al., 2016; Morillas et al., 2020) or salt and wind weathering combination (e.g. the impact of marine spray in windy areas) (Grimmer, 1984; Morillas et al., 2020; Rodriguez-Navarro et al., 1999), freeze-thaw cycles or thermal fluctuations (Morillas et al., 2020).

Surface blackening (environmental pollution)

Also called soiling, the deposition of a very thin layer of exogenous particles (e.g. soot) which imparts a dirty appearance to the stone surface (ICOMOS and ISCS, 2008). When the conditions are suitable (high humidity content, condensation on the surface, carbonate composition of the substrate) a sulphation process can take place, determining the formation of the famous black crusts on the surface of materials. Luckily, having the ceramic materials mainly a silicatic composition, the surface soiling does not frequently determine the crusts' formation. It can eventually happen to the expenses of Ca-bearing minerals if present, as for example plagioclase (Cultrone et al., 2000; Pozo-Antonio et al., 2019; Simão et al., 2006) or when gypsum is deposited on the silicatic surface by the environment (as secondary gypsum), not chemically involving the substrate (Del Monte and Sabbioni, 1984; Fugazzotto, 2012; Fugazzotto and Braga, 2012; Mazzeo, 2005). Thus, the implications on silicatic substrate are not intense.

Differential degradation on masonries structures

Differential degradation is a term used to describe the different entity/kinds of decay affecting a heterogeneous material (ICOMOS and ISCS, 2008).

Anyhow if we consider a brick masonry as a unique element, this term could be translated to indicate the diffusion of different degradation mechanisms or different severities of the decay occurred regarding the constituent materials, according to their different characteristics. It is the case of the preferential erosion of the bricks on a masonry containing cementitious bedding mortars (Grimmer, 1984). A further differential degradation on masonry units could be ascribable to the different porosity characterizing bricks and mortars, that in presence of salts crystallization would preferentially determine the degradation of mortar joints when the porosity is higher on the mortars, or, on the contrary, of the bricks if these are the more porous materials (Charola and Lazzarini, 1986).

Therefore, the properties of ancient brick masonries will depend on the mortars and bricks types (Esbert et al., 1997), which in turn depends on the quality of the raw materials used and on the technological manufacturing process (Fernandes et al., 2010).

Decays involve further decays, thus creating a sort of vicious cycle which could compromise the integrity and structural stability of a material, hence of a monument/architecture.

1.3 Conservation and restoration issues: the traditional restoration materials and their problems

The restoration products usually adopted in conservation and restoration interventions of artificial materials (with exception of glass materials) are those used for the restoration of natural stones with high porosity (Lazzarini and Laurenzi Tabasso, 1986). Two problems can come from this: first of all, the low efficiency and durability, as well as compatibility and reversibility, of the traditional, often obsolete, materials; and secondly, the fact that even if similar, the artificial materials are not the natural ones. The application of products and procedures born to face conservation problems studied on natural stones, often cannot be considered perfectly transferable to the field of ceramic materials.

What about the traditional restoration materials for stones? Cement or lime mortars and organic resins are the most conventional traditional materials used to repair stone monuments and architecture, but they generally show numerous drawbacks in terms of compatibility, efficiency and thus durability (Geraldes et al., 2016; Sassoni et al., 2016).

Cements and lime mortars

About cement mortars, it is today universally admitted their unsuitability over time and in particular the highest, often not reversible, serious damages of structures and materials “restored” with them.

The examples could be numerous; I will focus only on the most frequent.

First of all, the already mentioned excessive use of cement mortars to repoint masonries, namely their use as bedding mortars on softer bricks, in presence of external aggressive factors, have determined all over the world the preferential degradation of bricks, both from a mechanical and chemical points of view (Grimmer, 1984; Sassoni et al., 2016).

Furthermore, the frequent reintegration of mortars and plasters with low permeability cement mortars has created hard and compact impermeable external layers, with imaginable negative consequences (Fiori et al., 2003; Lazzarini and Laurenzi Tabasso, 1986).

Cement could also be the cause of salt migration in the structure, with efflorescence and sub-florescence formation (Grimmer, 1984; Lazzarini and Laurenzi Tabasso, 1986; Pecchioni et al., 2008; Rizzi, 1914).

Regarding lime mortars, instead, usually employed precisely to be less invasive than cement (Grimmer, 1984), their high susceptibility to acid attacks makes the outdoor interventions not durable. Lime mortars indeed suffer of all the decays affecting carbonate materials, which means chemical dissolution, problems linked to water penetration, black crusts and these could represent the starting point of the degradation processes in case they are used on composite monuments (Matteini and Moles, 2007).

Additionally, studies pointed out the appearance of microbial contamination on a silicate-based stone masonry repaired with lime mortars, while it did not show this problem before the restoration (Warscheid and Braams, 2000).

From further researches it is inferred, moreover, that lime mortars are, among the traditional inorganic materials, those showing the highest bioreceptivity. The higher amount of calcite in a mortars determines a highest biological decay (Caneva et al., 2007). Brick masonries with lime bedding mortars or mosaic walls indeed show a deterioration by bio-organisms attack which starts from the bedding mortar and extends only in a second moment to the silicatic materials, namely bricks or the mosaic tesserae (Caneva et al., 2007).

Organic resins

Born for application on paintings, organic resins (as acrylic and silicon-based products) are also found as protective and consolidation materials for stones (Amoroso, 2002), particularly natural stones. They are also sometimes used for repairing (e.g. epoxy resin) with regard to small areas (Grimmer, 1984). However, both restorers and the scientific community very quickly observed their limited efficiency over time (Favaro et al., 2006; Grimmer, 1984; Munnikendam, 1967), due to their natural perishability (Favaro et al., 2006).

Another factor which influences their incompatibility is the total difference in chemical composition with respect to stone substrates.

Among their negative drawbacks, it is necessary to mention the aesthetical alteration, mainly appearing as a yellowing of the surfaces when applied outdoors as protectives (Favaro et al., 2006; Melo et al., 1999); as well as the difficulties in their removal once penetrated in the porosity, as in consolidation practices (Favaro et al., 2006).

Further materials traditionally used in restoration of stone are inorganic compounds, like limewater or Ba-hydroxides, mainly used for consolidation treatments. For this reason, they were not treated in this PhD thesis.

The synergy of different parameters which are responsible of the decay, make the degradation mechanisms hardly predictable or easy to simplify, and the conservation approach extremely complex.

Once the high dependency of the kind and entity of degradation phenomena from the materials and the exposure contexts has been noted, an accurate compositional and microclimatic study becomes indispensable in order to understand which is the most suitable conservation practice and restoration intervention with a case by case approach.

A perfect restoration intervention does not exist; it is not possible to find a unique product which can preserve the materials from the degradation. This is a natural process and it is also continuous. What we can do is a detailed analysis of the context, considering internal and external factors and their mutual interaction, adjusting every time the selection of materials and kind of interventions (Lazzarini and Laurenzi Tabasso, 1986).

Considered all these aspects, the utility of studying new alterative restoration materials comes out (Sassoni et al., 2016).

References

Amoroso, G., 2002. Trattato di Scienza della Conservazione dei Monumenti. Alinea Editrice, Firenze.

Barry Carter, C., Grant Norton, M., 2007. Ceramic Materials. Science and Engineering. Springer, New York.

Bonetto, J., 2016. Diffusione ed uso del mattone cotto nella Cisalpina romana tra ellenizzazione e romanizzazione., in: Bukowiecki, E., Volpe, R., Wulf-Rheidt, U. (Eds.), Archeologia Dell'Architettura, XX. All'insegna del giglio, Roma.

Campanella, G., 1928. Trattato generale teorico pratico dell'arte dell'ingegnere civile, industriale ed architetto. Dottor Francesco Vallardi, Milano.

Caneva, G., Nugari, M.P., Salvadori, O., 2007. La biologia vegetale per i beni culturali. Biodeterioramento e Conservazione., 2nd ed. Nardini Editore, Firenze.

Charola, A.E., 2000. Salts in the deterioration of porous materials: An overview. J. Am. Inst. Conserv. 39, 327–343. https://doi.org/10.1179/019713600806113176

Charola, A.E., Lazzarini, L., 1986. Deterioration of Brick Masonry Caused By Acid Rain. ACS Symp. Ser. 250–258. https://doi.org/10.1021/bk-1986-0318.ch017

Costa, C., Cerqueira, Â., Rocha, F., Velosa, A., 2019. The sustainability of adobe construction: past to future. Int. J. Archit. Herit. 13, 639–647. https://doi.org/10.1080/15583058.2018.1459954

Cultrone, G., Carrillo Rosua, F.J., 2020. Growth of metastable phases during brick firing: Mineralogical and microtextural changes induced by the composition of the raw material and the presence of additives. Appl. Clay Sci. 185, 105419. https://doi.org/10.1016/j.clay.2019.105419

Cultrone, G., De La Torre, M.J., Sebastian, E.M., Cazalla, O., Rodriguez-Navarro, C., 2000. Behavior of brick samples in aggressive environments. Water. Air. Soil Pollut. 119, 191–207. https://doi.org/10.1023/a:1005142612180

Cuomo di Caprio, N., 2007. Ceramica in archaeologia 2. "L'Erma" di Bretschneider, Roma.

Curioni, G., 1868. L'arte di fabbricare. Resistenza dei materiali e stabilità delle costruzioni.

Augusto Federico Negro Editore, Torino.

Del Monte, M., Sabbioni, C., 1984. Gypsum crusts and fly ash particles on carbonatic outcrops. Arch. Meteorol. Geophys. Bioclimatol. Ser. B 35, 105–111. https://doi.org/10.1007/BF02269413

Delgado, J.M.P.Q., Guimarães, A.S., De Freitas, V.P., Antepara, I., Kočí, V., Černý, R., 2016. Salt Damage and Rising Damp Treatment in Building Structures. Adv. Mater. Sci. Eng. 2016. https://doi.org/10.1155/2016/1280894

Elert, K., Bel-Anzué, P., Monasterio-Guillot, L., Pardo, S., 2019. Performance of alkaline activation for the consolidation of earthen architecture. J. Cult. Herit. 39, 93–102. https://doi.org/10.1016/j.culher.2019.03.004

Esbert, R.M., Ordaz, J., Alonso, F.J., Montoto, M., 1997. Manual de diagnosis y tratamiento de materiales pétreos y ceramicos. Collegi d'Aparelladors i Arquitectes Tècnics de Barcelona, Barcelona.

Favaro, M., Mendichi, R., Ossola, F., Russo, U., Simon, S., Tomasin, P., Vigato, P.A., 2006. Evaluation of polymers for conservation treatments of outdoor exposed stone monuments. Part I: Photo-oxidative weathering. Polym. Degrad. Stab. 91, 3083–3096. https://doi.org/10.1016/j.polymdegradstab.2006.08.012

Fernandes, F.M., Lourenço, P.B., Castro, F., 2010. Ancient Clay Bricks: Manufacture and Properties., in: Dan M.B., Přikryl R., Török A. (Eds.), Materials, Technologies and Practice in Historic Heritage Structures. Springer, pp. 29–48.

Fiori, C., Lorusso, S., Pentrella, R., 2003. Restauro, manutenzione, conservazione dei Beni Culturali: materiali, prodotti, tecniche, I Beni Culturali e l'Ambiente. Pitagora Editrice, Bologna.

Franzoni, E., 2014. Rising damp removal from historical masonries: A still open challenge. Constr. Build. Mater. 54, 123–136. https://doi.org/10.1016/j.conbuildmat.2013.12.054

Fugazzotto, M., 2012. Portali e manufatti lapidei a Barcellona Pozzo di Gotto. Caratterizzazione petrografica e diagnosi dello stato di conservazione finalizzate al restauro del patrimonio monumentale. Ilmiolibro self publishing, Torino.

Fugazzotto, M., Braga, R., 2012. A petrographic gateway to the Barcellona Pozzo di Gotto (NE Sicily) built environment. Rend. Online Soc. Geol. Ital. 21, 661–663.

Geraldes, C.F.M., Lima, A.M., Delgado-Rodrigues, J., Mimoso, J.M., Pereira, S.R.M., 2016. Geopolymers as potential repair material in tiles conservation. Appl. Phys. A Mater. Sci. Process. 122, 1–10. https://doi.org/10.1007/s00339-016-9709-3

Grimmer, A.E., 1984. A glossary of historic masonry deterioration problems and preservation treatments. Government Printing Office, Washington D.C.

Hodges, H., 1989. Artifacts. An introduction to early materials and technology., 3rd ed. General Duckworth & Co., London.

ICOMOS, ISCS, 2008. Illustrated glossary on stone deterioration patterns.

Lazzarini, L., Laurenzi Tabasso, M., 1986. Il restauro della pietra. CEDAM, Padova.

Lisø, K.R., Kvande, T., Hygen, H.O., Thue, J.V., Harstveit, K., 2007. A frost decay exposure index for porous, mineral building materials. Build. Environ. 42, 3547–3555. https://doi.org/10.1016/j.buildenv.2006.10.022

Maggetti, M., 1982. Phase analysis and its significance for technology and origin., in: Olin J.S., Franklin A.D. (Eds.), Archaeological Ceramics. Smithsonian Institution, pp. 121–133.

Matteini, M., Moles, A., 2007. La chimica nel restauro. I materiali dell'arte pittorica. Nardini Editore, Firenze.

Mazzeo, R., 2005. Patine su manufatti metallici., in: Tiano, P., Pardini, C. (Eds.), Le Patine. Genesi, Significato, Conservazione. Nardini Editore, Firenze, pp. 29–43.

Melo, M.J., Bracci, S., Camaiti, M., Chiantore, O., Piacenti, F., 1999. Photodegradation of acrylic resins used in the conservation of stone. Polym. Degrad. Stab. 66, 23–30. https://doi.org/10.1016/S0141-3910(99)00048-8

Morillas, H., Maguregui, M., Gallego-Cartagena, E., Marcaida, I., Carral, N., Madariaga, J.M., 2020. The influence of marine environment on the conservation state of Built Heritage: An overview study. Sci. Total Environ. 745. https://doi.org/10.1016/j.scitotenv.2020.140899

Munnikendam, R.A., 1967. Preliminary notes on the consolidation of porous building materials by impregnation with mononlers. Stud. Conserv. 12, 158–162. https://doi.org/10.1179/sic.1967.016

Pecchioni, E., Fratini, F., Cantisani, E., 2008. Le malte antiche e moderne tra tradizione ed innovazione. Pàtron Editore, Bologna.

Pozo-Antonio, J.S., Papanikolaou, A., Philippidis, A., Melessanaki, K., Rivas, T., Pouli, P., 2019. Cleaning of gypsum-rich black crusts on granite using a dual wavelength Q-Switched Nd:YAG laser. Constr. Build. Mater. 226, 721–733. https://doi.org/10.1016/j.conbuildmat.2019.07.298

Riccardi, M.P., Messiga, B., Duminuco, P., 1999. An approach to the dynamics of clay firing. Appl. Clay Sci. 15, 393–409. https://doi.org/10.1016/S0169-1317(99)00032-0

Rizzi, G., 1914. Manuale del capomastro. Impiego e prove dei materiali idraulici-cementizi., 3rd ed. Hoepli, Milano.

Rodrigues, J.D., Grossi, A., 2007. Indicators and ratings for the compatibility assessment of conservation actions. J. Cult. Herit. 8, 32–43. https://doi.org/10.1016/j.culher.2006.04.007

Rodriguez-Navarro, C., Doehne, E., Sebastian, E., 1999. Origins of honeycomb weathering: The role of salts and wind. Bull. Geol. Soc. Am. 111, 1250–1255. https://doi.org/10.1130/0016-7606(1999)111<1250:OOHWTR>2.3.CO;2

Sandrolini, F., Franzoni, E., 2006. An operative protocol for reliable measurements of moisture in porous materials of ancient buildings. Build. Environ. 41, 1372–1380. https://doi.org/10.1016/j.buildenv.2005.05.023

Sassoni, E., Pahlavan, P., Franzoni, E., Bignozzi, M.C., 2016. Valorization of brick waste by alkali-activation: A study on the possible use for masonry repointing. Ceram. Int. 42, 14685–14694. https://doi.org/10.1016/j.ceramint.2016.06.093

Simão, J., Ruiz-Agudo, E., Rodriguez-Navarro, C., 2006. Effects of particulate matter from gasoline and diesel vehicle exhaust emissions on silicate stones sulfation. Atmos. Environ. 40, 6905–6917. https://doi.org/10.1016/j.atmosenv.2006.06.016

Vidale, M., 2007. Ceramica e archeologia. Carocci editore, Roma.

Warren, J., 1999. Conservation of Brick. Butterworth Heinemann, Oxford.

Warscheid, T., Braams, J., 2000. Biodeterioration of stone: A review. Int. Biodeterior. Biodegrad. 46, 343–368. https://doi.org/10.1016/S0964-8305(00)00109-8

Chapter 2

Alkali-activated materials and geopolymers: the state of art

2.1 Alkali-activated materials, geopolymers and their evolution over time

Alkali activated materials (AAMs) are hydraulic binders with amorphous structure and ceramic-like properties, chemically synthetized by the reaction between an alkaline solution and a alumino-silicate powder (Davidovits, 1991; Pachego-Torgal et al., 2014; Provis and Bernal, 2014; Van Deventer et al., 2010). These products are called "alkali activated" precisely because the alumino-silicate precursor, once milled to a suitable granulometry, is activated, i.e. made reactive, by means of a solution of high pH, based on alkaline or alkaline earth metals as K, Na, Ca, etc. Within the term alkaline-activated materials a large group of materials are considered, which could have different proportions of Si, Al, Na or Ca according to the chemical composition of the solid precursors, and will therefore show different performances, because of the formation of different structures. As a whole, the final products are characterized by high mechanical resistance and chemical stability (Van Deventer et al., 2010).

Their performances can be considered similar to those of the traditional cements, for that they are nowadays considered a suitable alternative, actually a more sustainable one (Davidovits, 1991).

The sustainability of alkali-activated materials is due to many factors, first of all the possibility of consolidating at room temperature, or at temperatures much lower than those required by traditional ceramics or cements (e.g. Portland cement requires firing at 1450-1550 °C; while ceramics firing ranges between 800 and 1400 °C – see Chapter 1), thus reducing considerably the environmental impact due to CO_2 emissions. Portland cement production is considered indeed one of the primary causes of global warming (Van Deventer et al., 2010). Furthermore, suitable materials for the synthesis of alkali-activated binders include waste materials characterized by alumino-silicate compositions, as natural wastes (e.g. volcanic ash) or industrial by-products (e.g. fly ash from coal combustion, blast furnace slag, construction and demolition waste (C&D)). The recycling of waste helps, at the same time, to solve the disposal problems linked to their high volume and to reduce the over-exploitation of natural resources.

Among this large group of materials, this PhD thesis focuses on geopolymers. Geopolymers are alkali-activated materials characterized by the highest content of Al and Na and the simultaneous lowest content of Ca, as shown in Fig. 2.1 (Leonelli and Romagnoli, 2013; Van Deventer et al., 2010). A specification is needed, the low Ca content is referred to the reactive Ca; the geopolymer process *stricto sensu* can indeed involve also raw materials with a relatively high amount of Ca, that however will not take part completely in the reaction (Yip et al., 2008).

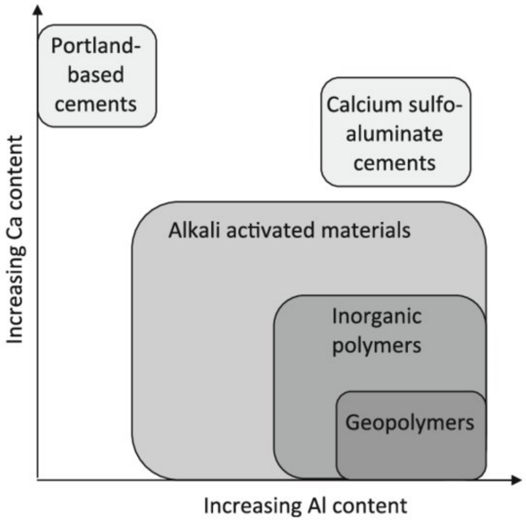

Fig. 2.1 – Classes of Alkali Activated Materials according to Van Deventer et al. (2010).

The research around these materials actually started in the 1940s and 1950s with Purdon and Glukhovsky respectively. The latest in particular studied the alkaline activation of clays, feldspars, volcanic ash and by-products of metallurgical industries of Kiev region, describing a reaction mechanism very similar to those recognized by current literature of dissolution and condensation (Leonelli and Romagnoli, 2013). Glukhovsky described the process in four steps, disruption, coagulation, condensation and crystallization, and called the final products as soils cements (Leonelli and Romagnoli, 2013). Rapidly these materials gained interest in the application as firing resistant materials, but their use still remains limited as niche products (Van Deventer et al., 2010).

After more than 40 years, these materials are still under experimentation and continuously improved for a larger basin of applications.

Regarding the terminology: the term geopolymer was coined by Davidovits (1991), one of the pioneers in this field of research. In the 1970s, he patented geopolymers obtained from metakaolin. Nowadays this name has been extended to all the alkali-activated materials which are part of the range showed in Fig. 2.1, regardless of the type of precursors involved in the synthesis.

Other terms could be found in literature for indicating AAMs and/or geopolymers, inducing a generally confusing nomenclature (Duxson et al., 2007; Van Deventer et al., 2010); the most frequent terms are mineral polymers (Wastiels et al., 1994) or inorganic polymers (Barbosa et al., 2000), thus referring to their characteristic polymeric structure; hydroceramic (Siemer, 2002) or zeoceramic (Fernández-Jiménez et al., 2008), indicating their affinity with the ceramic materials (chemical composition, refractoriness, aspect…); furthermore, it is possible to find terms as zeocements (Krivenko and Kovalchuk, 2007), where what is highlighted is their affinity with cements and zeolites simultaneously (Duxson et al., 2005; Palomo et al., 1999; Van Deventer et al., 2010). Currently, the above defined definitions of AAMs and the subgroup of geopolymers constitute an internationally recognized terminology.

It is not easy to summarize the wide range of characteristics of this class of materials. Their properties are mainly determined by their microstructural characteristics; which in its turn depends on the chemical composition of the raw materials (Duxson et al., 2007), as already said, and by their crystalline or amorphous nature, as well as on the chemical process of geopolymerization (Duxson et al., 2005; Leonelli and Romagnoli, 2013). Other important properties commonly characterizing the AAMs are in particular the resistance to acid attacks and to freezing, the easy workability, the fast setting and curing time, and the low shrinkage.

Advantages in respect to the traditional cements and traditional ceramics could be pointed out as the lower environmental impact, the higher versatility (giving the possibility to obtain very different products according to the requirements desired for the application), the costs and energy reduction, and the better performance.

2.2 The geopolymer's structure, raw materials and synthesis process

The geopolymeric structure could remind one of that of a glassy material; it is indeed amorphous or partially crystalline. Its polymeric organization is due by silicon and aluminum tetrahedra linked together by oxygen atoms. The negative charges determined by the substitution of silicon-containing tetrahedra with aluminum ones in the polymeric chain is then balanced by cations as Na^+ or K^+ coming from the alkaline solution used for the synthesis (Leonelli, 2013; Pachego-Torgal et al., 2014; Provis and Bernal, 2014).

If cations turn out to be in excess in respect to those required for the negative charge compensation of the polymeric chain, a carbonation process could happen by the action of atmospheric CO_2 with consequent sodium carbonates crystallization (Criado et al., 2005; Leonelli, 2013; Lloyd et al., 2010; Najafi Kani et al., 2012; Zhang et al., 2018). These are the typical efflorescences found on geopolymeric products. This effect could be in some way avoided by studying the formulation in a stoichiometric way. About that, better results could be obtained by increasing the alumina content of the mixture in order to achieve a better cross-linking and lower the mobility of the alkali (Najafi Kani et al., 2012; Pacheco-Torgal et al., 2013). The presence of Al in the chain in fact is the responsible of the complexity of the geopolymeric structure; indeed, while the typical structure of Portland cement sees long silicatic chains, when Al is present the structure becomes tridimensional (Leonelli, 2013).

Efflorescences, in fact, could be partly ascribed to the relatively weak bonding of Na in the gel, thus easily available for exchanges (Bortnovsky et al., 2008; Najafi Kani et al., 2012). Indeed, being more strongly bonded to the geopolymer chains, K has been sometimes used instead of Na, as the hydroxide solution used for activating the process (Najafi Kani et al., 2012). Further attempts have seen the application of hydrothermal curing (Najafi Kani et al., 2012).

According to the amorphous content and the solubility of the mineral phases constituting the alumino-silicate precursors, the liquid components able to activate the process will be different (in terms of type, molarity, pH and proportions) (Buchwald et al., 2003). The higher the amorphous content and the solubility of phases containing alumina and silica, the higher the reactivity of the precursor will be (Buchwald et al., 2003). Other factors which affect the reactivity of the precursors are the granulometry of the particles (the lower the particle size, the higher the available surface for the contact with alkaline solutions, the easier the activation process will be (Buchwald et al., 2003; Wong et al., 2018)) and the pre-treatment of the powder. Alumino-silicate materials which do not naturally show high reactivity, such as for example different clays, could increase their reactivity by being previously treated by thermal processes (Buchwald et al., 2003). It is the case in particular of the already mentioned metakaolin, which is the product of a thermal treatment at around 700 °C of kaolinite clays.

With these premises, it is logic that the evaluation of the sustainability of a geopolymeric product must take into consideration all the factors, from the supplying of the raw materials, to their eventual preparation, to the synthesis parameters and the proportions of the liquid components. Overall, literature affirms the lower environmental impact produced by creating geopolymers with respect to the cement binders, and often to the traditional ceramics (Duxson et al., 2007; Pacheco-Torgal et al., 2008; Puertas et al., 2010, 2008; Sassoni et al., 2016).

The most studied raw materials for the alkali-activation process are metakaolin, fly ash and blast furnace slag; where metakaolin and fly ash are characterized by high amount of silica and alumina (until 60% and 30% respectively) and low amounts of CaO (from 8 to 38% depending on the type of fly ash), while the slags instead show a higher amount of CaO (until 50%), more similar to those of the Portland cement, and relatively high amount of silica and alumina (until 40% and 30% respectively) (Pachego-Torgal et al., 2014).

Concerning the bricks, which have been chosen as geopolymeric precursor for this research, they generally contain high levels of silica and alumina, while the content of CaO is moderate (Reig et al., 2013a).

A general overview of the chemical composition of the raw materials used for geopolymerization is shown in Fig. 2.2.

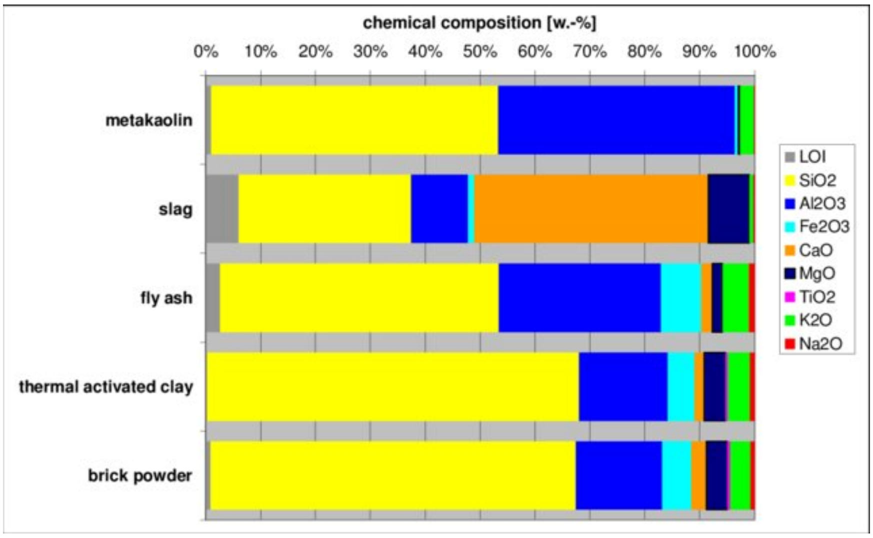

Fig. 2.2 – Example of the chemical composition of the alumino-silicate materials that can be used as geopolymeric precursors, investigated by Buchwald et al. (2003).

Regarding the alkaline activators, hydroxides, carbonates and silicates are suitable materials. The most used are sodium/potassium hydroxides (NaOH or KOH) and sodium/potassium soluble silicates, commonly known as waterglass. The general formula of these is $M_2O*nSiO_2$ where M=Na or K.

Even if, because of their high alkalinity, these products are classified as dangerous materials, actually, if used in the correct way, they show a very low toxicological risk. Soluble silicates indeed are totally inorganic compounds which when diluted do not have a real environmental impact. Even if their pH could be very high, once diluted in superficial water they tend to react with cations naturally available, forming amorphous silica or insoluble silicates, which are innocuous and already present in nature in rocks and soils (Medri, 2013).

According to the proportions of the cementitious components (CaO-SiO_2-Al_2O_3) two main categories could be defined: low calcium and high calcium alkaline cements. Two different patterns characterize their geopolymerization process, with the formation of two different gels. The low calcium system, described as $(Na,K)_2O$-Al_2O_3-SiO_2-H_2O, is formed when low calcium raw materials are involved (CaO around 10% in weight). Aggressive working conditions are required to activate the process, as high alkaline media or a thermal treatment until 200 °C. The geopolymerization reaction determines the formation of an alkaline alumino-silicate hydrate gel called N-A-S-H, where N=Na_2O; A=Al_2O_3; S=SiO_2; H=H_2O (Pachego-Torgal et al., 2014).

When the amount of SiO_2+CaO exceeds 70% the system is easier to be activated, with moderate alkaline conditions and often without pre-treatment. This high calcium system is described as $(Na, K)_2O$-CaO-Al_2O_3-SiO_2-H_2O. The reaction product obtained is a calcium silicate hydrate gel, C-A-S-H gel where C=CaO. This structure is very similar to those of the cements, C-S-H, with a difference in Al uptake (Pachego-Torgal et al., 2014).

Apart from these two geopolymerization processes described in literature, hybrid alkaline cements must be taken into consideration. Hybrid (or blended) alkaline cements are a third group, constituted by a mixing of the first two (Alonso and Palomo, 2001; Garcia-Lodeiro et al., 2013, 2011, 2010; García-Lodeiro et al., 2013; Pachego-Torgal et al., 2014; Puertas et al., 2010; Yip et al., 2005). This is the typical situation occurring when also a mixing of raw materials of different characteristics are used as precursors, as for example fly ash or slag with few amount of Portland cement; blast furnace slag and fly ash, etc. The final gel formed could be an intermediate gel among N-A-S-H and C-A-S-H, as for example a N-A-S-H gel with high content of Ca inside its structure, defined as (N,C)-A-S-H gel or, on the contrary, a C-A-S-H gel with high proportion of Na inside (Garcia-Lodeiro et al., 2013a, 2013b, 2011, 2010; Pachego-Torgal et al., 2014). The kinetics of the reaction in the hybrid systems is however still quite unclear (Garcia-Lodeiro et al., 2013a). The chemistry of the raw materials, therefore, strictly determines variations in the described geopolymerization process (Van Deventer et al., 2007). In Fig. 2.3 is reported a scheme of the geopolymerization process.

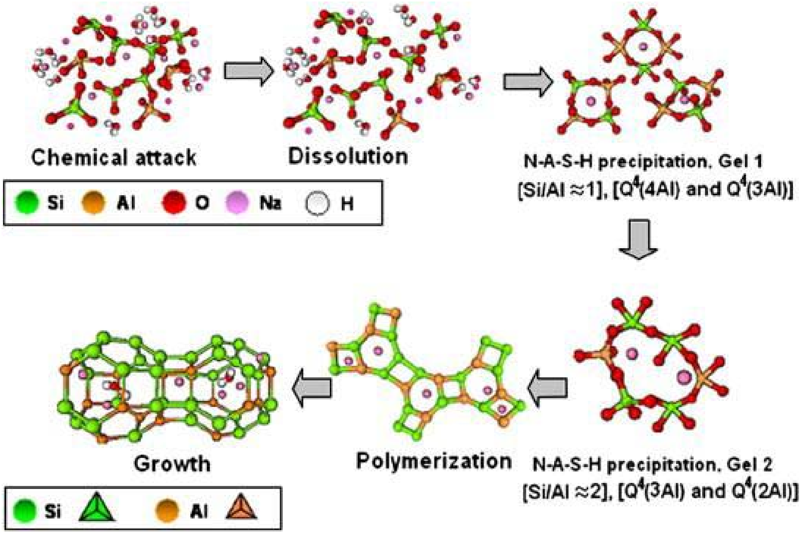

Fig. 2.3 – Geopolymerization process schematized by Shi et al. (2011), particularly referring to the N-A-S-H gel formation (see the N-A-S-H description later on in this chapter).

In order to understand the complex mechanism of geopolymerization a schematic description is here reported (Provis and Bernal, 2014):

a) The alumino-silicate species of the raw materials undergo dissolution in the alkaline environment;

b) A re-arrangement among the dissolved species and involving also those coming from the activating solution occurs;

c) The gel starts to nucleate according to two different systems (or a combination of them):

c$_1$) Low calcium gel (N-A-S-H) will grow in a three-dimensional structure with Al- and Si- containing tetrahedra randomly distributed and the balancing cations positioned in the cavities of the polymeric skeleton. This process could give the formation of secondary crystalline products, namely zeolites.

c$_2$) In high calcium systems, the (C-A-S-H) gel will grow mainly in a two-dimensional way. Each chain contains (3n-1) tetrahedra, where n = integer number. In the interlayers Ca^{2+} cations fit in, as well as water of hydration and alkalis. Contrarily to the N-A-S-H gel, water is here part of the gel structure.

The gel nucleation furthermore occurs in two steps: a first intermediate Al-rich gel is formed (Gel1), because of the faster dissolution of Al in respect to Si due to weaker Al-

O bond; then the progressive dissolution of Si determines the enriching of the gel in this element (Gel2) (Fernández-Jiménez et al., 2006; Shi et al., 2011).

d) The gel solidifies, hardens and develops strength.

When hybrid cements are involved, a co-precipitation of N-A-S-H and C-A-S-H gels will happen, determining a more complex structure where the two gels seem not to precipitate separately but with an interconnection. An interaction, still under study, will involve the two type of gels, by means of a different structural and compositional geopolymeric process (Garcia-Lodeiro et al., 2011).

2.3 Ceramic-based geopolymers

Solid waste produced from construction and demolition activities (e.g. excavations or building and roads construction, demolition and renovation) amounts to several million tons globally (Wong et al., 2018). Its recycling becomes then of strategic importance.

One of the most prominent wastes is ceramic waste, among which bricks, representing around the 45% of the C&D waste total amount (Reig et al., 2013b; Wong et al., 2018). The same kind of waste could come furthermore by industrial activities, as bricks and tile industries, as residue of working or because of broken or not well formed pieces (Tuyan et al., 2018). Waste generated by construction and demolition or by ceramic industries are classified as non-hazardous waste, because it does not contain asbestos (Bernal et al., 2016). Thanks to this, it could be re-used without pre-treatment as new prime materials. Working with demolition waste could be challenging because of its high heterogeneity and the difficulty in controlling its composition. Furthermore, the extraction of eventual contaminants, as wood, paper, plaster, glass, plastic and rubber, etc. is not so easy (Bernal et al., 2016; Cazacliu et al., 2014; Robayo et al., 2016b). Working with construction waste or waste coming from industries would be preferable in order to avoid these limits and to make the experimental studies reproducible, by reducing compositional variability of the raw materials themselves (Bernal et al., 2016).

In recent years, there have been increasing numbers of researches carried out on recycling brick waste to produce eco-friendlier materials. They have been used as aggregates (Wong et al., 2018 and references therein - table 5) or as partial raw material replacement for example in cement-based concrete and mortars (Wong et al., 2018 and references therein - table 2). Little literature is also available investigating the possible alkaline-activation of powdered ceramic waste, and red brick waste in particular (Wong et al., 2018 and reference therein - table 3).

Generally, a combination of sodium hydroxide and sodium silicates, in different proportions and concentration, has been found suitable for alkaline-activation of ceramic precursors (Allahverdi and Najafi Kani, 2009; Azevedo et al., 2018; Puertas et al., 2006; Reig et al., 2013b, 2013a; Robayo et al., 2016b, 2016a; Tuyan et al., 2018).

Both solid (e.g. Komnitsas et al., 2015) and hollow (e.g. Rovnaník et al., 2018) bricks, as well as tiles (e.g. Komnitsas et al., 2015), have been studied, obtaining ceramic-based products with compressive resistances going from around 7 MPa after 28 days of curing (Robayo et al., 2016b) to values higher than 40 MPa already after 7 days of curing (Komnitsas et al., 2015) or 71 MPa at 28 days (Sun et al., 2013).

The observed low reactivity of ceramic materials in respect to the most common alumino-silicate precursors (Buchwald et al., 2003), suggested the experimentation of binary mixtures involving more reactive components. Metakaolin, already mentioned, is one of the most frequent reactive additives used in combination with ceramic powdered waste (Azevedo et al., 2018; Rovnaník et al., 2018). It is indeed one of the first materials used for the geopolymerization and characterized by a very high percentage of amorphous, thus reactive, silica and alumina.

The ceramic reactivity, thus the pozzolan properties, depends on its amorphous component of alumino-silicate composition, which is formed during the firing of the original clay (Baronio and Binda, 1997; Böke et al., 2006).

The pozzolanic behavior of ceramic materials is commonly known and their use as additives for lime mortars is attested since ancient time, allowing to obtain a final product with hydraulic properties, more resistant and durable over time because of the formation of insoluble products with binding properties (Baronio and Binda, 1997). Crushed bricks have been documented as substitutes for naturally occurring pozzolanic materials.

Nevertheless, the research into utilizing brick dust as the source materials for alkali activated materials production is still in early stage and little is the information available

(Wong et al., 2018). From here the necessity to further investigate them and assess their feasibility (Wong et al., 2018).

2.4 Geopolymers application in the field of Cultural Heritage

Notwithstanding geopolymers have been commonly studied as functional ceramics or building materials, the experiences of geopolymers application on Cultural Heritage are limited. Few studies are reported on geopolymers for Cultural Heritage occurred regarding the consolidation of earthen architectures (Costa et al., 2019; Elert et al., 2015); repairing binders and mortars, as well as pre-casted elements, have also been tested (Barone et al., 2020; Clausi et al., 2016b, 2016a; Geraldes et al., 2016; Hanzlíček et al., 2009; Moutinho et al., 2019; Occhipinti et al., 2020; Rescic et al., 2011; Ricciotti et al., 2017; Sassoni et al., 2016). These preliminary results are surely promising, demonstrating the real possibility to optimize the performance and the appearance of the geopolymeric products, based on the kind of intervention (consolidation, repointing, retrofitting and so on…) and on the different supports (ornamental stones, terracotta sculptures and so on…). There again, as reported by Rescic and Fratini (2013), Davidovits himself was promoting a product for the realization of three-dimensional elements in the artistic field, the so-called geopolystone.

An appreciable advantage to restoration of monuments and architectural heritage with the geopolymeric technology is that it allows to choose the best raw materials from local areas (local quarries/outcropping or local industries), thus promoting at the same time a compatible intervention and the circular economy (Occhipinti et a., 2020; Barone et al., 2020). Despite this high potential of applicability of geopolymers in the conservation and restoration field, the scientific and technological aspects related to their applicability have been until now little explored (Geraldes et al., 2016).

2.5 Curiosities: the idea of the geopolymers use as building materials for the Pyramids

In 1978 Davidovits suggested that the hard and resistant materials constituting the Egyptian Pyramids were geopolymers, rather than limestone quarried blocks (Davidovits and Morris, 1988)! If true, this would be the absolutely first appearance of geopolymers linked with Cultural Heritage (Rescic and Fratini, 2013). The theory of Davidovits was based on the assumption that petrographic studies of thin sections of rocks under the microscope was unable in order to discriminate the limestone historically recognized as Pyramids' building material from a very similar artificial cementitious material. The fragments analyzed were constituted indeed by little amounts of binder (3-5%) in respect to the aggregates, mainly due to fossils and carbonate minerals, such as calcite; interpreted as a newly formed mineral. The hypothesis of Davidovits foresaw the production of geopolymers by disaggregation of a fossiliferous limestone with high percentage of kaolinitic clay inside, typical of those regions around the Pyramids. This mud would be than alkali activated by using natron (an available in loco sodium carbonate hydrate – the one used for the mummification process) and hydrated lime. The last would be obtained by the calcination (heating at high temperature – around 800 °C) of carbonate rocks and plants' ashes commonly used in the hearths.

Many archaeometric researches have followed one another, trying to confirm or deny this assumption (Barsoum et al., 2006; Demortier, 2004; Harrell and Penrod, 1993; Škvára et al., 2008). Even so, these theories are still part of an international current debate (Rescic and Fratini, 2013) .

References

Allahverdi, A., Najafi Kani, E., 2009. Construction wastes as raw materials for geopolymer binders. Int. J. Civ. Eng. 7, 154–160.

Alonso, S., Palomo, A., 2001. Alkaline activation of metakaolin and calcium hydroxide mixtures: Influence of temperature, activator concentration and solids ratio. Mater. Lett. 47, 55–62. https://doi.org/10.1016/S0167-577X(00)00212-3

Azevedo, A.G. de S., Strecker, K., Lombardi, C.T., 2018. Produção de geopolímeros à base de metacaulim e cerâmica vermelha. Cerâmica 64, 388–396. https://doi.org/10.1590/0366-69132018643712420

Barbosa, V.F.F., MacKenzie, K.J.D., Thaumaturgo, C., 2000. Synthesis and characterisation of materials based on inorganic polymers of alumina and silica: Sodium polysialate polymers. Int. J. Inorg. Mater. 2, 309–317. https://doi.org/10.1016/S1466-6049(00)00041-6

Barone, G., Caggiani, M.C., Coccato, A., Finocchiaro, C., Fugazzotto, M., Lanzafame, G., Occhipinti, R., Stroscio, A., Mazzoleni, P., 2020. Geopolymer production for conservation-restoration using Sicilian raw materials: Feasibility studies. IOP Conf. Ser. Mater. Sci. Eng. 777. https://doi.org/10.1088/1757-899X/777/1/012001

Baronio, G., Binda, L., 1997. Study of the pozzolanicity of some bricks and clays. Constr. Build. Mater. 11, 41–46. https://doi.org/10.1016/S0950-0618(96)00032-3

Barsoum, M.W., Ganguly, A., Hug, G., 2006. Microstructural evidence of reconstituted limestone blocks in the Great Pyramids of Egypt. J. Am. Ceram. Soc. 89, 3788–3796. https://doi.org/10.1111/j.1551-2916.2006.01308.x

Bernal, S.A., Rodríguez, E.D., Kirchheim, A.P., Provis, J.L., 2016. Management and valorisation of wastes through use in producing alkali-activated cement materials. J. Chem. Technol. Biotechnol. 91, 2365–2388. https://doi.org/10.1002/jctb.4927

Böke, H., Akkurt, S., Ipekoğlu, B., Uğurlu, E., 2006. Characteristics of brick used as aggregate in historic brick-lime mortars and plasters. Cem. Concr. Res. 36, 1115–1122. https://doi.org/10.1016/j.cemconres.2006.03.011

Bortnovsky, O., Dědeček, J., Tvarůžková, Z., Sobalík, Z., Šubrt, J., 2008. Metal ions as probes for characterization of geopolymer materials. J. Am. Ceram. Soc. 91, 3052–3057. https://doi.org/10.1111/j.1551-2916.2008.02577.x

Buchwald, A., Kaps, C., Hohmann, M., 2003. Alkali-Activated Binders and Pozzolan Cement Binders – Compete Binder Reaction or Two Sides of the Same Story ? 11th Int. Congr. Chem. Cem. 1238–1247.

Cazacliu, B., Sampaio, C.H., Miltzarek, G., Petter, C., Le Guen, L., Paranhos, R., Huchet, F., Kirchheim, A.P., 2014. The potential of using air jigging to sort recycled aggregates. J. Clean. Prod. 66, 46–53. https://doi.org/10.1016/j.jclepro.2013.11.057

Clausi, M., Magnani, L.L., Occhipinti, R., Riccardi, M.P., Zema, M., Tarantino, S.C., 2016a. Interaction of metakaolin-based geopolymers with natural and artificial stones and implications on their use in cultural heritage. Int. J. Conserv. Sci. 7, 871–884.

Clausi, M., Tarantino, S.C., Magnani, L.L., Riccardi, M.P., Tedeschi, C., Zema, M., 2016b. Metakaolin as a precursor of materials for applications in Cultural Heritage: Geopolymer-based mortars with ornamental stone aggregates. Appl. Clay Sci. 132–133, 589–599. https://doi.org/10.1016/j.clay.2016.08.009

Costa, C., Cerqueira, Â., Rocha, F., Velosa, A., 2019. The sustainability of adobe construction: past to future. Int. J. Archit. Herit. 13, 639–647. https://doi.org/10.1080/15583058.2018.1459954

Criado, M., Palomo, A., Fernández-Jiménez, A., 2005. Alkali activation of fly ashes. Part 1: Effect of curing conditions on the carbonation of the reaction products. Fuel 84, 2048–2054. https://doi.org/10.1016/j.fuel.2005.03.030

Davidovits, J., 1991. Geopolymers - Inorganic polymeric new materials. J. Therm. Anal. 37, 1633–1656. https://doi.org/10.1007/BF01912193

Davidovits, J., Morris, M., 1988. The Pyramids: an enigma solved. Hippocrene Books, New York.

Demortier, G., 2004. PIXE, PIGE and NMR study of the masonry of the pyramid of Cheops at Giza. Nucl. Instruments Methods Phys. Res. Sect. B Beam Interact. with Mater. Atoms 226, 98–109. https://doi.org/10.1016/j.nimb.2004.02.024

Duxson, P., Fernández-Jiménez, A., Provis, J.L., Lukey, G.C., Palomo, A., Van Deventer, J.S.J., 2007. Geopolymer technology: The current state of the art. J. Mater. Sci. 42, 2917–2933. https://doi.org/10.1007/s10853-006-0637-z

Duxson, P., Provis, J.L., Lukey, G.C., Mallicoat, S.W., Kriven, W.M., Van Deventer, J.S.J., 2005. Understanding the relationship between geopolymer composition, microstructure and mechanical properties. Colloids Surfaces A Physicochem. Eng. Asp. 269, 47–58. https://doi.org/10.1016/j.colsurfa.2005.06.060

Elert, K., Pardo, E.S., Rodriguez-Navarro, C., 2015. Alkaline activation as an alternative method for the consolidation of earthen architecture. J. Cult. Herit. 16, 461–469. https://doi.org/10.1016/j.culher.2014.09.012

Fernández-Jiménez, A., Monzó, M., Vicent, M., Barba, A., Palomo, A., 2008. Alkaline activation of metakaolin-fly ash mixtures: Obtain of Zeoceramics and Zeocements. Microporous Mesoporous Mater. 108, 41–49. https://doi.org/10.1016/j.micromeso.2007.03.024

Fernández-Jiménez, A., Palomo, A., Sobrados, I., Sanz, J., 2006. The role played by the reactive alumina content in the alkaline activation of fly ashes. Microporous Mesoporous Mater. 91, 111–119. https://doi.org/10.1016/j.micromeso.2005.11.015

Garcia-Lodeiro, I., Fernandez-Jimenez, A., Palomo, A., 2013a. Hydration kinetics in hybrid binders: Early reaction stages. Cem. Concr. Compos. 39, 82–92. https://doi.org/10.1016/j.cemconcomp.2013.03.025

García-Lodeiro, I., Fernández-Jiménez, A., Palomo, A., 2013b. Variation in hybrid cements over time. Alkaline activation of fly ash-portland cement blends. Cem. Concr. Res. https://doi.org/10.1016/j.cemconres.2013.03.022

Garcia-Lodeiro, I., Fernandez-Jimenez, A., Palomo, A., Macphee, D.E., 2010. Effect of Calcium Additions on N–A–S–H Cementitious Gels. J. Am. Ceram. Soc. 93, 1934–1940. http://doi.org/10.1111/j.1551-2916.2010.03668.x

Garcia-Lodeiro, I., Palomo, A., Fernandez-Jimenez, A., Macphee, D.E., 2011. Compatibility studies between N-A-S-H and C-A-S-H gels. Study in the ternary diagram Na2O–CaO–Al2O3–SiO2–H2O. Cem. Concr. Res. 41, 923–931. http://doi.org/10.1016/j.cemconres.2011.05.006

Geraldes, C.F.M., Lima, A.M., Delgado-Rodrigues, J., Mimoso, J.M., Pereira, S.R.M.,

2016. Geopolymers as potential repair material in tiles conservation. Appl. Phys. A Mater. Sci. Process. 122, 1–10. https://doi.org/10.1007/s00339-016-9709-3

Hanzlíček, T., Steinerová, M., Straka, P., Perná, I., Siegl, P., Švarcová, T., 2009. Reinforcement of the terracotta sculpture by geopolymer composite. Mater. Des. 30, 3229–3234. https://doi.org/10.1016/j.matdes.2008.12.015

Harrell, J.A., Penrod, B.E., 1993. The Great Pyramid Debate – Evidence from the Lauer Sample. J. Geol. Educ. 41, 358–363. https://doi.org/10.5408/0022-1368-41.4.358

Komnitsas, K., Zaharaki, D., Vlachou, A., Bartzas, G., Galetakis, M., 2015. Effect of synthesis parameters on the quality of construction and demolition wastes (CDW) geopolymers. Adv. Powder Technol. 26, 368–376. https://doi.org/10.1016/j.apt.2014.11.012

Krivenko, P. V., Kovalchuk, G.Y., 2007. Directed synthesis of alkaline aluminosilicate minerals in a geocement matrix. J. Mater. Sci. 42, 2944–2952. https://doi.org/10.1007/s10853-006-0528-3

Leonelli, C., 2013. Definizione, preparazione, proprietà ed applicazioni., in: Leonelli, C., Romagnoli, M. (Eds.), Geopolimeri: Polimeri Inorganici Attivati Chimicamente. ICerS, Bologna, pp. 1–22.

Leonelli, C., Romagnoli, M., 2013. Geopolimeri: Polimeri Inorganici Attivati Chimicamente., 2nd ed. ICerS, Bologna.

Lloyd, R.R., Provis, J.L., Van Deventer, J.S.J., 2010. Pore solution composition and alkali diffusion in inorganic polymer cement. Cem. Concr. Res. 40, 1386–1392. https://doi.org/10.1016/j.cemconres.2010.04.008

Medri, V., 2013. Materie Prime., in: Leonelli, C., Romagnoli, M. (Eds.), Geopolimeri: Polimeri Inorganici Attivati Chimicamente. ICerS, Bologna, pp. 23–41.

Moutinho, S., Costa, C., Cerqueira, Â., Rocha, F., Velosa, A., 2019. Geopolymers and polymers in the conservation of tile facades. Constr. Build. Mater. 197, 175–184. https://doi.org/10.1016/j.conbuildmat.2018.11.058

Najafi Kani, E., Allahverdi, A., Provis, J.L., 2012. Efflorescence control in geopolymer binders based on natural pozzolan. Cem. Concr. Compos. 34, 25–33.

https://doi.org/10.1016/j.cemconcomp.2011.07.007

Occhipinti, R., Stroscio, A., Finocchiaro, C., Fugazzotto, M., Leonelli, C., Lo Faro, M.J., Megna, B., Barone, G., Mazzoleni, P., 2020. Alkali activated materials using pumice from the Aeolian Islands (Sicily, Italy) and their potentiality for cultural heritage applications: Preliminary study. Constr. Build. Mater. 259, 120391. https://doi.org/10.1016/j.conbuildmat.2020.120391

Pacheco-Torgal, F., Castro-Gomes, J., Jalali, S., 2008. Alkali-activated binders: A review. Part 1. Historical background, terminology, reaction mechanisms and hydration products. Constr. Build. Mater. 22, 1305–1314. https://doi.org/10.1016/j.conbuildmat.2007.10.015

Pacheco-Torgal, F., Tam, V.W.Y., Labrincha, J.A., Ding, Y., de Brito, J., 2013. Handbook of Recycled Concrete and Demolition Waste. Woodhead Publishing.

Pachego-Torgal, F., Labrincha, J.A., Leonelli, C., Palomo, A., Chindaprasirt, P., 2014. Handbook of Alkali-activated cements, mortars and concretes. Elsevier.

Palomo, A., Grutzeck, M.W., Blanco, M.T., 1999. Alkali-activated fly ashes: A cement for the future. Cem. Concr. Res. 29, 1323–1329. https://doi.org/10.1016/S0008-8846(98)00243-9

Provis, J.L., Bernal, S.A., 2014. Geopolymers and related alkali-activated materials. Annu. Rev. Mater. Res. 44, 299–327. https://doi.org/10.1146/annurev-matsci-070813-113515

Puertas, F., Barba, A., Gazulla, M.F., Gómez, M.P., Palacios, M., Martínez-ramírez, S., 2006. Ceramic wastes as raw materials in portland cement clinker fabrication: Characterization and alkaline activation. Mater. Constr. 56, 73–84. https://doi.org/10.3989/mc.2006.v56.i281.94

Puertas, F., García-Díaz, I., Barba, A., Gazulla, M.F., Palacios, M., Gómez, M.P., Martínez-Ramírez, S., 2008. Ceramic wastes as alternative raw materials for Portland cement clinker production. Cem. Concr. Compos. 30, 798–805. https://doi.org/10.1016/j.cemconcomp.2008.06.003

Puertas, F., García-Díaz, I., Palacios, M., Gazulla, M.F., Gómez, M.P., Orduña, M., 2010. Clinkers and cements obtained from raw mix containing ceramic waste as a raw material. Characterization, hydration and leaching studies. Cem. Concr. Compos. 32, 175–186. https://doi.org/10.1016/j.cemconcomp.2009.11.011

Reig, L., Tashima, M.M., Borrachero, M. V., Monzó, J., Cheeseman, C.R., Payá, J., 2013a. Properties and microstructure of alkali-activated red clay brick waste. Constr. Build. Mater. 43, 98–106. https://doi.org/10.1016/j.conbuildmat.2013.01.031

Reig, L., Tashima, M.M., Soriano, L., Borrachero, M. V., Monzó, J., Payá, J., 2013b. Alkaline activation of ceramic waste materials. Waste and Biomass Valorization 4, 729–736. https://doi.org/10.1007/s12649-013-9197-z

Rescic, S., Fratini, F., 2013. Geopolimeri e Beni Culturali., in: Leonelli, C., Romagnoli, M. (Eds.), Geopolimeri: Polimeri Inorganici Attivati Chimicamente. ICerS, Bologna, pp. 252–278.

Rescic, S., Plescia, P., Cossari, P., Tempesta, E., Capitani, D., Proietti, N., Fratini, F., Mecchi, A.M., 2011. Mechano-chemical activation: An ecological safety process in the production of materials to stone conservation. Procedia Eng. 21, 1061–1071. https://doi.org/10.1016/j.proeng.2011.11.2112

Ricciotti, L., Molino, A.J., Roviello, V., Chianese, E., Cennamo, P., Roviello, G., 2017. Geopolymer composites for potential applications in cultural heritage. Environ. - MDPI 4, 1–15. https://doi.org/10.3390/environments4040091

Robayo, R.A., de Guitiérrez, R.M., Muldford, A.J., 2016a. Production of building elements based on alkali-activated red clay brick waste. Rev. Fac. Ing. 25, 21–30.

Robayo, R.A., Mulford, A., Munera, J., Mejía de Gutiérrez, R., 2016b. Alternative cements based on alkali-activated red clay brick waste. Constr. Build. Mater. 128, 163–169. https://doi.org/10.1016/j.conbuildmat.2016.10.023

Rovnaník, P., Rovnaníková, P., Vyšvařil, M., Grzeszczyk, S., Janowska-Renkas, E., 2018. Rheological properties and microstructure of binary waste red brick powder/metakaolin geopolymer. Constr. Build. Mater. 188, 924–933. https://doi.org/10.1016/j.conbuildmat.2018.08.150

Sassoni, E., Pahlavan, P., Franzoni, E., Bignozzi, M.C., 2016. Valorization of brick waste by alkali-activation: A study on the possible use for masonry repointing. Ceram. Int. 42, 14685–14694. https://doi.org/10.1016/j.ceramint.2016.06.093

Shi, C., Jiménez, A.F., Palomo, A., 2011. New cements for the 21st century: The pursuit of an alternative to Portland cement. Cem. Concr. Res. 41, 750–763. https://doi.org/10.1016/j.cemconres.2011.03.016

Siemer, D.D., 2002. Hydroceramic a "new" cementitious waste from materials for US defence-type reprocessing waste. Mater. Res. Innov. 6, 96–104. https://doi.org/10.1007/s10019-002-0193-3

Škvára, F., Svoboda, P., Doležal, J., Bittnar, Z., Šmilauer, V., Kopecký, L., Šulc, R., 2008. Geopolymer concrete - An ancient material too? Ceram. - Silikaty 52, 296–298.

Sun, Z., Cui, H., An, H., Tao, D., Xu, Y., Zhai, J., Li, Q., 2013. Synthesis and thermal behavior of geopolymer-type material from waste ceramic. Constr. Build. Mater. 49, 281–287. https://doi.org/10.1016/j.conbuildmat.2013.08.063

Tuyan, M., Andiç-Çakir, Ö., Ramyar, K., 2018. Effect of alkali activator concentration and curing condition on strength and microstructure of waste clay brick powder-based geopolymer. Compos. Part B Eng. 135, 242–252. https://doi.org/10.1016/j.compositesb.2017.10.013

Van Deventer, J.S.J., Provis, J.L., Duxson, P., Brice, D.G., 2010. Chemical research and climate change as drivers in the commercial adoption of alkali activated materials. Waste and Biomass Valorization 1, 145–155. https://doi.org/10.1007/s12649-010-9015-9

Van Deventer, J.S.J., Provis, J.L., Duxson, P., Lukey, G.C., 2007. Reaction mechanisms in the geopolymeric conversion of inorganic waste to useful products. J. Hazard. Mater. 139, 506–513. https://doi.org/10.1016/j.jhazmat.2006.02.044

Wastiels, J., Wu, X., Faignet, S., Patfoort, G., 1994. Mineral polymer based on fly ash. J. Resour. Manag. Technol. 22, 135–141.

Wong, C.L., Mo, K.H., Yap, S.P., Alengaram, U.J., Ling, T.C., 2018. Potential use of brick waste as alternate concrete-making materials: A review. J. Clean. Prod. 195, 226–239. https://doi.org/10.1016/j.jclepro.2018.05.193

Yip, C.K., Lukey, G.C., Van Deventer J.S.J., 2005. The coexistence of geopolymeric gel and calcium silicate hydrate at the early stage of alkaline activation. Cem. Concr. Res. 32, 1688–1697. https://doi.org/10.1016/j.cemconres.2004.10.042

Yip, C.K., Lukey, G.C., Provis, J.L., Van Deventer J.S.J., 2008. Effect of calcium silicate sources on geopolymerisation. Cem. Concr. Res. 38, 554–564. https://doi.org/10.1016/j.cemconres.2007.11.001

Zhang, Z., Provis, J.L., Ma, X., Reid, A., Wang, H., 2018. Efflorescence and subflorescence induced microstructural and mechanical evolution in fly ash-based geopolymers. Cem. Concr. Compos. 92, 165–177. https://doi.org/10.1016/j.cemconcomp.2018.06.010

Chapter 3

Materials and methods

3.1 The experimental protocol

The experimental protocol has been organized in three phases (Table 3.1):

- firstly, different raw ceramic materials have been selected among ceramic industrial waste, in order to identify two potential geopolymeric precursors for the aim of this research project;
- in the second phase, the geopolymeric binders have been experimented in laboratory and simultaneously characterized, continuously improving them on an empirical basis, until reaching the mortars' formulations, which in turn have been characterized;
- in the third phase, the selected geopolymeric products have been tested on archaeological remains.

For the characterization of raw materials and geopolymers, both usual analytical techniques such as X-Ray Diffractometry, Scanning Electron Miscroscopy, IR spectroscopy etc. and more innovative approaches (as the application of Raman spectroscopy and Diffuse Reflectance Infrared Spectroscopy, not usually used for this kind of materials) have been used.

The analytical investigations were performed mainly in the laboratories of the Department of Biological, Geological and Environmental Sciences of University of Catania. Some further analyses were performed in collaboration with other laboratories in Catania (Department of Physics and Astronomy), in Italy (University of Modena and Reggio Emilia, University of Florence, University of Pisa) or in Spain (University of Granada).

In detail, the characteristics of the raw materials have been compared according to their potential reactivity in alkaline media, by means of leaching test, followed by inductively coupled plasma – optical emission spectrometry (ICP-OES); their chemical, molecular and mineralogical characteristics have been investigated by means of X-Ray Fluorescence (XRF), Fourier Transform Infrared Spectroscopy with Attenuated Total Reflectance

(FTIR-ATR), Diffuse Reflectance Infrared Spectroscopy (DRIFT) and Raman spectroscopy, Thermo-gravimetric analysis (TGA) and X-Ray Diffractometry (XRD). Laser granulometry was furthermore performed and followed by Brunauer–Emmett–Teller (BET) analysis. Morphological features have been investigated by means of Scanning Electron Microscopies (SEM).

The geopolymeric products have then been investigated in their chemical composition by the already mentioned spectroscopic techniques; furthermore, chemical data were obtained by the Energy Dispersive X-Ray analysis (EDS) coupled to Scanning Electron Microscopy (SEM) and Transmission Electron Microscopy (TEM). These information, together with the related micrographs and diffraction patterns, allowed also to improve the knowledge of the chemistry of the gel in function of the morphologies. The porosimetric structure and the absorption properties have been also investigated, with Mercury Intrusion Porosimetry (MIP) and Capillary Water Absorption Tests. Finally, the mechanical performance, both compressive and flexural strengths, were tested.

The chemical stability of the products was tested by measuring the pH and ionic conductivity of the solution in which fragments were immersed. The adhesion properties to the archaeological substrate at the interface geopolymer/substrate have been studied by Scanning Electron Microscopy, and also mechanically studied by an adhesion test developed *ad hoc*.

RAW MATERIALS

- ✓ XRF
- ✓ REACTIVITY TEST
- ✓ TGA
- ✓ SELECTION OF 2 RAW MATERIALS
- ✓ LASER GRANULOMETRY+BET
- ✓ XRD
- ✓ FTIR-ATR
- ✓ DRIFT
- ✓ RAMAN
- ✓ SEM

GEOPOLIMERIC BINDERS

- ✓ XRD
- ✓ SEM-EDS
- ✓ TEM-EDS
- ✓ FTIR-ATR
- ✓ DRIFT
- ✓ RAMAN
- ✓ MIP
- ✓ COMPRESSION TEST
- ✓ COLORIMETRY

GEOPOLIMERIC PRODUCTS FOR RESTORATION

- ✓ ADHESION TEST
- ✓ SEM-EDS
- ✓ PH&CONDUCTIVITY MEASUREMENTS
- ✓ COMPRESSION TEST
- ✓ FLEXURAL TEST
- ✓ MIP
- ✓ CAPILLARY WATER ABSORPTION TEST
- ✓ COLORIMETRY

Table 3.1 – Analytical protocols followed for the different categories of materials studied.

3.2 Analytical techniques

3.2.1 Leaching test and Inductively Coupled Plasma – Optical Emission Spectroscopy (ICP-OES)

The test have been performed following the experiments of Fernández-Jiménez and Palomo (2003) and Ruiz-Santaquiteria et al. (2013); however while they usually use HF, in this research the tests have been carried out reproducing the solubility conditions chosen for the alkaline activating process, namely ambient T and pH of a NaOH 8M solution.

1 ± 0.05 g powder of each material has been subjected to a leaching attack by using NaOH 8M (NaOH, 99%, J. T. Baker; water Millipore purified by Milli-Q UV, resistivity > 18 MΩ·cm) in 100 ml of solution. The system was mechanically agitated (300 rpm) for 12 hours at room temperature.

The analysis of the eluate allowed the determination by gravimetric method of the solid residue and to obtain by ICP-OES the amount of soluble Si and Al.

In particular, after the basic attack, the eluates have been filtered with Whatman paper and diluted with Milli-Q water until reaching the volume of 1 L. The washing of the filters was carried out until reaching a neutral pH. The solid residues have been than obtained after drying in an oven at 110 °C for 1 hour.

A Varian 720-ES ICP – OES has been used for the chemical analysis of the eluates by introducing the sample via spray chamber. The quantification has been obtained by using the internal standard method of Ge (1 mg/L); the calibration curve has been realized considering 6 points in the 2 - 200 μg/L interval.

The test has been conducted at the University of Florence thanks to Prof. Emiliano Carretti.

3.2.2 Thermogravimetric analysis (TGA)

Thermogravimetric analysis have been performed by using a thermobalance TA Instrument, model Q5000IR. The analyses have been performed on about 10-15 mg of sample in a nitrogen flux, with gradual increases of 20 °C/minute, considering a temperature range from the environmental temperature to a maximum of 900 °C.

The analyses have been conducted at the University of Pisa, thanks to Prof. Maria Rosaria Tiné.

3.2.3 Laser granulometry and Brunauer–Emmett–Teller analysis (BET)

Granulometric measurements have been carried out by using the Laser Granulometer Mastersizer 2000, Hydro 2000S model (Malvern Instrument). The measurements have been conducted in humid conditions; after the acquisition of a “white” reference, 10 successive acquisitions for each sample are elaborated by the software, which gives back an average curve. The results are then expressed with a cumulative curve and a curve representing the granulometric distribution.

BET analysis have also been performed. The analyses have been performed by using the Micromeritics Instrument, Gemini Model 2380, with the following technical specifications: N_2 analysis adsorptive, 10 s equilibration time, 779.905 mmHg pressure.

All these measurements have been done at the University of Modena and Reggio Emilia thanks to Profs. Cristina Leonelli and Isabella Lancellotti.

3.2.4 X-Ray Fluorescence (XRF)

Chemical analyses by X-Ray Fluorescence have been performed on pearls by a PANalytical instrument, model Zetium, with ceramic tube with Rh anode; ultra-fine high transmission Beryllium front window, at least 75 μm and tube geometry below the sample; High Stability Power 4 kW X-ray Generator; decoupled goniometer $\theta/2\theta$ with optical positioning system and high angular reproducibility (0.0001°). The major elements have been quantified by using the OMNIAN software, while the traces elements by Pro-Trace.

All the measurements have been conducted at the CIC (Centro de Instrumentation Cientifica) of the University of Granada.

The only exception is the metakaolin sample, which was analyzed at the University of Catania by means of a portable X-Ray Fluorescence, particularly the Bruker Tracer IV-SD system equipped with a Rh target X-ray tube with Pd slits and a Silicon Drif Detector (SDD), with 60 s live time accumulations.

3.2.5 X-Ray Diffractometry (XRD)

Mineralogical investigations have been performed by a PANalytical X'Pert PRO X-Ray Diffractometer, with Cu Kα radiation and operating at 45 kV and 40 mA; the following operative conditions were used: time 20 seconds, step 0.04 in a range of 3-70 2Θ.

The qualitative analysis was then conducted by using High Score Plus software v.4.8, while for the quantitative data Profex software was chosen (Doebelin and Kleeberg, 2015).

In order to quantify the amorphous content, the Rietveld Refinement (Gualtieri and Zanni, 1998) has been used, by adding to the sample 5% in weight of corundum as internal standard (NIST SRM 676a). The analyses have been performed at the University of Granada.

3.2.6 Fourier Transform Infrared Spectroscopy – Attenuated Total Reflectance (FTIR-ATR)

FTIR-ATR spectra were obtained on the powdered samples by means of a Thermo Fisher Scientific Nicolet 380 FT-IR spectrometer with a Smart Orbit diamond attenuated total reflectance (ATR) cell. The spectra were collected at room temperature in the 400-4000 cm^{-1} range, with 4 cm^{-1} resolution and averaging 64 scans. For each sample, in order to have a representative result, three measurements have been acquired and the spectra averaged.

Principal component analysis has been performed on the ATR spectra by means of Orange Data Mining 3.30.2 software.

The analyses have been performed at the Department of Biological, Geological and Environmental Sciences at University of Catania.

3.2.7 Diffused Reflectance Infrared Fourier Transform Spectroscopy (DRIFT)

DRIFT spectra were collected on fragments by means of an Agilent technologies Cary 630 FTIR infrared spectrometer. Data were recorded at room temperature and the spectra were calculated in reflectance with 512 interferometer scans in the wavenumber range of 5500-450 cm^{-1}, with resolution of 4 cm^{-1}. The software Agilent MicroLab PC controls the system. In order to have representative data, the spectrum shown for each sample is the average of three measurements on three different portions of the same samples.

Statistical principal component analysis has been performed on the DRIFT spectra by means of Orange Data Mining 3.30.2 software.

The analyses have been performed at the Department of Biological, Geological and Environmental Sciences at University of Catania.

3.2.8 Raman Spectroscopy

Micro-Raman spectroscopy has been performed on fragments by a Jasco NRS3100 spectrometer equipped with a Notch filter and a Peltier-cooled (-49°C) 1024x128 CCD. The 532 nm excitation wavelength was used, reaching, with the 1800 gr/mm grating, a spectral resolution of ~3 cm^{-1}. The calibration of the system was verified using the 520.7 cm^{-1} Raman band of silicon before each experimental session. Different particles for each samples have been selected for analysis by using an Olympus (Japan) 20× objective (N.A.=0.45), with a spatial resolution of about 4 µm. The laser power value is controlled through neutral optical density filters and it was kept around 1 mW to avoid heating effects. Time and number of accumulations were regulated according to the sample response. In all cases, both the low wavenumber region (130-1200 cm^{-1}) and the high wavenumber one (3100-3700 cm^{-1}) were investigated.

The Qn notation developed by Engelhardt et al. (1975) in the field of Nuclear Magnetic Resonance will be used for describing the connectivity of the alumino-silicate gel: Q stands for the Si atom and n (0-4) indicates the number of bridging oxygen atoms (Vidal. et al., 2016).

The analyses have been performed at the Department of Biological, Geological and Environmental Sciences at University of Catania.

3.2.9 Scanning Electron Microscopy with Energy Dispersive X-Ray Probe (SEM-EDS)

The SEM-EDS analyses have been performed in three different structures according to the availability of the instruments and/or the necessity of investigating some features at different magnifications.

In particular, SEM-EDS instrumentation at the Department of Biological, Geological and Environmental Science and at the Department of Physics and Astronomy (thanks to Prof. Francesco Ruffino and Dr. Stefano Boscarino) of the University of Catania, and at the CIC of the University of Granada have been used. The samples analysed were very thin fragments previously carbon-coated. The equipments and conditions of analysis are respectively reported below:

- Tescan Vega LMU Scanning Electron Microscope equipped with energy dispersive X-ray spectroscopy (EDS) microanalysis. Data were collected by focusing the e-beam on the sample at an energy of 25kV and current of 0.2 nA.
- Zeiss FEG-SEM Supra 25 Microscope Field Emission Scanning Electron Microscope equipped with InLens detector coupled with an energy dispersive X-ray spectroscopy (EDS) microanalysis. Data were collected by focusing the e-beam on the sample at an energy of 25kV and current of 0.2 nA.
- Carl Zeiss SMT Field Emission Scanning Electron Microscope (AURIGA Series) equipped with InLens detector and an energy dispersive X-ray spectroscopy (EDS) microanalysis. The energy was of of 20 kV and current of 0.2 nA.

3.2.10 Transmission Electron Microscopy with Energy Dispersive X-ray Spectroscopy (TEM-EDS)

Thermo Fisher Scientific TALOS F200X Transmission Electron Microscopy has been used equipped energy dispersive X-ray spectroscopy (EDS) operating at 200 kV and equipped with an EDAX solid-state energy-dispersive X-ray detector. Powder samples were deposited on carbon-coated Cu grids. Quantitative chemical analyses were obtained in STEM mode using a scan window of 20 × 100 nm. The analysis has been performed at the CIC of the University of Granada.

3.2.11 Mercury Intrusion Porosimetry (MIP)

For Mercury Intrusion Porosimetric analysis, a Thermoquest Pascal 240 porosimeter was used in order to explore the pore size distribution with radii comprised between 0.0074 mm and 15 mm, and a Thermoquest Pascal 140 porosimeter to investigate the pore radii range 3.8 mm-116 mm. Before the analysis, the fragments have been dried in an oven for 24 hours at 100 °C.

The analyses have been performed at the Department of Biological, Geological and Environmental Sciences at the University of Catania.

3.2.12 Capillary water absorption test

The test has been performed according to the standard UNI 10859:2000. Six cubes of 2*2*2 cm for each formulation to test have been put in contact with water and their weight have been measured at fixed intervals of time (1, 3, 10, 15, 30, 60, 480, 1440 min). Before the test, the samples were dried in an oven at 70 °C during 24 hours.

The analyses have been performed at the Department of Biological, Geological and Environmental Sciences at University of Catania.

3.2.13 Uniaxial compressive test

Three samples of 2*2*2 cm for preliminary tests have been analysed at the University of Florence, at the University of Modena and Reggio Emilia and at the University of Granada, respectively with the following instrumentations and measurements' conditions:

- Instron Model 5592 instrumentation, maximum charge of 600 kN and a velocity of 0.5 MPa/s, according to UNI EN 1926:2007 standard;
- Instron Model 5567 instrumentation, maximum charge of 30 kN and a velocity of 3 mm/min, according to UNI EN 826:2013 standard;
- Ibertest Model Tetronic-100-MD2 instrumentation, maximum charge of 100 kN and a velocity of 3 mm/min.

Then, six replicates of 2*2*2cm for each formulation have been subjected compressive tests using a 70-T1182 Uniframe (Controls) mechanical press at the Department of Biological, Geological and Environmental Sciences at University of Catania and with the following operative conditions: 2000 kN of maximum peak, 0.1 cell load and a velocity of 2400 N/s.

3.2.14 Three points flexural test

Three replicates of 2*2*8 cm for each formulation have undergone the three points flexural test with 70-T1182 Uniframe (Controls) mechanical press according to the following operative conditions: knifes' length of 60 mm, 0.3 kN peak, 0.05 cell loading and velocity of 25 N/s.

The analyses have been performed at the Department of Biological, Geological and Environmental Sciences at University of Catania.

3.2.15 pH measurements and conductivity test

Chemical stability has been tested by measuring at fixed intervals of time (0, 5,15,30, 60, 120, 240, 480, 1440 min) the pH of the water in which geopolymeric samples were immersed during 24 hours in stirring conditions, according to a water/sample ratio of 10/1. The same solution was also subjected to ionic conductivity measurements, at the same intervals of time.

The analyses have been performed at the University of Modena and Reggio Emilia, thanks to Profs. Cristina Leonelli and Isabella Lancellotti.

3.2.16 Colorimetry

Colorimetric measurements have been carried out by a Konica Minolta CM-2600d instrument. A circular area with a diameter of 8 mm was observed. All measurements were performed under D65 illuminant and 10° observer conditions. The values are expressed in the CIELAB (L*, a*, b*) colour coordinates system, where L* defines lightness and ranges from 0 (total absorption or black) to +100 (white), whereas a* and b* denote the green/red and blue/yellow values, respectively, both ranging between -60 and +60. Three measurements have been performed on each sample, in order to obtain a representative average value.

The analyses have been performed at the Department of Biological, Geological and Environmental Sciences at the University of Catania.

3.2.17 Adhesion test

In the case of mortars to be used for restoration purposes for reintegration of bricks, an adhesion test was performed on sandwiches (brick/mortar/brick). This test was performed in an unusual way, by repeating the three points flexural test, with the data indicated in the paragraph 3.2.14, positioning the sandwich horizontally on the knifes, with the median knife pointing towards the mortar joint and the two external knifes directed toward the bricks.

The analyses have been performed at the Department of Biological, Geological and Environmental Sciences at University of Catania.

References

Doebelin, N., Kleeberg, R., 2015. Profex: A graphical user interface for the Rietveld refinement program BGMN. J. Appl. Crystallogr. 48, 1573–1580. https://doi.org/10.1107/S1600576715014685

Engelhardt, G., Zeigan, D., Jancke, H., Hoebbel, D., Weiker, Z., 1975. High resolution 29Si NMR of silicates and zeolites. Zeitschrift für Anorg. und Allg. Chemie 418, 17–28.

Fernández-Jiménez, A., Palomo, A., 2003. Characterisation of fly ashes. Potential reactivity as alkaline cements. Fuel 82, 2259–2265. https://doi.org/10.1016/S0016-2361(03)00194-7

Gualtieri, A., Zanni, M., 1998. Quantitative determination of crystalline and amorphous phase in traditional ceramics by combined Rietveld-RIR method. Trans Tech Publ Ltd 278, 834–839.

Ruiz-Santaquiteria, C., Fernández-Jiménez, A., Skibsted, J., Palomo, A., 2013. Clay reactivity: Production of alkali activated cements. Appl. Clay Sci. 73, 11–16. https://doi.org/10.1016/j.clay.2012.10.012

UNI, 2013. Isolanti termici per edilizia - Determinazione del comportamento a compressione. EN 826.

UNI, 2007. Natural stone test methods - Determination of uniaxial compressive strength. EN 1926.

UNI, 2000. Beni culturali - Materiali lapidei naturali ed artificiali - Determinazione dell’assorbimento d’acqua per capillarità. 10859.

Vidal., L., Joussein, E., Colas, M., Cornette, J., Sanz, J., Sobrados, I., Gelet, J.L., Absi, J., Rossignol, S., 2016. Controlling the reactivity of silicate solutions: A FTIR, Raman and NMR study. Colloids and surfaces 503, 101–109. https://doi.org/10.1016/j.colsurfa.2016.05.039

Chapter 4

Raw materials and characterization

4.1 Ceramic precursors

Different types of industrial ceramic wastes have been collected as precursors for alkaline activation. They are showed in the Fig. 4.1 and listed in the Table 4.1.

Industrial and handmade tiles have been provided by a local industry, La Bottega Calatina, located in Caltagirone (CT). In addition, different types of red clay bricks have been recovered from the local industry Laquattro, located in Rometta (ME).

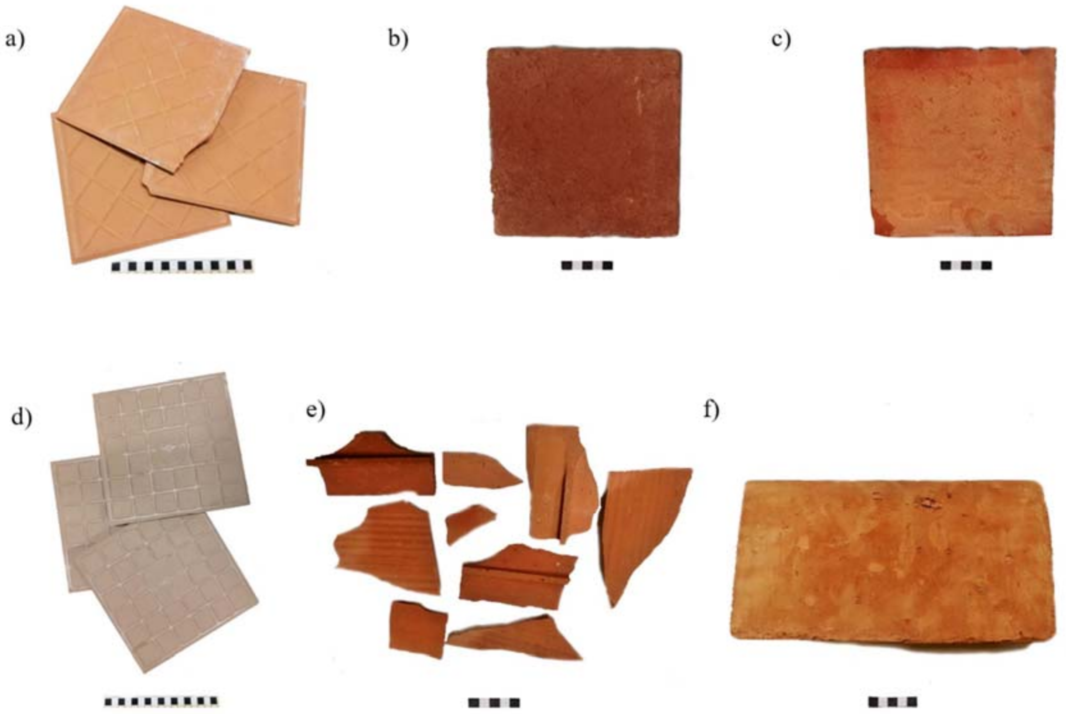

Fig. 4.1 – Ceramic waste retrieved by local industries: LBCa a), LBCb b), LBCc c), LBCf d), CWF e), CWM f). Abbreviations in Table 4.1.

Label	Ceramic waste type	Company	Country
LBCa	Industrial ceramic tiles	La Bottega Calatina	Caltagirone (CT)
LBCb	Hand-made ceramic tiles	La Bottega Calatina	Caltagirone (CT)
LBCc	Semi-industrial ceramic tiles	La Bottega Calatina	Caltagirone (CT)
LBCf	Gress	La Bottega Calatina	Caltagirone (CT)
CWF	Hollow red clay bricks	Laquattro	Rometta (ME)
CWM	Solid red clay bricks	Laquattro	Rometta (ME)

Table 4.1 – Ceramic waste materials studied as geopolymeric precursors.

La Bottega Calatina (LBC), founded in 2001 by Rosario Parrinello, is a company specialized in manufacturing and decoration of ceramic and lava stone, according to the ancient local traditions (Fig. 4.2). It offered different kind of tiles, semi-industrial and completely handmade with different characteristics. All these materials are labelled as LBC, plus an alphabetic sequence as LBCa, LBCb and so on.

Laquattro, founded in 1982 by Pietro La Fauci, began as roof tiles producer and then moved on to red clay bricks, bocoming one of the most important references in the production of hollow bricks (Fig. 4.3).

This company provided two different types of red bricks, labelled as CWF (Construction material Waste "Forato" – where *forato* means hollow brick) and CWM (Construction material Waste "Mattone" – where *mattone* means brick, specifically solid brick). All the products selected are made by local clayey materials and aggregates and are available as waste in large amount, because of damages occurring during the manufacturing, the decoration or the transport. Regarding the decorated ones there are also a lot of materials which, even if intact from the ceramic body point of view, show defects on the glaze, becoming unsaleable materials and so necessary to be disposed. In case of glazed materials, this layer has been mechanically removed before starting to work.

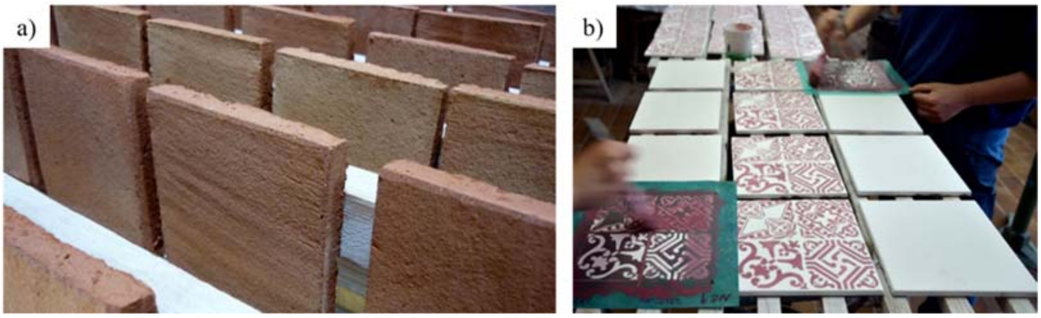

Fig. 4.2 – Example of terracotta tiles a) and handmade decorations b) at La Bottega Calatina.

Fig. 4.3 – The area of storage and transportation of the hollow bricks at Laquattro.

The general characteristics of the selected ceramics are described below:

- LBCa: tile waste characterized by a fine and homogeneous grain body, industrially made by mixing commercial clay with 3% of water and fired at around 1100 °C, after natural drying. When present, the glaze has been applied by airbrush, followed by a second firing to fix it. The colour of the body is pinkish.
- LBCb: tile waste characterized by a coarse grain body, handmade by mixing local clay with a higher water percentage, volcanic and sand aggregates are present. The firing temperature to obtain this kind of material is between 900 and 1100 °C. The glaze is applied, when present, following the same procedure of the LBCa tiles. The colour of the body is dark red.
- LBCc: tile waste of medium grain size, semi-industrially produced, of reddish colour and homogeneous texture. Also in this case the glaze, when present, is applied with the airbrush and fixed by a second firing step.

- LBCf: gres tile waste; the colour is greyish, perfectly homogeneous and smooth. This kind of product is produced by industrial process starting from kaolinitic clay, with temperature higher than 1100 °C, usually between 1300 and 1400 °C.
- CWF: hollow bricks, ceramic materials fired at low temperature, around 870 °C, starting from local clay of the Plio-Pleistocene Rometta Formation retrieved in the areas of Fondachelli, San Pier Niceto and Barcellona Pozzo di Gotto and local sand aggregates. The texture is quite heterogeneous, light red in colour with fine grain size and sporadically interrupted by white spots, probably of carbonate nature, and dark ones of millimetric size.
- CWM: solid brick, retrieved from Laquattro but produced by Latersud, a Calabrian company, today leader in the production of this materials. The colour is light red, the grain size is fine and the general texture appearance is homogeneous. Sporadic silver/gold-like millimetric lamellae are visible together with some white spots.

All the information about the firing temperature are directly supplied by the companies.

According to the suggestions of the producers, LBCa and CWF have been selected for experimenting alkali activation. Among all the ceramic waste supplied, indeed, these are the more abundant, thus those mainly responsible of the highest disposal problem. They are furthermore the most representative as industrial products and they are available in greater amounts for the tests. These precursors have been thoroughly characterized by means of XRF, XRD, TGA, reactivity tests and FTIR and SEM. DRIFT and Raman have been also carried out for testing the techniques on geopolymers. However, to avoid repetitions, the DRIFT and Raman spectra of raw materials will be shown in Chapter 6 only, as a reference for interpreting the geopolymeric materials obtained. Granulometric analysis furthermore have been performed in view of the precursors preparation.

Nevertheless, all the other ceramic waste has been characterized in order to have an idea of the chemical and mineralogical differences and of their potential reactivity. The analyses carried out are XRF, TGA and reactivity tests.

4.1.1 Selected precursors characterization

4.1.1.1 Chemical characterization (XRF)

The raw materials selected for alkaline activation have been studied from the chemical point of view by means of X-Ray Fluorescence on beads. The results are shown in Table 4.2.

Major elements (as oxides) (wt %)	SiO_2	Al_2O_3	Fe_2O_3	MnO	MgO	CaO	Na_2O	K_2O	TiO_2	P_2O_5	LOI	Tot.
LBCa	60.67	16.30	5.69	0.08	2.31	8.73	1.35	3.27	0.69	0.14	0.47	99.70
CWF	57.33	14.32	5.51	0.08	2.43	11.99	1.16	2.49	0.73	0.17	3.46	99.67

Trace elements (ppm)	Sr	Cr	Ba	Ni	Pb	Rb	V	Y	Zn	Zr
LBCa	243	104	338	46	48	159	60	39	107	185
CWF	457	76	291	38	27	106	52	33	80	208

Table 4.2 – XRF results on the ceramic waste materials selected as precursors.

Both ceramics show a high amount of SiO_2 (around 60%), followed by Al_2O_3 (around 15%). Calcium is the third component of the chemistry of these materials, with values around 10%. Another important element, as normal, is iron. The two materials show a different LOI%, with very low values for LBCa and a higher value for CWF, which suggests the presence of carbonate phases in the latter. In this context, the Ca content of LBCa would be attributable to non-carbonate phases, as Ca-rich silicates. This would require confirmation by XRD analysis.

SiO_2%, Al_2O_3% and CaO% have been plotted in the triangular diagram showing the usual range of composition of the alumino-silicate materials most commonly used as precursors in the field of AAMs (Fig. 4.4). It is evident that the ceramic waste has an intermediate composition, with high percentages of silica in respect to the other materials, a bit less of alumina and an intermediate content of CaO. Relatively to this component, the studied ceramic waste are placed between the materials known as "low-calcium" (as metakaolin and fly ash) and those of "high calcium" (as blast furnace slag) (Pachego-Torgal et al., 2014). Particularly, they are located near the limit area of the fly ash, with a higher silica content.

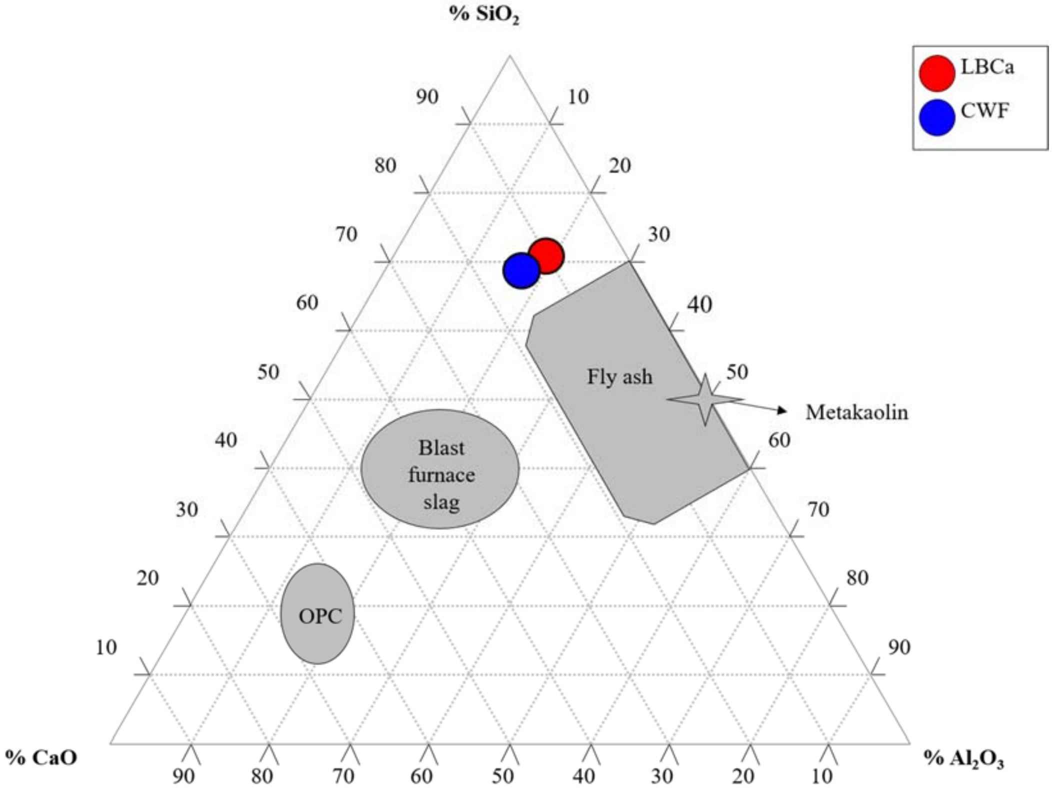

Fig. 4.4 – Triangular diagram CaO-SiO$_2$-Al$_2$O$_3$ for the raw materials composition. The colored circles represent the ceramic waste analyzed, while the grey areas, sketched approximately considering Pachego-Torgal et al. (2014), indicate the compositional range of typical raw materials used for geopolymerization. The compositional range of typical OPC is also marked on the diagram.

4.1.1.2 Mineralogical characterization (XRD)

The mineralogical characterization of the two raw materials selected for the synthesis has been performed by XRD. The phases individuated (Fig. 4.5) are quartz, diopside, gehlenite, haematite, feldspars (microcline and Ca-plagioclase) and wollastonite for the LBCa ceramic; quartz, diopside, gehlenite, haematite, feldspars (microcline and plagioclases), calcite and muscovite/illite for the CWF ceramic. Their quantification has been calculated by using the Rietveld method (Gualtieri and Zanni, 1998) by corundum internal standard addition and it is shown in Table 4.3. The amorphous content calculated is 32.83% for LBCa and 40.89% for CWF.

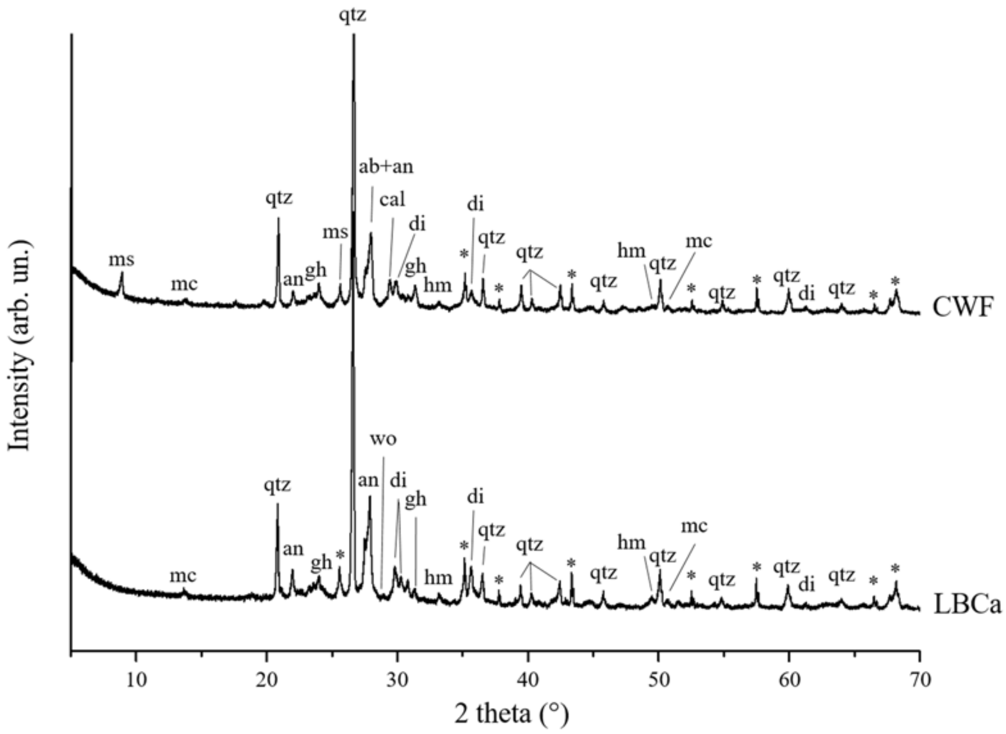

*Fig. 4.5 – Diffraction patterns of the raw materials LBCa and CWF. Qtz=quartz; di=diopside; gh=gehlenite; hm=haematite; mc=microcline; an=anorthite; ab=albite; wo=wollastonite; cal=calcite; ms=muscovite/illite; * indicates corundum, added as internal standard.*

Sample	Quartz	Diopside	Gehlenite	Haematite	K-Feldspars	Plagioclases	Wollastonite	Calcite	Muscovite/ Illite
LBCa	21.28	7.40	2.29	1.49	11.08	21.43	2.21	0.00	0.00
CWF	22.09	4.94	3.71	1.20	5.43	15.97	0.00	2.97	2.79

Table 4.3 – Quantitative mineralogical composition (%) of the raw materials LBCa and CWF, calculated by the Rietveld Method.

4.1.1.3 Thermo-gravimetric characterization (TGA)

From the TG curves reported in Fig. 4.6 and the values of Table 4.4 it is possible to see a high mass loss, with a residue at 850-900 °C of 99.7% for the LBCa and of 97% for the CWF. In particular, it is possible to notice as the two samples are characterized by different pattern of mass loss. Apart for the mass loss occurring in the temperature interval 80-200 °C, attributed to the loss of superficial or hygroscopic water, different steps attributable to the dehydroxilation of clay minerals are visible in LBCa. The CWF TG curve is dominated by the step at 600-900 °C typical of a decarbonation process, attributable to the calcite, already detected by XRD.

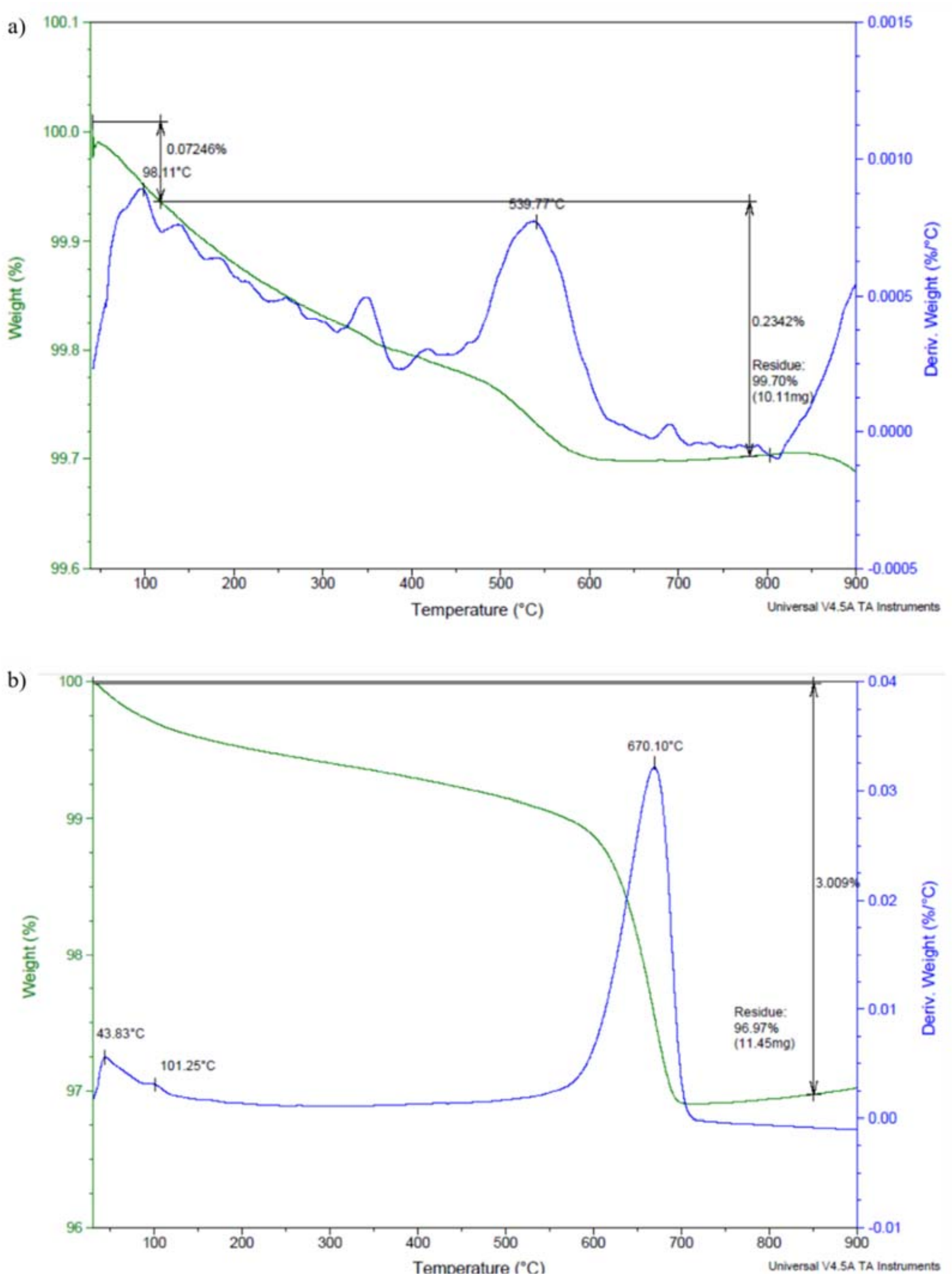

Fig. 4.6 – TG curves of the ceramic waste selected as geopolymeric precursors: LBCa a) and CWF b).

Sample	0-80 °C	80-130 °C	130-200 °C	200-500 °C	500-600 °C	600-900 °C	Residue (%)
LBCa		0.15		0.05	0.09		99.7
CWF	0.36					2.7	97

Table 4.4 – Degradation temperatures and mass loss of the two ceramic precursors selected. Residual mass at 850 °C.

4.1.1.4 Reactivity test (basic attack and ICP-OES)

As it is well known, not all the silica and alumina present in a ceramic material could be considered reactive (Pachego-Torgal et al., 2014). In order to investigate how much of these components are potentially reactive, and so important for the geopolymeric process (Pachego-Torgal et al., 2014), a reactivity test has been performed on all the raw material selected evaluating their solubility in a 8M NaOH solution at room temperature, and the obtained solution analysed by ICP-OES.

By the gravimetric measurement of the solid residue, the soluble phase (that means potentially reactive) has been obtained. LBCa shows a higher value of soluble phases in respect to CWF, respectively with a solid residue of 90% and 94%.

Table 4.5 shows the Si and Al concentrations determined on the eluates by the ICP-OES. As expected the solubility results higher for Si than for Al. Table 4.6 shows instead the contribution sum of Si and Al and their % in the soluble phase, with the highest value calculated for CWF.

Sample	Si (mg/L)	Si - reproducibility %	Al (mg/L)	Al - reproducibility %
LBCa	9.5	4.7	3.1	2.7
CWF	10	3.8	3.6	2

Table 4.5 – Analytical results of the Si and Al concentration, expressed in mg/L. The reproducibility of the measures is also shown.

Sample	Si+Al (mg/L)	Soluble fraction %	(Si+Al)/Soluble fraction %
LBCa	12.63	10	12
CWF	13.61	6	22

Table 4.6 – Comparison between the Si and Al amount solubilized with the leaching test and the soluble fraction (in % as solid completion).

The high percentage of solid residue after NaOH treatment has been observed in literature. Different researches indeed demonstrate as the basic attack, even performed at different conditions of sodium hydroxide concentration, temperature or treatment time, give only a partial dissolution of Si and Al of the alumino-silicate material studied (Mostafa et al., 2001; Panagiotopoulou et al., 2007; Xu and Van Deventer, 2000). Their % solubility in alkaline solution is also linked to the nature of the alumino-silicate materials, for example it seems that tectosilicates are more sensible to this kind of treatment than phyllosilicates, inosilicates or ciclosilicates (Xu and Van Deventer, 2000). Also the ability of the alumino-silicate material to cation exchange, the Al^{3+} coordination and the surface area influence the Si and Al dissolution (Mostafa et al., 2001; Panagiotopoulou et al., 2007).

In order to understand the percentage of silica and alumina potentially reactive, the obtained results have been recalculated. The final data are exposed in Table 4.7.

Sample	SiO_2 % s tot	Al_2O_3 % s tot	SiO_2 % s silica tot	Al_2O_3 % s alumina tot	$[SiO_2]/[Al_2O_3]_{reactive}$
LBCa	0.002	0.001	0.328	0.359	3.397
CWF	0.002	0.001	0.373	0.475	3.145

Table 4.7 – Amount of silica and alumina dissolved after basic attack, calculated on the total silica and alumina amount measured from the bulk chemical composition of ceramic precursors tested. SiO_2% s tot= SiO_2% soluble with respect to the total chemical composition of the sample; Al_2O_3% s tot= Al2O3% soluble with respect to the total chemical composition of the sample; SiO_2 s silica tot=SiO_2% soluble with respect to the total SiO_2% present in the sample; Al_2O_3% s alumina tot=Al_2O_3% soluble with respect to the total Al_2O_3% present in the sample.

The amount of soluble silica and alumina of the ceramic precursors at these conditions (NaOH 8M solution at room temperature) is very low, less than 1% of the total silica and alumina detected by XRF. For this reason, we could imagine to have the necessity to add more reactive materials to the ceramic precursors, as for example metakaolin (MK). However, the low measured value could be highly affected by the reprecipitation of SiO_2 and Al_2O_3 as, for instance, sodium silicates and aluminates.

Nevertheless, the $([SiO_2]/[Al_2O_3])_{reactive}$ ratio of the studied ceramic materials is on average around 3. This is considered a critical parameter which in order to obtain a good mechanical performance in geopolymers should be between 2 and 4 (Pachego-Torgal et al., 2014).

4.1.1.5 Molecular characterization (FTIR-ATR)

In Fig. 4.7 are shown the ATR spectra respectively of LBCa and CWF ceramics, that will be compared with the ATR spectra acquired on the geopolymers, in Chapter 6.

The spectra show the typical wide band of the alumino-silicate phases in the region 1240-815 cm^{-1} and the signals related to quartz at 798 and 779 cm^{-1} (Reig et al., 2013a);

furthermore, in CWF the typical absorption bands of carbonates (1460 and 873 cm^{-1}) are also visible, which are linked to calcite individuated by XRD (Farmer, 1974; Hughes et al., 1995; Rodriguez-Blanco et al., 2011).

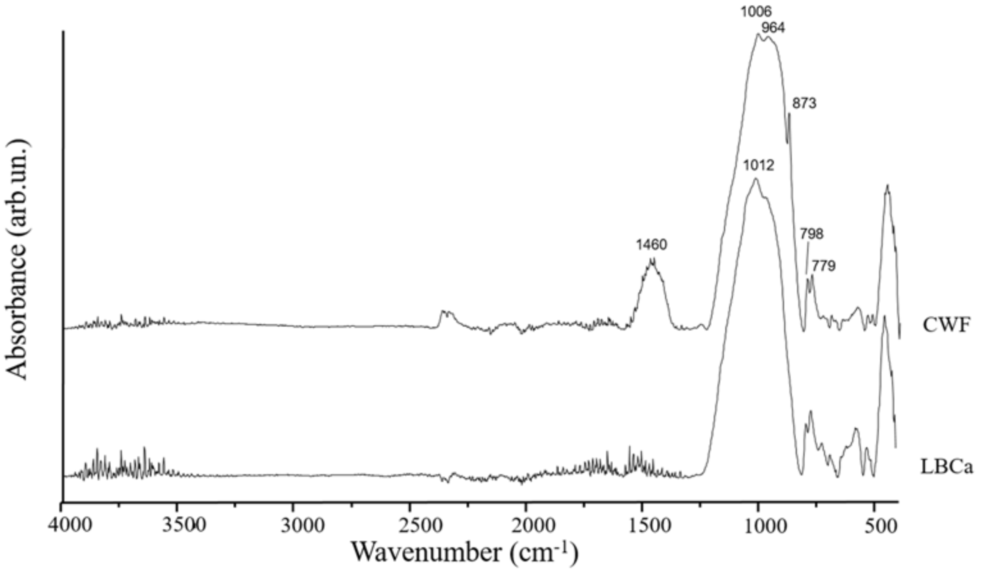

Fig. 4.7 – ATR spectra of the ceramic materials selected LBCa and CWF.

4.1.1.6 Morphological characterization (SEM)

The SEM micrographs obtained on fragments of the ceramic waste show the typical appearance of powdered ceramic, characterized mainly by irregular shape particles (Azevedo et al., 2018; Reig et al., 2013b, 2013a); furthermore, some alumino-silicate minerals are recognizable inside the matrix. The SEM micrographs are shown in Fig. 4.8.

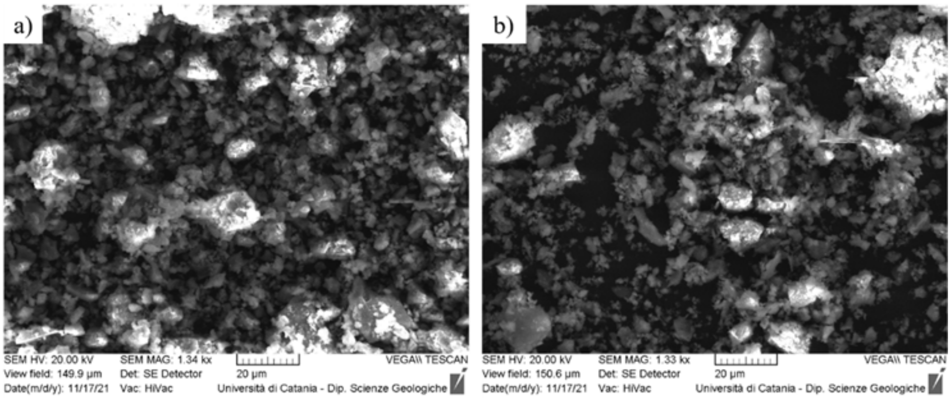

Fig. 4.8 – SEM micrographs of powdered LBCa a) and CWF b).

4.1.1.7 Granulometric analysis (Laser granulometry and BET)

The granulometry of the raw materials plays an important role for the alkaline activation process: the higher the surface available for contact with the activating solutions, the easier the reaction will be (Buchwald et al., 2003; Wong et al., 2018).

Preliminary activation tests revealed that a ceramic powder of around 75 µm does not give good outcomes, resulting in a very slow consolidation and curing rate, together with a complete failure of the integrity tests (see Chapter 5). A lower granulometry, at least of 15 µm is preferred. Starting from centimetre-sized fragment of ceramics (1-2 cm) different grounding procedures have been tested in order to reach the desired granulometry. The preferred procedure individuated consists in 40 minutes grounding in a porcelain jar with alumina spheres, in accordance with literature (Reig et al., 2013a). A granulometry of about 15 µm and 12 µm, measured by laser diffraction, are obtained respectively for LBCa and CWF ceramics (Fig. 4.9).

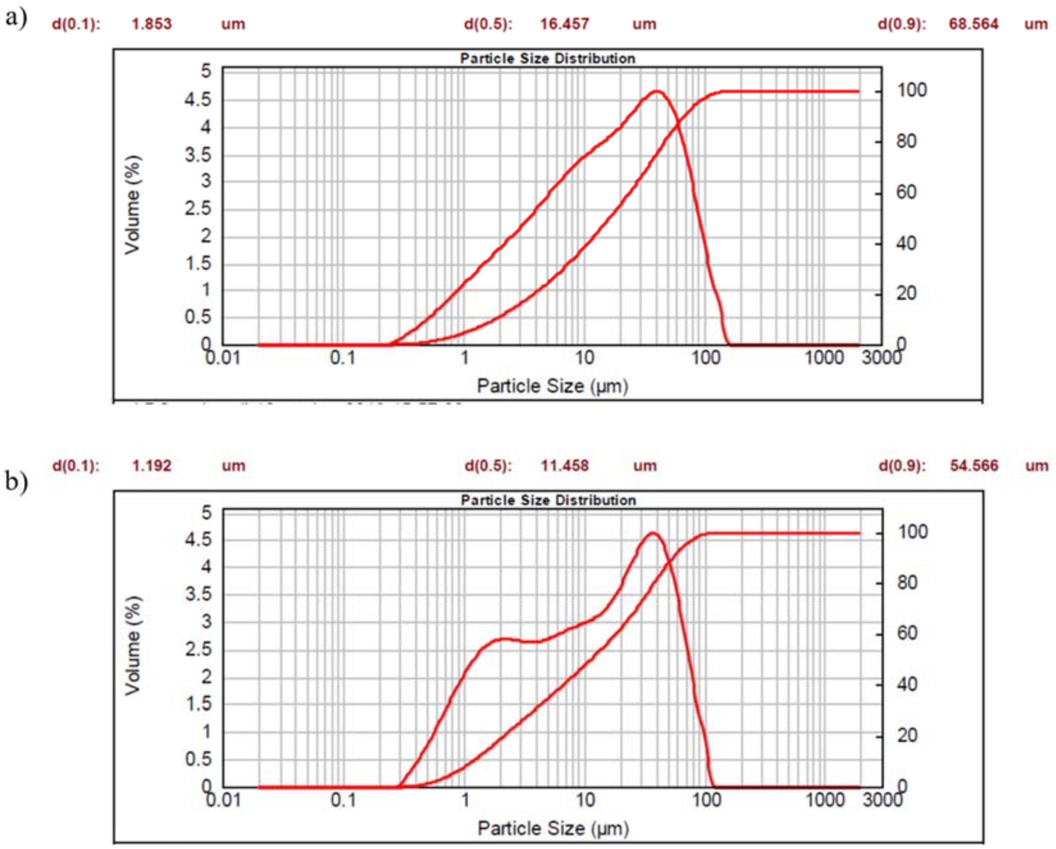

Fig. 4.9 – Particle size distributions of the LBCa a) and CWF b) raw materials, measured by laser granulometry. D(0.5)=50% of volume with the particle size less than this dimension; D(0.9)=90% of volume with the particle size less than this dimension.

As immediately visible, furthermore, LBCa particle size distribution shows a unimodal pattern, with mean particle size around 10 µm, while CWF is characterized by a bimodal particle size distribution, with mean particle sizes around 1 µm and 10 µm. The obtained powder fineness is similar to that of Portland cement, having particles in the size range 1-100 µm (Tuyan et al., 2018) and to that of MK which is going to be used in this research project (Finocchiaro, 2020).

During a material processing its specific surface could change, thus BET analyses have been performed in order to evaluate the correlation between the granulometric analysis and the superficial area (Fagerlund, 1973). It has been found that when the granulometry decreases, the specific area of LBCa ceramic increases, while that of CWF decreases (Table 4.8).

Sample	Granulometry	Surface area (m^2/g)
LBCa	1-2 mm	0.5272
	~15 µm	1.0155
CWF	>125 µm	47.8880
	~12 µm	43.1090

Table 4.8 – BET analysis results on the precursors selected.

4.1.2 Characterization of further potential precursors

The other collected ceramic waste has been characterized in order to verify the variety in terms of chemico-mineralogical composition and eventual reactivity for further geopolymerization studies. XRF, TGA and leaching test are hereafter shown.

4.1.2.1 Chemical characterization (XRF)

As for LBCa and CWF materials the analyses have been conducted by means of X-Ray Fluorescence on beads. The results are shown in the Table 4.9.

The materials show similar characteristics, with the exception of gres LBCf. In general, all the materials show a SiO_2 content over 55%, as more abundant component; it is followed by Al_2O_3 with values around 18%. Calcium and iron are further important components, with values between 5 and 10%. Sample LBCf, instead, shows the highest percentage of SiO_2, with a value over 72%, and the lowest percentages of CaO, almost absent, as well as of Fe_2O_3.

Major Oxides (%)	SiO_2	Al_2O_3	Fe_2O_3	MnO	MgO	CaO	Na_2O	K_2O	TiO_2	P_2O_5	LOI	Tot.
LBCb	57.91	17.33	7.53	0.11	2.58	7.41	2.35	2.30	1.13	0.35	0.47	99.47
LBCc	61.17	17.03	5.63	0.04	2.08	7.81	0.49	4.02	0.76	0.17	0.51	99.71
LBCf	72.37	18.37	0.99	0.01	0.54	0.80	3.22	2.37	0.68	0.12	0.35	99.82
CWM	56.83	15.20	5.63	0.07	2.52	10.15	1.39	2.80	0.70	0.18	4.32	99.79

Trace elements (ppm)	Sr	Cr	Ba	Ni	Pb	Rb	V	Y	Zn	Zr
LBCb	591	76	452	27	57	87	96	37	104	247
LBCc	261	62	375	32	163	190	33	40	138	286
LBCf	191	253	319	32	119	151	12	46	312	677
CWM	398	144	319	55	31	120	57	37	94	200

Table 4.9 – XRF results on the additional ceramic waste materials studied.

SiO_2, Al_2O_3 and CaO percentages have been plotted in the triangular diagram showing the usual range of composition of the alumino-silicate materials most commonly used as precursors in the field of AAMs (Fig. 4.10). Apart for sample LBCf, the materials fall in the same area of the two already studied ceramic materials, LBCa and CWF, that means in an area close to the fly ash, but richer in silica. LBCf instead falls much closer to the SiO_2-Al_2O_3 axis, because of the absence of the CaO component.

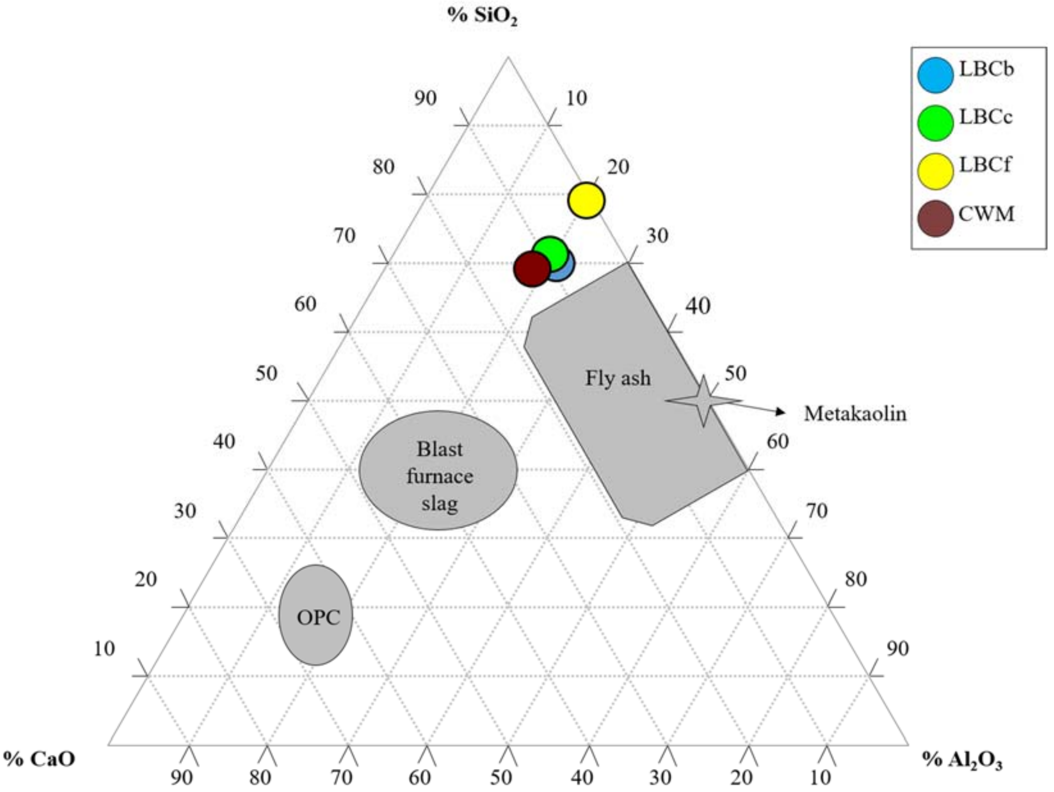

Fig. 4.10 – Triangular diagram CaO-SiO$_2$-Al$_2$O$_3$ for the raw materials composition. The colored circles represent the ceramic waste analyzed, while the grey areas, sketched approximately considering Pachego-Torgal et al. (2014), indicate the compositional range of the typical raw materials used for the geopolymerization. The compositional range of typical OPC is also marked on the diagram.

4.1.2.2 Thermo-gravimetric characterization (TGA)

The additional ceramic waste materials retrieved have been subjected to thermo-gravimetric analysis.

All the ceramic materials studied show low mass loss, with a residue of about 99.6% at 850-900 °C, with the exception of CWM that shows the lowest value attesting on 95.8%. The observed patterns are similar to those of the already studied LBCa and CWF, where the samples from LBC (namely LBCb, LBCc and LBCf) show TG curves similar to those of LBCa; and the other sample from Laquattro (namely CWM) shows a similar trend of CWF. Indeed, apart from the mass loss occurring in the temperature interval 80-200 °C, attributed to the loss of superficial or hygroscopic water, the LBC samples show steps related to the dehydroxilation of clay minerals, while CWM shows a step linked to the de-carbonation process. The mass loss at the different temperatures and the residual mass at 850 °C for all the studied samples are visible in Fig. 4.11 and summarized in Table 4.10.

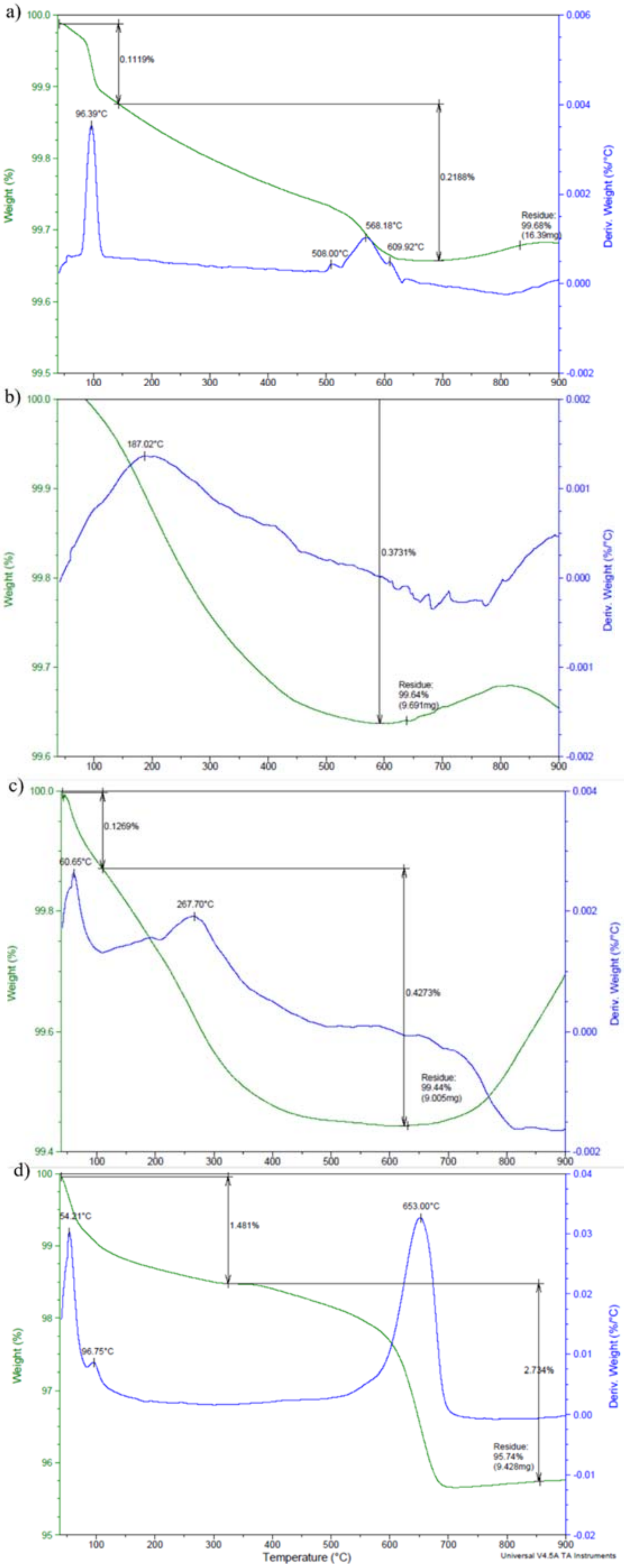

Fig. 4.11 – TG curves of further ceramic waste: LBCb a), LBCc b), LBCf c) and CWM d).

Sample	0-80°C	80-130°C	130-200°C	200-500°C	500-600°C	600-900°C	Residue (%)
LBCb		0.14			0.19		99.7
LBCc			0.4				99.6
LBCf	0.12			0.4			99.5
CWM	0.78	0.24				3.2	95.8

Table 4.10 – Degradation temperatures and mass loss of further ceramic waste. Residual mass at 850 °C.

4.1.2.3 Reactivity test (basic attack and ICP-OES)

In order to investigate how much of these components are potentially reactive, the reactivity test has been performed in the same conditions as for LBCa and CWF samples. It was not possible to test LBCc.

By gravimetric measurement of the solid residue, the soluble phase (the potentially reactive) has been obtained. In particular, as shown in Table 4.11 the sample with the highest value of soluble phase is CWM, with 30 wt% of soluble phase, while LBCb shows the lowest value. Table 4.12 shows the Si and Al concentrations determined on the eluates by ICP-OES. As expected, the solubility is higher, in all the samples, for Si than for Al. The Table 4.13 shows instead the contribution sum of Si and Al and their % in the soluble phase, with the highest value calculated for CWM.

Sample	LBCb	LBCf	CWM
Solid residue (%)	84	83	70

Table 4.11 – Percentage of solid residue after leaching test.

Sample	Si (mg/L)	Si - reproducibility %	Al (mg/L)	Al - reproducibility %
LBCb	8.1	3.6	3	2.9
LBCf	15.7	2.9	3.8	0.9
CWM	22.1	5.5	14.6	0.8

Table 4.12 – Analytical results of the Si and Al concentration, expressed in mg/L. The reproducibility of the measurements is also shown.

Sample	Si+Al (mg/L)	Soluble fraction %	(Si+Al)/Soluble fraction %
LBCb	11.07	16	7
LBCf	19.48	17	11
CWM	36.7	30	12

Table 4.13 – Comparison between the amount of Si and Al solubilized with the leaching test and the soluble fraction (in % as solid completion).

In order to understand the potentially reactive percentages of silica and alumina, the obtained results have been recalculated. The final data are exposed in Table 4.14.

The amount of soluble silica and alumina of the ceramic materials at these conditions (NaOH 8M solution at room temperature) is very low, less than 1% of the total silica and alumina detected by XRF. However, also in this case, the low measured value could be highly affected by the reprecipitation of SiO_2 and Al_2O_3 as, for instance, sodium silicates and aluminates.

The $([SiO_2]/[Al_2O_3])_{reactive}$ ratio of the studied ceramic materials is within the range indicated in literature for obtaining a good geopolymer in terms of mechanical strength, that is between 2 and 4 (Pachego-Torgal et al., 2014). Only sample CWM is quite below the threshold.

Sample	SiO_2 % s tot	Al_2O_3 % s tot	SiO_2 % s silica tot	Al_2O_3 % s alumina tot	$[SiO_2]/[Al_2O_3]_{reactive}$
LBCb	0.002	0.001	0.299	0.327	3.057
LBCf	0.003	0.001	0.464	0.391	4.678
CWM	0.005	0.003	0.832	1.815	1.714

Table 4.14 – Amounts of silica and alumina dissolved after basic attack, calculated on the total silica and alumina measured from the bulk chemical composition of ceramic materials tested. SiO_2% s tot= SiO_2% soluble with respect to the total of the sample; Al_2O_3% s tot= Al2O3% soluble with respect to the total of the sample; SiO_2 s silica tot=SiO_2% soluble with respect to the total SiO_2% present in the sample; Al_2O_3% s alumina tot=Al_2O_3% soluble with respect to the total Al_2O_3% present in the sample.

4.2 Alkali activating solutions

According to literature (Allahverdi and Najafi Kani, 2009; Geraldes et al., 2016; Komnitsas et al., 2015; Moutinho et al., 2019; Reig et al., 2013b, 2013a; Ricciotti et al., 2017; Robayo et al., 2016; Rovnaník et al., 2018; Tuyan et al., 2018), and after some preliminary tests, sodium hydroxide (NaOH) mixed in different proportions with sodium silicate (Na_2SiO_3) has been selected as alkaline activating solution. The only activation by sodium hydroxide or waterglass did not give satisfactory results.

8M NaOH has been chosen, in order to have an enough alkaline medium, preventing eventual excessive efflorescences, but not excessively aggressive towards the environment. The desired molarity has been obtained by diluting a commercial 10M NaOH solution, supplied by Carlo Erba company.

The sodium silicate used has been provided by Ingessil srl; it is characterized by a module $SiO_2/Na_2O=3.3$ and pH=11.5.

4.3 Additives

4.3.1 Metakaolin

Metakaolin (MK) is one of the main raw materials commonly used for the production of geopolymers, because of its high reactivity (Barone et al., 2020; Djobo et al., 2014; Yip et al., 2005). It is produced by the calcination of kaolin. It is here used in few amounts (maximum 20% of the solid precursor) in order to increase the reactivity and the performance of the ceramic-based geopolymers to experiment. The MK used is ARGICAL^{TM} M-1000, supplied by IMERYS (France). In order to have comparative analysis with the other precursors used, chemical, mineralogical and molecular characterizations have been performed. As well as for the ceramic precursors, DRIFT and Raman spectroscopy have been carried out and their results are directly reported on the Chapter 6 only, as a reference for interpreting the geopolymeric materials obtained.

4.3.1.1 Chemical characterization (XRF)

The elemental composition of MK has been determined by means of pXRF analysis. Na_2O, MgO could not be accurately measured, because of the instrumentation limit, which registers a high analytical error for light elements. The chemical composition by weight%

results as follow: Al_2O_3 = 34.03, SiO_2 = 58.56, P_2O_5 = 0.20, K_2O = 0.69, CaO = 2.08, TiO_2 = 1.88 and Fe_2O_3 = 2.57 (Barone et al., 2020).

4.3.1.2 Mineralogical characterization (XRD)

The diffraction pattern shown in Fig. 4.12 reveals as mineralogical components illite, anatase and quartz, respectively in 4.93%, 0.89% and 16.62%, with an amorphous fraction of 77.55% (Occhipinti et al., 2020). The phases quantifications have been obtained by the Rietveld Method (Gualtieri and Zanni, 1998) and corundum internal standard.

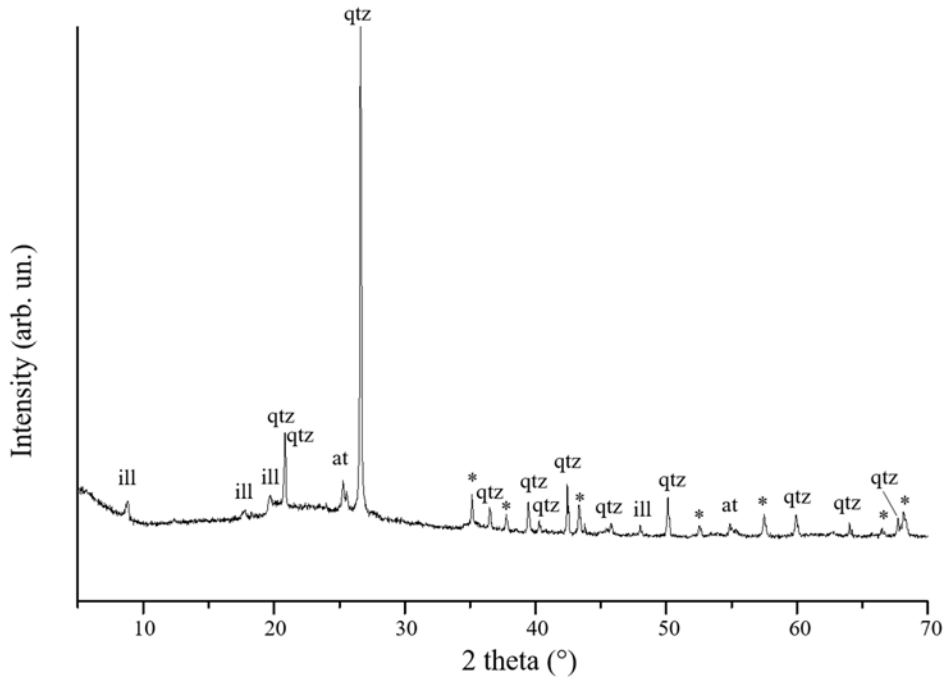

*Fig. 4.12 – Diffraction pattern of metakaolin. Qtz=quartz; ill=illite; at=anatase; * indicates the corundum, added as internal standard.*

4.3.1.3 Molecular characterization (FTIR-ATR)

Fig. 4.13 shows the FTIR-ATR spectrum. This spectrum will be used for comparison with the geopolymers where percentages of MK are added. It shows the alumino-silicate band centered at 1038 cm^{-1}.

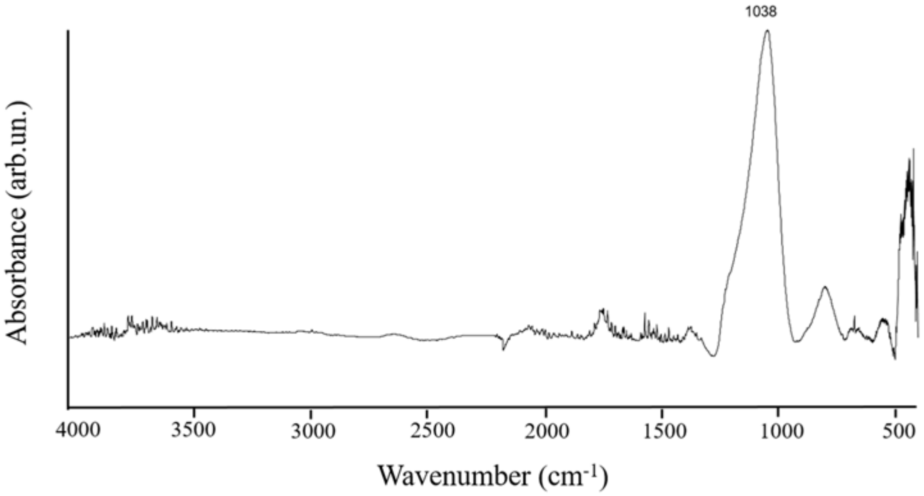

Fig. 4.13 – ATR spectrum of metakaolin.

4.3.2 Prompt Vicat

Prompt is a natural cement prepared and supplied by Vicat Group, in France. It is commonly known as roman cement and it is characterized by a rapid setting (2-3 min) and hardening. It is obtained by the firing at 500-1200 °C of a calcareous clay. The chemical composition is similar to that of a Portland cement and to that of the natural hydraulic lime; according to the data sheet it is composed as follow (wt%): SiO_2 = 18.09, Al_2O_3 = 7.24, Fe_2O_3 = 3.2, CaO = 53.07, MgO = 3.84, SO_3 = 3.24, K_2O = 1.16, Na_2O = 0.28. LOI = 9.28.

It has been used as additive in order to promote the reactivity of the ceramic precursors in the form of binary mixtures, whose workability has been compared to ceramic-only geopolymers. Because of its high environmental impact and the short setting time when alkaline activated - not a suitable property for a restoration product - Prompt has been used only in the preliminary tests. For this reason, no further investigations have been conducted on it.

4.4 Aggregates

Fig. 4.14 – Selected aggregates: siliceous sand a), carbonate sand b) and ceramic waste aggregates c).

In order to create mortars, different kinds of aggregates have been selected (Fig. 4.14). Siliceous commercial sand has been used in order to replicate the typical aggregates used in the construction field. Furthermore, a carbonate sand, coming from the streams of the Tyrrhenian area of the province of Messina, was provided from a local construction industry. The composition of the carbonate sand has been assessed by XRF on beads and it is here reported: major oxides (%) SiO_2 = 8.29, Al_2O_3 = 1.74, Fe_2O_3 = 0.82, MnO = 0.09, MgO = 0.61, CaO = 48.88, Na_2O = 0.21, K_2O = 0.39, TiO_2 = 0.10, P_2O_5 = 0.04, LOI = 38.12. Trace elements (ppm) as follow: Zr = 108, Sr = 3444, Ni = 9, Pb = 13, Rb = 14, Y = 12, Zr = 9.

However, the use of natural aggregates constitutes a relevant issue in environmental safeguard. As they are highly requested in the construction field, their mining process can cause the scarring of land use, loss of agricultural land, noise, erosion problems and so on; and huge amounts of water expenditure for their preparation. Thus, for the production of innovative and sustainable materials, the use of recycled aggregates would be beneficial (Wong et al., 2018). It is for this reason, and not only for compatibility, that for this PhD thesis it was decided to test also the same ceramic waste (specifically LBCa) used as geopolymeric precursors as aggregates. Thus, large amounts of locally available waste materials can be recycled.

The granulometric curves of the selected aggregates are here reported, obtained with different sieves for the siliceous sand, and for the carbonate sand and ceramic (Table 4.15). The standard granulometry of CEN Standard Sand (certified according to UNI EN 196-

1:2016 which is compliant with the normative ISO 679:2009) has been followed. Fig. 4.15 shows a comparison of the granulometric curves.

Siliceous sand		Carbonate sand and ceramic aggregates	
mm	%	mm	%
2-1.6	7	2-0.85	33
1.6-1	26	0.85-0.5	34
1-0.5	34	0.5-0.125	20
0.5-0.16	20	0.125-0.063	12
0.16-0.08	12		

Table 4.15 – Granulometry of the selected aggregates.

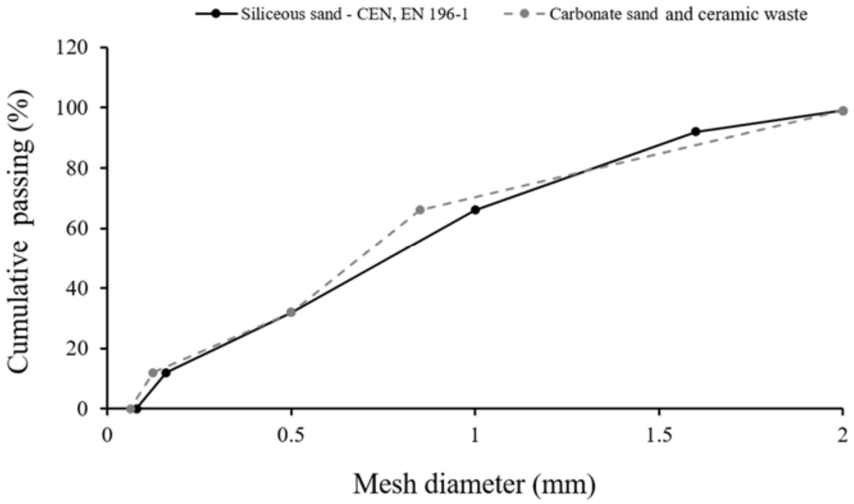

Fig. 4.15 – Granulometric curves of the selected aggregates.

For the purpose of applicability tests, finely powdered white marble was also considered. This is one of the most widely diffused aggregates in the field of restoration and it was supplied directly by the restorers (Fig. 4.16). No technical information is available.

Fig. 4.16 – Powdered white marble used as aggregate in the mortars realized for the case-studies.

References

Allahverdi, A., Najafi Kani, E., 2009. Construction wastes as raw materials for geopolymer binders. Int. J. Civ. Eng. 7, 154–160.

Azevedo, A.G. de S., Strecker, K., Lombardi, C.T., 2018. Produção de geopolímeros à base de metacaulim e cerâmica vermelha. Cerâmica 64, 388–396. https://doi.org/10.1590/0366-69132018643712420

Barone, G., Caggiani, M.C., Coccato, A., Finocchiaro, C., Fugazzotto, M., Lanzafame, G., Occhipinti, R., Stroscio, A., Mazzoleni, P., 2020. Geopolymer production for conservation-restoration using Sicilian raw materials: Feasibility studies. IOP Conf. Ser. Mater. Sci. Eng. 777. https://doi.org/10.1088/1757-899X/777/1/012001

Buchwald, A., Kaps, C., Hohmann, M., 2003. Alkali-Activated Binders and Pozzolan Cement Binders – Compete Binder Reaction or Two Sides of the Same Story ? 11th Int. Congr. Chem. Cem. 1238–1247.

Djobo, J.N.Y., Tchadjié, L.N., Tchakoute, H.K., Kenne, B.B.D., A., E., D., N., 2014. Synthesis of geopolymer composites from a mixture of volcanic scoria and metakaolin. J. Asian Ceram. Soc. 2, 387–398. https://doi.org/10.1016/j.jascer.2014.08.003

Fagerlund, G., 1973. Determination of specific surface by the BET method. Matériaux Constr. 6, 239–245. https://doi.org/10.1007/BF02479039

Farmer, V.C., 1974. The infrared spectra of minerals. Mineralogical Society, London.

Finocchiaro, C., 2020. Evaluation of new uses of volcanic ashes and paleo-soils coming from Mt.Etna volcano in the geopolymer production. University of Catania.

Geraldes, C.F.M., Lima, A.M., Delgado-Rodrigues, J., Mimoso, J.M., Pereira, S.R.M., 2016. Geopolymers as potential repair material in tiles conservation. Appl. Phys. A Mater. Sci. Process. 122, 1–10. https://doi.org/10.1007/s00339-016-9709-3

Gualtieri, A., Zanni, M., 1998. Quantitative determination of crystalline and amorphous phase in traditional ceramics by combined Rietveld-RIR method. Trans Tech Publ Ltd 278, 834–839.

Hughes, T.L., Methven, C.M., Jones, T.G.J., Pelham, S.E., Fletcher, P., Hall, C., 1995.

Determining cement composition by Fourier transform infrared spectroscopy. Adv. Cem. Based Mater. 2, 91–104. https://doi.org/10.1016/1065-7355(94)00031-X

Komnitsas, K., Zaharaki, D., Vlachou, A., Bartzas, G., Galetakis, M., 2015. Effect of synthesis parameters on the quality of construction and demolition wastes (CDW) geopolymers. Adv. Powder Technol. 26, 368–376. https://doi.org/10.1016/j.apt.2014.11.012

Mostafa, N.Y., El-Hemaly, S.A.S., Al-Wakeel, E.I., El-Korashy, S.A., Brown, P.W., 2001. Characterization and evaluation of the pozzolanic activity of Egyptian industrial by-products: I: Silica fume and dealuminated kaolin. Cem. Concr. Res. 31, 467–474. https://doi.org/10.1016/S0008-8846(00)00485-3

Moutinho, S., Costa, C., Cerqueira, Â., Rocha, F., Velosa, A., 2019. Geopolymers and polymers in the conservation of tile facades. Constr. Build. Mater. 197, 175–184. https://doi.org/10.1016/j.conbuildmat.2018.11.058

Occhipinti, R., Stroscio, A., Finocchiaro, C., Fugazzotto, M., Leonelli, C., Lo Faro, M.J., Megna, B., Barone, G., Mazzoleni, P., 2020. Alkali activated materials using pumice from the Aeolian Islands (Sicily, Italy) and their potentiality for cultural heritage applications: Preliminary study. Constr. Build. Mater. 259, 120391. https://doi.org/10.1016/j.conbuildmat.2020.120391

Pachego-Torgal, F., Labrincha, J.A., Leonelli, C., Palomo, A., Chindaprasirt, P., 2014. Handbook of Alkali-activated cements, mortars and concretes. Elsevier.

Panagiotopoulou, C., Kontori, E., Perraki, T., Kakali, G., 2007. Dissolution of aluminosilicate minerals and by-products in alkaline media. J. Mater. Sci. 42, 2967–2973. https://doi.org/10.1007/s10853-006-0531-8

Reig, L., Tashima, M.M., Borrachero, M. V., Monzó, J., Cheeseman, C.R., Payá, J., 2013a. Properties and microstructure of alkali-activated red clay brick waste. Constr. Build. Mater. 43, 98–106. https://doi.org/10.1016/j.conbuildmat.2013.01.031

Reig, L., Tashima, M.M., Soriano, L., Borrachero, M. V., Monzó, J., Payá, J., 2013b. Alkaline activation of ceramic waste materials. Waste and Biomass Valorization 4, 729–736. https://doi.org/10.1007/s12649-013-9197-z

Ricciotti, L., Molino, A.J., Roviello, V., Chianese, E., Cennamo, P., Roviello, G., 2017.

Geopolymer composites for potential applications in cultural heritage. Environ. - MDPI 4, 1–15. https://doi.org/10.3390/environments4040091

Robayo, R.A., Mulford, A., Munera, J., Mejía de Gutiérrez, R., 2016. Alternative cements based on alkali-activated red clay brick waste. Constr. Build. Mater. 128, 163–169. https://doi.org/10.1016/j.conbuildmat.2016.10.023

Rodriguez-Blanco, J.D., Shaw, S., Benning, L.G., 2011. The kinetics and mechanisms of amorphous calcium carbonate (ACC) crystallization to calcite, via vaterite. Nanoscale 3, 265–271. https://doi.org/10.1039/c0nr00589d

Rovnaník, P., Rovnaníková, P., Vyšvařil, M., Grzeszczyk, S., Janowska-Renkas, E., 2018. Rheological properties and microstructure of binary waste red brick powder/metakaolin geopolymer. Constr. Build. Mater. 188, 924–933. https://doi.org/10.1016/j.conbuildmat.2018.08.150

Tuyan, M., Andiç-Çakir, Ö., Ramyar, K., 2018. Effect of alkali activator concentration and curing condition on strength and microstructure of waste clay brick powder-based geopolymer. Compos. Part B Eng. 135, 242–252. https://doi.org/10.1016/j.compositesb.2017.10.013

UNI, 2016. Metodi di prova dei cementi - Parte 1: Determinazione delle resistenze meccaniche. EN 196-1.

Wong, C.L., Mo, K.H., Yap, S.P., Alengaram, U.J., Ling, T.C., 2018. Potential use of brick waste as alternate concrete-making materials: A review. J. Clean. Prod. 195, 226–239. https://doi.org/10.1016/j.jclepro.2018.05.193

Xu, H., Van Deventer, J.S.J., 2000. The geopolymerisation of alumino-silicate minerals. Int. J. Miner. Process. 59, 247–266. https://doi.org/10.1016/S0301-7516(99)00074-5

Yip, C.K., Lukey, G.C., Van Deventer J.S.J., 2005. The coexistence of geopolymeric gel and calcium silicate hydrate at the early stage of alkaline activation. Cem. Concr. Res. 32, 1688–1697. https://doi.org/10.1016/j.cemconres.2004.10.042

Chapter 5

Experimental: synthesis process and first evaluations

The synthesis process has been carried out prior preparation of the solid and liquid raw materials. First of all, the LBCa and CWF raw materials have been ground by porcelain jars in order to reach the desired granulometry. The first tests have been performed with a LBCa ground at around 75 µm. The poor results obtained in terms of activation of the geopolymerization process (the pastes did not harden – Fig. 5.1a and b), highlighted the necessity to reduce the granulometry (Fig. 5.1c and d). Smaller granulometry indeed produces an increase in the surface available for contact with the activating solution, thus promoting the reaction (Buchwald et al., 2003; Wong et al., 2018). A granulometry similar to that of commercial MK has been chosen (~10 µm).

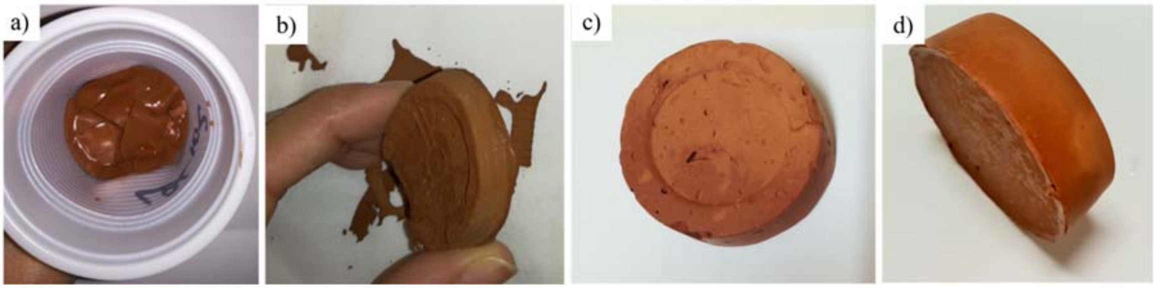

Fig. 5.1 – Samples after alkaline activation of ceramic waste LBCa of 75 µm a) and b) and of 10 µm c) and d).

In addition to pure ceramic slurries, binary mixtures were also experimented by the addition of different proportions of MK. MK is dried in the oven and sieved before adding it to the ceramic, in order to avoid the formation of MK granules. The powdered components were carefully homogenized in a porcelain jar before the addition of the activating solution.

Concerning the activating solutions, sodium hydroxide 8M has been obtained by diluting the commercial 10M stock and letting it rest for a while. The dilution was requested in order to reduce the potential environmental hazard of the material, increasing the user-friendly property of this kind of solution.

Preliminary tests by using only sodium hydroxide yielded poor results in setting and curing of the pastes. Alkali activated mixtures with only waterglass were also tested. Sodium hydroxide was mixed with waterglass according to defined weight proportions, and again let to rest for some minutes before the synthesis, in order to avoid the effect of the exothermal reaction between the two liquids on the geopolymerization (Ahmari et al., 2012; Lancellotti et al., 2013).

Few tests were also performed with Prompt as additive, in order to appreciate the differences in workability and setting time.

The liquid was then poured on the powders, and immediately subjected to mechanical mixing for 5 minutes. The so-obtained slurries were then poured into molds and manually agitated for 1 minute in order to facilitate the escape of air bubbles from the mixture (Duxson et al., 2005; Komnitsas et al., 2015; Panizza et al., 2018; Robayo et al., 2016). After 24 hours at room temperature, the samples were demolded and wrapped with polyethylene film for the remaining curing time (fixed at 28 days). Maturation has been carried out at room temperature, around 25 °C, avoiding firing procedures in order to reduce environmental impact. However, some formulations replicates were also subjected to a low-temperature firing (65 °C) for the first 24 hours after synthesis (Reig et al., 2013a), in order to assess the effect of different curing strategies.

The best L/S ratio for each formulation has been defined according to the workability of the slurry during the synthesis, while considering also the setting and curing times. It was improved empirically via further synthesis tests after the evaluation of each slurry. The entire synthesis process is represented in Fig. 5.2.

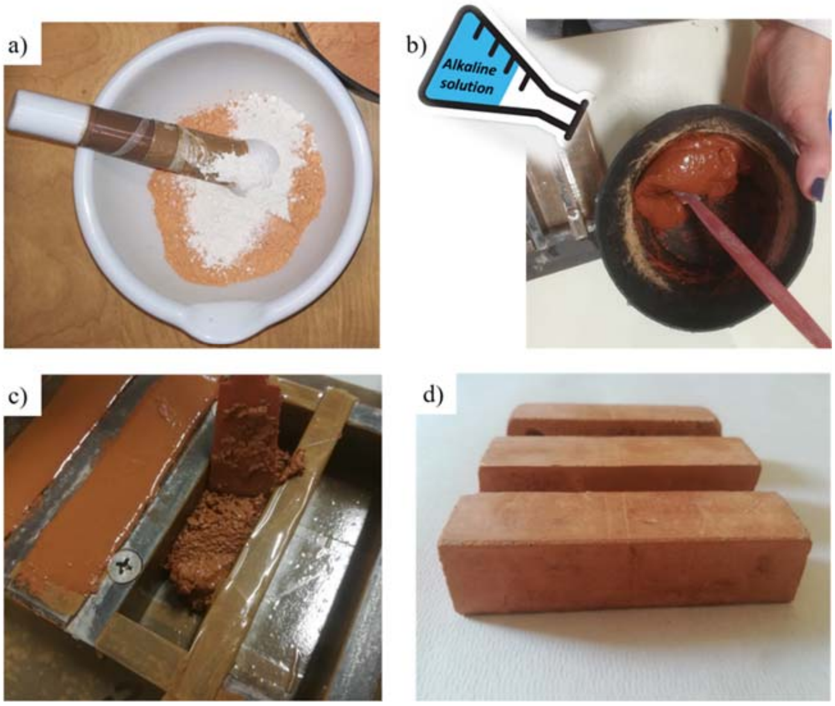

Fig. 5.2 – Synthesis process: mixing of powdered precursors a), solid and liquid components mixing b), pouring of the slurries into molds c); geopolymers after curing d).

The first tests have been performed with LBCa as raw material. Further tests have been planned for CWF and improvements on other LBCa formulations.

Around fifty formulations have been synthesized and, after 28 days of curing, submitted to preliminary considerations and to the integrity test. Preliminary evaluations of the pastes are conducted by simple observation of a few criteria, and concern the curing time required to demold the geopolymers, their complete hardening (when the surfaces are completely dry), the tendency to shrink, the appearance in terms of homogeneity and the efflorescences crystallization (Fig. 5.3) (Lancellotti et al., 2013; Pecchioni et al., 2008).

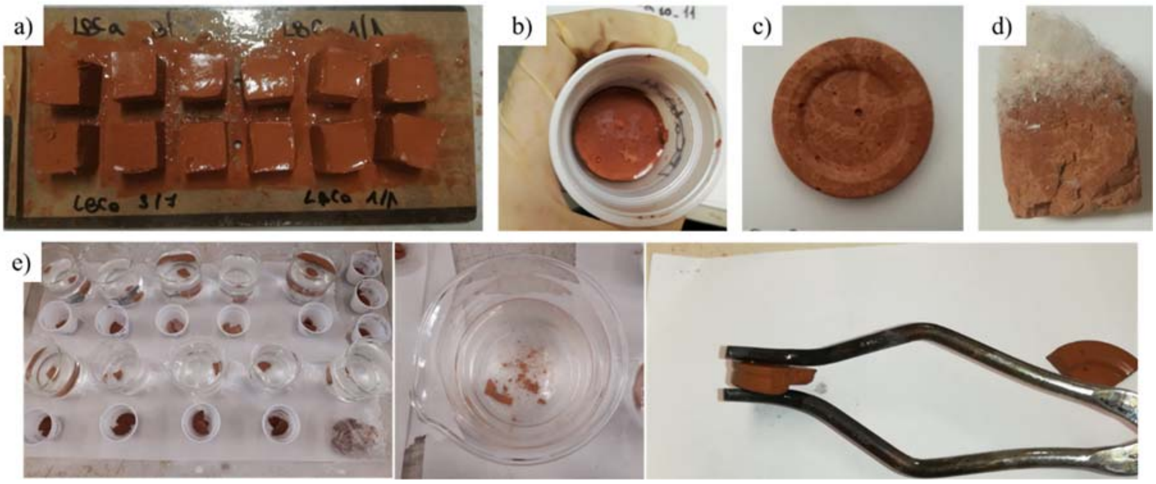

Fig. 5.3 – Preliminary criteria to evaluate the synthetized products: hardening a), shrinkage b), homogeneity c), efflorescence d), integrity e).

The integrity test, instead, is a preliminary test generally adopted by the scientific community working with geopolymers in order to see the stability of the material in water, when soaked for 24 hours (Lancellotti et al., 2013). The integrity test could be, thus, considered a first step of evaluation of the occurred geopolymerization process (Lancellotti et al., 2013). The visible parameters considered to check the sample's integrity were the appearance of water (clear, with residues, turbid) and the tendency of the geopolymeric fragment to be broken by a metallic pincer with hand pressure. A formulation passes the test if the water remains clear and the geopolymer does not break with the pincer (Fig. 5.4).

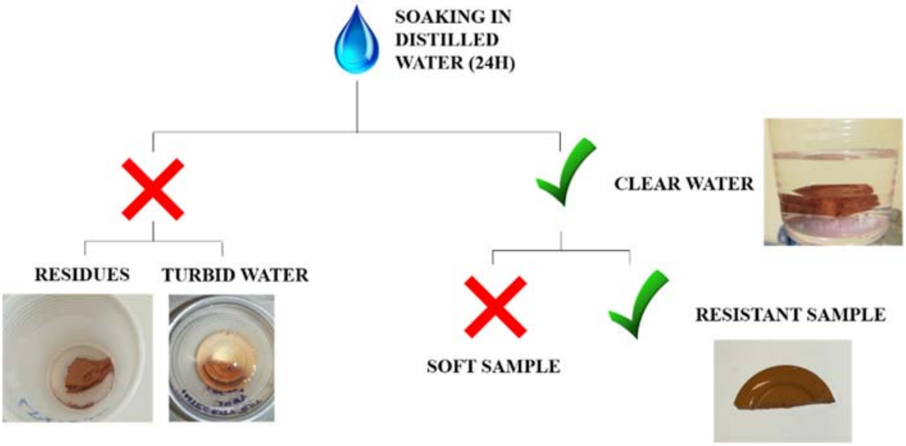

Fig. 5.4 – Integrity test scheme.

In Table 5.1 all the formulations are reported, together with their synthesis parameters, the preliminary evaluations and the results of the integrity test. The formulations that failed during the synthesis (i.e. insufficient workability, not setting…) have not been reported.

The first observation, already disclosed, is the failure of the formulations made with 75 µm powders, which do not set and harden just because of drying after very long times. Indeed, they totally failed the integrity tests, with the exception of the sample with 50% of Prompt. The setting time is then accelerated by the decrease of the granulometry of the ceramic precursor, fixating on 5 min. The curing time instead ranges between 1 to 7 days, likely depending on the liquid content and on the grade of reactivity involved in the process (Azevedo et al., 2018; Clausi et al., 2016; Rovnaník et al., 2018). The majority of the samples show a fairly homogeneous visual appearance, with some exceptions probably due to insufficient mixing of the different components in binary mixtures, or due to a separation of the waterglass which tends to stratify in the poured samples, when in excess. In some cases, the lack of workability observed during the synthesis makes the surface of the dried samples rough, because of an increased difficulty in pouring the slurry into the mold. The tendency to shrink characterizes all the samples, with the exception of those with the highest amount of MK. Nevertheless, the entity of the shrinkage could be considered low and it should be normal, as intrinsic characteristic of this kind of materials, due to the evaporation of part of the water content (Komnitsas and Zaharaki, 2007). In order to reduce it in the final products, inert materials are going to be added (Pecchioni et al., 2008). No cracks or micro-cracks were observable. Regarding the efflorescences, it is evident that these appear when the sodium hydroxide proportion in the liquid component is too high (e.g. sodium hydroxide/waterglass = 2.33), or when moderate amounts of sodium hydroxide (e.g. sodium hydroxide/waterglass ~ 0.5) is combined with high amounts of water added during the synthesis. Furthermore, they appear in samples which have been subjected to the above-mentioned, low-temperature firing step, probably because of a faster evaporation of water with respect to the replicates cured completely at room temperature (Amin et al., 2017; Komnitsas et al., 2015; Robayo et al., 2016). For what concerns the stability in water and the resistance to the pincer cut after soaking, it is possible to see how the first synthesis tests totally failed both criteria of the integrity test, with the exception of the fired samples and of the binary mixtures (Table 5.1). The apparent quick setting and regular curing of all the samples which tend to disintegrate in water could probably be ascribed to the hardening action of the waterglass (Ahmari et al., 2012; Komnitsas et al., 2015; Pacheco-Torgal et al., 2013), generally present in high amounts. Thus, we could hypothesize a hardening of the product by water evaporation but the not occurrence of a geopolymerization process.

In the second part of the table the results of the integrity tests get better and the samples completely pass the integrity tests, leaving the water clear and resisting to the pincer cut.

Among these, the formulations obtained by adding some percentage of Prompt are characterized by a very quick setting time, resulting in inadequate workability when restoration practices are involved.

Sample	Raw material		Additives		NaOH/ Waterglass	H_2O **	L/S	Tc	St	Ct	Homogeneity	Shrinkage	Cracks	Salts	Integrity tests***		New labels
	Type	Granulometry	MK*	P*											Stability in water	Resistance to pincer	
LBCa$_{75}$ 1	LBCa	75 µm	0%	0%	only waterglass	30%	0.58	22 ± 5 °C	/	28 dd	not	X	/	/	3	breaks	
LBCa$_{75}$ 2	LBCa	75 µm	0%	0%	0.71	11%	0.54	22 ± 5 °C	/	28 dd	not	X	/	/	3	breaks	
LBCa$_{75}$ 3	LBCa	75 µm	0%	50 %	only NaOH	0%	1.00	22 ± 5 °C	/	28 dd	yes	X	/	/	1	breaks	
LBCa$_{75}$ 4	LBCa	75 µm	0%	0%	only waterglass	53%	0.53	22 ± 5 °C	/	28 dd	not	X	/	/	3	breaks	
LBCa 1	LBCa	10 µm	0%	0%	only waterglass	17%	0.48	22 ± 5 °C	5 min	28 dd	yes	X	/	/	3	breaks	
LBC 2	LBCa	10 µm	0%	0%	0.71	0%	0.48	22 ± 5 °C	5 min	28 dd	yes	X	/	/	3	breaks	
LBCa 3	LBCa	10 µm	0%	50 %	only NaOH	0%	0.05	22 ± 5 °C	5 min	1 dd	yes	X	/	/	1	breaks	
LBCa 4	LBCa	10 µm	0%	0%	only waterglass	39%	0.41	22 ± 5 °C	5 min	28 dd	not	X	/	/	2	breaks	
LBCa 5	LBCa	10 µm	0%	0%	only waterglass	26%	0.38	22 ± 5 °C	5 min	1 dd	not	X	/	/	2	breaks	
LBCa 5A	LBCa	10 µm	0%	0%	only waterglass	26%	0.38	65°C (24h)	5 min	1 dd	not	X	/	X	1	breaks	
LBCa 5+10MK	LBCa	10 µm	10%	0%	only waterglass	22%	0.36	22 ± 5 °C	5 min	1 dd	yes	X (very low)	/	/	1	breaks	
LBCa 5+10MK_A	LBCa	10 µm	10%	0%	only waterglass	22%	0.36	65°C (24h)	5 min	1 dd	not	X	/	X	1	breaks	
LBCa 5+20MK	LBCa	10 µm	20%	0%	only waterglass	22%	0.36	22 ± 5 °C	5 min	1 dd	yes	X (very low)	/	/	1	breaks	
LBCa 6	LBCa	10 µm	0%	0%	only waterglass	20%	0.4	22 ± 5 °C	5 min	1 dd	yes	X	/	/	2	breaks	
LBCa 6+10MK	LBCa	10 µm	10%	0%	only waterglass	11%	0.36	22 ± 5 °C	5 min	1 dd	not	X (very low)	/	/	2	breaks	

LBCa 6+20MK	LBCa	10 µm	20%	0%	only waterglass	11%	0.36	22 ± 5 °C	5 min	1 dd	yes	X (very low)	/	/	2	breaks	
LBCa 7	LBCa	10 µm	0%	0%	only waterglass	14%	0.42	22 ± 5 °C	5 min	1 dd	yes	X	/	/	3	breaks	
LBCa 8	LBCa	10 µm	0%	0%	only waterglass	9.50%	0.42	22 ± 5 °C	5 min	1 dd	yes	X	/	/	3	breaks	
LBCa 9	LBCa	10 µm	0%	0%	0.5	0%	0.48	22 ± 5 °C	5 min	7 dd	yes	X	/	/	2	breaks	
LBCa 10	LBCa	10 µm	0%	0%	0.5	5%	0.38	22 ± 5 °C	5 min	7 dd	yes	X	/	/	3	breaks	
LBCa 11	LBCa	10 µm	0%	0%	only waterglass	24%	0.38	22 ± 5 °C	5 min	1 dd	not	X	/	/	1	breaks	
LBCa 12	LBCa	10 µm	0%	0%	0.53	27%	0.38	22 ± 5 °C	5 min	1 dd	yes	X	/	X	1	breaks	
LBCa 12A	LBCa	10 µm	0%	0%	0.53	27%	0.38	65°C (24h)	5 min	1 dd	yes	X	/	X	1	breaks	
LBCa 13	LBCa	10 µm	0%	0%	0.43	0%	0.45	22 ± 5 °C	5 min	7 dd	yes	X	/	/	1	resistant	LBCa 3/7
LBCa 13+10MK	LBCa	10 µm	10%	0%	0.43	0%	0.45	22 ± 5 °C	5 min	1 dd	yes	X (very low)	/	X (very low)	1	resistant	LBCa 3/7+10MK
LBCa 13+20MK	LBCa	10 µm	20%	0%	0.43	0%	0.47	22 ± 5 °C	5 min	1 dd	yes	/	/	/	1	resistant	LBCa 3/7+20MK
LBCa 14	LBCa	10 µm	0%	0%	1	0%	0.44	22 ± 5 °C	5 min	7 dd	yes	X	/	/	1	resistant	LBCa 1/1
LBCa 14+10MK	LBCa	10 µm	10%	0%	1	0%	0.43	22 ± 5 °C	5 min	1 dd	yes	X (very low)	/	/	1	resistant	LBCa 1/1+10MK
LBCa 14+20MK	LBCa	10 µm	20%	0%	1	0%	0.45	22 ± 5 °C	5 min	1 dd	yes	/	/	/	1	resistant	LBCa 1/1+20 MK
LBCa 14+5P	LBCa	10 µm	0%	5%	1	0%	0.45	22 ± 5 °C	5 min	< 1 dd	yes	X	/	/	1	resistant	
LBCa 14+10P	LBCa	10 µm	10%	10 %	1	0%	0.44	22 ± 5 °C	2 min	< 1 dd	yes	X	/	/	1	resistant	

LBCa 14+20P	LBCa	10 µm	20%	20 %	1	0%	0.47	22 ± 5 °C	2 min	< 1 dd	yes	X	/	/	1	resistant	
LBCa 15	LBCa	10 µm	0%	0%	2.33	0%	0.43	22 ± 5 °C	5 min	7 dd	yes	X	/	X	1	breaks	LBCa 7/3
LBCa 15+10MK	LBCa	10 µm	10%	0%	2.33	0%	0.44	22 ± 5 °C	5 min	1 dd	yes	X (very low)	/	X	1	resistant	LBCa 7/3+10MK
LBCa 15+20MK	LBCa	10 µm	20%	0%	2.33	0%	0.44	22 ± 5 °C	5 min	1 dd	yes	/	/	X	1	resistant	LBCa 7/3+20MK
CWF 3/7	CWF	10 µm	0%	0%	0.43	0%	0.36	22 ± 5 °C	5 min	7 dd	yes	X	/	/	1	resistant	
CWF 3/7+10MK	CWF	10 µm	10%	0%	0.43	0%	0.40	22 ± 5 °C	5 min	1 dd	yes	X (very low)	/	/	1	resistant	
CWF 3/7+20MK	CWF	10 µm	20%	0%	0.43	0%	0.40	22 ± 5 °C	5 min	1 dd	not	/	/	/	1	resistant	
CWF 1/1	CWF	10 µm	0%	0%	1	0%	0.37	22 ± 5 °C	5 min	7 dd	yes	X	/	/	1	resistant	
CWF 1/1+10MK	CWF	10 µm	10%	0%	1	0%	0.36	22 ± 5 °C	5 min	1 dd	yes	X (very low)	/	/	1	resistant	
CWF 1/1+20 MK	CWF	10 µm	20%	0%	1	0%	0.41	22 ± 5 °C	5 min	1 dd	yes	/	/	/	1	resistant	
CWF 7/3	CWF	10 µm	0%	0%	2.33	0%	0.43	22 ± 5 °C	5 min	7 dd	yes	X	/	X	2	resistant	
CWF 7/3+10MK	CWF	10 µm	10%	0%	2.33	0%	0.40	22 ± 5 °C	5 min	1 dd	yes	X (very low)	/	X	2	resistant	
CWF 7/3+20MK	CWF	10 µm	20%	0%	2.33	0%	0.41	22 ± 5 °C	5 min	1 dd	yes	/	/	X	2	resistant	

**the % is calculated on total solid ; **the % is calculated on total liquid; ***1=clear water; 2=residues; 3=turbid water*

Table 5.1 – Synthesis parameters of binders and mortars experimented; Tc= curing temperature; St=setting time and Ct=curing time.

The formulations tested both with curing at room temperature and after a low-temperature firing step have been partially analyzed. Uniaxial compressive tests and Mercury Intrusion Porosimetry have been performed in order to investigate the effect of the firing step on the performance of the product. The uniaxial compressive tests have been carried out on cubic samples of 2*2*2 cm by the University of Florence, according to the UNI EN 1926:2007, as indicated in Chapter 3. The porosimetric analyses have been performed at University of Catania with the specifics indicated already in Chapter 3. The results are summarized below, in the scheme of Fig. 5.5. All the results are shown in Attachments 5.1 and 5.2.

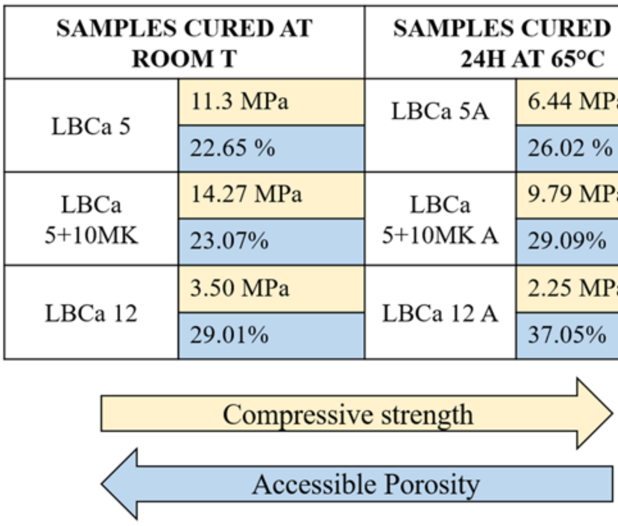

SAMPLES CURED AT ROOM T		**SAMPLES CURED FOR 24H AT 65°C**	
LBCa 5	11.3 MPa	LBCa 5A	6.44 MPa
	22.65 %		26.02 %
LBCa 5+10MK	14.27 MPa	LBCa 5+10MK A	9.79 MPa
	23.07%		29.09%
LBCa 12	3.50 MPa	LBCa 12 A	2.25 MPa
	29.01%		37.05%

Fig. 5.5 – Porosimetric and mechanical results obtained from samples LBCa 5, LBCa 5+10MK and LBCa 12, cured at ambient temperature, and on the respective samples fired during 24 hours at 65 °C and then leaved maturing at room temperature, LBCa 5A, LBCa 5+10MK_A and LBCa 12A.

The samples LBCa 5 and LBCa 5+10MK do not show visible efflorescences, while the same formulations after the firing step (LBCa 5A and LBCa 5+10MK_A) are characterized by visible efflorescences as well as a decrease in compressive strength of about 5 MPa. The simultaneous occurrence of these features could be correlated. As a matter of fact, the crystallization of crypto-efflorescence would interrupt the structural continuity of the alkaline gel in the samples, compromising their compactness and resistance (Rowles and O'Connor, 2009). Compressive strength decreases are also individuated in LBCa 12A (same formulation as LBCa 12, but fired), but in this case efflorescences are already visible in the non-fired sample. In general, the resistance of both samples is very poor. Looking also at the porosimetric data, it is furthermore possible to notice an inverse pattern, with an increase of the accessible porosity after firing. Again, the fired samples show worse performances than those cured at room temperature. The higher accessible porosity volume would indeed determine a higher vulnerability of the products to environmental decays. These results allowed to decide to continue the study with curing at room temperature only, pursuing the aim of this research of reducing the environmental costs in restoration material production.

In order to investigate the efflorescences formed on the samples, few samplings have been carried out on the "barbetta" when present (Fig. 5.3d), otherwise the salt samples have been scratched from the surface with a scalpel. In this latter case we have to consider the possibility to have sampled the geopolymer as well. X-ray powder Diffraction has been carried out on samples LBCa 12A, LBCa 7/3, LBCa 7/3+10MK, LBCa 7/3+20MK and LBCa 3/7+10MK. Only qualitative analysis is carried out, just to define which kind of salts are formed. The diffraction pattern of salts collected from sample LBCa 7/3+20MK is shown in Fig. 5.6 as representative. From this analysis, mainly sodium carbonates with different hydration grades have been detected, as expected (Criado et al., 2005; Leonelli, 2013; Lloyd et al., 2010; Najafi Kani et al., 2012; Provis and Van Deventer, 2009; Rowles and O'Connor, 2009; Yip et al., 2008; Zhang et al., 2018). Some further peaks cannot be attributed to sodium carbonates, and are mainly compatible with the presence of gypsum, however its presence cannot be confirmed by XRF analysis, since S is not revealed. In detail, trona ($Na_3(CO_3)(HCO_3)*2(H_2O)$) and thermonatrite ($Na_2CO_3(H_2O)$) have been individuated in sample LBCa 7/3, in samples LBCa 3/7+10MK and LBCa 7/3+20MK (with the possible presence of gypsum ($CaSO_4*2H_2O$)) and in sample LBCa 12A (with the possible presence of ettringite ($Ca_6Al_2(SO_4)_3(OH)_{12}*26(H_2O)$)); only thermonatrite was detected in sample LBCa 7/3+10MK. In some samples peaks attributable to quartz, most likely due to the geopolymeric substrate scratched unintentionally during sampling, are also present.

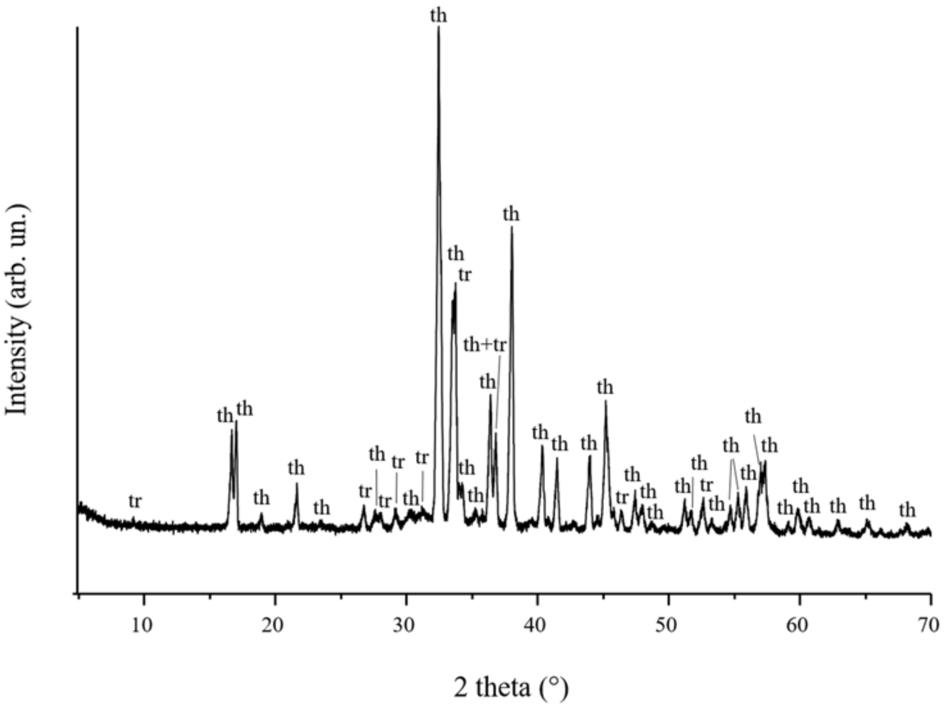

Fig. 5.6 – Representative diffraction pattern of the salts collected from the samples LBCa 12A, LBCa 7/3, LBCa 7/3+10MK, LBCa 7/3+20MK and LBCa 3/7+10MK. In particular, in the image is shown the diffraction pattern of the sample LBCa 7/3+20MK. Th=thermonatrite; tr=trona.

After considering the preliminary results of the empirically adjusted slurries in the lab, a batch of LBCa-based formulations has been selected to be improved and to be studied in depth for the objectives of this PhD thesis. The same batch of formulations was replicated using CWF as precursor. All the formulations selected are highlighted in grey on Table 5.1. The series is based on fixed proportions of sodium hydroxide/waterglass and of ceramic/MK, in order to investigate the effects of these parameters, keeping the others fixed. In particular, according to the sodium hydroxide/waterglass ratio three series have been experimented (3/7, 1/1 and 7/3); each series is constituted by three formulations, without or with 10 or 20% of MK (weight% on the solid precursor). Thus, for each starting material (LBCa and CWF) three formulations were obtained directly mixing the ceramic precursor with the alkaline solutions and six formulations are indeed binary mixtures (ceramic waste and MK as additive). The CWF formulations are shown in Fig. 5.7, as example.

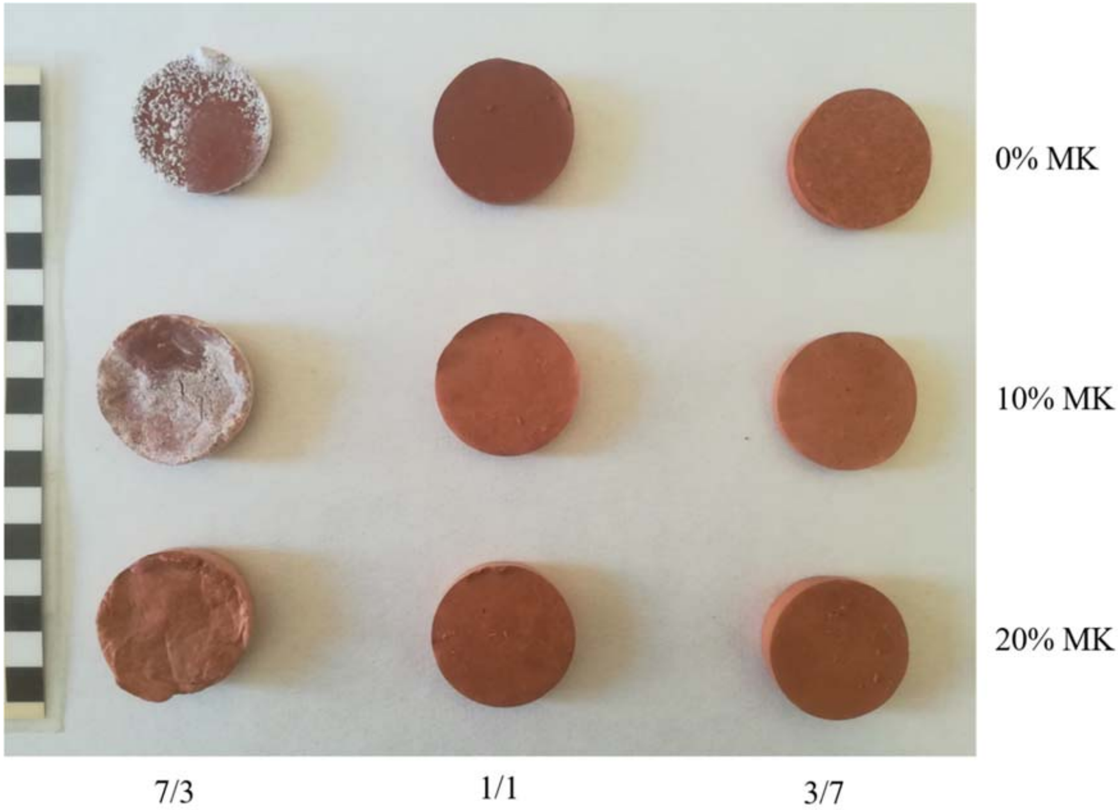

Fig. 5.7 – Samples of the studied formulations starting from CWF raw material.

To facilitate the comprehension of the compositional differences of the studied formulations they have been re-labelled as described in Fig. 5.8.

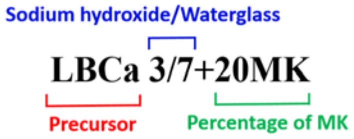

Fig. 5.8 – Description of the talking labels.

The weight and molar ratio of the synthesis components of these binders are shown in Table 5.2.

		weight ratio			molar ratio		
	Formulations LBCa	L/S	Water/Solid	Na_2SiO_3/NaOH	SiO_2/Al_2O_3	Al_2O_3/Na_2O	Water/Alkali
Binders from LBCa raw ceramic	LBCa 3/7	0.45	0.30	2.33	7.22	1.37	5.45
	LBCa 1/1	0.44	0.31	1.00	6.95	1.16	5.19
	LBCa 7/3	0.43	0.31	0.43	6.69	1.02	4.96
	LBCa 3/7+10MK	0.45	0.30	2.33	6.25	1.60	5.86
	LBCa 1/1+10MK	0.43	0.30	1.00	6.01	1.37	5.50
	LBCa 7/3+10MK	0.44	0.32	0.43	5.79	1.16	5.34
	LBCa 3/7+20MK	0.47	0.32	2.33	5.54	1.76	6.53
	LBCa 1/1+20MK	0.45	0.31	1.00	5.30	1.53	6.02
	LBCa 7/3+20MK	0.44	0.32	0.43	5.10	1.33	5.71
	Formulations CWF						
Binders from CWF raw ceramic	CWF 3/7	0.36	0.22	2.33	4.03	2.78	4.03
	CWF 1/1	0.37	0.25	1.00	3.92	2.26	4.06
	CWF 7/3	0.43	0.30	0.43	7.22	0.91	4.38
	CWF 3/7+10MK	0.40	0.25	2.33	6.51	1.64	4.68
	CWF 1/1+10MK	0.36	0.24	1.00	6.24	1.48	4.26
	CWF 7/3+10MK	0.40	0.28	0.43	6.07	1.17	4.44
	CWF 3/7+20MK	0.40	0.25	2.34	5.64	1.90	5.17
	CWF 1/1+20MK	0.41	0.27	1.00	5.46	1.55	5.05
	CWF 70/30+20MK	0.41	0.29	0.43	5.26	1.32	4.92

Table 5.2 – Weight and molar ratio synthesis parameters of binders under study.

Regarding the restoration materials to develop, different kinds of aggregates have been selected in order to see the different behavior in respect to mechanical resistance, tendency to shrinkage, adhesion properties and colour appearance. Specifically, commercial siliceous sand, locally available carbonate sand, the same ceramic waste used as precursor and commercial powdered marble have been used, as already described in Chapter 4. These are added to the studied binders during the synthesis, modifying the L/S ratio by adding water in order to improve the workability of the slurry. The amount of aggregates has been determined according to preliminary tests, trying to aim at the usual 1/3 binder/aggregate ratio used (Binda et al., 2003; Haach et al., 2011; Reig et al., 2013b; Schueremans et al., 2011). After the first tests, it was decided to use a 1/1 ratio instead, in order to avoid adding too much water for adjusting the workability. This could indeed affect the already studied binder, changing its performance and the geopolymerization process itself.

The developed mortars have also been tested directly on fragments of archaeological materials and left to dry at room temperature without any cover, in order to simulate curing in an outdoor setting and making conditions as realistic as possible (Clausi et al., 2016). Further details on the final products' synthesis are exposed in Chapters 6 and 7; their planning is indeed strictly correlated to the results obtained on the studied binders.

References

Ahmari, S., Ren, X., Toufigh, V., Zhang, L., 2012. Production of geopolymeric binder from blended waste concrete powder and fly ash. Constr. Build. Mater. 35, 718–729. https://doi.org/10.1016/j.conbuildmat.2012.04.044

Amin, S.K., El-Sherbiny, S.A., El-Magd, A.A.M.A., Belal, A., Abadir, M.F., 2017. Fabrication of geopolymer bricks using ceramic dust waste. Constr. Build. Mater. 157, 610–620. https://doi.org/10.1016/j.conbuildmat.2017.09.052

Azevedo, A.G. de S., Strecker, K., Lombardi, C.T., 2018. Produção de geopolímeros à base de metacaulim e cerâmica vermelha. Cerâmica 64, 388–396. https://doi.org/10.1590/0366-69132018643712420

Binda, L., Baronio, G., Tiraboschi, C., Tedeschi, C., 2003. Experimental research for the choice of adequate materials for the reconstruction of the Cathedral of Noto. Constr. Build. Mater. 17, 629–639. https://doi.org/10.1016/S0950-0618(03)00059-X

Buchwald, a, Kaps, C., Hohmann, M., 2003. Alkali-Activated Binders and Pozzolan Cement Binders – Compete Binder Reaction or Two Sides of the Same Story ? 11th Int. Congr. Chem. Cem. 1238–1247.

Clausi, M., Tarantino, S.C., Magnani, L.L., Riccardi, M.P., Tedeschi, C., Zema, M., 2016. Metakaolin as a precursor of materials for applications in Cultural Heritage: Geopolymer-based mortars with ornamental stone aggregates. Appl. Clay Sci. 132–133, 589–599. https://doi.org/10.1016/j.clay.2016.08.009

Criado, M., Palomo, A., Fernández-Jiménez, A., 2005. Alkali activation of fly ashes. Part 1: Effect of curing conditions on the carbonation of the reaction products. Fuel 84, 2048–2054. https://doi.org/10.1016/j.fuel.2005.03.030

Duxson, P., Provis, J.L., Lukey, G.C., Mallicoat, S.W., Kriven, W.M., Van Deventer, J.S.J., 2005. Understanding the relationship between geopolymer composition, microstructure and mechanical properties. Colloids Surfaces A Physicochem. Eng. Asp. 269, 47–58. https://doi.org/10.1016/j.colsurfa.2005.06.060

Haach, V.G., Vasconcelos, G., Loureno, P.B., 2011. Influence of aggregates grading and water/cement ratio in workability and hardened properties of mortars. Constr. Build.

Mater. 25, 2980–2987. https://doi.org/10.1016/j.conbuildmat.2010.11.011

Komnitsas, K., Zaharaki, D., 2007. Geopolymerisation: A review and prospects for the minerals industry. Miner. Eng. 20, 1261–1277. https://doi.org/10.1016/j.mineng.2007.07.011

Komnitsas, K., Zaharaki, D., Vlachou, A., Bartzas, G., Galetakis, M., 2015. Effect of synthesis parameters on the quality of construction and demolition wastes (CDW) geopolymers. Adv. Powder Technol. 26, 368–376. https://doi.org/10.1016/j.apt.2014.11.012

Lancellotti, I., Catauro, M., Ponzoni, C., Bollino, F., Leonelli, C., 2013. Inorganic polymers from alkali activation of metakaolin: Effect of setting and curing on structure. J. Solid State Chem. 200, 341–348. https://doi.org/10.1016/j.jssc.2013.02.003

Leonelli, C., 2013. Definizione, preparazione, proprietà ed applicazioni., in: Leonelli, C., Romagnoli, M. (Eds.), Geopolimeri: Polimeri Inorganici Attivati Chimicamente. ICerS, Bologna, pp. 1–22.

Lloyd, R.R., Provis, J.L., Van Deventer, J.S.J., 2010. Pore solution composition and alkali diffusion in inorganic polymer cement. Cem. Concr. Res. 40, 1386–1392. https://doi.org/10.1016/j.cemconres.2010.04.008

Najafi Kani, E., Allahverdi, A., Provis, J.L., 2012. Efflorescence control in geopolymer binders based on natural pozzolan. Cem. Concr. Compos. 34, 25–33. https://doi.org/10.1016/j.cemconcomp.2011.07.007

Pacheco-Torgal, F., Tam, V.W.Y., Labrincha, J.A., Ding, Y., de Brito, J., 2013. Handbook of Recycled Concrete and Demolition Waste. Woodhead Publishing.

Panizza, M., Natali, M., Garbin, E., Tamburini, S., Secco, M., 2018. Assessment of geopolymers with Construction and Demolition Waste (CDW) aggregates as a building material. Constr. Build. Mater. 181, 119–133. https://doi.org/10.1016/j.conbuildmat.2018.06.018

Pecchioni, E., Fratini, F., Cantisani, E., 2008. Le malte antiche e moderne tra tradizione ed innovazione. Pàtron Editore, Bologna.

Provis, J.L., Van Deventer, J.S.J., 2009. Geopolymers. Structure, processing, properties and industrial applications. Woodhead Publishing Limited, Cambridge.

Reig, L., Tashima, M.M., Borrachero, M. V., Monzó, J., Cheeseman, C.R., Payá, J., 2013a. Properties and microstructure of alkali-activated red clay brick waste. Constr. Build. Mater. 43, 98–106. https://doi.org/10.1016/j.conbuildmat.2013.01.031

Reig, L., Tashima, M.M., Soriano, L., Borrachero, M. V., Monzó, J., Payá, J., 2013b. Alkaline activation of ceramic waste materials. Waste and Biomass Valorization 4, 729–736. https://doi.org/10.1007/s12649-013-9197-z

Robayo, R.A., Mulford, A., Munera, J., Mejía de Gutiérrez, R., 2016. Alternative cements based on alkali-activated red clay brick waste. Constr. Build. Mater. 128, 163–169. https://doi.org/10.1016/j.conbuildmat.2016.10.023

Rovnaník, P., Rovnaníková, P., Vyšvařil, M., Grzeszczyk, S., Janowska-Renkas, E., 2018. Rheological properties and microstructure of binary waste red brick powder/metakaolin geopolymer. Constr. Build. Mater. 188, 924–933. https://doi.org/10.1016/j.conbuildmat.2018.08.150

Rowles, M.R., O'Connor, B.H., 2009. Chemical and structural microanalysis of aluminosilicate geopolymers synthesized by sodium silicate activation of metakaolinite. J. Am. Ceram. Soc. 92, 2354–2361. https://doi.org/10.1111/j.1551-2916.2009.03191.x

Schueremans, L., Cizer, Ö., Janssens, E., Serré, G., Balen, K. Van, 2011. Characterization of repair mortars for the assessment of their compatibility in restoration projects: Research and practice. Constr. Build. Mater. 25, 4338–4350. https://doi.org/10.1016/j.conbuildmat.2011.01.008

UNI, 2007. Natural stone test methods - Determination of uniaxial compressive strength. EN 1926.

Wong, C.L., Mo, K.H., Yap, S.P., Alengaram, U.J., Ling, T.C., 2018. Potential use of brick waste as alternate concrete-making materials: A review. J. Clean. Prod. 195, 226–239. https://doi.org/10.1016/j.jclepro.2018.05.193

Yip, C.K., Lukey, G.C., Provis, J.L., Van Deventer J.S.J., 2008. Effect of calcium silicate sources on geopolymerisation. Cem. Concr. Res. 38, 554–564. https://doi.org/10.1016/j.cemconres.2007.11.001

Zhang, Z., Provis, J.L., Ma, X., Reid, A., Wang, H., 2018. Efflorescence and subflorescence induced microstructural and mechanical evolution in fly ash-based geopolymers. Cem. Concr. Compos. 92, 165–177. https://doi.org/10.1016/j.cemconcomp.2018.06.010

Chapter 6

Geopolymers from industrial tiles waste

6.1 Geopolymeric binders

6.1.1 Mineralogical characterization (XRD)

The XRD patterns collected on the studied binders after 28 days of curing are reported in Figg. 6.1 (binders from ceramic waste) and 6.2 (binary mixtures from ceramic waste and MK). The XRD patterns of the ceramic and MK precursors have been reported for comparison. All diffraction patterns display peaks of the precursors, namely quartz, diopside, gehlenite, haematite, feldspars (microcline and Ca-plagioclase) and wollastonite, with the addition of illite in the binary samples. Furthermore, new phases related to the carbonation of efflorescence (mainly thermonatrite) are individuated. Other new crystalline phases are not evidenced and no significant differences are highlighted between geopolymer series with different alkaline solution ratios. Unlike other common alkali-activated binders (Clausi et al., 2018; Criado et al., 2005; Duxson et al., 2007; Fernández-Jiménez et al., 2006; Fernández-Jiménez and Palomo, 2005; Lancellotti et al., 2013), no zeolites are here detected; this could be explained because of the scarse amount of reactive alumina, together with the temperature of curing that does not cause its solubilisation (D'Elia et al., 2020).

The Rietveld refinement gave the possibility to study the amorphous content increment between the precursors and the relative geopolymers. It is summarized in Fig. 6.3, together with the content of efflorescences. These are indeed two important parameters to consider in order to establish the quality of the geopolymer for further improvements.

The amorphous content is not linear with the increase of sodium hydroxide and MK in the paste, as instead we could assume. In fact, it is higher in the 1/1 set and in the 3/7+20MK sample and it decreases drastically in the set richer in sodium hydroxide, i.e. the set 7/3 (except the sample without MK). According to the amount of MK it is evident that the samples with 10% of MK show lower increase with respect to the samples with 20% of MK, or without MK. Regarding the efflorescences, it is possible to notice as the samples characterized by a higher amount of salts are those with higher sodium hydroxide/waterglass ratio; the salts content furthermore decreases with increasing amounts of MK in the slurry.

Considering the decrease of the single phases it was possible to individuate the higher contribution in the dissolution for the geopolymerization process of gehlenite (c.a. decrease of 70%), microcline and haematite (c.a. 60% each) and Ca-plagioclase (c.a. 30%).

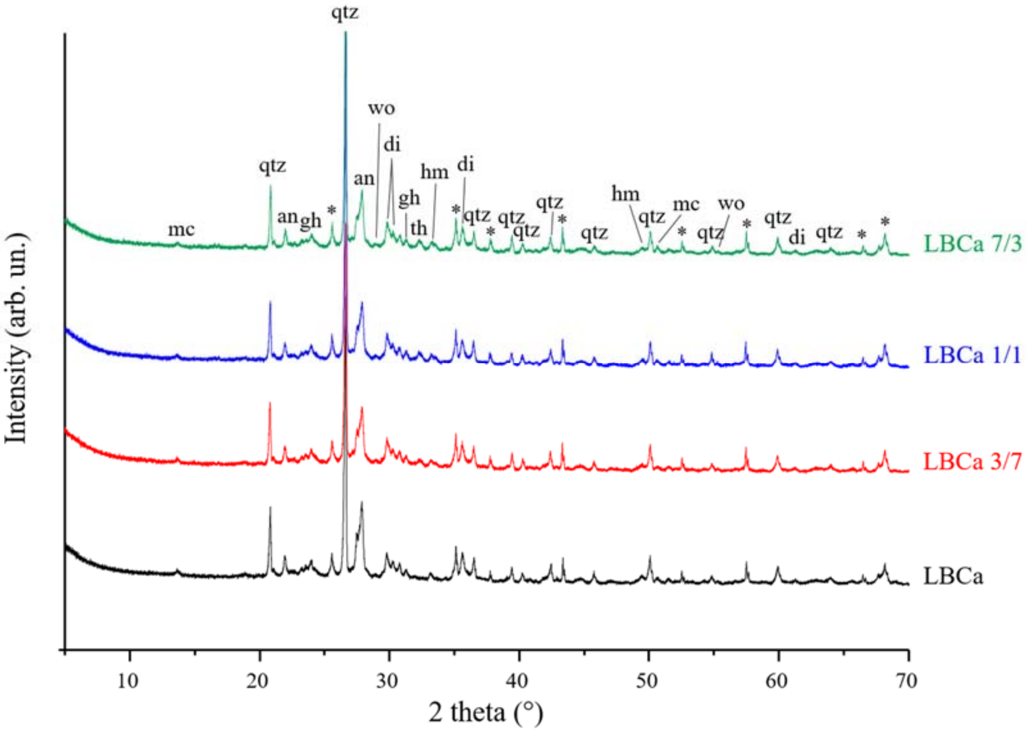

*Fig. 6.1 – Diffraction patterns of LBCa 3/7, LBCa 1/1, LBCa 7/3 and LBCa raw material samples; qtz=quartz; di=diopside; gh=gehlenite; hm=haematite; mc=microcline; an=anorthite; wo=wollastonite; th=thermonatrite; * indicates corundum, added as internal standard.*

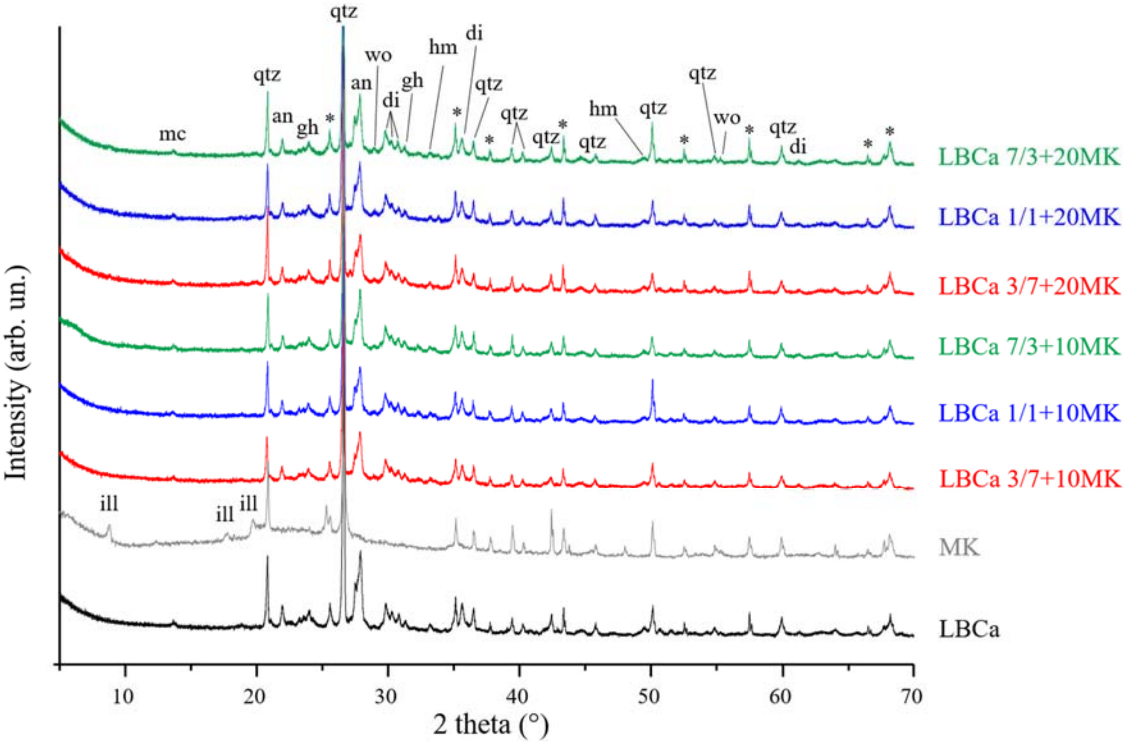

*Fig. 6.2 – Diffraction patterns of 10% MK and 20% MK samples and the relative raw materials LBCa and MK; qtz=quartz; di=diopside; gh=gehlenite; hm=haematite; mc=microcline; an=anorthite; wo=wollastonite; ill=illite; * indicates corundum, added as internal standard.*

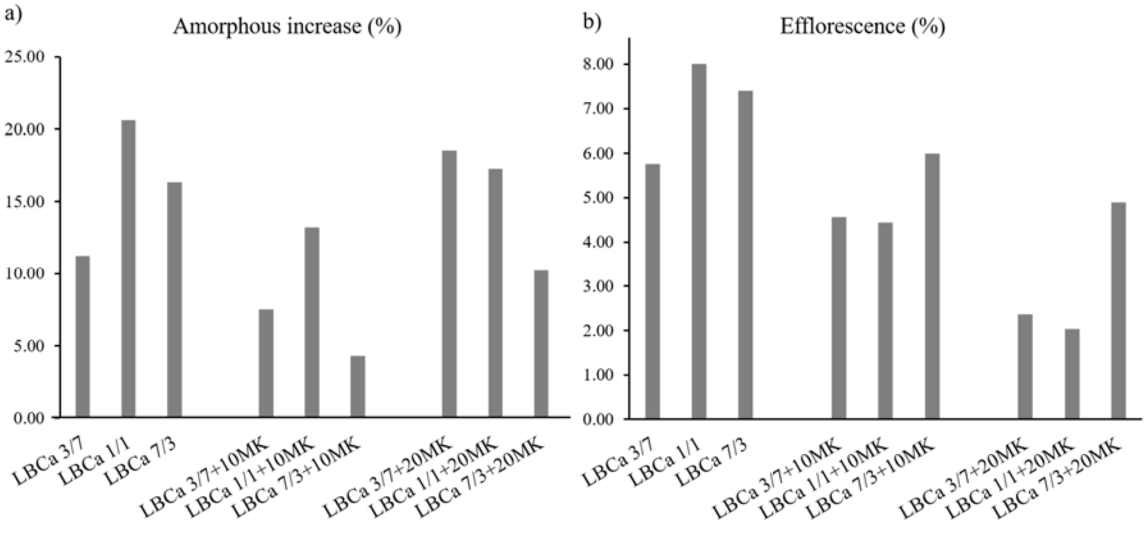

Fig. 6.3 – Histograms of the geopolymer series showing the amorphous content increase a) and efflorescence amounts b). The amorphous content has been calculated after the normalization of the data without efflorescences amounts.

6.1.2 Microstructural characterization and gel chemical investigation (SEM-EDS, TEM-EDS)

SEM-EDS

To point out the differences in the microstructure and chemical composition of the developed geopolymers, SEM-EDS analyses at different magnifications have been carried out.

The SEM images will show in sequence the low magnification images of the samples without MK, with the relative collected spectra (Fig. 6.4); the low magnification of the samples with 10% of MK (Fig. 6.5) and those with 20% of MK (Fig. 6.6). Images at higher magnification showing details or particular morphologies with EDS spectra follow, in particular those acquired on samples without MK (Fig. 6.7), on samples with 10% of MK (Fig. 6.8) and on samples with 20% of MK (Fig. 6.9).

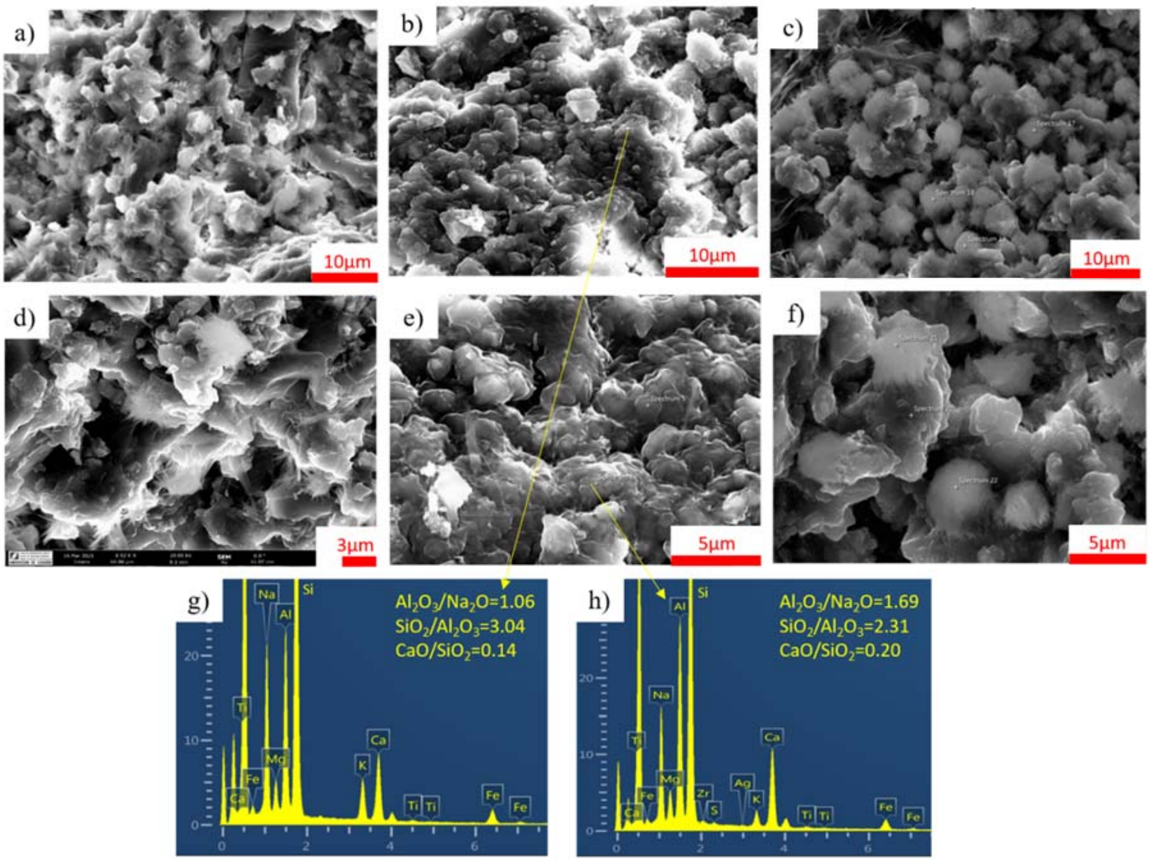

Fig. 6.4 – SEM images at different magnification of LBCa 3/7 a) and d); LBCa 1/1 b) and e); and LBCa 7/3 c) and f). The images show details of tufts particles d) and f), and of a representative dense matrix e). The EDS spectra relative to the matrix are also shown (g and h).

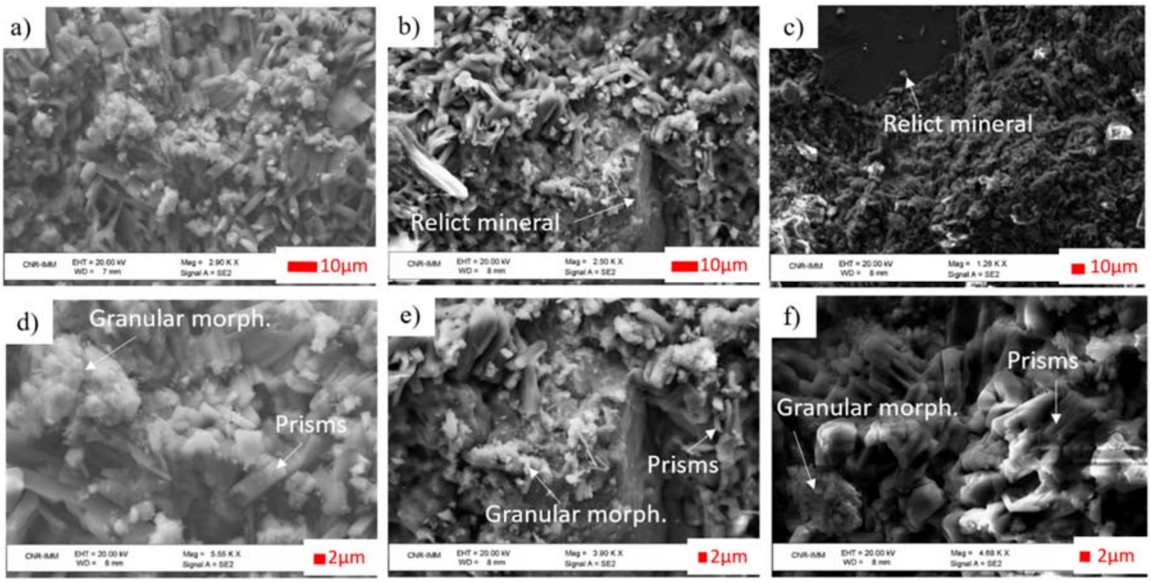

Fig. 6.5 – SEM images at different magnifications of LBCa 3/7+10MK a) and d); LBCa 1/1+10MK b) and e); and LBCa 7/3+10MK c) and f), showing the two characteristics morphologies of granular particles and prisms, together with some relict minerals.

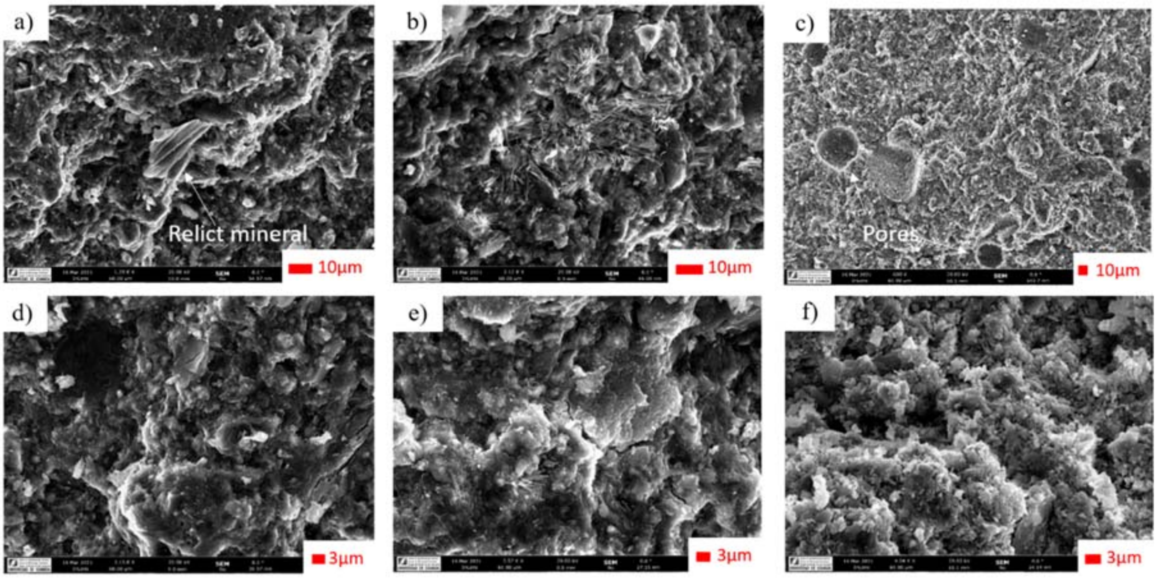

Fig. 6.6 – SEM images at different magnifications of LBCa 3/7+20MK a) and d); LBCa 1/1+20MK b) and e); and LBCa 7/3+20MK c) and f).

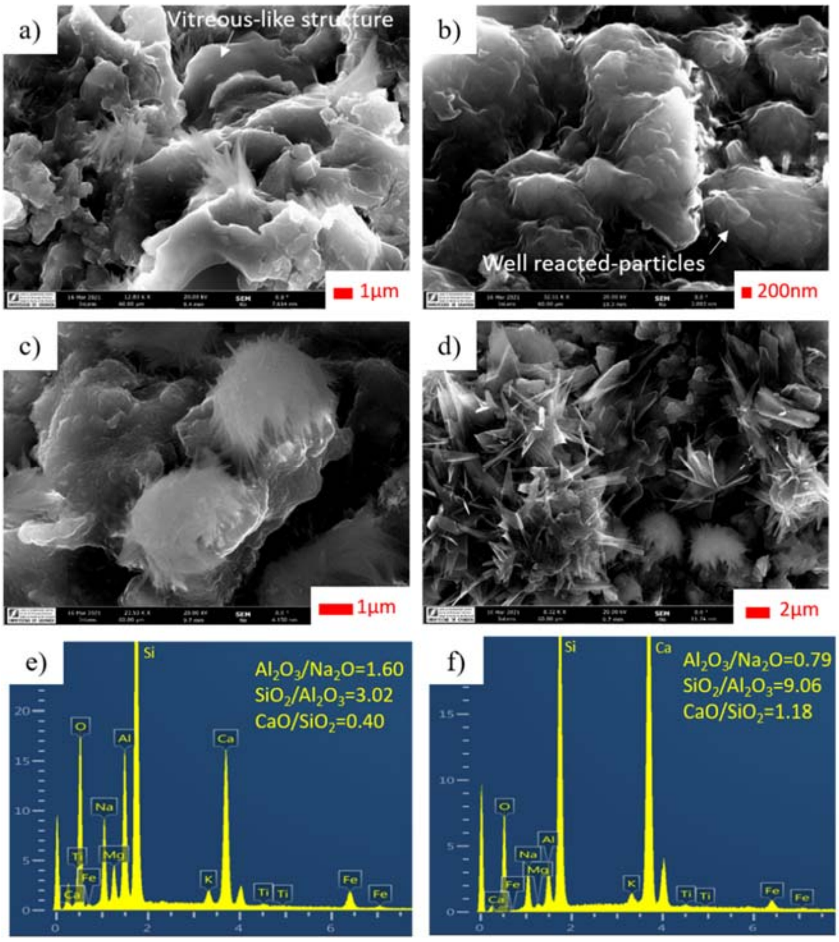

Fig. 6.7 – SEM images of LBCa 3/7 a); LBCa 1/1 b) and LBCa 7/3 c) and d). The images show details of tufts particles a) and c), of a representative dense matrix (b) and of the acicular crystals (d). The spectra e) and f) show respectively the chemical composition of the crystals/tufts individuated on sample LBCa 3/7 and the tufts characterizing sample 7/3.

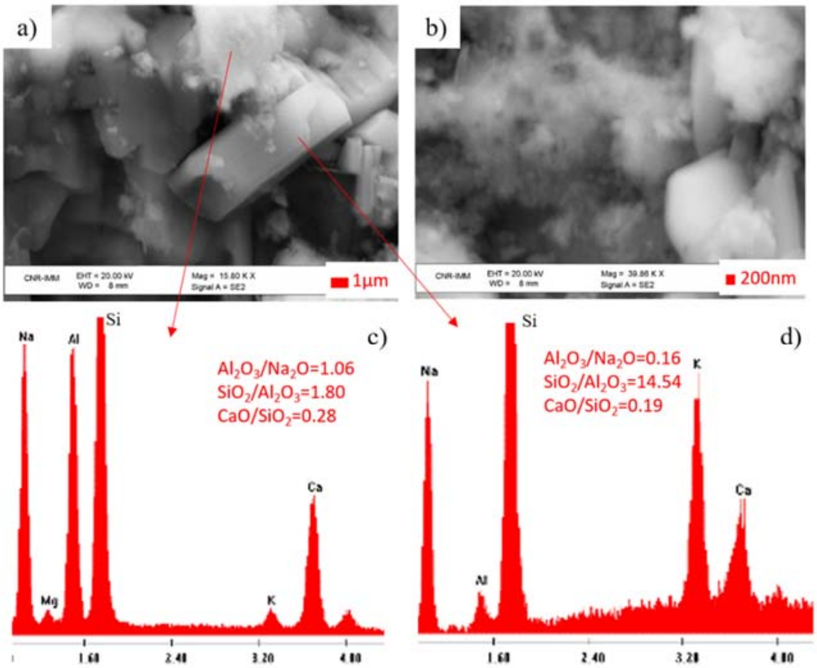

Fig. 6.8 – SEM images of LBCa 3/7+10MK a) and LBCa 1/1+10MK b). The images show details of amorphous granular particles with the relative spectrum c); a detail of a hollow prism with its spectrum d).

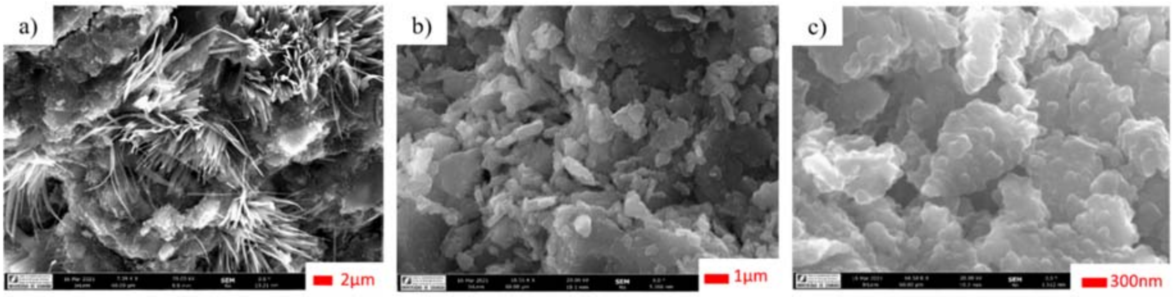

Fig. 6.9 – Detailed SEM images of LBCa 1/1+20MK secondary crystals a) and of the botryoidal morphology of sample LBCa 7/3+20MK b) and c).

Overall, the samples show a homogeneous and well reacted microstructure, bonding the particles at micrometric scale (Figg. 6.4, 6.5 and 6.6), similar to those observed in the literature relative to ceramic-based geopolyemers (Azevedo et al., 2018; Reig et al., 2013; Robayo et al., 2016; Sun et al., 2013). All matrices appear compact with a dense, and in some points vitreous-like, texture. Comparing the samples, the structure seems to become denser with decreasing sodium hydroxide/waterglass ratio, as expected (Pachego-Torgal et al., 2014).

Morphologically, the matrix appears characterized by “sintered” granules, arising both as surface and internal features, which is possible to associate to the geopolymeric gel morphology (He et al., 2012), mainly N-A-S-H or (N,C)-A-S-H (García-Lodeiro et al., 2012). According to these observations, the development of an amorphous phase is confirmed.

The chemical composition acquired in different points of the matrices is compatible with a multi-component system of (N,C)-A-S-H (e.g. Fig. 6.4g and h), with the granular matrix and massive areas sharing more or less the same composition.

A distinctive feature characterizes the samples with 10% of MK, where, beside the granular morphology, smooth prisms, apparently hollow, are also visible (Fig. 6.5 and 6.8a). Similar structures are interpreted by Wan et al. (2019) as a geopolymeric gel, but no further explanation is present in the actual literature, in the author’s knowledge.

The chemical composition of the samples with 10% of MK is heterogeneous; chemical clusters are detected, but not reflecting the different morphologies. Both the matrix and the prisms appear sometimes more sodic sometimes richer in Ca and Si. For their heterogeneity the spectra shown in Fig. 6.8c and d could not be considered as representative but only as examples.

Furthermore, 7/3+20MK stands out from the other samples because it shows a unique morphology characterized by mammillary-botryoidal aspect, appreciable at high magnification (Fig. 6.9b and c).

Nevertheless, the chemical composition of the botryoidal features characterizing sample 7/3+20MK do not deviate from the averaged chemical composition of the gels detected in the other samples.

No new further minerals are detected, while some relict minerals not completely dissolved (e.g. Figg. 6.5b and c and 6.6a) are visible as residual particles of the alumino-silicate precursors. Among the phases detected quartz, K-feldspar and MK lamellae have been identified.

The general massive structure of the samples is interrupted by a porosity, heterogeneously distributed. As visible in Fig. 6.6c spherical voids of 20-50 μm in size characterize the pores structure at low magnification, probably due to air bubbles trapped in the matrix during the synthesis (Duxson et al., 2005; Komnitsas et al., 2015; Panizza et al., 2018; Robayo et al., 2016).

Different secondary products are distinguishable:

- soft-looking tufts of about 3 μm wide are spread all over the surface in samples 3/7 (Fig. 6.4d) and 7/3 (Fig. 6.4f). Increasing the magnification, these products show a different morphologies and patterns: while the tufts appearing in sample 3/7 seem to be of secondary precipitation growing in the interstices and in the pores (Fig. 6.7a), the tufts characterizing sample 7/3 appear as aggressive particles attached to the massive substrate (Fig. 6.7c);
- acicular/star-like crystals embedded in the amorphous matrix, thus interrupting its continuity, are visible in sample 7/3 (Fig. 6.7d);
- few superficial filaments are visible as secondary products on the surface of the sample 1/1 (Fig. 6.4e);
- long whiskers growing inside cavities and interstices, which could be interpreted as sodium carbonate (Reig et al., 2013a), are observed at high magnification in the sample 1/1+20MK (Fig. 6.9a).

The EDS analyses performed on the tufts that were present in samples 3/7 (Fig. 6.7e) and 7/3 (Fig. 6.7f) confirmed their different nature: the tufts of sample 7/3 are almost completely composed of Ca and Si, while Na and Al are also relevant in the tufts precipitating in sample 3/7.

EDS analyses on the other secondary products were unable to identify their composition because of their small dimensions.

From semi-quantitative EDS analyses of more than 150 points, the type of gel has been better identified (Figg. 6.10 and 6.11).

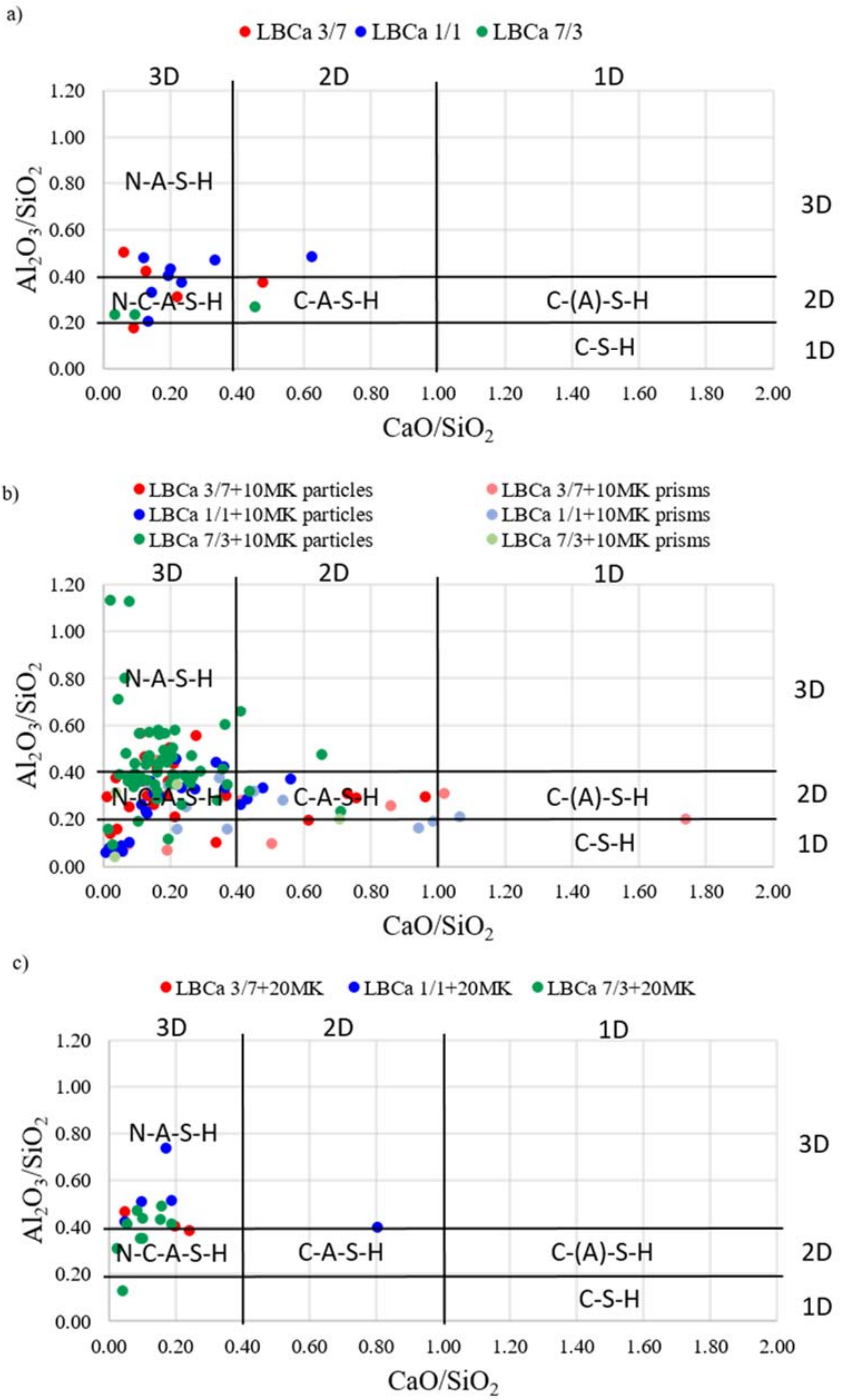

Fig. 6.10 – Al_2O_3/SiO_2 vs. CaO/SiO_2 ratios for gels precipitating in hybrid cements (based on EDS findings); a) LBCa binders without MK; b) LBCa binders with 10% of MK; c) LBCa binders with 20% of MK. The gel ranges indicated are reported from the literature (Garcia-Lodeiro et al., 2011; Pardal et al., 2009).

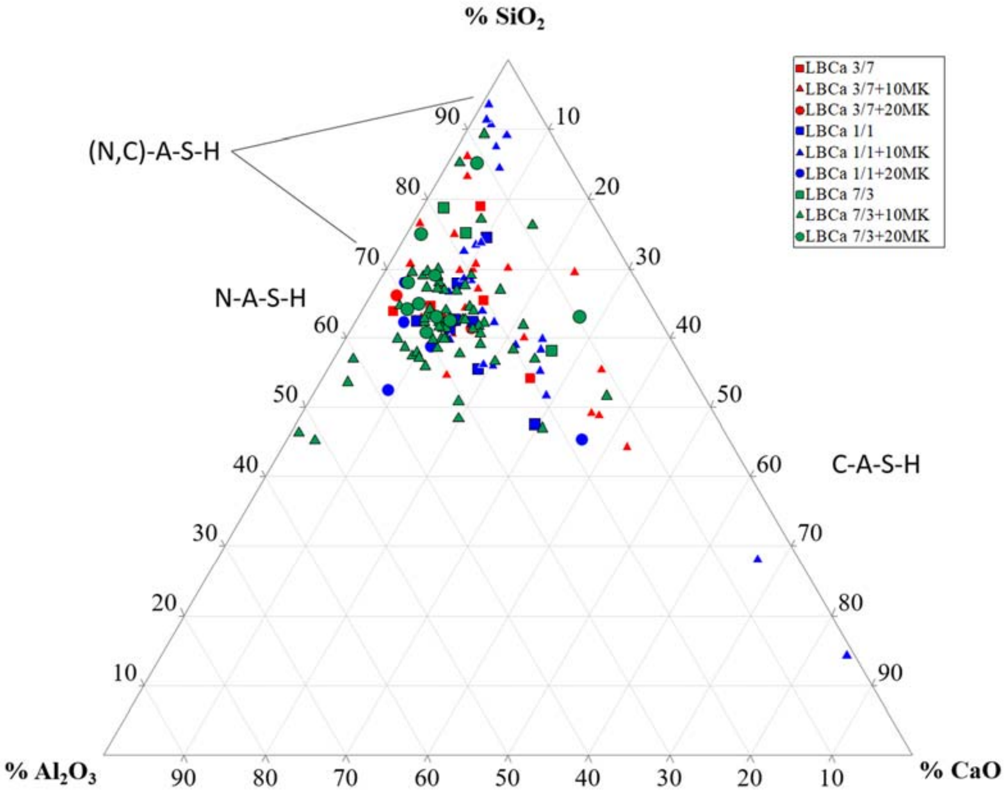

Fig. 6.11 – SiO_2-Al_2O_3-CaO ternary diagram for the gel detected on all the AAMs series developed: LBCa 3/7 series, LBCa 1/1 series and LBCa 7/3 series. The gel ranges indicated in the diagram proceed from the literature (García-Lodeiro et al., 2013; Pachego-Torgal et al., 2014).

The Al_2O_3/SiO_2 and CaO/SiO_2 ratios have been plotted in Fig. 6.10; the composition ranges which characterize the main types of gels, (C-S-H, C-(A)-S- H, C-A-S-H, N-A-S-H and (N,C)-A-S-H), are also marked in the figure according to literature (Garcia-Lodeiro et al., 2011; Pardal et al., 2009). Overall, all the points analyses acquired on the different samples show a chemical composition with a prevalent attribution to (N,C)-A-S-H and only partially to N-A-S-H (mainly for samples with 20% of MK) or C-A-S-H (mainly for samples with 10% of MK). Regarding the samples with 10% of MK, plotting both the data acquired on the granular morphology and those acquired on the prisms two clusters could be drawn, with partial overlap. Indeed, while the majority of the points related to the first morphology falls in the (N,C)-A-S-H and N-A-S-H region, with only some point toward the C-A-S-H region; the composition of the prisms is distributed between (N,C)-A-S-H and C-A-S-H, always with a moderate alumina/silica ratio. These interpretations are confirmed by the visualization of data in the SiO_2-Al_2O_3-CaO ternary diagram for the gel reported in Fig. 6.11 and compared with the literature data (Pachego-Torgal et al., 2014).

The chart exposed in Fig. 6.12 summarizes the SEM-EDS observations. From this, it is possible to deduce that while the sodium hydroxide/waterglass ratio influences the density of the structure, producing denser matrix with higher waterglass proportions (Robayo et al., 2016), it does not seem to have any particular effect on the type of gel formed. This latter is instead mainly determined by the different proportions of MK to the ceramic precursor. Indeed, it is possible to notice that samples with the same MK percentage show globally the same kind of gel. From a hybrid, homogeneous (N,C)-A-S-H gel of the samples without MK, the gel changes composition with the addition of MK, enriching in sodium. Furthermore, C-A-S-H clusters are individuated in the intermediate samples, particularly in correspondence of the prismatic structures. This unusual behaviour is not well understood, but I would speculate that it could be attributable to particular stoichiometric conditions which negatively affect the continuity of the geopolymerization process. Being unvaried all the other synthesis parameters (as liquid components proportions or molarity, environmental conditions and so on), the only parameter which could determine variations is the elemental proportions. It would be possible that: in the only presence of ceramic precursor, the alkaline activation starts to dissolve the Ca-species, giving a hybrid gel with a slower but homogeneous growing; while with the addition of some amounts of MK, the geopolymerization process readily affects the more reactive phases (MK), somehow inhibiting the participation of the dissolved ceramic phases to the polycondensation reaction. This could determine the reprecipitation of Ca-rich phases (e.g. calcium alumino-silicate hydrates as strätlingite, or AFm phases – already found together with C-A-S-H gel in blended systems (Garcia-Lodeiro et al., 2011; García-Lodeiro et al., 2013; Pardal et al., 2009)), and represented by the prismatic morphologies. The higher amount of alumina in the samples with 20% of MK could justify the absence of the prisms, because of the more cross-linked structure which could allow the blocking of the eventual Ca excess within the gel structure. Further investigations are needed in order to confirm this hypothesis.

After all, in the blended systems the type of the final product is determined, besides the reaction conditions and the system's chemistry, by the reaction mechanisms which can involve the evolution of a gel into another and different phase equilibria (Garcia-Lodeiro et al., 2011; García-Lodeiro et al., 2013, 2012; Pachego-Torgal et al., 2014; Yip et al., 2005, 2008). The compatibility of the two gels (N-A-S-H and C-A-S-H) characterizing the hybrid systems is still a key theme of current research (García-Lodeiro et al., 2012).

An exhaustive sequence of SEM image collected on all the samples is exposed in Attachment 6.1.

	3/7	1/1	7/3
0% MK	Compact matrix Granular appearance N,CASH Tufts precipitates (Na+Al+Ca+Si)	Compact matrix Granular appearance N,CASH Filaments	Compact matrix Granular appearance N,CASH Tufts attaching (Ca+Si)
10% MK	Compact matrix Granular appearance Prisms NASH - N,CASH CASH	Compact matrix Granular appearance Prisms NASH - N,CASH CASH	Compact matrix Granular appearance Prisms NASH - N,CASH CASH
20% MK	Compact matrix Granular appearance NASH N,CASH	Compact matrix Granular appearance NASH N,CASH Long whiskers	Compact matrix Granular appearance Botryoidal matrix NASH N,CASH

← Texture density

Fig. 6.12 – Gel type chart of LBCa binders: schematic summary of the SEM-EDS results.

TEM-EDS

Two samples, LBCa 1/1 and LBCa 1/1+20MK, considered representative of the geopolymeric series have been selected and analysed under TEM after 28 days of curing in order to investigate the differences in the geopolymeric gel characteristics between pure ceramic samples and binary mixtures. Fig. 6.13 shows the formation of a different structure of the gel between the two samples. While the one without MK has a quite angular structure, where the profile of pseudo-geometric elements is identifiable, in that with MK these shapes disappear and the general appearance of the fragment analysed is cloudier (granular) and amorphous-like. The diffraction analyses performed in some points of the samples' fragments confirm the amorphous nature of the gel, being sometimes also semi-crystalline. In order to understand the possible distribution of type of gels, N-A-S-H and/or C-A-S-H, a chemical mapping have been carried out. Hereafter it has been reported an overlap of the distribution of Ca and Na elements. As it is possible to see in Fig. 6.14 there is a strictly intermingled Ca-Na composition in this geopolymeric gel. These results could be interpreted as a contemporary formation of both C-A-S-H and N-A-S-H as two phases strictly linked in nanometric structure. The results are consistent with those from the literature (Garcia-Lodeiro et al., 2011).

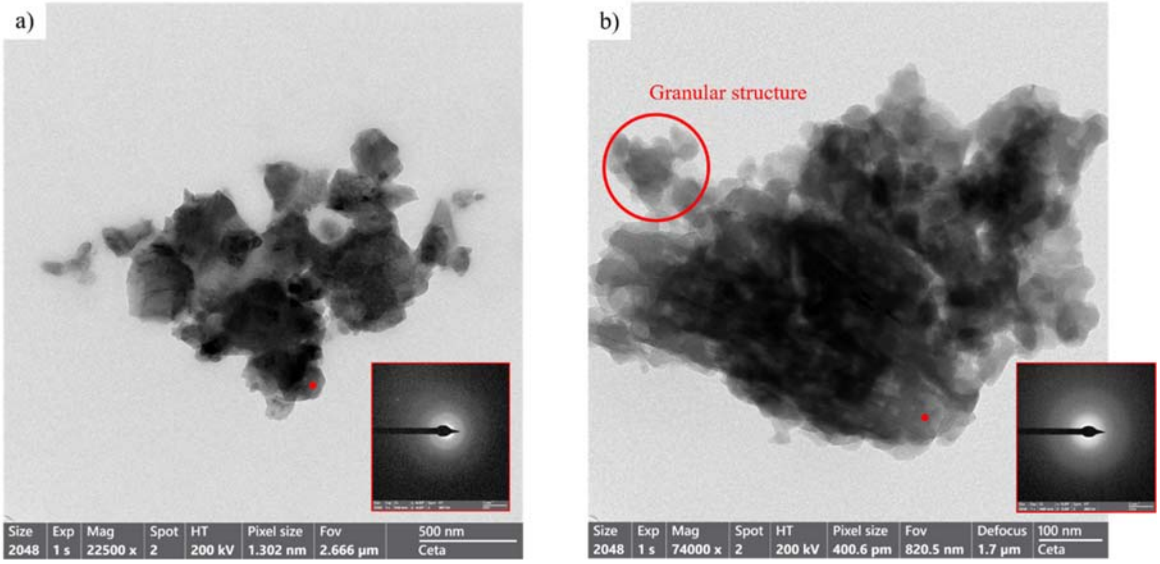

Fig. 6.13 – TEM micrographs of a fragment of sample LBCa 1/1 a) and of LBCa 1/1+20MK b). The image shows also two diffraction patterns obtained in two representative areas, red square.

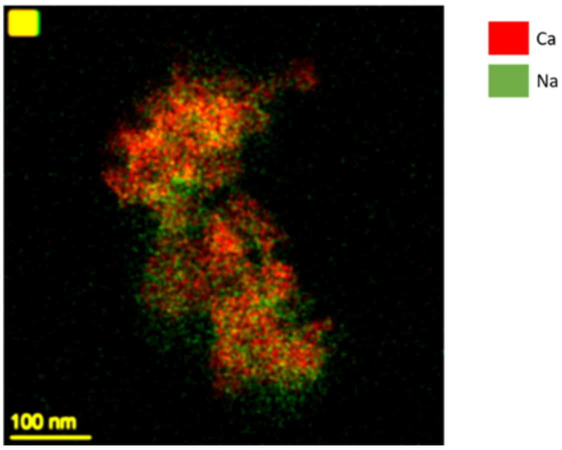

Fig. 6.14 – TEM map overlapping the distribution of Ca and Na on the fragment of LBCa 1/1+20MK visible in Fig. 6.13 b).

6.1.3 Molecular characterization (FTIR-ATR, DRIFT, Raman Spectroscopy)

FTIR-ATR

The FTIR-ATR analysis has been performed on all the binders at 28 days of curing and the obtained spectra have been compared with those of the raw materials (Fig. 6.15). Furthermore, for the comparison of the binary geopolymers, dry mixtures of the raw materials (10% and 20% of MK added to powdered ceramic waste) have been considered.

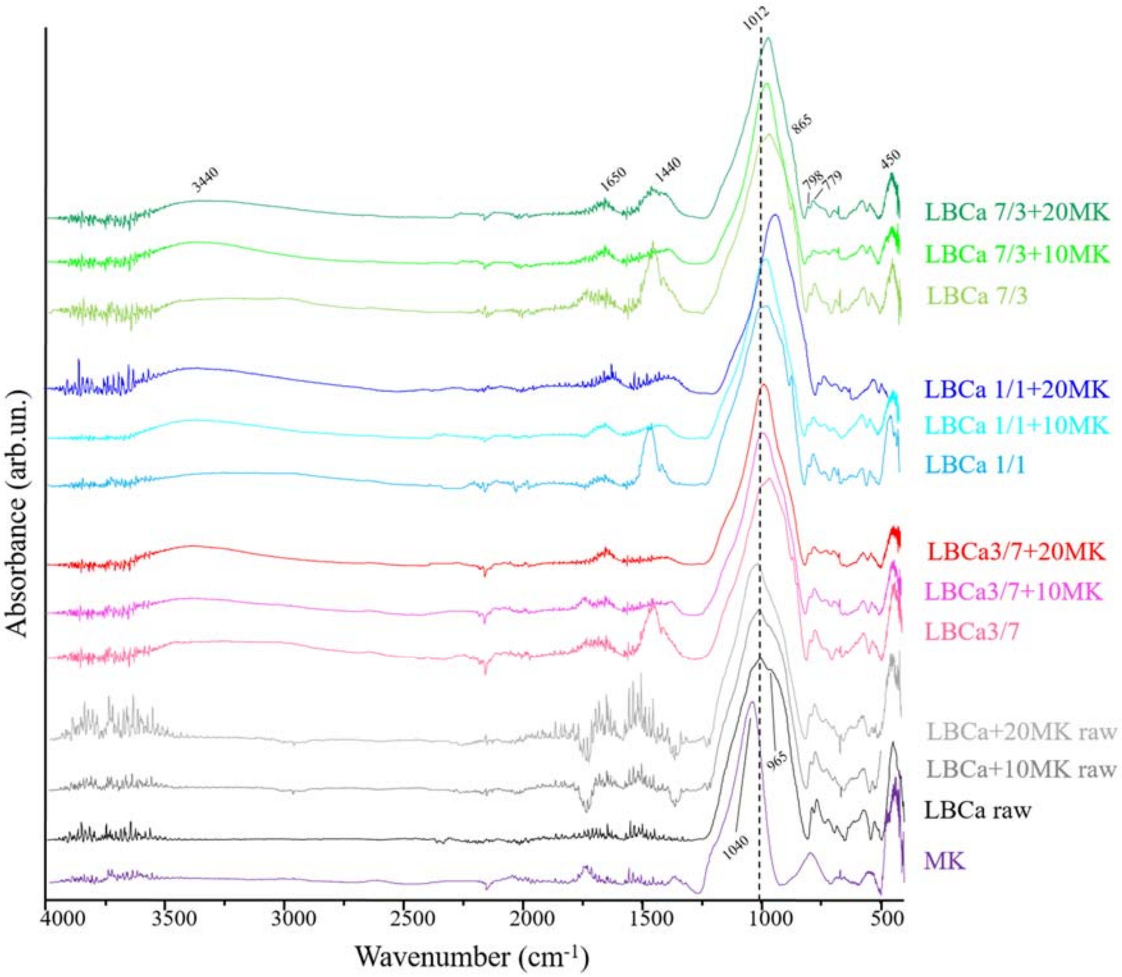

Fig. 6.15 – ATR spectra of the LBCa 3/7, LBCa 1/1 and LBCa 7/3 series, together with the raw materials LBCa, MK and the dry mixtures LBCa+10MK and LBCa+20MK. The spectra have been normalized in order to allow direct comparisons and stacked for clarity.

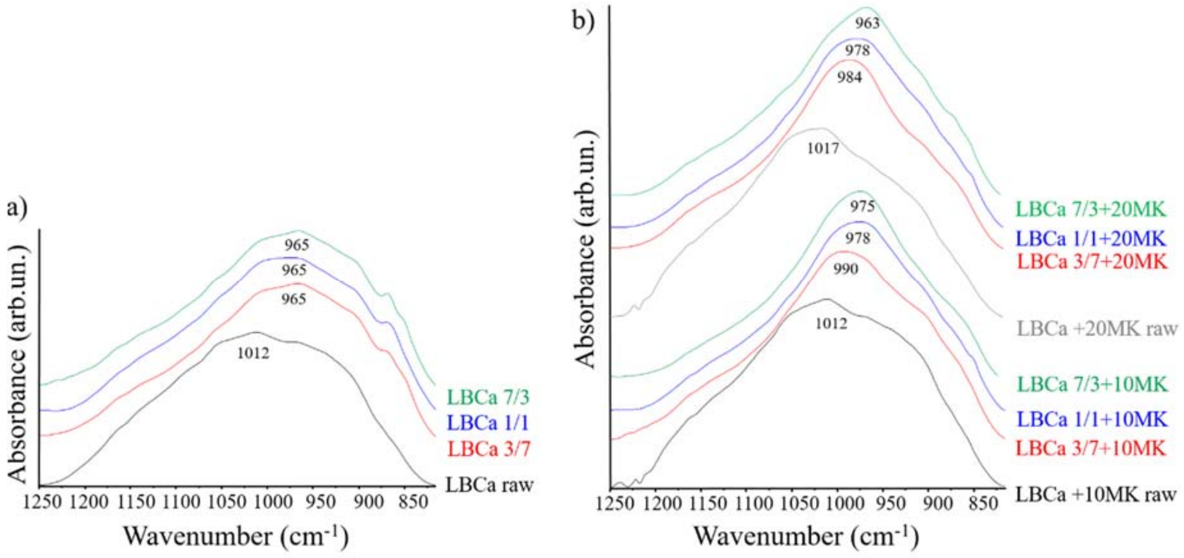

Fig. 6.16 – Zoom of the main band observed in LBCa geopolymer samples without MK, compared with the ceramic raw material LBCa a); zoom of the main band observed in the LBCa geopolymer samples with 10% of MK and 20% of MK, respectively compared with the dry mixtures of the raw materials LBCa with 10% and 20% of MK b). The spectra have been normalized in order to allow direct comparisons and stacked for clarity.

As expected, all the spectra are characterized by a wide and intense band appearing between 1240 and 815 cm^{-1}, the alumino-silicates absorption band (main band). The interpretation of this region may be difficult because of the overlap of the vibrational signals of different compounds, thus determining a highly complex spectrum (Reig et al., 2013).

Overall, Fig. 6.15 highlights a change in the shape of the main band, which is characterized in the raw materials by a broad profile, organized in different components: the position relative to the maximum intensity (marked with a black dotted line in figure), indicating the Si-O-T (T=Al, Si) stretching vibration (Khan et al., 2016; Rovnaník et al., 2018; Tuyan et al., 2018), is centred at 1012 cm^{-1}. A shoulder at 965 cm^{-1} is also highlighted. In the geopolymer spectra, the maximum peak undergoes a shift towards lower wavenumbers. While the samples without MK, maintaining more or less the same shape of the raw material, show the shoulder at 965 cm^{-1} as the new maximum of the main band (Fig. 6.16a), the binary samples show a narrower band with the maximum between 990 and 963 cm^{-1}. In order to obtain more accurate interpretations related to the shift of the maximum of the alumino-silicate band, the region of the main band has been extracted from each spectrum and compared with those of the precursors dry mixtures. Hence, the dry mixture with 20% of MK shows the maximum at 1017 cm^{-1}, conveying the influence of the main absorption band of MK, attested at 1040 cm^{-1}, and the relative geopolymer samples 3/7+20MK, 1/1+20MK and 7/3+20MK respectively at 984, 978 and 963 cm^{-1}, while the dry mixture with 10% of MK shows the maximum at 1012 cm^{-1} and its relative geopolymers 3/7+10MK, 1/1+10MK and 7/3+10KM respectively at 990, 978 and 975 cm^{-1}. The shift appears greater for the geopolymers without MK, while for those with MK it increases with the increase of sodium hydroxide in the slurry and with MK.

This shift occurs due to the formation of alumino-silicate gel (Khan et al., 2016; Robayo et al., 2016), as the asymmetric stretching vibrations of the newly formed Si-O-T bonds promotes the appearance of a new band around 950 cm^{-1} (Hajimohammadi et al., 2011; Rees et al., 2007).

Apart from the main band, other significant ones appear in the geopolymer spectra. The broad band at 3440 cm^{-1} together with the signal at 1650 cm^{-1} represent the stretching and bending vibration of the OH bonds and of the absorbed water molecules in the geopolymer mixtures (Azevedo et al., 2018; Khan et al., 2016; Rovnaník et al., 2018; Tuyan et al., 2018), which is more evident in the samples with MK; the signals at 1440 and 865 cm^{-1}, mostly visible in the samples without MK, represent the O-C-O asymmetric stretching linked to the formation of carbonate phases (Azevedo et al., 2018; Fernández-Jiménez and Palomo, 2005; Komnitsas et al., 2015; Robayo et al., 2016; Rovnaník et al., 2018). The band at around 450 cm^{-1} decreases in intensity comparing the geopolymers in respect to the raw materials: this could be attributed to the dissolution of Al-O and Si-O species with subsequent formation of Si-O-Al bonds, as reported by Azevedo et al. (2018).

Furthermore, looking at the doublet 798 and 779 cm^{-1}, distinctive of quartz, it is possible to notice a consistent intensity reduction in the geopolymer spectra in comparison with the raw material, thus indicating quartz partial reaction (Reig et al., 2013).

In order to acquire deeper information related to the possible correlations among the samples, Principal Component Analysis (PCA) has been performed. The results are reported in Fig. 6.17. The first three PCs represent a cumulative variance of 99%.

In the score plot (Fig.6.17a), small clusters are visible. According to PC1, samples without MK (positive values) and binary mixtures (negative values) can be distinguished. PC2, instead, differentiates samples according to the sodium hydroxide/waterglass ratio: the negative values influence the samples with 7/3 ratio and the positive ones those with 3/7 ratio; 1/1 samples are intermediate. The loadings diagram (Fig.6.17b), indeed, shows that negative values of PC2 are linked to lower wavenumber positions of the main alumino-silicate band, as observed for 7/3 samples in Fig. 6.16, with a gradual increasing trend towards 3/7 ones.

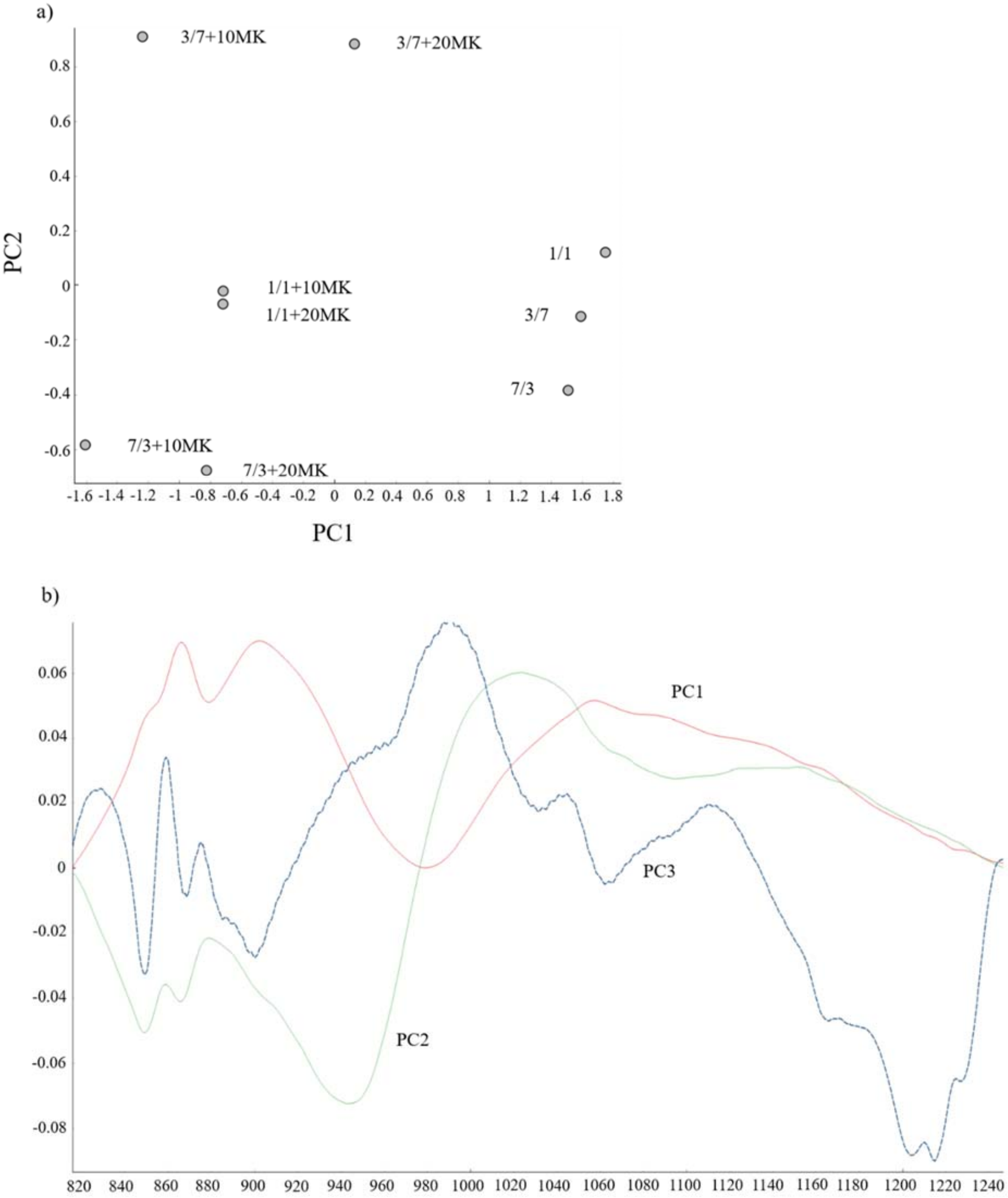

Fig. 6.17 – Score plot (PC1 and PC2) of the 9 ATR spectra with PCA treatment a); Loadings diagram of the first three principal components b).

DRIFT (focus on the application of the technique for the geopolymers investigation)

In order to study the applicability of this technique on the geopolymeric materials, all the LBCa geopolymer series have been analysed after 28 days of curing. For comparison the raw materials have also been investigated.

Representative DRIFT spectra of both raw materials (MK and raw LBCa ceramic) and geopolymers are shown together in Fig. 6.18.

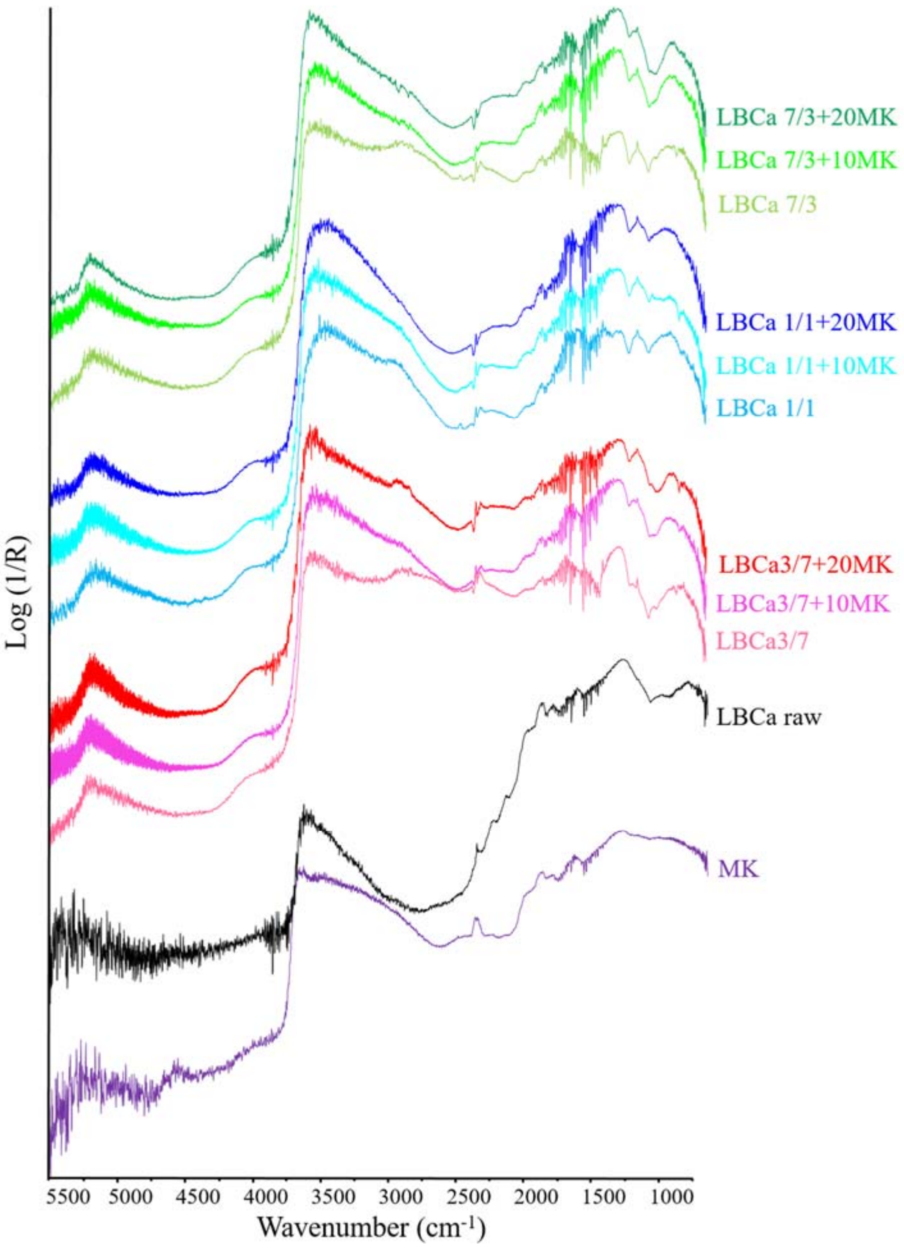

Fig. 6.18 – DRIFT spectra of LBCa geopolymer samples and the relative raw materials. The spectra are stacked for clarity.

The spectra are quite noisy, nevertheless it is possible to discern:

1) a water-connected band around 5200 cm^{-1} (Frost and Jonansson, 1998; Madejová and Komadel, 2001), better defined for the geopolymers;

2) a very broad band ranging from 3700 to 2700 cm^{-1} probably linked, together with the noisy signal around 1620 cm^{-1}, to the hydroxyl groups (Belver et al., 2005; Mladenović et al., 2020); since it appears broader for MK rather than for raw ceramic it may also be attributed to alumina, silica-alumina, or γ-Al_2O_3 (Belver et al., 2005). The band profile of the geopolymers shows additional shoulders (i.e. newly formed bonds);

3) the alumino-silicates signals in the region 1300-900 cm^{-1} (Aly et al., 2008).

The latter deserve a closer observation and a detailed analysis. For this reason, all the spectra were cut to extract the region of interest (1300-900 cm^{-1}) and subjected to a linear baseline subtraction, they were then smoothed and normalized to the intensity of the band between 1064 and 1079 cm^{-1}. The results are visible in Fig. 6.19.

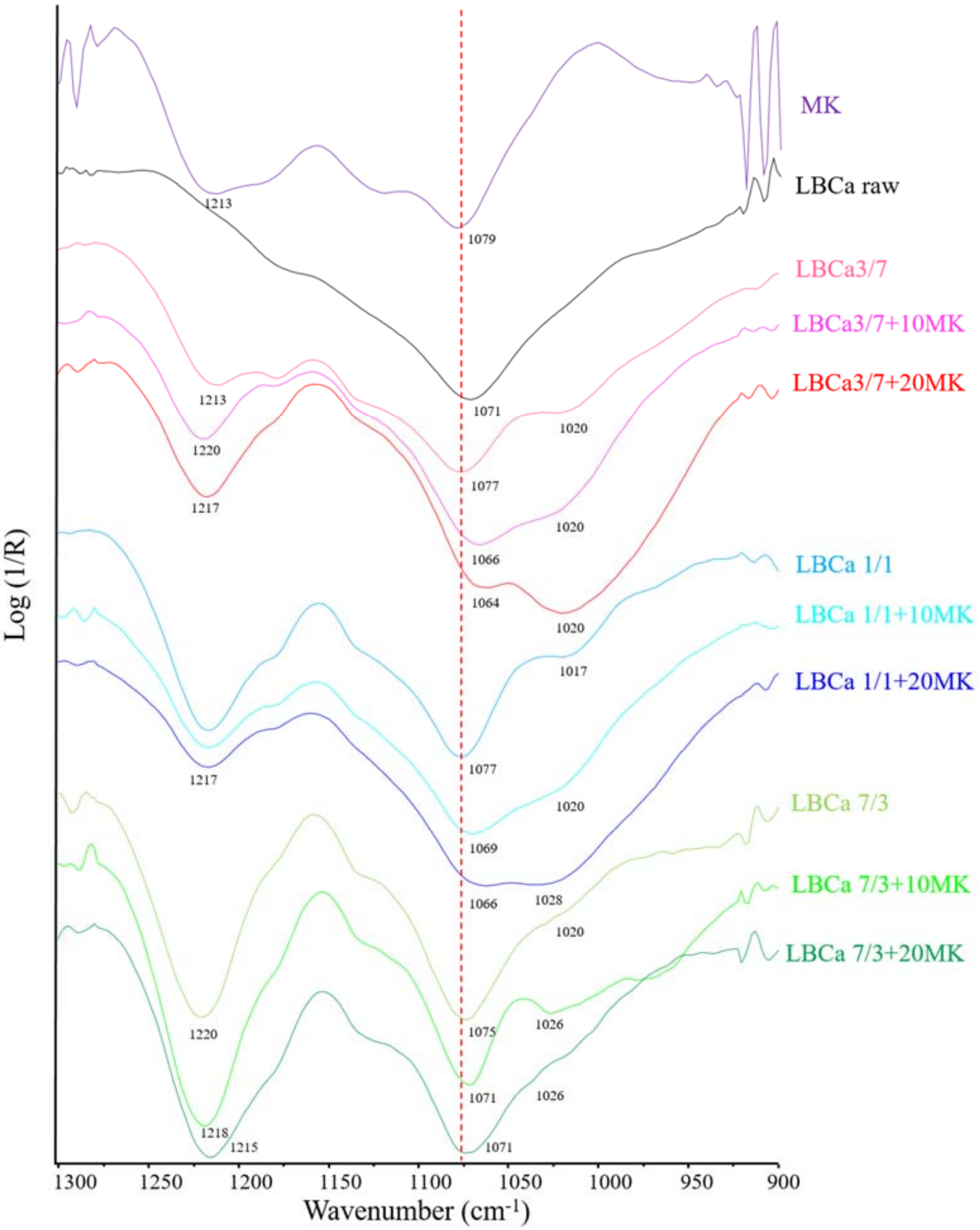

Fig. 6.19 – DRIFT spectra of the MK and ceramic precursor and the respective geopolymers in the 1400-700 cm^{-1} range. The spectra are stacked for clarity.

Overall, a shift towards lower wavenumber of the principal band (1064-1077 cm^{-1}) is observed with respect to MK main position (1079 cm^{-1}). On the other hand, with respect to raw ceramic precursor (1071 cm^{-1}), the shift is more visible for geopolymers formulations including MK, especially for 3/7 and 1/1 mixtures (1064-1069 cm^{-1}). According to Mladenović et al. (2020) the band shift indicates the occurred geopolymerization, as much as it does for absorbance infrared spectra.

Another event must be underlined in the geopolymers DRIFT spectra: the appearance of a shoulder centred between 1017 and 1028 cm^{-1}. In two cases, coinciding with the samples showing the largest shift, i.e. samples 1/1+20MK and 3/7+20MK, this new band cannot be considered anymore a shoulder, since it respectively reaches or overcomes in intensity the one at ca. 1065 cm^{-1}. Following the experimentation of Aly et al. (2008), a principal band centred at about 1065 cm^{-1} would imply a high Si/Al ratio (~4), whilst, the appearance of a component at lower wavenumbers as the most intense band (~1020 cm^{-1}) would mean a lowering of the Si/Al ratio to a value between 2.5 and 3.

Furthermore, even though a band decomposition would lead to more precise considerations, it seems clear that a higher intensity of the ~1220 cm^{-1} band in the samples of the 7/3 set, to which corresponds a lower intensity of the newly formed ~1020 cm^{-1} band, could be linked to a higher crosslinking, assigned to the formation of Q4 species (SiO_4 tetrahedra connected at all four corners with Si/Al species) (Alipour et al., 2016).

Lastly, differently to what observed in the FTIR-ATR spectra, the shift of the ~1070 cm^{-1} signal of the 7/3 samples is less noticeable in respect to the others.

This difference is confirmed by the PCA carried out on the treated spectra (Fig. 6.20): negative PC1 and positive PC2 characterize all the 7/3 spectra, LBCa 1/1 score is located very close to them. Another spectrum with low intensity of the ~1020 cm^{-1} shoulder is that of sample 3/7 without MK, separated from the other 3/7 samples due to its negative PC1, while the spectrum with the most intense ~1020 cm^{-1} band is that with the highest value of PC1: LBCa 3/7+20MK, as it can be observed in the PC1 loadings curve.

The first three PCs account to a cumulative variance of 96.2%.

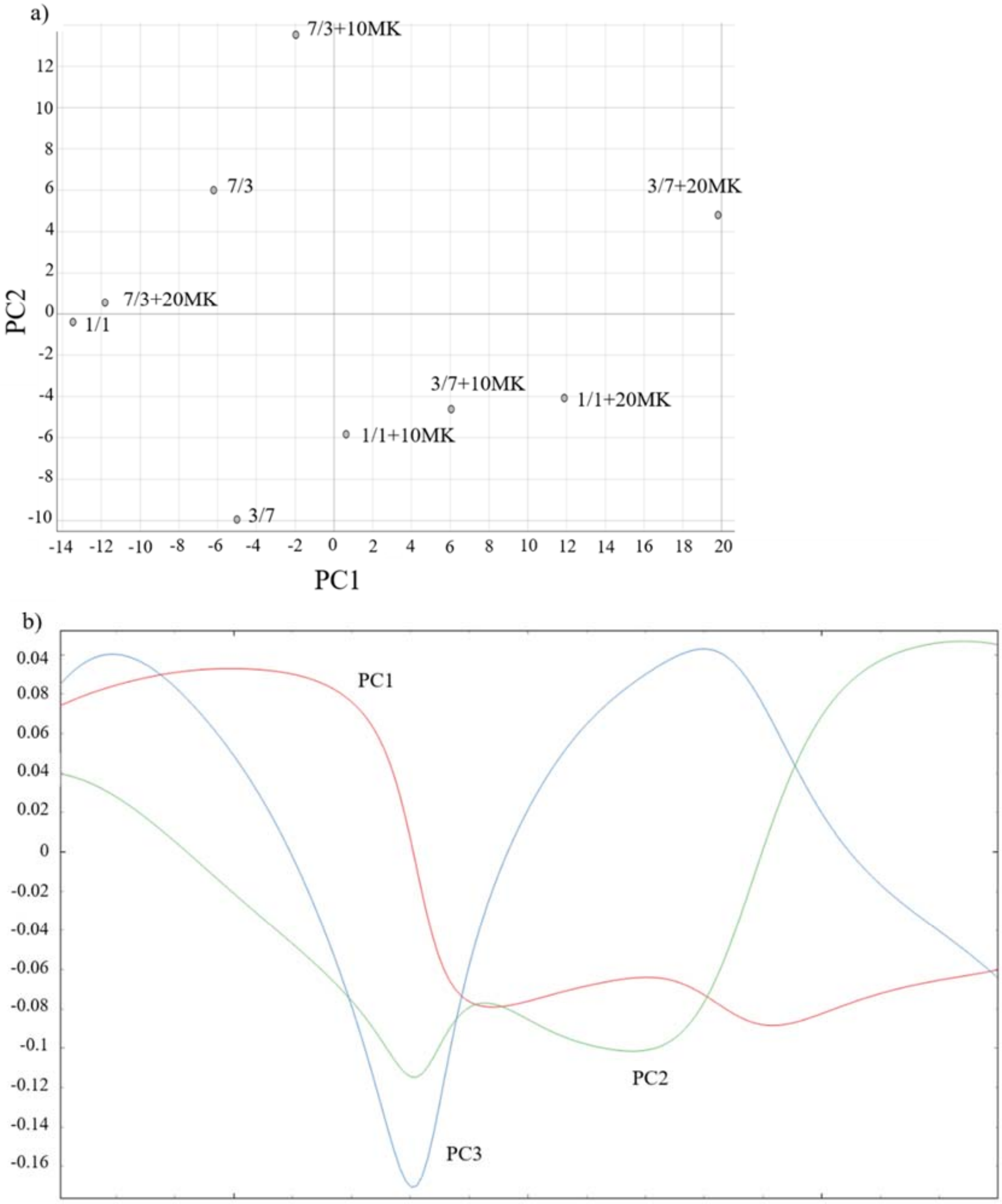

Fig. 6.20 – Score plot (PC1 and PC2) of the 9 DRIFT spectra with PCA treatment a); Loadings diagram of the first three principal components b).

Raman Spectroscopy (focus on the application of the technique for geopolymers investigation)

Representative Raman results obtained on the ceramic precursor and the different geopolymers formulations are reported in Fig. 6.21.

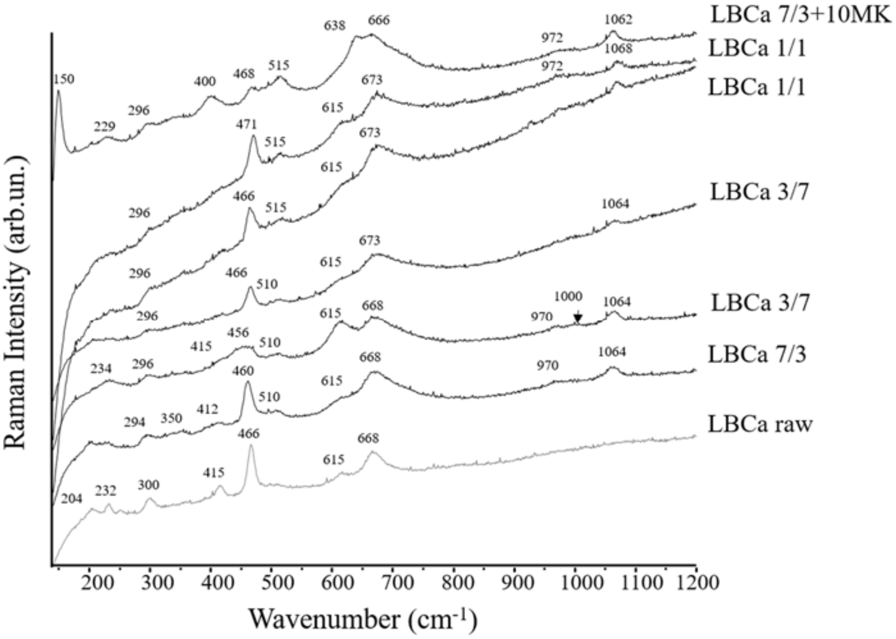

Fig. 6.21 – Representative Raman spectra of LBCa ceramic waste precursor and respective geopolymers. The spectra are stacked for clarity.

Firstly, it is observed the recurrence of haematite signature (around 232, 294 and 415 cm^{-1}) (Froment et al., 2008); furthermore, the samples including MK show anatase signals too, as expected. In MK TiO_2 is present (=1.88% by XRF), in the Raman measurements this clearly appears as anatase from the band at 145 (here cut by Notch filter and appearing as a broad, intense feature at the beginning of the spectrum), 200, 395, 518, 638 cm^{-1} (Murad, 1997). Attention must be paid to the band ranging from 460 to 471 cm^{-1} connected to quartz: according to (Kosor et al., 2016a), its broadening and shift would hint to the formation of a differently structured alumino-silicate material. This is evident especially in the case of 3/7 sample where it appears broadened and shifted to 456 cm^{-1} and connected to the 615 cm^{-1} band, whose intensity excludes its association to haematite. It could be due instead to the broken Si–O–Si bonds of siloxane rings vibrations (Kosor et al., 2016a). The 456 cm^{-1} band is too shifted to ascribe these signals to rutile (Murad, 1997). Almost all the spectra exhibit a band between 1062 and 1068 cm^{-1}, together with a weaker one around 970 cm^{-1}.

The attribution to Q3 and Q2 type stretching vibration of the silicate tetrahedron with aluminium presence can be hypothesized (Kosor et al., 2016a, 2016b; Renaudin et al., 2009; Rüscher et al., 2010; Xu et al., 2018). On the other hand, the finding of small quantities of thermonatrite by means of XRD measurements, which is reported to display its principal band at about 1067 cm^{-1}, could question this attribution (Jentzsch et al., 2013). Considering the most diffused interpretation of these bands in the literature as connected to the alumino-silicate structure of geopolymers, a focus on the region between 890 and 1160 cm^{-1} was carried out comparing the ceramic precursor and the different geopolymers formulations (Fig. 6.22). These spectra were baseline-subtracted with LabSpec software using linear segments at fixed points for all the samples.

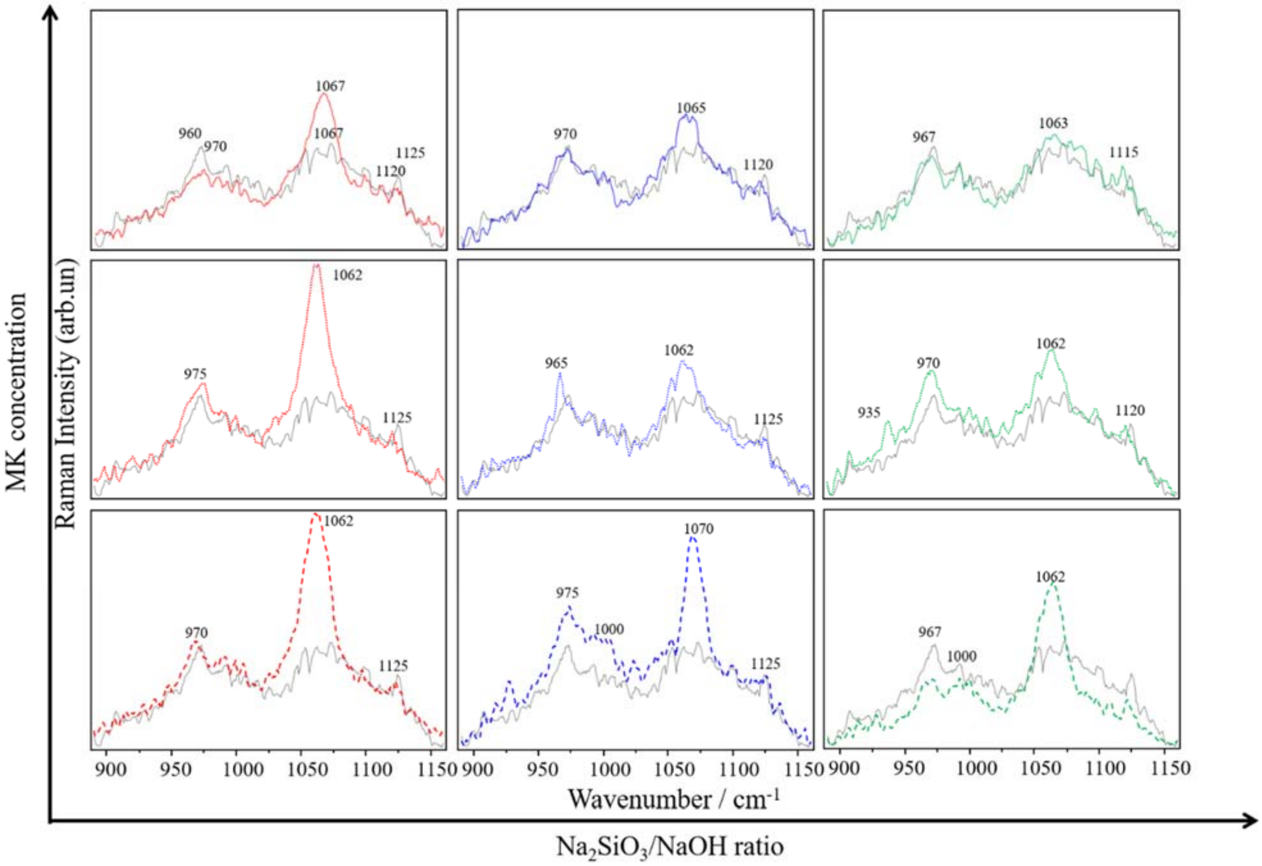

Fig. 6.22 – Representative baseline-subtracted Raman spectra in the 890–1160 cm^{-1} region of LBCa ceramic waste precursor (in grey) and respective AAMs (dashed: no MK addition; dotted: 10% MK; full: 20% MK; red: NaOH/Na_2SiO_3=7/3; blue: NaOH/ Na_2SiO_3=1/1; green: NaOH/Na_2SiO_3=3/7).

The 1062–1070 cm^{-1} band is observed to decrease in intensity going with increasing MK content; the same trend is visible with the increase of waterglass to NaOH in the activators mixture. If the band at ca. 1065 cm^{-1} band is associated to Q3 units (Kosor et al., 2016a, 2016b; Rüscher et al., 2010; Xu et al., 2018), it must be deducted that samples activated with a higher percentage of NaOH and those with 0% or 10% of MK in the precursor perform a higher structural crosslinking (higher three-dimensional structural organization), as already highlighted by FTIR-ATR. Furthermore, it can be noted how the spectrum of sample 3/7 does not exhibit the shoulder at approximately 1120 cm^{-1} characterizing all the other materials and probably to be interpreted as Q4 units (Arnoult et al., 2018). However, it should be considered that the geopolymeric systems are heterogeneous and complex systems, while these measurements are punctual.

Sample 3/7+20MK was chosen to carry out Raman analyses during geopolymerization because it displayed the shortest setting time. The most significant results are shown in Fig. 6.23. The spectrum of the material 10 min after its synthesis shows a 970 cm^{-1} band, interpreted as Q2 units (Kosor et al., 2016a, 2016b; Renaudin et al., 2009; Rüscher et al., 2010; Xu et al., 2018) and a much weaker one at 1044 cm^{-1}; the latter must be due to the used activating solution with maximum at approximately 1038 cm^{-1}. The first evidence of quartz (460 cm^{-1}, blue line) appears after 90 min, whereas anatase's presence or absence (red line) could be due to micro-movements of the sample during setting exceeding the spatial resolution of the used microscope. After 370 min, the spectrum flattens and, as visible in Fig. 6.23b where the spectra are shown without stacking, fluorescence gradually increases with time. It can be hypothesized that at this moment, the different processes involved in the geopolymerization mechanism take place at the same time.

The analyses performed in the high wavenumber region on mature samples (Fig. 6.24) highlighted the appearance of the OH stretching band at 3440 cm^{-1} in sample 7/3+20MK (Mierzwiński et al., 2019; Steinerová and Schweigstillová, 2013; Szechyńska-Hebda et al., 2019), better visible in sample 7/3, and at 3630 cm^{-1} in 1/1+20MK. The latter could account for Si-OH cohesive interactions similar to the non-hydrogen-bonded OH groups in liquid water (Walrafen, 1975).

A correlation between the spectral components (position/relative intensity) in the region 890–1160 cm^{-1} and the different formulations could lead to useful indications about their final local structure. The latter is indeed strongly dependent on the reactivity of the raw materials but also on the mix design (raw materials and alkali solution proportion); therefore, it can preliminarily suggest if the chosen parameters lead toward a more or less crystalline or amorphous product. The hydroxyl group revelation in the high wavenumber region of the spectra furthermore proved as Raman spectroscopy could be successfully applied when information about the degree of AAM hydration is required (Caggiani et al., 2021).

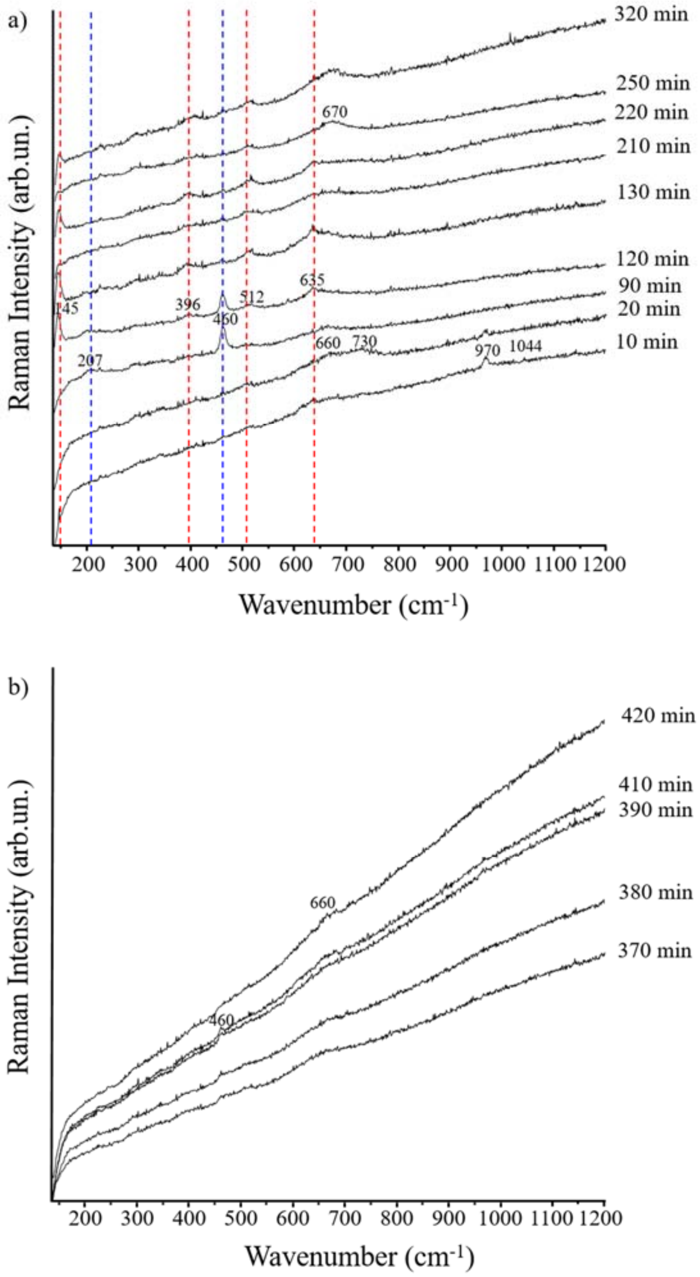

Fig. 6.23 – Representative Raman spectra of LBCa 3/7+20MK during geopolymerization.

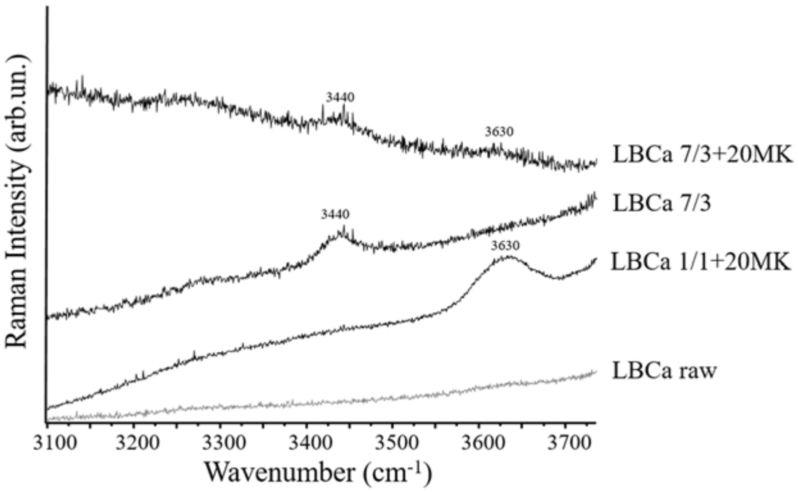

Fig. 6.24 – Representative Raman spectra of clay and LBCa ceramic waste precursors and respective AAMs in the 3100–3700 cm^{-1} spectral region. The spectra are stacked for clarity.

6.1.4 Mercury Intrusion Porosimetry (MIP)

All the binders have been studied with Mercury Intrusion Porosimetry in order to investigate their porous structure. The bulk density is also obtained. All the data (bulk density, accessible porosity, total pore volume, average pore diameter, modal pore diameter and incremental volume of the pores) are shown in Table 6.1.

		LBCa 7/3	LBCa 7/3+10 MK	LBCa 7/3+20 MK	LBCa 1/1	LBCa 1/1+10 MK	LBCa 1/1+20 MK	LBCa 3/7	LBCa 3/7+10 MK	LBCa 3/7+20 MK
Bulk density (g/cm^3)		1.84	1.84	1.76	1.92	2.16	1.65	1.85	1.79	1.76
Accessible Porosity (%)		32.37	28.11	32.09	26.85	30.56	28.42	27.88	27.15	26.92
Total Pore Volume (cm^3/g)		0.18	0.15	0.18	0.14	0.14	0.17	0.15	0.15	0.15
Average Pore Diameter (μm)		0.29	0.26	0.24	0.94	0.13	0.04	0.46	0.09	0.04
Modal Pore Diameter (μm)		0.77	0.60	0.47	2.19	0.25	0.06	2.19	0.14	0.05
Incremental Volume (cm^3/g)	100-10 μm	0.07	0.02	0.00	0.08	0.01	0.00	0.02	0.01	0.00
	10-1 μm	0.72	0.21	0.02	7.22	0.03	0.01	6.96	0.02	0.00
	1-0.1 μm	76.84	39.99	37.24	16.07	38.78	0.01	24.71	19.96	0.00
	0.1-0.01 μm	45.52	21.96	24.18	13.78	26.28	109.47	17.85	46.21	98.02
	0.01-0.001 μm	16.91	7.49	9.09	6.14	7.05	9.77	7.36	7.56	9.45

Table 6.1 – Porosimetric data of the LBCa geopolymeric slurries.

Bulk density and percentage of accessible porosity, as well as the total pore volume, remain more or less on the same values for all the samples (accessible porosity of ca. 30%); what changes is the porosimetric distribution on the different ranges. The more abundant porosimetric range is represented by the fractions 1-0.1 and 0.1-0.01 μm, with a prevalence of the coarser one, excepting for the samples 1/1+20MK and 3/7+20MK where the most prevalent is the 0.1-0.01 μm fraction.

In order to study the influence of MK in the formulation, each series has been considered separately (Figg. 6.25, 6.26 and 6.27); furthermore, for comparison the extreme samples of the whole series have been observed together (Fig. 6.28). Overall, with the increase of MK in the slurries the pore diameter decreases. This phenomenon is well visible for the 3/7 series where the addition of 20% of MK determines a decrease of the average pore diameter from the range 10-1 μm (with a peak at 2.5 μm) to 0.1-0.01 μm, while it is only slightly visible for the 7/3 series.

In order to study the influence of waterglass content in the slurry, the samples without MK have been compared (Fig. 6.29). Sample 7/3, with lower waterglass, shows a porosity characterized by a visibly smaller pore dimension, while the other two samples could be considered identical.

From this data overview it is possible to affirm that the parameters which mainly affect the porous structure of these geopolymers is MK and that, if from one side it is responsible of the reduction of pore diameters, it does not affect the volume percentage.

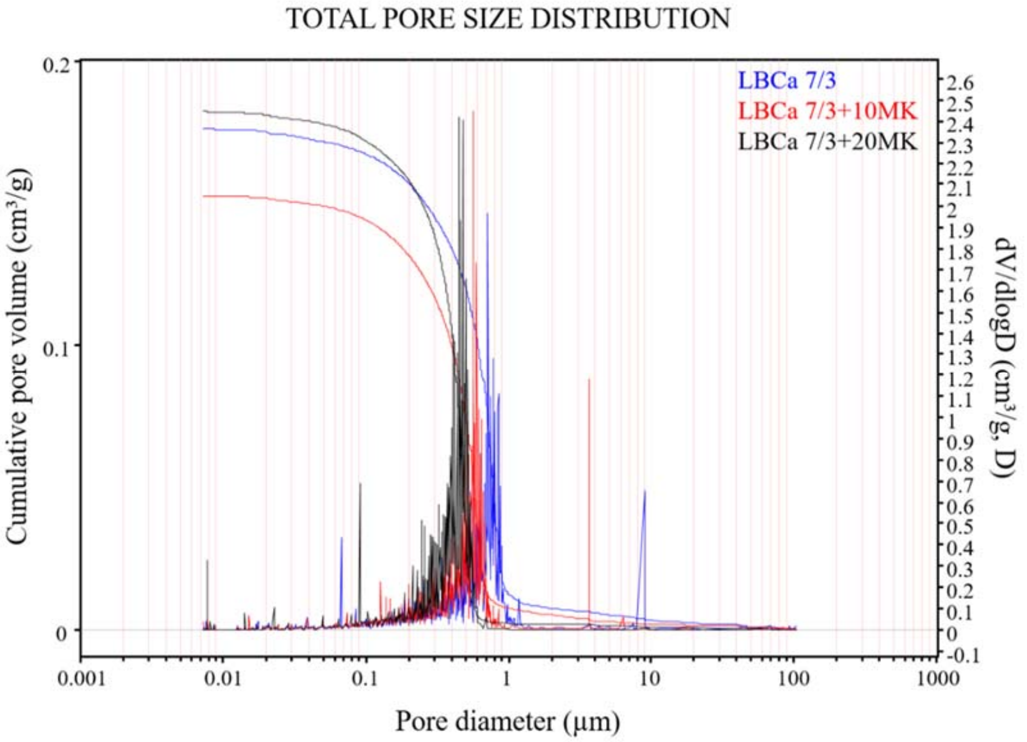

Fig. 6.25 – Total pore size distribution of the 7/3 series.

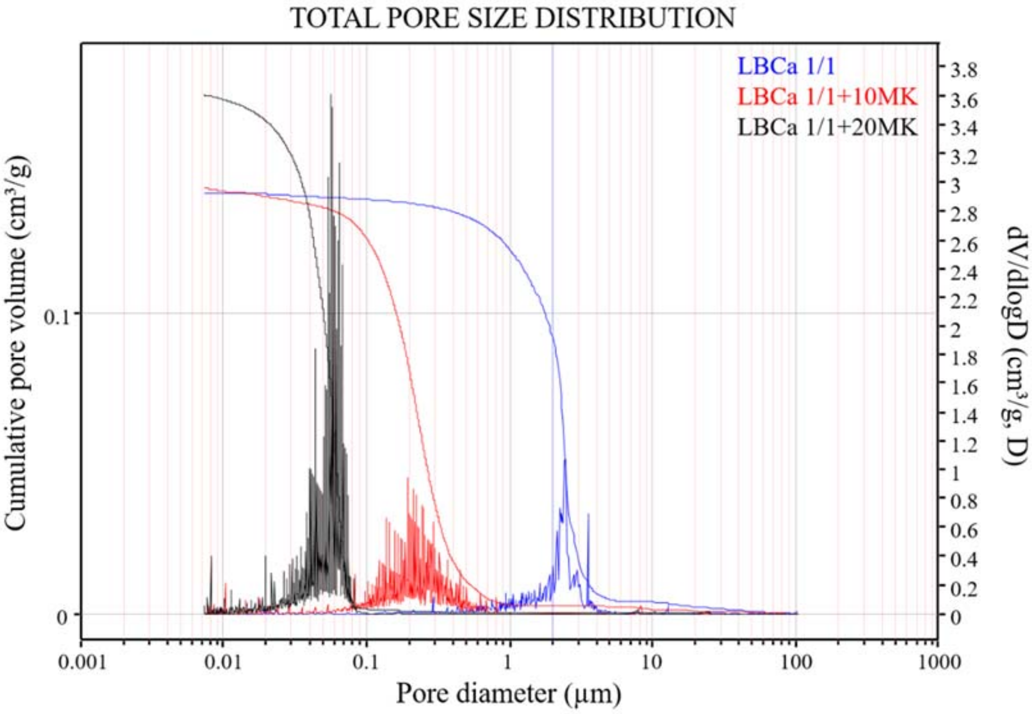

Fig. 6.26 – Total pore size distribution of the 1/1 series.

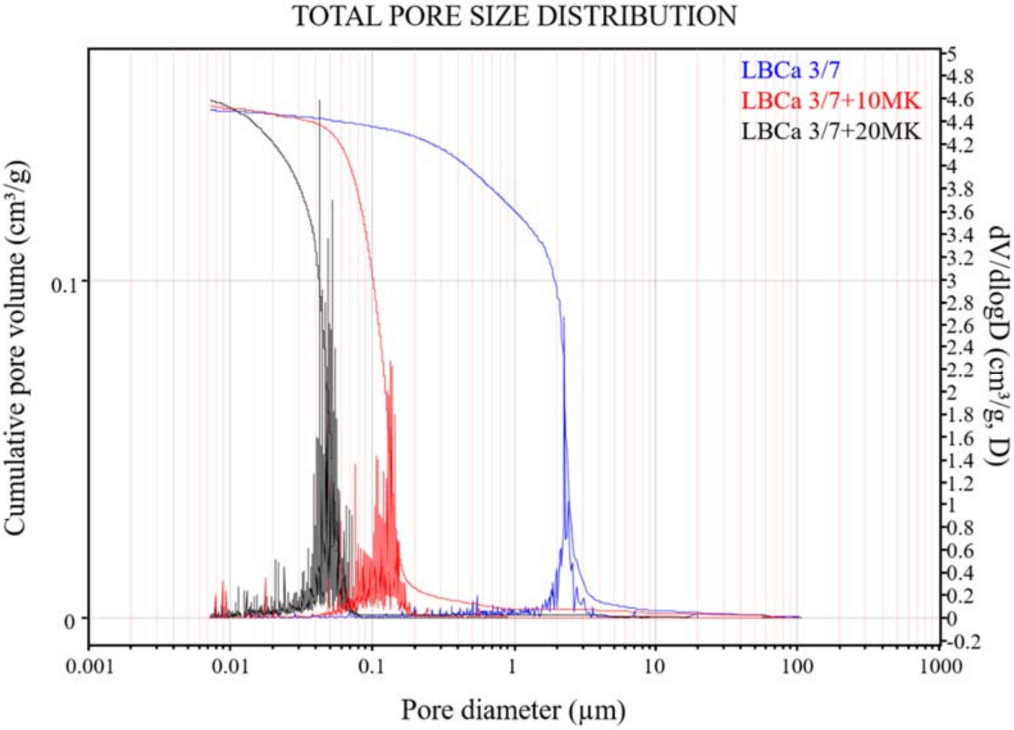

Fig. 6.27 – Total pore size distribution of the 3/7 series.

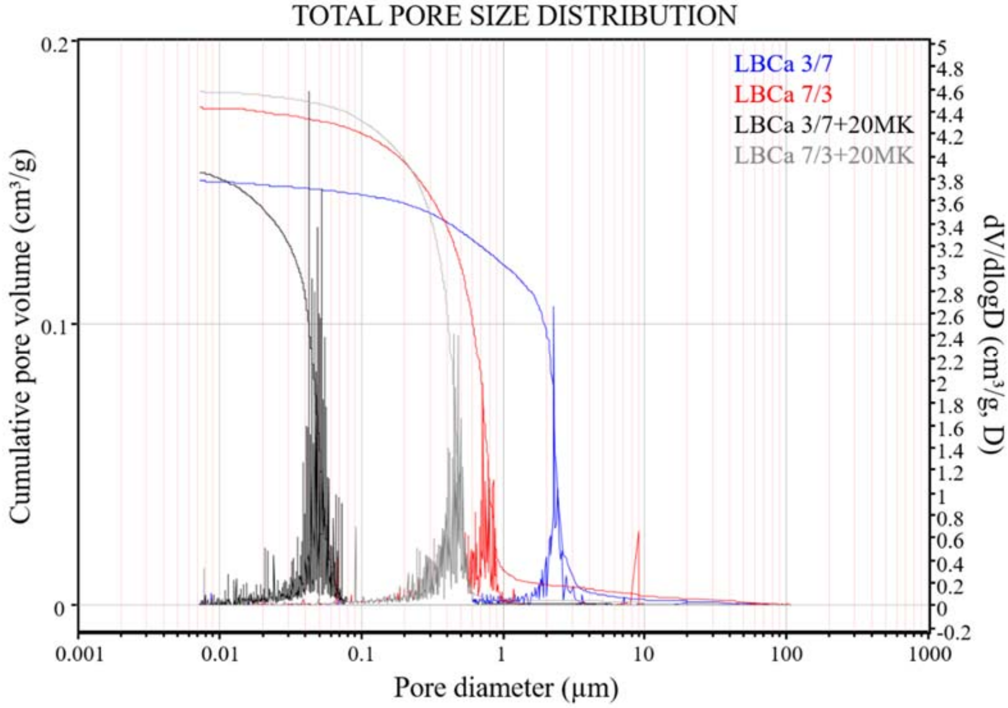

Fig. 6.28 – Comparison of the total pore size distributions characterizing the extremes of the series: LBCa 3/7, LBCa 3/7+20MK; LBCa 7/3 and LBCa 7/3+20MK, representative samples of the entire studied geopolymers.

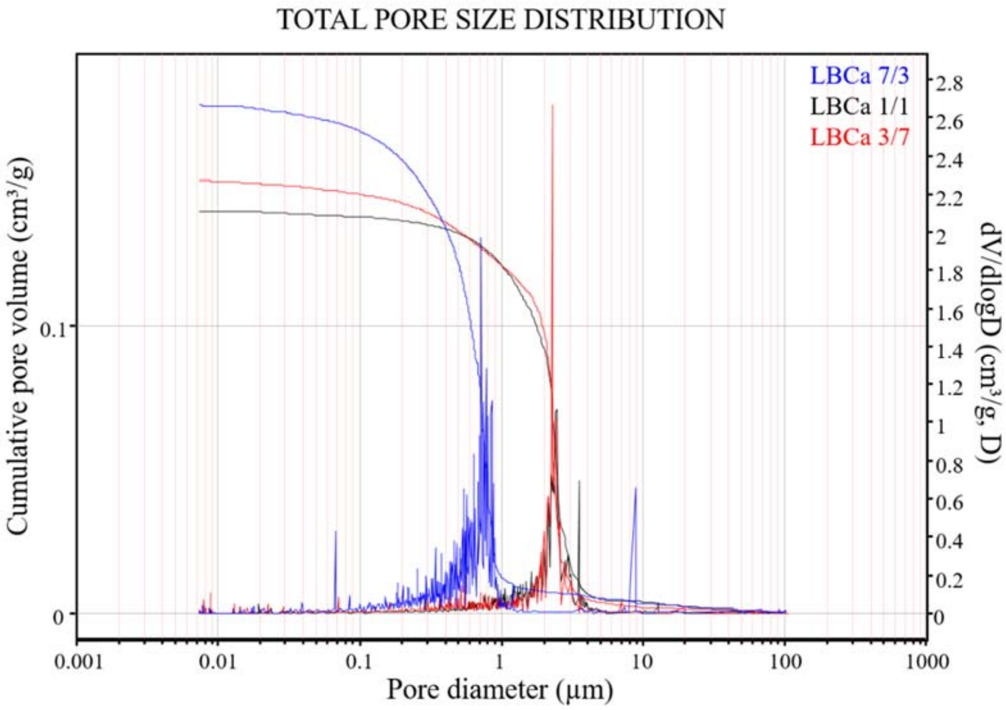

Fig. 6.29 – Comparison of the total pore size distributions characterizing samples without MK, in order to study the influence of waterglass on the porous structure.

6.1.5 Mechanical characterization – uniaxial compressive test

The results obtained by uniaxial compressive test, performed at University of Granada on three samples of 2*2*2 cm for each formulation, showed a not homogeneous behaviour, barely attributable to mixing design variations; it is possible to notice how the samples with 10% of MK registered very variable values from one sample to another, showing a very high standard deviation. The data relative to the samples with 20% of MK could be considered instead more reliable (Fig. 6.30). The samples without MK have not been tested because they did not harden even after one week of curing, thus they have been lost when demoulded.

The Coefficient of Variation (CoV), measured as standard deviation/data average, has been calculated on these results, obtaining values exceeding the threshold of acceptability (fixed at 0.15 by the actual legislation - D. Min. Infrastrutture 14/01/2008).

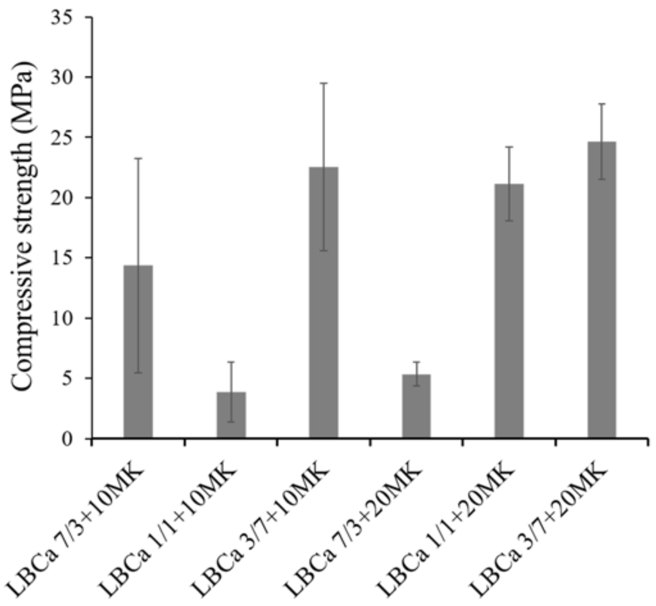

Fig. 6.30 – Compressive strength average, measured on the samples with MK at University of Granada. The standard deviation bar is indicated.

Due to these results, it was decided to perform again the test increasing the number of samples, in order to obtain a more reliable standard deviation. The samples without MK have also been tested this time, as they were allowed to harden for two weeks before demoulding. The tests have been performed at University of Catania and the results are shown in the Fig. 6.31, while all the data are visible in Table 6.2.

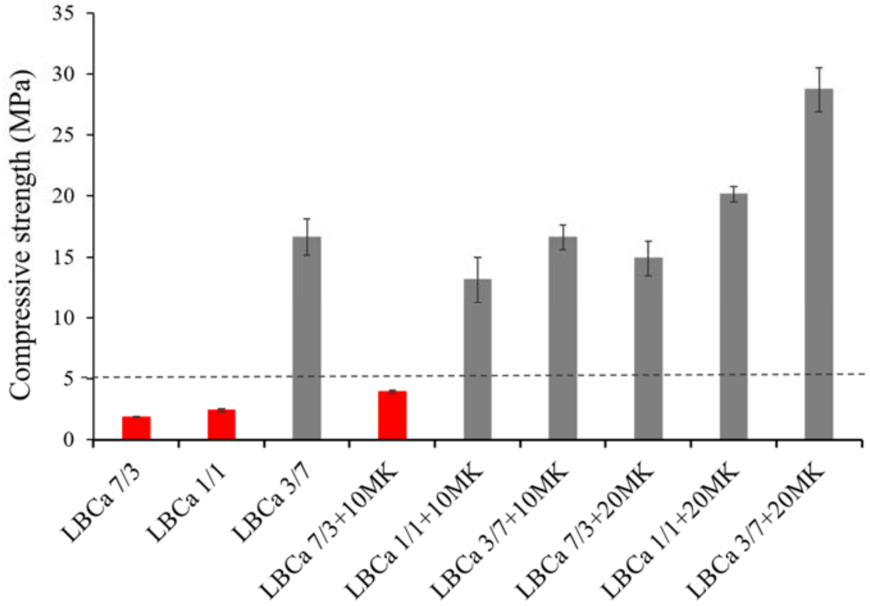

Fig. 6.31 – Compressive strength average, measured on all the experimented geopolymers, at University of Catania. The standard deviation bar is indicated.

The compressive strength seems to increase with the increase of the percentage of MK and waterglass in the binders, as expected (Azevedo et al., 2018; Granizo et al., 2007; Komnitsas and Zaharaki, 2007; Occhipinti et al., 2020; Panizza et al., 2018; Pathak et al., 2014; Reig et al., 2013; Robayo et al., 2016; Rovnaník et al., 2018). The higher value is indeed registered for sample 3/7+20MK, followed by sample 1/1+20MK, respectively with 28.72 and 20.14 MPa. Intermediate values are instead registered for the intermediate formulations, those with 10% of MK, respectively with 16.61 and 13.11 MPa. The binders with the 7/3 ratio of sodium hydroxide/waterglass show the lowest values of resistance and a low brittle behaviour; in particular, samples 7/3 and 7/3+10MK do not meet the threshold of 5 MPa, arbitrarily chosen to consider the geopolymeric binder acceptable according to the desired applications in this research project. Also, sample 1/1 does not overcome that value.

Worth to note is the peculiar behaviour of sample 3/7, which reaches resistances comparable to samples with 10% of MK.

According to the standard deviation, the sample with more reliable results is 1/1+20MK.

All the data acquired, after the exclusion of the aberrant ones, show CoV values well below the threshold and can be considered of high quality with respect to the technical legislation of concretes (D. Min. Infrastrutture 14/01/2008).

Many factors could influence the compressive strength of this type of materials, as the curing conditions, the compactness, etc. The latter could depend on the moulding step, as well as on air bubbles not expelled during the vibration step which could leave behind very important pores (Winter, 2009). Hence, it is important to consider a high number of samples paying attention to the standard deviation and CoV values.

Fig. 6.32 shows the typical failure mode of the compressive tests on the tested samples. Under compression, the samples have shown abrupt failure, typical of cements (Deere and Miller, 1966; Occhipinti et al., 2020), with a detachment of the external walls. Only the samples with compressive strength lower than 10 MPa show a soft disintegration under compression.

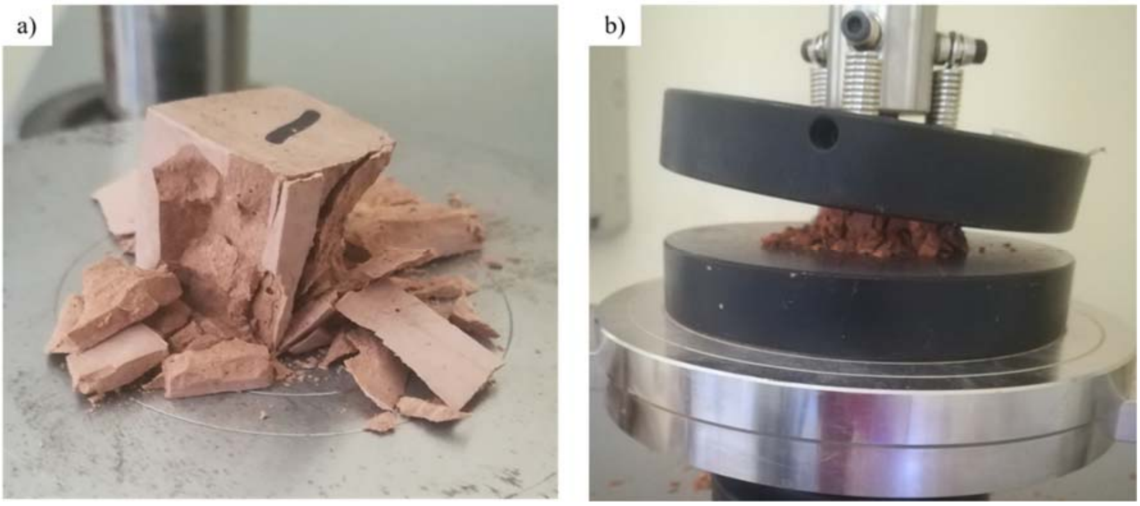

Fig. 6.32 – Typical failure mode of the majority of the samples a) and of the softer ones b).

Sample	Resistance (MPa)	Average value	St. Dev.	Bottom limit	Up limit	Accepted values	New average	New St. Dev.	Bottom limit	Up limit	Variation coeff.
LBCa 3/7_1	13.00	17.63	3.68	13.95	21.32	15.03	16.62	1.48	15.14	18.09	0.09
LBCa 3/7_2	14.68					14.68					
LBCa 3/7_3	18.34					18.34					
LBCa 3/7_4	17.71					17.71					
LBCa 3/7_5	17.32					17.32					
LBCa 3/7_6	24.75										
LBCa 1/1_1	2.37	2.48	0.18	2.30	2.66	2.37	2.42	0.12	2.30	2.53	0.05
LBCa 1/1_2	2.26					2.26					
LBCa 1/1_3	2.59					2.59					
LBCa 1/1_4	2.81										
LBCa 1/1_5	2.50					2.50					
LBCa 1/1_6	2.36					2.36					
LBCa 7/3_1	1.83	1.87	0.05	1.82	1.92	Being the standard deviation already acceptable, no more data elaboration has been performed.					0.03
LBCa 7/3_2	1.90										
LBCa 7/3_3	1.83										
LBCa 7/3_4	1.96										
LBCa 7/3_5	1.83										
LBCa 7/3_6	/										
LBCa 3/7+10MK_1	17.88	17.48	3.42	14.06	20.90	17.88	16.61	1.01	15.60	17.62	0.06
LBCa 3/7+10MK_2	15.08					15.08					
LBCa 3/7+10MK_3	16.54					16.54					
LBCa 3/7+10MK_4	13.87										

LBCa 3/7+10MK_5	16.96					16.96					
LBCa 3/7+10MK_6	24.56										
LBCa 1/1+10MK_1	15.38	12.76	2.60	10.16	15.36		13.11	1.85	11.25	14.96	0.14
LBCa 1/1+10MK_2	9.77										
LBCa 1/1+10MK_3	11.25					11.25					
LBCa 1/1+10MK_4	9.63										
LBCa 1/1+10MK_5	15.56										
LBCa 1/1+10MK_6	14.96					14.96					
LBCa 7/3+10MK_1	4.11	3.84	0.40	3.44	4.24	4.11	3.94	0.12	3.82	4.06	0.03
LBCa 7/3+10MK_2	3.02										
LBCa 7/3+10MK_3	3.88					3.88					
LBCa 7/3+10MK_4	3.80					3.80					
LBCa 7/3+10MK_5	3.99					3.99					
LBCa 7/3+10MK_6	4.27										
LBCa 3/7+20MK_1	30.99	28.43	3.12	25.31	31.56	30.99	28.72	1.80	26.93	30.52	0.06
LBCa 3/7+20MK_2	32.58										
LBCa 3/7+20MK_3	27.05					27.05					
LBCa 3/7+20MK_4	26.88					26.88					
LBCa 3/7+20MK_5	23.13										
LBCa 3/7+20MK_6	29.97					29.97					
LBCa 1/1+20MK_1	23.00	18.96	2.91	16.05	21.87		20.14	0.65	19.49	20.78	0.03
LBCa 1/1+20MK_2	19.24					19.24					
LBCa 1/1+20MK_3	20.46					20.46					
LBCa 1/1+20MK_4	20.72					20.72					
LBCa 1/1+20MK_5	14.70										

LBCa 1/1+20MK_6	15.66										
LBCa 7/3+20MK_1	13.75	15.77	2.37	13.40	18.14	13.75	14.89	1.43	13.46	16.31	0.10
LBCa 7/3+20MK_2	17.56					17.56					
LBCa 7/3+20MK_3	20.19										
LBCa 7/3+20MK_4	13.66					13.66					
LBCa 7/3+20MK_5	14.43					14.43					
LBCa 7/3+20MK_6	15.03					15.03					

Table 6.2 – Compressive strength results of LBCa geopolymeric samples.

6.1.6 Colorimetry

Colorimetric measurements have been performed on raw ceramic and on the studied geopolymers, as well as on the archaeological materials to restore (more information about the selected archaeological materials are available in paragraph 6.2).

Regarding the geopolymeric samples, the colour measurement has been performed on both surfaces of the samples: the bottom surface that was in contact with the mold and the up surface. The latter sometimes show a very thin shiny layer, probably because of waterglass concentration. Thus, Table 6.3 shows the results on the bottom surfaces, as they are considered more reliable of the product colour. All data of bottom and upper surfaces are reported in Supplementary materials (Attachment 6.2).

				Comparison with LBCa raw						Comparison with ME brick						Comparison with GL brick					
Sample	L*	a*	b*	ΔL*	Δa*	Δb*	ΔE*	ΔC*	ΔH*	ΔL*	Δa*	Δb*	ΔE*	ΔC*	ΔH*	ΔL*	Δa*	Δb*	ΔE*	ΔC*	ΔH*
LBCa 3/7	45	15	21	-12	2	-1	13	1	2	-2	0	-4	5	-4	2	-14	5	-1	15	2	5
LBCa 1/1	39	15	20	-18	2	-1	19	1	3	-8	0	-4	9	-4	2	-20	5	-1	21	2	5
LBCa 7/3	40	15	20	-17	2	-1	17	0	2	-7	-1	-5	8	-4	2	-19	5	-1	20	1	5
LBCa 3/7+10MK	53	11	15	-4	-2	-6	8	-6	1	6	-5	-10	12	-11	1	-6	1	-7	9	-5	4
LBCa 1/1+10MK	52	12	17	-5	-1	-4	7	-4	1	5	-4	-8	10	-8	1	-7	2	-4	8	-3	4
LBCa 7/3+10MK	63	11	18	5	-2	-4	7	-4	0	16	-5	-7	18	-9	0	4	1	-4	5	-3	2
LBCa 3/7+20MK	60	10	14	2	-2	-7	8	-7	2	13	-5	-11	17	-12	2	1	1	-8	8	-6	4
LBCa 1/1+20MK	63	10	12	6	-3	-9	11	-9	2	16	-6	-13	21	-14	2	4	0	-9	10	-8	5
LBCa 7/3+20MK	69	9	14	11	-4	-8	14	-9	1	21	-7	-11	25	-13	0	9	-1	-8	12	-8	3

*Table 6.3 – CIE-L*a*b* chromatic parameters measured on LBCa geopolymeric binders; colorimetric data results in comparison with references raw material LBCa and archaeological bricks (namely ME brick and GL brick – see paragraph 6.2).*

The L*, a* and b* values measured on the binder surfaces are compared with those measured on the original raw material LBCa, in order to understand possible correlations with the MK addition in the mixture and with the sodium hydroxide and waterglass proportions (Fig. 6.33). Further important information in order to develop suitable restoration mortars is obtained by comparing the binders' values with those measured on the archaeological references (Figg. 6.34 and 6.35).

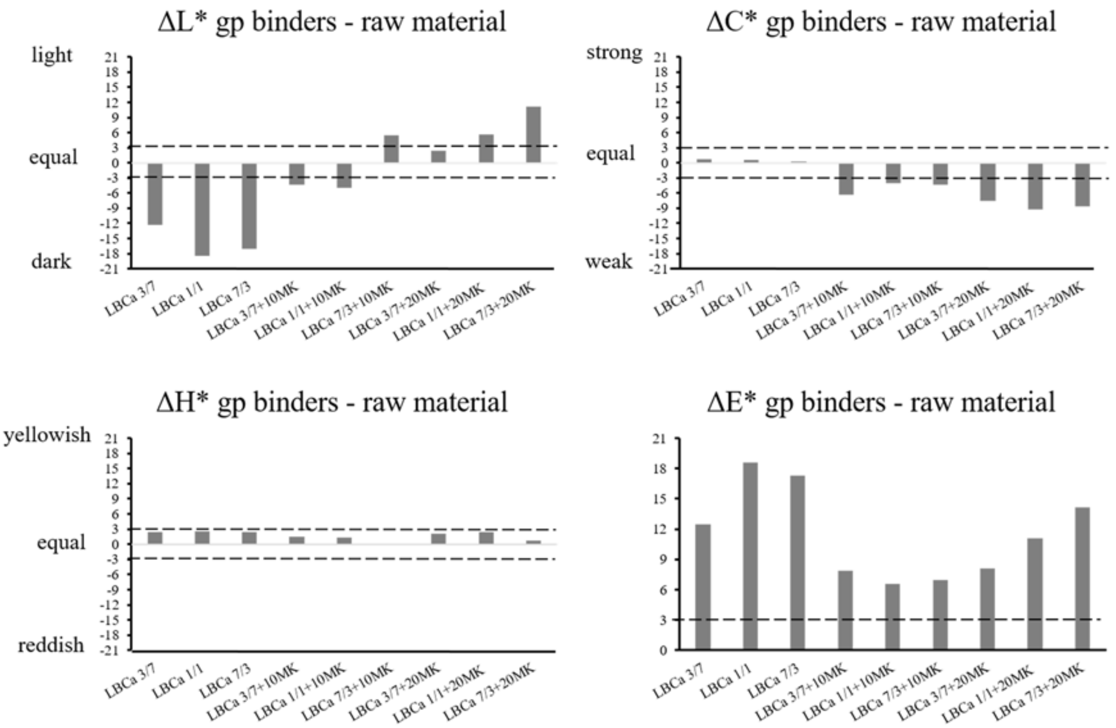

Fig. 6.33 – Partial and total colour differences of the LBCa geopolymeric binders in respect to the ceramic precursor LBCa. In the partial colour differences ΔL, ΔC* and ΔH* the same vertical numeric scales are used to show the relative weight of three chromatic variables on the total colour differences ΔE*. ΔL=lightness variation, ΔC=chroma variation and ΔH=hue variation. The dashed lines indicate the perceptibility limit, which is equal to 3 units (Benavente et al., 2003).*

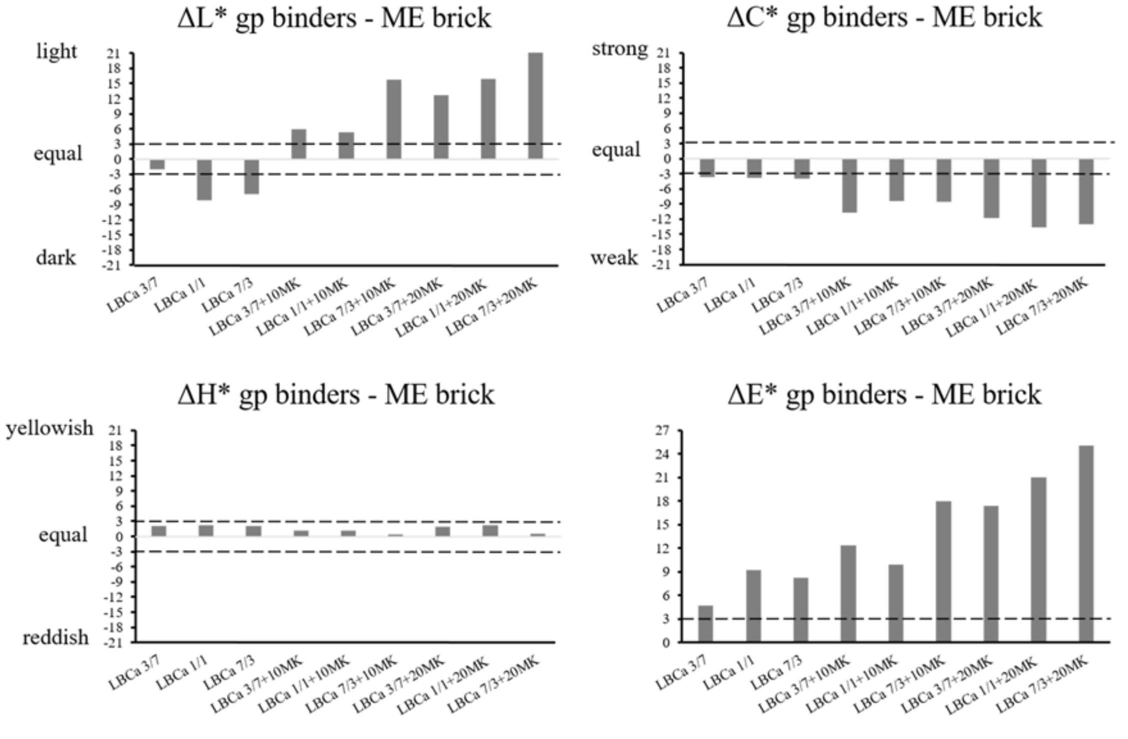

Fig. 6.34 – Partial and total colour differences of the LBCa geopolymeric binders in respect to the ME brick. In the partial colour differences ΔL, ΔC* and ΔH* the same vertical numeric scales are used to show the relative weight of three chromatic variables on the total colour differences ΔE*. ΔL=lightness variation, ΔC=chroma variation and ΔH=hue variation. The dashed lines indicate the perceptibility limit, which is equal to 3 units (Benavente et al., 2003).*

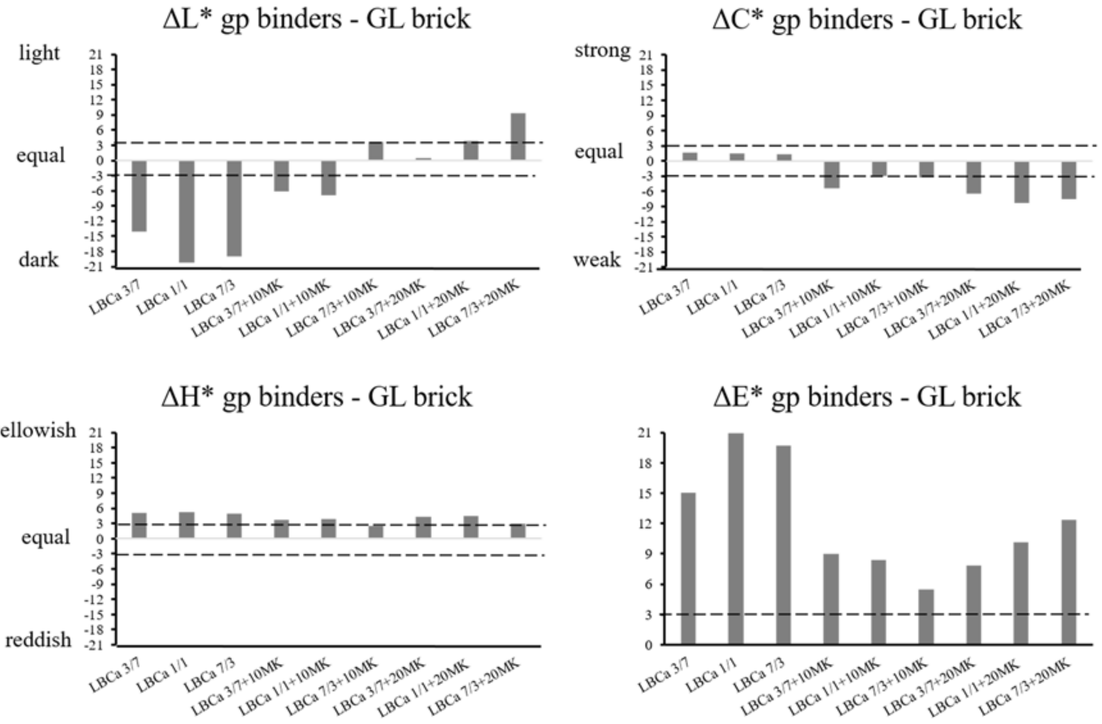

Fig. 6.*35 – Partial and total colour differences of the LBCa geopolymeric binders in respect to the GL brick. In the partial colour differences ΔL*, ΔC* and ΔH* the same vertical numeric scales are used to show the relative weight of three chromatic variables on the total colour differences ΔE*. ΔL=lightness variation, ΔC=chroma variation and ΔH=hue variation. The dashed lines indicate the perceptibility limit, which is equal to 3 units* (Benavente et al., 2003).

As reported by Benavente et al. (2003), considering the references Berns (2000) and Volz (2001), the general limit of perceptibility of the colour parameters changes is defined at 3 units in CIELAB space. Thus, the data interpretation has been made considering the range between -3 and +3 units as a range of not perceivable changes. It is necessary to keep in mind that this threshold does not determine a limit towards the acceptability of the material in a conservation intervention, which instead could require a visible colour difference between original materials and restoration ones (see Chapter 8). Many studies are available regarding the acceptable colour difference between the original material and, alternatively, its appearance once treated (consolidation, protection). In these cases, values generally between 6 units are accepted (Barone et al., 2008); on the other hand, few studies indicate specific values for considering a restoration mortar or a substitution material adequate (i.e. 11 units for Clausi et al., 2016). As formal norms do not exist in this sense, colour variations up to 15 units are arbitrarily considered adequate for the purpose of this study.

Looking at the differences between the geopolymeric formulations and LBCa precursor (Fig. 6.33) it is noticeable as the addition of MK determines a lightness increase (ΔL* increase), while the samples only made by the ceramic precursor show a very visible darkening (L* negative values). This behaviour is more evident for the set with higher sodium hydroxide. The chroma variation (ΔC*) in respect to the used raw material is not perceivable (between -3 and 3 units) for the majority of the samples while it is barely above the limit for sample 3/7+10MK and for the samples with 20% of MK, reaching the value of -10 units. We can assume that the increase in MK in the mixture determines a lowering of the a* and b* values, thus the colour saturation. Concerning the chroma, furthermore, the different proportions of the activating solutions do not seem to have an important role. The hue maintains the same values of the precursor, with changes located in the range individuated as not perceivable. Therefore, the total colour appearance is mainly influenced by variations in lightness and chroma, directly linked with the amount of MK added in the slurry and, with less weight, to the sodium hydroxide/waterglass ratio.

Figg. 6.34, 6.35 show the calculated variations in lightness, chroma, hue (ΔH*) and in total colour appearance of the formulations in respect to the two chosen archaeological materials (ME brick and GL brick). The most important visual effects are produced by lightness and chroma; both variables greatly influence the total colour difference (ΔE*), while the hue does not determine any appreciable change (with the exception of samples without MK in respect to GL brick, where a slight brightening occurs).

In detail, with respect to ME brick, most samples show a slight lightness variation, which however increases in the samples with the highest % of MK. Regarding the chroma, the values decrease for the samples with higher MK in the slurry, while the difference is quite perceivable only for those made with the ceramic precursor. Looking at the complete colour variation, it is noticeable at first sight as it exceeds the perceivable limit of 3 units, increasing in a way approximatively linear with MK and sodium hydroxide content in the mixture.

Considering the GL brick, excepting the samples without MK and the 7/3+20MK, most samples are located within the not perceivable lightness change range, or slightly out (with negative values for the samples with 10% of MK and positive ones for those with 20% of MK). Regarding the chroma only samples with MK in the slurry show visible changes, with negative values of low entity. Very slight changes are registered also for the hue, with positive values under 6 units. If we consider the total colour appearance it is immediately visible as the samples without MK are way too different compared to GL brick, while moderate values are shown by the binary mixtures.

In order to have an immediate perception of the colour relative appearance, a colour chart has been created, showing the "pseudo-colours" of all the binders obtained by LBCa raw material with the different % of MK and different sodium hydroxide/waterglass proportion (Fig. 6.36).

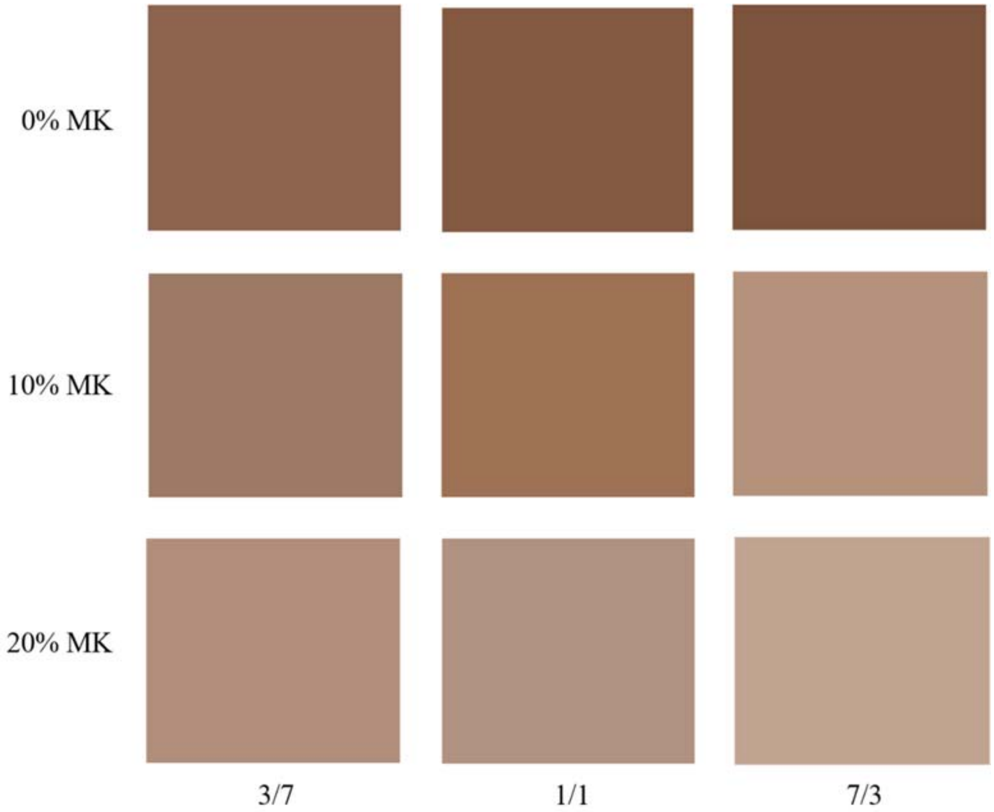

Fig. 6.36 – Pseudo-colours of the LBCa binders.

All things considered, the samples show colour parameters suitable for the implementation of restoration products. The variety of values obtained will allow, indeed, to choose binders with the desired colour aspect depending on the substrate on which to intervene. In the specific case, the bricks used as reference are really different between themselves, demonstrating as high versatility of restoration products is requested in order to face the great differences of original materials to restore. Furthermore, it is possible to choose a binder with a similar colour aspect, yet guaranteeing the recognition of the restoration intervention.

6.1.7 Binders evaluation for the development of restoration mortars

Overall, it is possible to confirm a good geopolymeric reaction of the waste ceramic raw material LBCa, which allows to create binders with good characteristics at room temperature.

In order to better understand the mechanisms and the performance of the binders produced, all the data have been compared. The data used to select the more suitable binders for the development of restoration mortars are reported in Table 6.4.

Sample	L/S	Theoretic SiO_2/Al_2O_3	Min. Curing time (gg)	Efflo resc. (%)	Amorp. (%)*	Amorp. increase (%)*	FTIR shift (cm^{-1})	Compres sive strength (MPa)	Accessible porosity (%)	Average pore diameter (µm)
LBCa 3/7	0.45	7.22	7	5.76	44.08	11.25	47	16.62	27.88	0.46
LBCa 1/1	0.44	6.95	7	8.01	53.43	20.60	47	2.42	26.85	0.94
LBCa 7/3	0.43	6.69	7	7.40	49.19	16.36	47	1.87	32.37	0.29
LBCa 3/7+10MK	0.45	6.25	1	4.57	44.82	7.51	22	16.61	27.15	0.09
LBCa 1/1+10MK	0.43	6.01	1	4.45	50.52	13.22	34	13.11	30.56	0.13
LBCa 7/3+10MK	0.44	5.79	1	6.00	41.60	4.29	37	3.94	28.11	0.26
LBCa 3/7+20MK	0.47	5.54	1	2.36	60.31	18.53	33	28.72	26.92	0.04
LBCa 1/1+20MK	0.45	5.3	1	2.03	59.05	17.27	39	20.14	28.42	0.04
LBCa 7/3+20MK	0.44	5.1	1	4.90	51.99	10.21	54	14.89	32.09	0.24

*Table 6.4 – Results comparison chart of the LBCa geopolymeric binders, including all the data useful for the selection of the suitable binders for mortars synthesis (efflorescence and amorphous %, FTIR shift, average compressive strength values and porosimetric data) and the synthesis parameters of L/S and theoretical silica/alumina ratios, together with the measured curing time. Min. curing time= minimum curing time; Effloresc.=Efflorescence; Amorp.=Amorphous content; Amorp. Increase=Amorphous Increase; *The amorphous amounts are calculated excluding the efflorescence data.*

According to the chemical (EDS), molecular (FTIR-ATR, DRIFT, Raman) and morphological (SEM, TEM) investigations, it has been possible to assess the accomplished geopolymeric process, enhancing some differences between the samples, particularly regarding the polymerization degree and network, as well as the formation of secondary salts. The XRD investigation confirmed the general increase of the amorphous phase in all the samples. Comparing the amorphous data with the compressive strengths, it was possible to notice a general increase of the resistance with the increase of the amorphous content. In particular, this is valid for the series 3/7, although not perfectly coherent in the series 1/1 and 7/3, where however other factors become relevant (for example, in series 7/3 the matrix is not well reacted and significant efflorescences formation occurs).

Considering the curing time and the theoretical parameters, we would expect a linear increase of those properties correlated to the geopolymer gel growth, as the amorphous amount and the compressive resistance, according to the amount of MK in the mixture. Nevertheless, a different behaviour has been noticed, which can be summarized in a higher amorphous amount and resistance for the samples without MK compared to those with only 10% of MK. The samples with 20% of MK show, instead, the highest results, as expected. Actually, when considering resistance only, this trend is valid strictly for the 3/7 series; while for 7/3 and 1/1 series the behaviour is more homogenous. The revealed uncommon pattern could be clarified thanks to SEM data, which illustrate a complex system.

Concerning the samples without MK, the good compressive resistance of sample 3/7 could be explained by the dense and vitreous texture of the matrix, likely due to the high silicate proportion in the slurry, which makes the matrix more compact despite the presence of efflorescence. The considerable increase in amorphous content for this sample is consistent with this interpretation.

On the contrary, sample 7/3 completely failed the compressive test. This could be associated to the abundance of crystalline structures which interrupt the continuity of the geopolymeric gel. The relatively high amount of amorphous moieties in this sample could be associated to the presence of dissolved material which is however not fully consolidated (probably the individuated tufts).

In addition to an apparently well-reacted compact structure, prismatic structures interrupting the matrix continuity are well visible in samples with 10% of MK. These crystalline structures certainly contribute, together with a high amount of efflorescences (with the exception of sample 1/1+10MK), to lower the general quantification of the amorphous fraction and the compressive resistance of sample 3/7+10MK.

Concerning samples with 20% of MK, as observed for those without MK, the higher the silicate proportion in the mixture, the denser is the matrix. This founds confirmation in the compressive resistance data and in the amorphous amount measured. Therefore, comparing all the data, the samples with the highest waterglass and MK amount show the best results. In this context, sample 7/3+20MK shows poor results, with medium-low resistance, low amorphous increase and simultaneous high efflorescences amount. Furthermore, its morphology observed with SEM at high magnifications appears poorly vitreous, with its particular botryoidal structure.

What observed regarding the formed gel determines a different porosity, which is another component influencing the mechanical resistance and durability of a material (Leonelli and Romagnoli, 2013). A material interacts with the environment through its open porosity. If on one hand the open pores ensure a good permeability of the material, at the same time they could be a preferential path for the penetration of water and aggressive agents, often causing consistent decays. The higher the pore diameter, the greater the permeability will be, as well as the susceptibility to the access of degradation agents (Leonelli and Romagnoli, 2013). Thus, considering the necessity of different permeability levels, depending on the kind of restoration product and the environment of the monument to restore, the preferable porosity could be very different. If a lower permeability determines a higher durability of a building material, in the conservation field a higher permeable material could be preferable.

The series 7/3 (with the exception of the first sample) is characterized by a more abundant and coarse porosity. It diminishes in the series 1/1 and 3/7, which show a similar porous structure. Noteworthy is the lower diameter of the porosity characterizing samples with 20% of MK.

Regarding the colour, it was possible to observe a suitability of the binder appearance in the context of ceramic restoration. The obtained different values allow to choose the binder according to the application. Nevertheless, we have to consider the possibility of a colour change of the binders when aggregates of different nature are added.

All things considered, in order to plan the development of restoration products, in particular bedding and reintegration mortars for brick masonries, the samples without MK and those belonging to the series 7/3 have been definitely excluded. The first are characterized by a very long curing time, not appropriate for *in situ* applications, which require a faster consolidation. Furthermore, all these samples show neither good mechanical nor aesthetical performance, with efflorescences often visible also by nacked eyes. The other results are nevertheless satisfactory; therefore, we could consider these binders for further optimization in the future.

Among the remaining four formulations (3/7+10MK, 3/7+20MK, 1/1+10MK and 1/1+20MK), all showing good properties, the samples with 20% of MK have higher performances. However, it was decided to also test sample 1/1+10MK, because of its much preferable workability. Not less important, it must be taken into consideration that, in the conservation field, "higher" does not necessary mean "better"; hence higher compressive resistance could be "too much" depending on the resistance of the substrate to restore (see Chapter 8). For this reason, testing sample 1/1+10MK, with intermediate values, could prove more adequate for the field of restoration.

Furthermore, we don't know how the binders could react with the aggregates addition, thus testing slurries with different mechanical resistance and porosity could help in finding the final best product.

Concerning the colour, the selected binders widen the possibility to find mortars with a suitable ΔE for the restoration of this kind of bricks.

6.2 Geopolymeric mortars

Starting from the selected binders, restoration mortars have been designed according to the scheme in Table 6.5, by adding different types of aggregates and adjusting the L/S ratio according to the changed workability. The scheme includes the new L/S ratios.

	Aggregates					
Binder selected	SS	SC	CER	Mortars	New L/S	
LBCa 1/1+10MK	X			LBCa 1/1+10MK SS	0.50	STEP 1
		X		LBCa 1/1+10MK SC	0.53	
			X	LBCa 1/1+10MK CER	0.78	
LBCa 1/1+20MK	X			LBCa 1/1+20MK SS	0.45	
		X		LBCa 1/1+20MK SC	0.55	
			X	LBCa 1/1+20MK CER	0.74	
LBCa 3/7+20MK		X		LBCa 3/7+20MK SC	0.51	STEP 2
			X	LBCa 3/7+20MK CER	0.71	

Table 6.5 – Scheme of geopolymeric restoration mortars and new L/S ratios. SS=siliceous sand; SC=carbonate sand and CER=ceramic aggregates.

Starting from a L/S ratio equal to 0.43, 0.45 and 0.47 respectively for the binders 1/1+10MK, 1/1+20MK and 3/7+20MK, the mortars required an increase of the liquid component, reaching at least a L/S ratio of 0.5. The only exception is mortar 1/1+20MK SS, which however did not show a good workability, thus more liquid would be required also in this case. Comparing the mortars realized from the same binder, it is clear that, according to the kind of aggregates added in the mixture, the required amount of liquid changes. The ceramic aggregates required a greater proportion of the liquid component (results consistent with literature (Pacheco-Torgal and Jalali, 2010)), with the best workability obtained between 0.7 and 0.8 L/S ratios; while the mortars with the siliceous sand required less additional liquid. The carbonate sand stands in the middle.

The syntheses have been performed in steps, firstly testing the binders 1/1+10MK and 1/1+20MK (those preferred according to the performances) with all the available aggregates (step 1); then, after the preliminary test of their adhesion properties to the substrates by flexural tests, the mortars with the binder 3/7+20MK have been realized by adding only the aggregates which passed this first performance evaluation (step 2).

Silicate sand, carbonate sand and crushed and sieved LBCa ceramic have been overall used in 1/1 binder to aggregate proportion. The aggregates' chemistry and granulometric curves are exposed in Chapter 4.

The intrinsic characteristics of the mortars, as the mechanical resistance, the microstructure and the colour, have been studied; but before, in order to understand the indispensable adhesion required to ceramic materials and their interaction, the slurries have been applied on two different kinds of brick of archaeological interest (see next paragraph) and the interface mortar-brick has been deeply investigated.

6.2.1 Mortars application on archaeological brick fragments and adhesion properties study

The reference brick samples of archaeological interest

Two bricks of very different characteristics have been chosen for the tests of applicability of the new geopolymeric mortars (Fig. 6.37). In particular a fragment of a solid brick retrieved during an excavation in the square in front of the Cathedral of Messina (Lentini et al., 2010) and a reference solid brick made by using local clay for the study of archaeological remains discovered in Gela (Caltanissetta) (Barone et al., 2012).

The brick from Messina, labelled as ME brick, is an archaeological finding related to the ancient urban pattern of the city of *Zancle-Messana*, the current Messina, in north-eastern of Sicily. During the excavation carried out in 2005-2006 by the Servizio Archeologico della Soprintendenza, for the construction of a civil building, many building phases have been discovered, revealing an interesting slice of the ancient city and of its urban pattern. Among the different structures identified, the remainings of a large peristyle building have been recognized. A relevant extended brick pavement arises (22.7*14 m), dated back to the III-II B.C. Furthermore, near to this area, the rests of a brick furnace have been found, attesting the importance of this type of materials. The brick fragment comes from the area of the furnace.

The possible presence of the ancient *agorà* in the proximity of the building with the brick pavement, indicating the centrality of the area excavated, have been considered decisive for the selection of a brick from this area, with the purpose to have a representative material of the Mediterranean region to study in this PhD thesis. The centrality of the furnace excavated, the fervid trade of ceramic materials at the time, the importance of the city of *Zancle-Messana* and the widespread presence of brick materials in ancient constructions, support the representativeness of the brick selected. There are not explicit testimonies of the commercial exchange of bricks, but we could assume it or assume at least technological exchanges.

The brick fragment coming from Gela, labelled as GL, is a modern reproduction of ancient bricks starting from local clayey material (clay pits in contrada Spinasanta-Priolo, 8 km to the east of Gela) and used as a reference material of the transport amphorae retrieved in Gela, an important Greek colony on the southern coast of Sicily (Barone et al., 2012). The selection of this material has been made in order to consider a typical brick which could be produced according to the local clay in that part of Sicily.

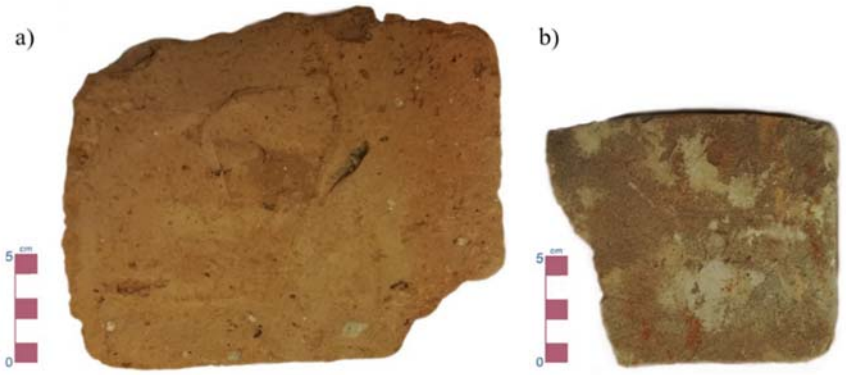

Fig. 6.37 – Bricks of archaeological interest chosen as reference material for the applicability study of geopolymeric mortars: brick fragment from Messina, ME brick a); brick fragment from Gela, GL brick b).

Label	Provenance	Age	Macroscopic observation
ME brick	Brick furnace, excavation in Piazza Duomo - Messina	c.a. III sec. B.C.	Heterogeneous texture, large aggregates and lumps, large porosity; crumbly; bright red-orange.
GL brick	Reproduction from raw materials retrieved 8 km east of Gela	Modern	Homogeneous texture, no aggregates are visible, low porosity; compact; pale pink-yellowish.

Table 6.6 – Reference bricks of archaeological interest for the Mediterranean region.

Their general features are shown in Table 6.6. It was decided to consider two types of brick so different in order to test at the same time the suitability of the geopolymeric mortars on representative Mediterranean archaeological bricks, and their versatility.

Considering the visual appearance of the obtained binders selected, it was decided to apply LBCa 1/1+10MK and +20MK mortars to ME brick, while mortar LBCa 3/7+20MK with a paler appearance was applied on GL brick. Then, the obtained mortars have been also studied by colorimetry for further colour comparisons.

The slurries have been spread with a spatula on eight prisms cut from the ancient bricks (six from ME brick, two from GL brick); other eight prisms of the same brick type have been laid down and pressed by hand, to create a sandwich brick/mortar/brick (Fig. 6.38). The surfaces of the ancient bricks in contact with the mortars have been previously wetted by deionized water, in order to avoid the preferential absorption of the liquid component of the mortar, which is fundamental in the geopoymerization process. At the same time this expedient helped the applicability of the mortar on the support, that otherwise tends to remain attached to the spatula because of its high viscosity. The applicability is further improved if a thin layer of *barbottina* is applied. More specifically, this was prepared by diluting the mortar's binder slurry by increasing its liquid components.

Fig. 6.38 – Application of mortars on fragments of original bricks: application of the mortar on a brick fragment a); positioning of the second fragment to create the sandwich brick/mortar/brick b); final sandwich brick/mortars once consolidated c); the example shows the applications made on ME brick.

Adhesion test

Three points flexural test has been used on the obtained sandwiches, in order to test the adhesion resistance of the system. A different behaviour is highlighted between the samples with ceramic or carbonate sand aggregates mortars with respect to those with silicate sand aggregates (Fig. 6.39). Those with ceramic and carbonate aggregates show a failure of the brick, while the interface brick/mortar resists to the test. The mortars with sand aggregates, on the contrary, tend to break at the interface showing a poor adhesion to the brick substrate.

Due to the failure of the adhesion test on the mortars with silicate sand of LBCa 1/1+10MK and LBCa 1/1+20MK, it was decided to abandon this type of aggregates, not synthetizing the mortar with silicate sand starting from the binder 3/7+20MK.

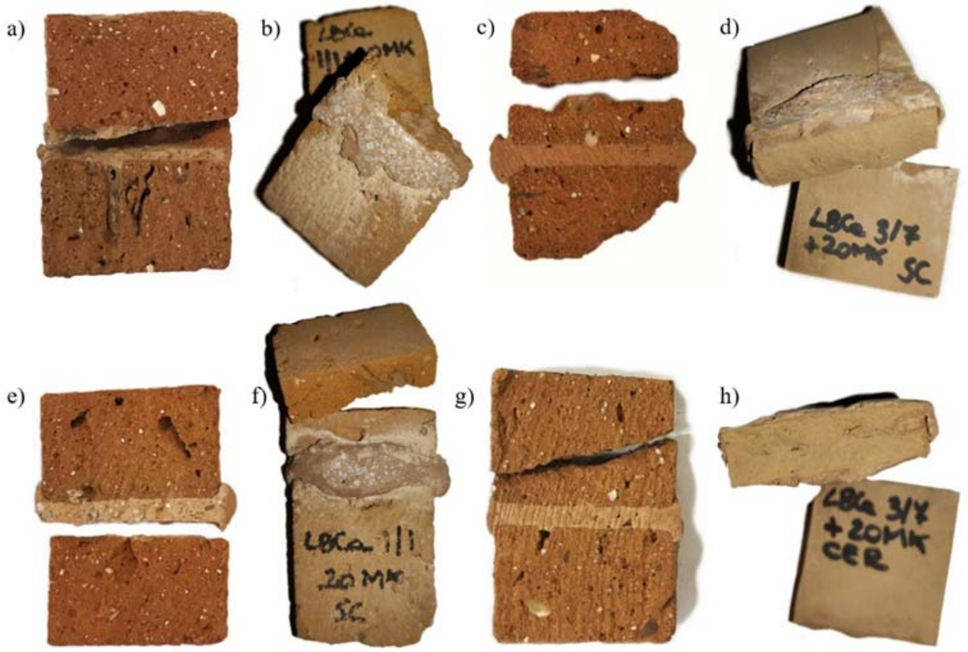

Fig. 6.39 – Sandwiches mortars/archaeological bricks after the adhesion test: LBCa 1/1+10MK SS a); LBCa 1/1+10MK SC b); LBCa 1/1+10MK CER c); LBCa 3/7+20MK SC d); LBCa 1/1+20MK SS e); LBCa 1/1+20MK SC f); LBCa 1/1+20MK CER g) and LBCa 3/7+20MK CER h).

Interface mortar/brick characterization by SEM-EDS analysis

In order to observe in detail a possible reaction along the contact surface between the geopolymer mortar and the archaeological substrate, the interface has been investigated on a fresh cut by means of SEM-EDS analysis. A focus on the mortars has been also performed.

The interface mortar/brick is characterized by blurred borders in all the mortars applied on the archaeological brick fragments from Messina: LBCa 1/1+10MK CER (Fig. 6.40), LBCa 1/1+10MK SS (Fig. 6.41), LBCa 1/1+10MK SC (Fig. 6.42), LBCa 1/1+20MK CER (Fig. 6.43), LBCa 1/1+20MK SS (Fig. 6.44) and LBCa 1/1+20MK SC (Fig. 6.45). This highlights a good penetration of the mortar inside the porosity of the archaeological substrate. This is valid also for the mortar LBCa 3/7+20MK SC applied to the archaeological brick from Gela (Fig. 6. 46), while the sample of the mortar LBCa 3/7+20MK CER applied on the brick from Gela shows a particular and unique reaction edge (Fig. 6.47).

No cracks or micro-cracks are visible at the interface, indicating a good adhesion.

The EDS spectra acquired at the interface show interesting data, indeed it is possible to individuate the formation of a Na-Si-Al or Na-Ca-Si-Al phase probably from the geopolymeric reaction, favouring the adhesion of the slurry to the ceramic.

Regarding the mortars appearance, no cracks are visible at the binder-aggregates interface which are thus well embedded in the matrix regardless to the type of aggregate (Fernández-Jiménez and Palomo, 2005).

The mortars obtained with ceramic aggregates show a homogeneous morphology, while those obtained by adding siliceous and carbonate aggregates appear highly heterogeneous. In particular, concerning the mortars with siliceous sands, Na-rich spots are evident, which are not homogeneously distributed in a matrix with the typical hybrid gel composition. It is possible that the new L/S ratio determines the precipitation of N-A-S-H spot separately by the (N,C)-A-S-H gel, creating discontinuities. Alternatively, these spots could be associated to Na-rich salts precipitation. Observing the mortars with carbonate aggregates, instead, it is noticed as these could not further be considered as inert component of the mortar since they appear to react in contact with the alkaline solutions. Indeed, LBCa 1/1+10MK SC, LBCa 1/1+20MK SC and LBCa 3/7+20MK SC mortars are characterized by Ca-rich clusters with ill defined edges, almost completely dissolved and very well embedded in the matrix.

The SEM-EDS observations are consistent with the adhesion behaviour registered by flexural tests. Indeed, we should consider the possibility that the samples with siliceous sand failed the adhesion tests because of the heterogeneous composition of the gel and of its discontinuities due to the presence of salts and siliceous aggregates not well bound to the matrix.

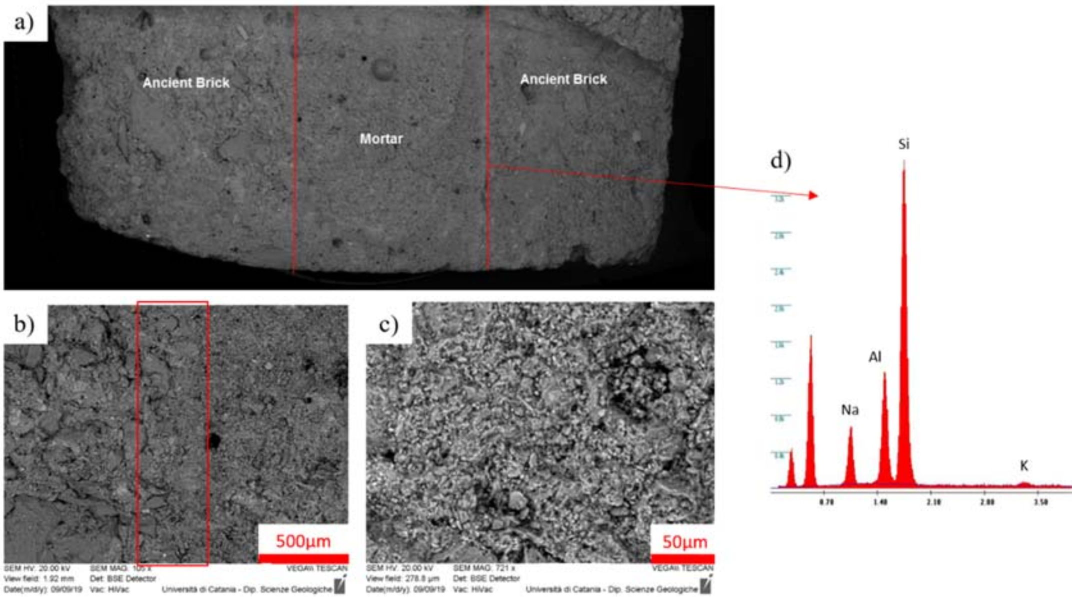

Fig. 6.40 – SEM images of the sandwich mortar/ancient brick, particularly of LBCa 1/1+10MK CER applied on ME brick: fish eye image a); interface surface, with the mortar at the right side of the picture b); detailed image of the mortar at higher magnification c); EDS spectrum acquired on the mortar at the interface with the brick.

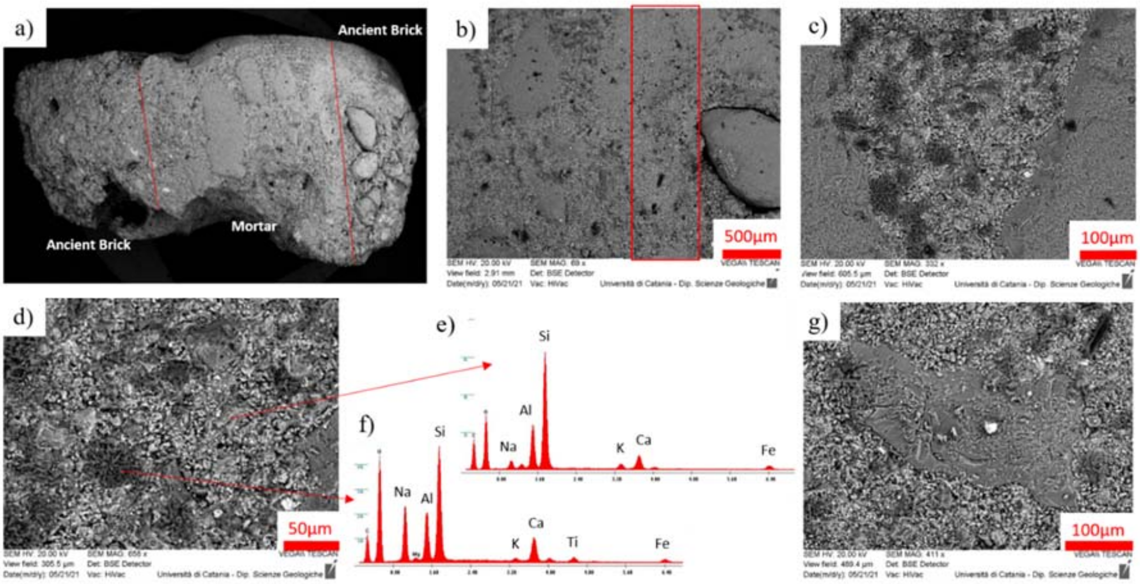

Fig. 6.41 – SEM images of the sandwich mortar/ancient brick, particularly of LBCa 1/1+10MK SS applied on ME brick: fish eye image a); interface surface, with the mortar on the left side of the picture b); detailed image of the mortar at different magnifications c) and d); EDS spectra of the two identified areas of the mortar, particularly the "white" area e) and the Na-rich spots f); detail of a silicate aggregate embedded in the mortar matrix g).

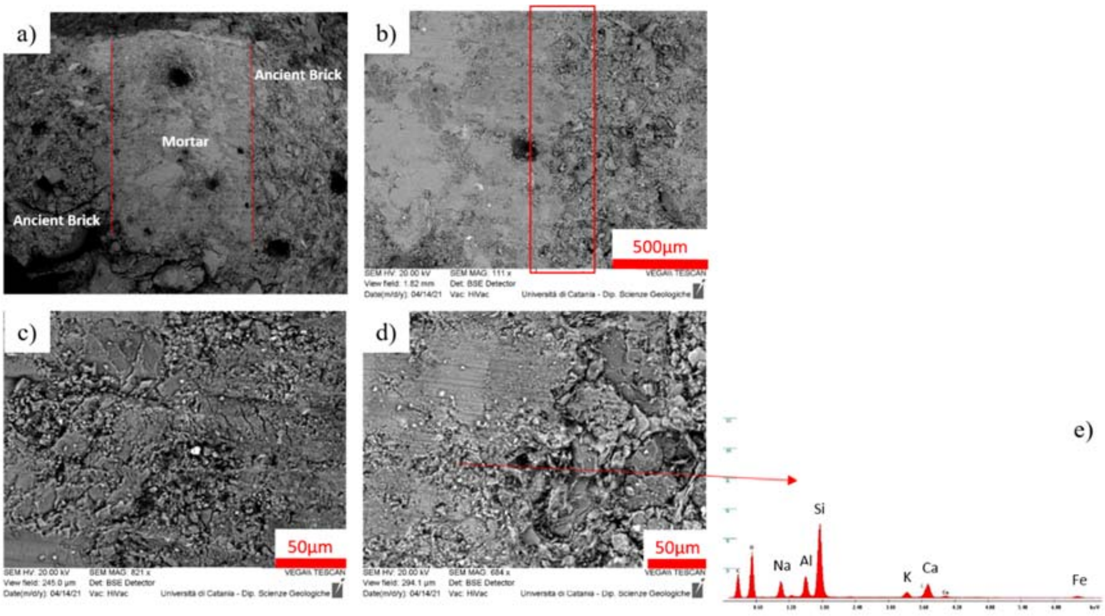

Fig. 6.42 – SEM images of the sandwich mortar/ancient brick, particularly of LBCa 1/1+10MK SC applied on ME brick: fish eye image a); interface surface, with the mortar on the left side of the picture b) and d); focus on the mortar c) EDS spectrum acquired on the mortar at the interface with the brick e).

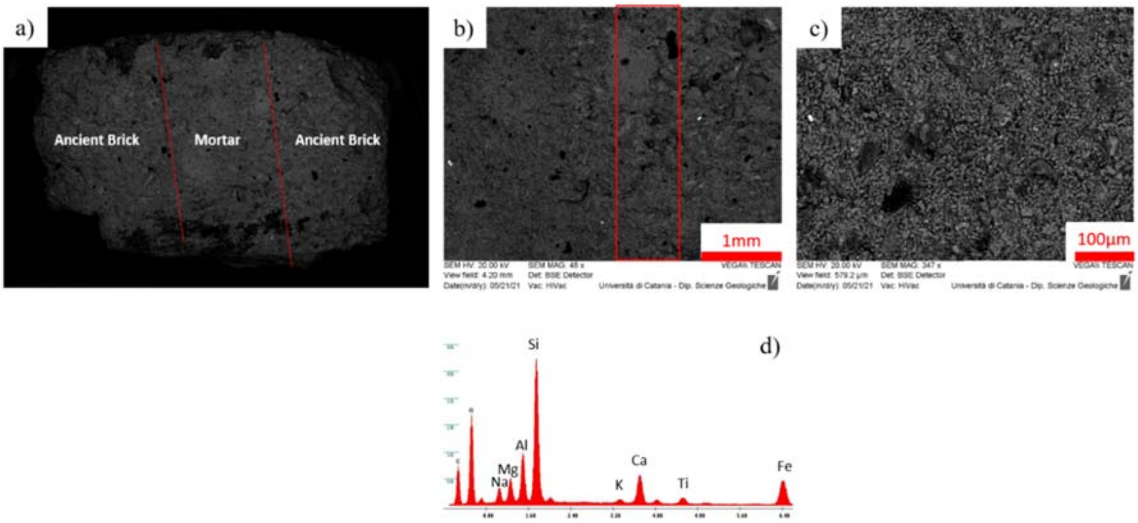

Fig. 6.43 – SEM images of the sandwich mortar/ancient brick, particularly of LBCa 1/1+20MK CER applied on ME brick: fish eye image a); interface surface with the mortar on the left side of the picture b); focus on the mortar c) EDS spectrum acquired on the mortar at the interface with the brick d).

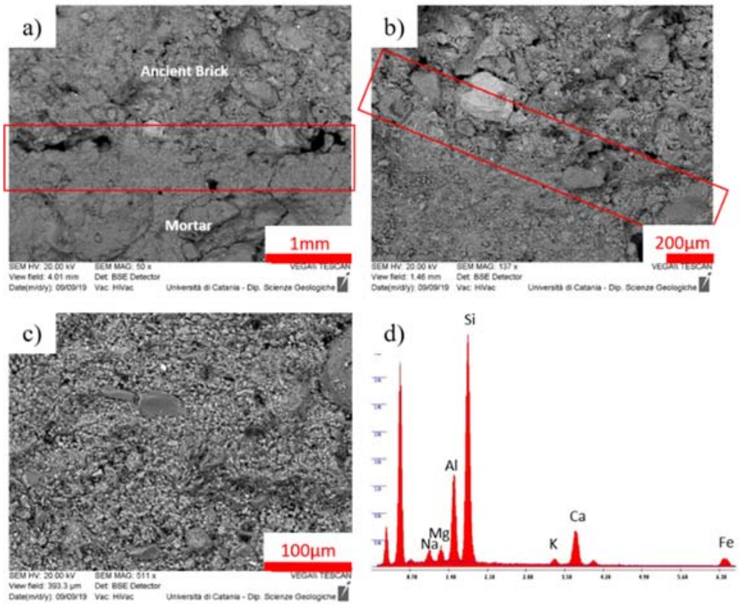

Fig. 6.44 – SEM images of the sandwich mortar/ancient brick, particularly of LBCa 1/1+20MK SS applied on ME brick: interface mortar/brick at low magnification a); interface surface b); focus on the mortar c) EDS spectrum acquired on the mortar at the interface with the brick d).

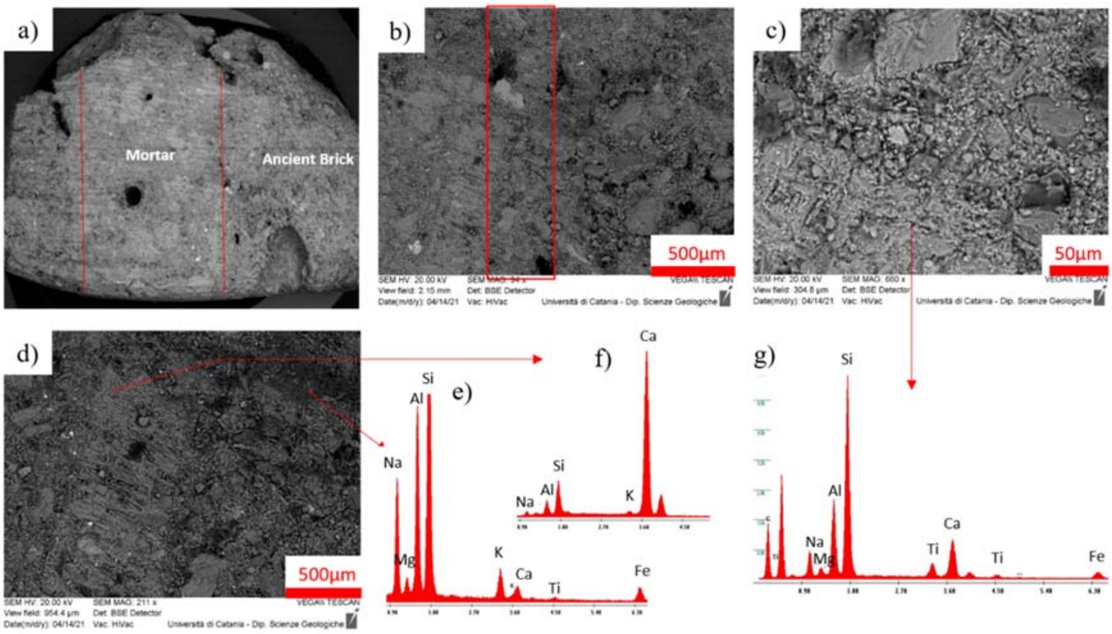

Fig. 6.45 – SEM images of the sandwich mortar/ancient brick, particularly of LBCa 1/1+20MK SC applied on ME brick: fish eye image of the mortar applied on ME brick a); interface mortar/brick with the mortar in the left side of the picture b); focus on the mortar c) and d) with representative EDS spectra acquired on a "grey" spot e), on a partially reacted carbonate aggregate f) and on a representative point of the matrix g).

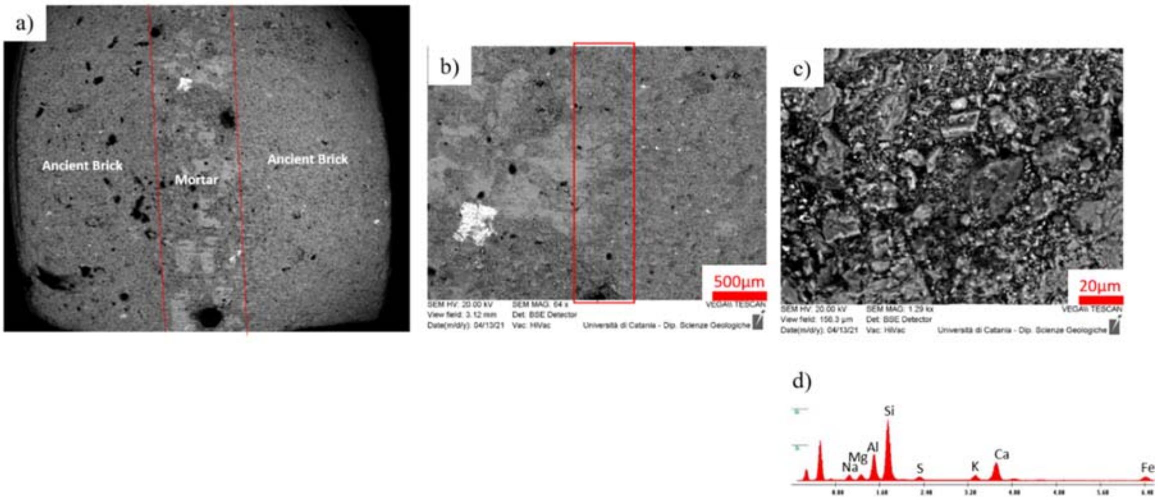

Fig. 6.46 – SEM images of the sandwich mortar/ancient brick, particularly of LBCa 3/7+20MK SC applied on GL brick: fish eye image of the mortar applied on the brick a); interface mortar/brick, with the mortar in the left side of the picture b); focus on the mortar c) EDS spectrum acquired on it d).

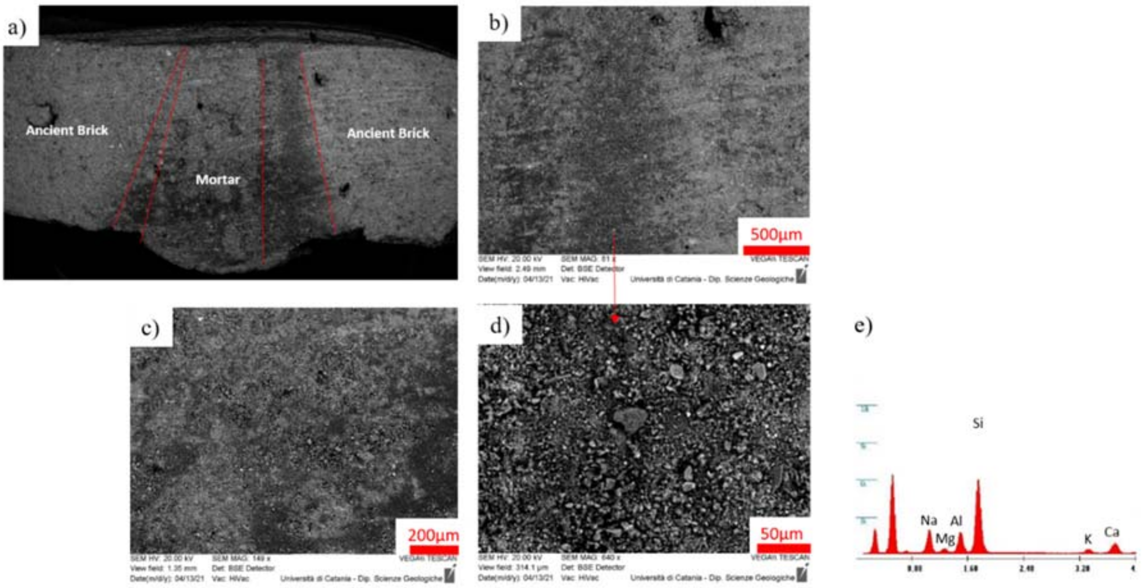

Fig. 6.47 – SEM images of the sandwich mortar/ancient brick, particularly of LBCa 3/7+20MK CER applied on GL brick: fish eye image of the mortar applied on the brick a); interface mortar/brick, with the mortar in the left side of the picture b); focus on the mortar c) and focus on the mortar inside the transition layer d) EDS spectrum acquired on it e).

6.2.2 pH measurements and conductivity test (focus on selected geopolymers)

Four different geopolymeric mortars based on LBCa ceramic waste with 10 and 20% of MK and two different types of aggregates (sand and ceramic) have been selected for the pH and conductivity test. Both pH and ionic conductivity measures are related to the ions released in water by the solid geopolymer, thus giving interesting information about chemical stability (Barone et al., 2021). Ionic conductivity is electrical conductivity due to the motion of all the free ionic charges present in the solution and it is linked directly to the total dissolved solids.

Concerning pH values, they remain fairly constant during the 24 h of test for all the samples, confirming the chemical stability of the material that shows a steady value already after 15 min and an average value around 11 (Fig. 6.48 and Table 6.7).

As regards the conductivity results, it can be noted that the conductivity increases with time, with a similar trend for all the samples (Fig. 6.49 and Table 6.8), but the higher values reached are linked to the presence of ceramic aggregates. Apparently, the amount of MK does not determine any considerable correlation. Even if the study should be deepened, the materials could be considered stable.

Just for comparison, drinking water is characterized by a conductivity value in the range of 5–50 mS/m, deionized water by a conductivity around 5.5 µS/m at 25 °C and sea water of about 5 S/m (or 5000000 µS/m) (Barone et al., 2021). Indeed, it is possible to affirm that the mortars studied shows values of ionic conductivity just one order of magnitude higher than the drinking water.

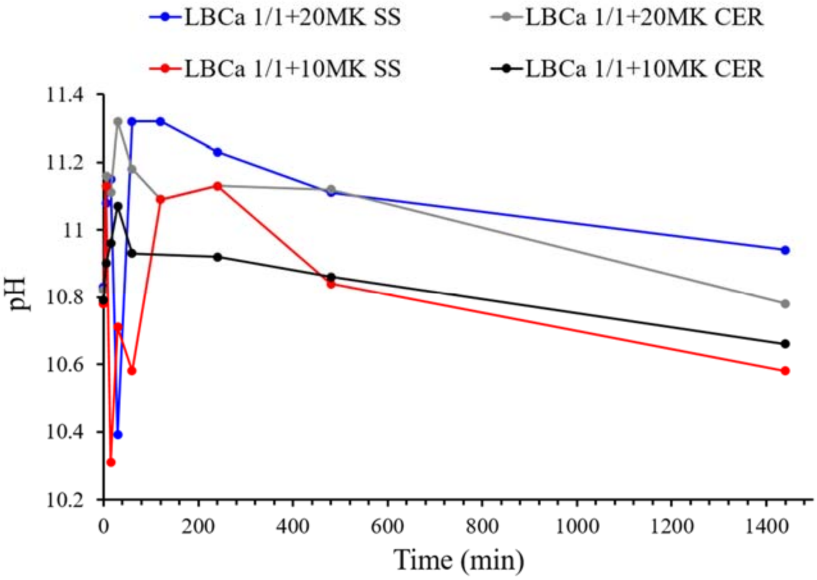

Fig. 6.48 – pH measures acquired on a selection of mortar samples: LBCa 1/1+20MK SS, LBCa 1/1+20MK SC, LBCa 1/1+10MK SS and LBCa 1/1+10MK CER.

	Time (min)								
Samples	0	5	15	30	60	120	240	480	1440
LBCa 1/1+10MK SS	10.78	11.13	10.31	10.71	10.58	11.09	11.13	10.84	10.58
LBCa 1/1+10MK CER	10.79	10.9	10.96	11.07	10.93	0.88	10.92	10.86	10.66
LBCa 1/1+20MK SS	10.83	11.08	11.15	10.39	11.32	11.32	11.23	11.11	10.94
LBCa 1/1+20MK CER	10.82	11.16	11.11	11.32	11.18	11.09	11.13	11.12	10.78

Table 6.7 – pH measurements on four examples of geopolymeric mortars based on LBCa ceramic waste and two different types of aggregates.

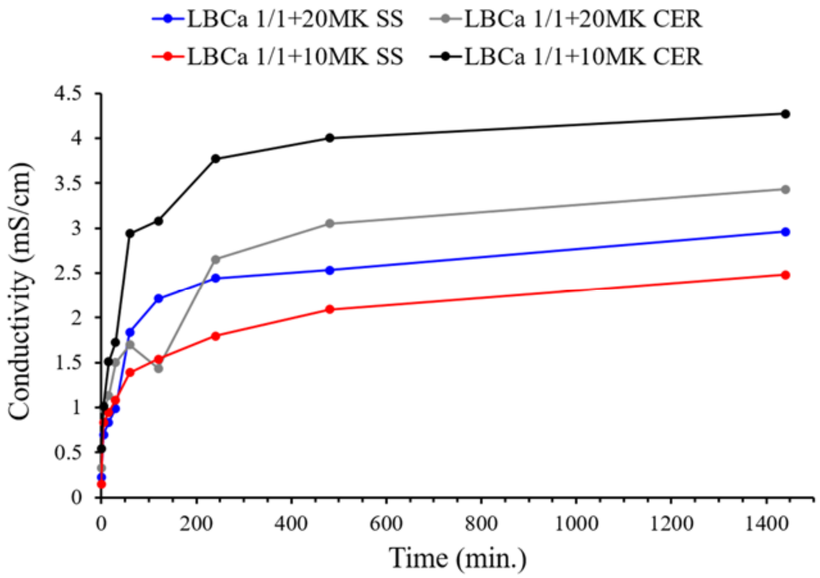

Fig. 6.49 – Conductivity results measured on a selection of mortar samples: LBCa 1/1+20MK SS, LBCa 1/1+20MK SC, LBCa 1/1+10MK SS and LBCa 1/1+10MK CER.

	Time (min)								
Samples	0	5	15	30	60	120	240	480	1440
LBCa 1/1+20MK SS	0.22	0.696	0.832	0.987	1.837	2.21	2.44	2.53	2.96
LBCa 1/1+20MK CER	0.325	0.977	1.13	1.499	1.697	1.434	2.65	3.05	3.43
LBCa 1/1+10MK SS	0.1442	0.83	0.947	1.084	1.387	1.538	1.792	2.09	2.48
LBCa 1/1+10MK CER	0.539	1.008	1.505	1.725	2.94	3.08	3.77	4	4.27

Table 6.8 – Conductivity measurements (mS/cm) on four examples of geopolymeric mortars based on LBCa ceramic waste and two different kind of aggregates.

6.2.3 Mechanical characterization (compressive and flexural tests)

Uniaxial compressive test

The uniaxial compressive test has been performed on six replicates of 2*2*2 cm for each mortar, after 28 days of curing. The analyses have been performed in part at University of Modena and Reggio Emilia and in part at University of Catania. All the data acquired are shown in Table 6.9. The results, presented in Fig. 6.50, highlight a higher compressive resistance for the mortars obtained by using carbonate aggregates, regardless to the type of binder; followed by the mortars with ceramic aggregates and then of those with siliceous sand. Hence it is possible to assume that the type of aggregate strictly determines, more than the original resistance of the binder, the final resistance of the product developed. Furthermore, the values of the mortars LBCa 1/1+10MK and +20MK with ceramic and siliceous aggregates are comparable to each other, under 10 MPa, while the resistance increases with the mortars from the binder 3/7, higher than 15 MPa. The highest resistance values were obtained by the mortars LBCa 1/1+20MK SC with 32 MPa and LBCa 3/7+20MK SC with 29 MPa.

Lastly, comparing the data obtained on the mortars with those on the original binders (Fig. 6.50) it is interesting to notice that the resistance only increases in the mortars with the carbonate aggregates, while it visibly decreases with the introduction of ceramic and siliceous aggregates. While in traditional OPC systems the compressive strength tends to increase with the aggregate addition (Lee and Van Deventer, 2004), it appears that, in geopolymeric systems, chemical and physical interactions between aggregates and binders probably determine more complex results. The intuitive assumption that a strong geopolymeric binder allows to obtain a strong mortar (Lee and Van Deventer, 2004) is not always true, as demonstrated by the abovementioned results.

Due to the poor results acquired on the mortars with silicate sands so far, no further characterizations have been performed on them, except for MIP.

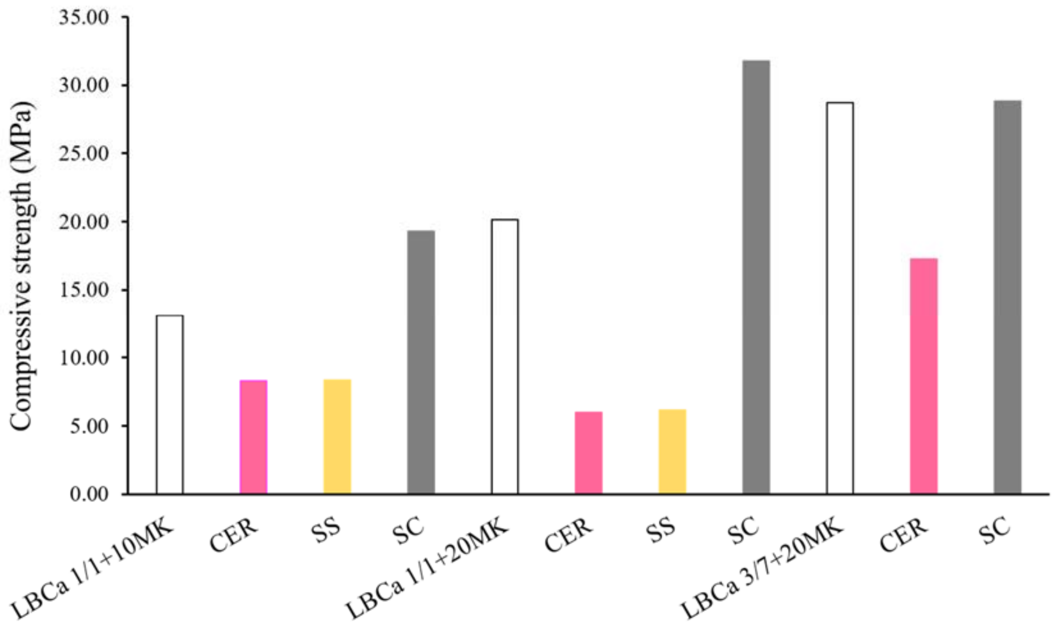

Fig. 6.50 – Average compressive strength values measured on the mortar samples and compared with those of the original binder: the original binders are indicated with an empty bar and are followed on the right side by the relative mortars with ceramic aggregates (CER, pink bar), siliceous sand aggregates (SS, yellow bar) and carbonate sand (SC, grey bar).

Sample	Resistance (MPa)	Aver age	St. Dev.	Bottom limit	Up limit	Accepted values	New average	New St. Dev.	Bottom limit	Up limit	Variati on coeff.
LBCa 1/1+10MK SS_1*	8.39	7.69	0.92	6.76	8.61	8.39	8.34	0.05	8.29	8.39	0.01
LBCa 1/1+10MK SS_2*	8.29					8.29					
LBCa 1/1+10MK SS_3*	6.38										
LBCa 1/1+10MK SC_1	12.97	18.85	3.06	15.79	21.90		19.30	1.01	18.29	20.31	0.05
LBCa 1/1+10MK SC_2	18.31					18.31					
LBCa 1/1+10MK SC_3	20.58					20.58					
LBCa 1/1+10MK SC_4	19.99					19.99					
LBCa 1/1+10MK SC_5	22.92										

LBCa 1/1+10MK SC_6	18.31					18.31					
LBCa 1/1+10MK CER_1*	8.19	8.32	1.79	6.53	10.11	8.19					**0.22
LBCa 1/1+10MK CER_2*	6.19										**The value is calculated on the original values
LBCa 1/1+10MK CER_3*	10.58										
LBCa 1/1+20MK SS_1*	6.65	6.31	0.27	6.04	6.58		6.14	0.16	5.98	6.30	0.03
LBCa 1/1+20MK SS_2*	5.98					5.98					
LBCa 1/1+20MK SS_3*	6.30					6.30					
LBCa 1/1+20MK SC_1	28.59	31.71	2.01	29.70	33.72		31.77	1.24	30.54	33.01	0.04
LBCa 1/1+20MK SC_2	34.58										
LBCa 1/1+20MK SC_3	30.53					30.53					
LBCa 1/1+20MK SC_4	32.08					32.08					
LBCa 1/1+20MK SC_5	33.66					33.66					
LBCa 1/1+20MK SC_6	30.82					30.82					
LBCa 1/1+20MK CER_1*	5.92	6.46	0.69	5.77	7.16	5.92	5.98	0.06	5.92	6.03	0.01
LBCa 1/1+20MK CER_2*	6.03					6.03					
LBCa 1/1+20MK CER_3*	7.44										
LBCa 3/7+20MK SC_1	28.15	30.23	2.71	27.52	32.94	28.15	28.85	1.04	27.81	29.89	0.04
LBCa 3/7+20MK SC_2	33.92										

LBCa 3/7+20MK SC_3	33.74										
LBCa 3/7+20MK SC_4	30.32					30.32					
LBCa 3/7+20MK SC_5	27.20										
LBCa 3/7+20MK SC_6	28.08					28.08					
LBCa 3/7+20MK CER_1	17.04	17.09	1.62	15.46	18.71	17.04	17.29	0.75	16.55	18.04	0.04
LBCa 3/7+20MK CER_2	16.56					16.56					
LBCa 3/7+20MK CER_3	17.04					17.04					
LBCa 3/7+20MK CER_4	19.22										
LBCa 3/7+20MK CER_5	14.11										
LBCa 3/7+20MK CER_6	18.54					18.54					

Table 6.9 – Compressive resistance results of the LBCa geopolymeric slurries. Tests marked with an asterisk have been performed at University of Modena and Reggio Emilia

Three points flexural test

The flexural test has been performed on three replicates for each mortar, with the exception of the mortars with siliceous sands which failed the previous tests. Prisms of 2*2*8 cm were tested for each formulation after 28 days of curing. Fig. 6.51 shows the resistances measured, which reach the highest values for samples LBCa 3/7+20MK CER and LBCa 1/1+20MK SC, respectively at 11 and at 9 MPa. It is possible to notice a correlation between flexural resistance with the obtained compressive data, particularly the resistance increases with MK and waterglass in the slurry, and higher values for the mortars with carbonate aggregates with respect to those with ceramic aggregates are also registered. In this context we should consider the low value measured on sample LBCa 3/7+20MK SC an exception, probably attributable to a failure during the synthesis process (for example as a consequence of air bubbles).

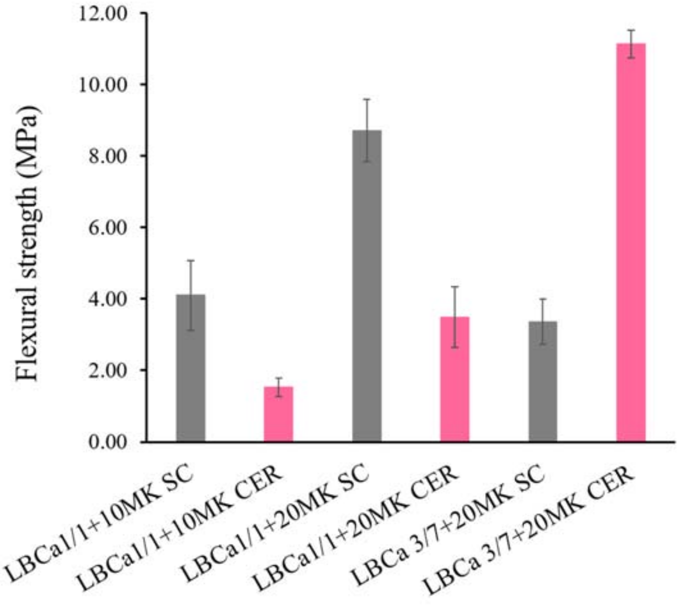

Fig. 6.51 – Flexural strength measured on the geopolymeric mortars with carbonate sand and ceramic aggregates.

6.2.4 Mercury Intrusion Porosimetry (MIP) and capillary water absorption test

MIP

The porosimetric data acquired on the geopolymeric mortars are shown in Table 6.10 and in Fig. 6.52.

Samples	LBCa 1/1+10MK CER	LBCa 1/1+10MK SS	LBCa 1/1+20MK CER	LBCa 1/1+20MK SS
Bulk density (g/cm^3)	2.54	2.24	1.66	2.30
Accessible Porosity (%)	49.33	30.84	32.64	30.03
Total pore volume (cm^3/ g)	0.19	0.14	0.20	0.13
Average Pore Diameter (µm)	0.22	0.12	0.24	0.14
Modal Pore Diameter (µm)	0.49	0.32	13.45	0.42

Table 6.10 – Porosimetric data on geopolymeric mortars studied.

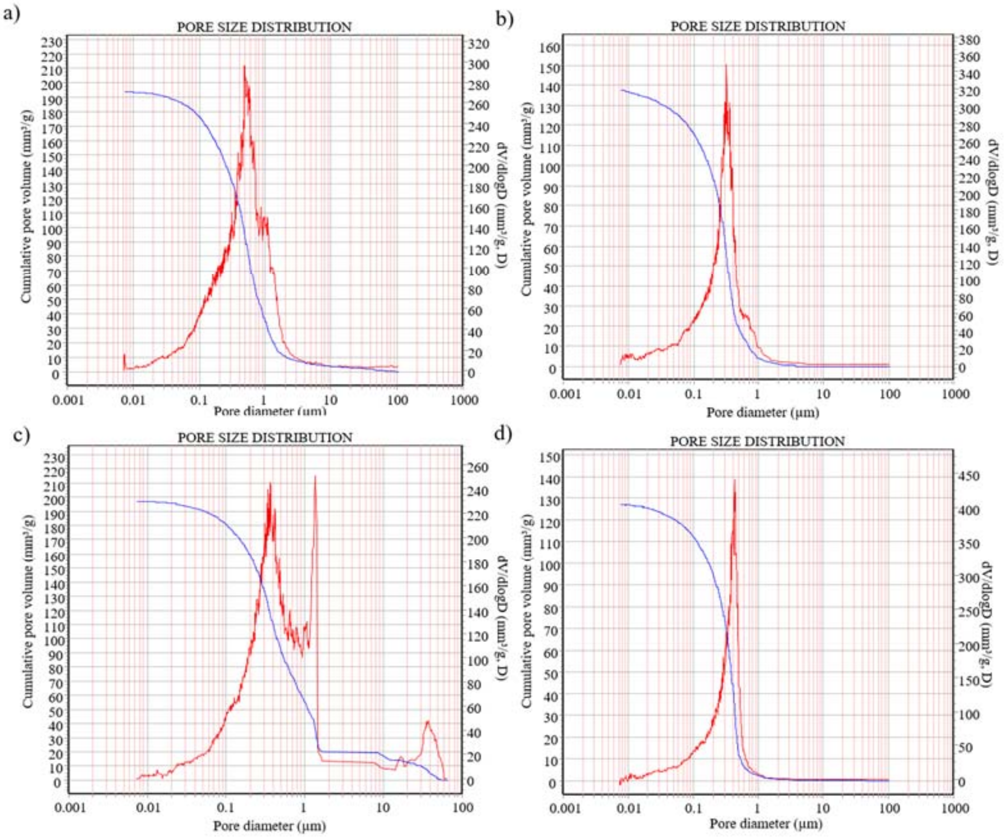

Fig. 6.52 – Pore size distribution of the geopolymeric mortars studied: LBCa 1/1+10MK CER a); LBCa 1/1+10MK SS b); LBCa 1/1+20MK CER c) and LBCa 1/1+20MK SS d).

Unfortunately, because of an irreparable failure of the instrument, it was not possible to perform these analyses on all the mortars developed. Nevertheless, the data obtained are interesting and could give a general overview of the changes occurred when the selected binders have been optimized with the addition of the aggregates.

The mortars investigated by MIP are LBCa 1/1+10MK SS and CER, and LBCa 1/1+20MK SS and CER.

The geopolymeric mortars show an average pore size distribution in the range of 0.12-0.24 µm, with pore diameter increasing with the increase of MK in the mixture (Fig. 6.53a). Larger pore diameter is also registered for the mortars with ceramic aggregates compared to those with silicate sand (Fig. 6.53b). Regarding the original binders, the accessible porosity slightly increases with the addition of ceramic aggregates, remaining more or less unvaried for the mortars with siliceous sand.

With the purpose to test the compatibility of the geopolymeric mortars with the materials to restore, a comparison with the archaeological material has been carried out. Particularly the mortars with 10% of MK with two different aggregates have been compared, as representative example, with the brick from ME (Fig. 6.54). It is highlighted how the dimension of the pores in the mortars is lower than that in the brick, as generally required in the restoration context (Rescic and Fratini, 2013).

The porosimetric results gave important clues about the suitability of this type of material in the context of restoration, but for obtaining information on all the mortars developed, due to the impossibility to follow the porosimetric analysis, their absorption behaviour has been studied. It is indeed a property strictly linked to the porous structure of a material and particularly important for restoration purposes. Thus, capillary absorption tests on all the mortars samples have been carried out.

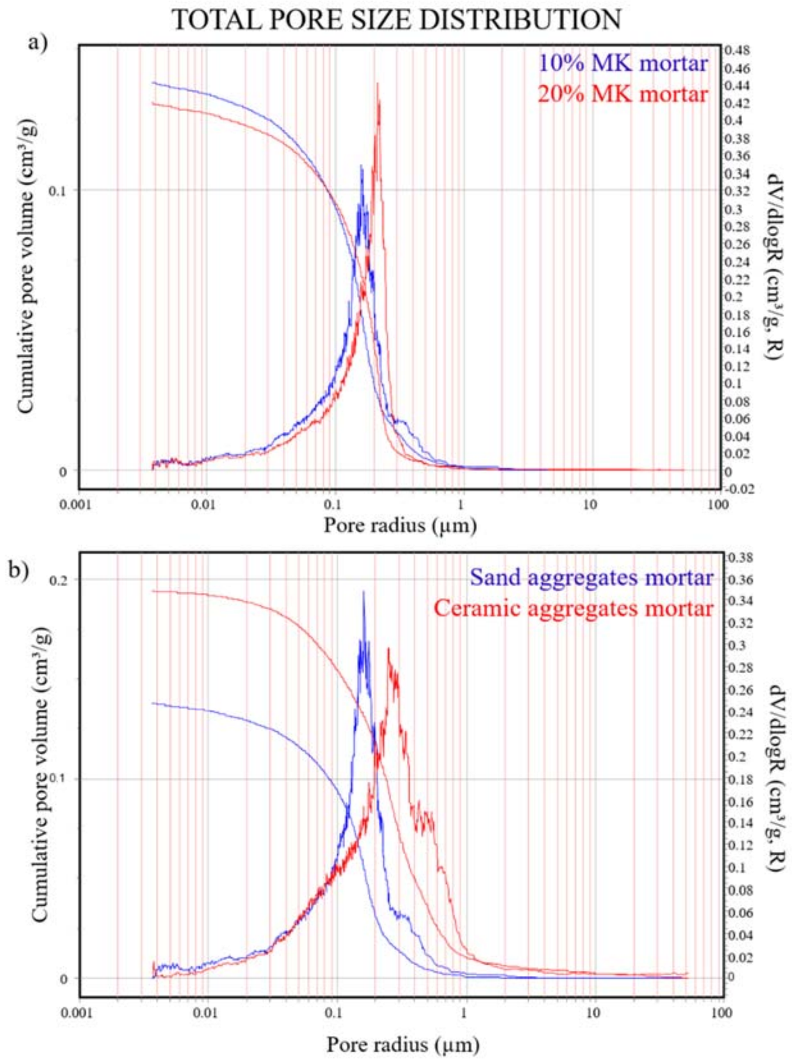

Fig. 6.53 – Comparison of pore size distribution depending on the % of MK, by plotting the pore size distribution of LBCa 1/1+10MK SS and LBCa 1/1+20MK SS a) and comparison of the pore size distribution depending on type of aggregates in the mortars.

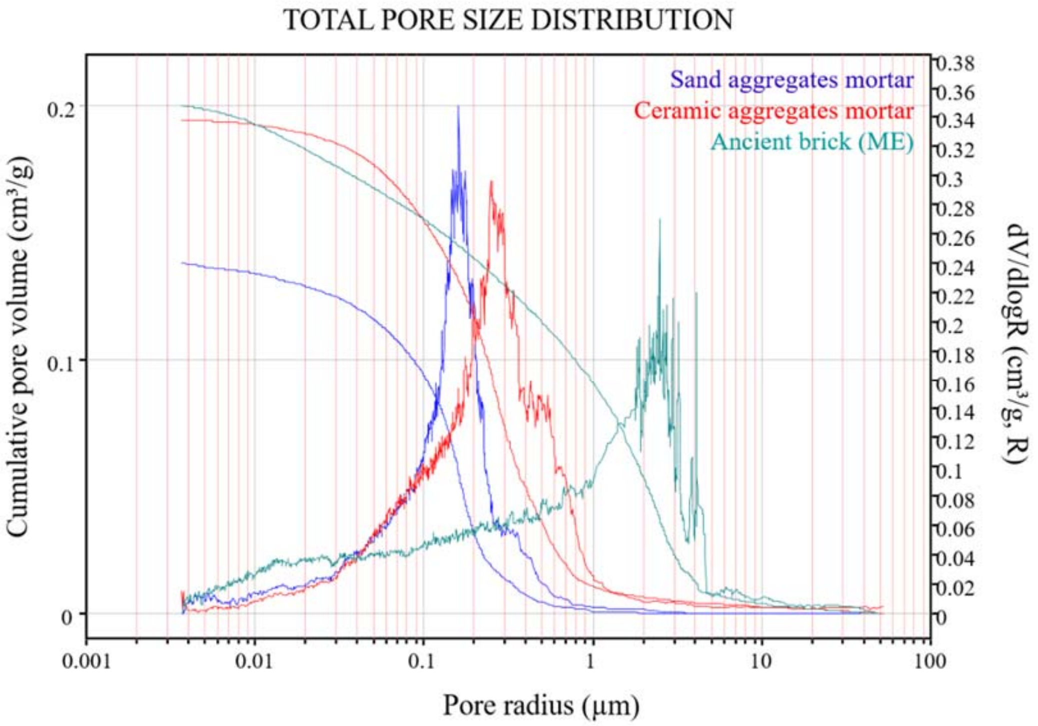

Fig. 6.54 – Comparison of the pore size distribution measured on mortars LBCa 1/1+10MK CER and LBCa 1/1+10MK SS with the archaeological brick from Messina, sample ME.

Capillary absorption test

Six replicates of 2*2*2 cm for each mortar have been tested according to the suggestion of the UNI 10859:2000 standard after 28 days of curing. More accurate results would be obtained by using bigger samples. In order to obtain the dry weight, samples have been put in an oven at 70 °C for 24 hours and left in a desiccator until the environmental temperature was reached. Then, the six cubes have been put on a plastic support in a plastic box, over a few millimeters of deionized water, as shown in Fig. 6.55.

At defined interval of times after water contact (1, 3, 10, 15, 30 minutes;1, 8 and 24 hours) their weight has been measured, upon buffering with a wet paper.

All the data measured and the relative elaborations are shown in the Attachment 6.3.

Fig. 6.56 a, c, e, g, i, m shows the average values of water absorption per surface unit in function of time, demonstrating that all the samples have reached the saturation level after 8 hours (seventh measure), as the appearance of a plateau demonstrates. Fig. 6.56 b, d, f, h, l, n, realized excluding the points of the plateau, show the regression line, whose angular coefficient is the capillary absorption coefficient for that mortar.

From the data of Table 6.11, showing all the capillary absorption coefficients calculated, it is evident that the mortars with higher amount of MK and with ceramic aggregates reach higher values.

Once again, the results obtained show good results for the restoration purposes.

Fig. 6.55 – Capillary water absorption test on geopolymeric cubic samples.

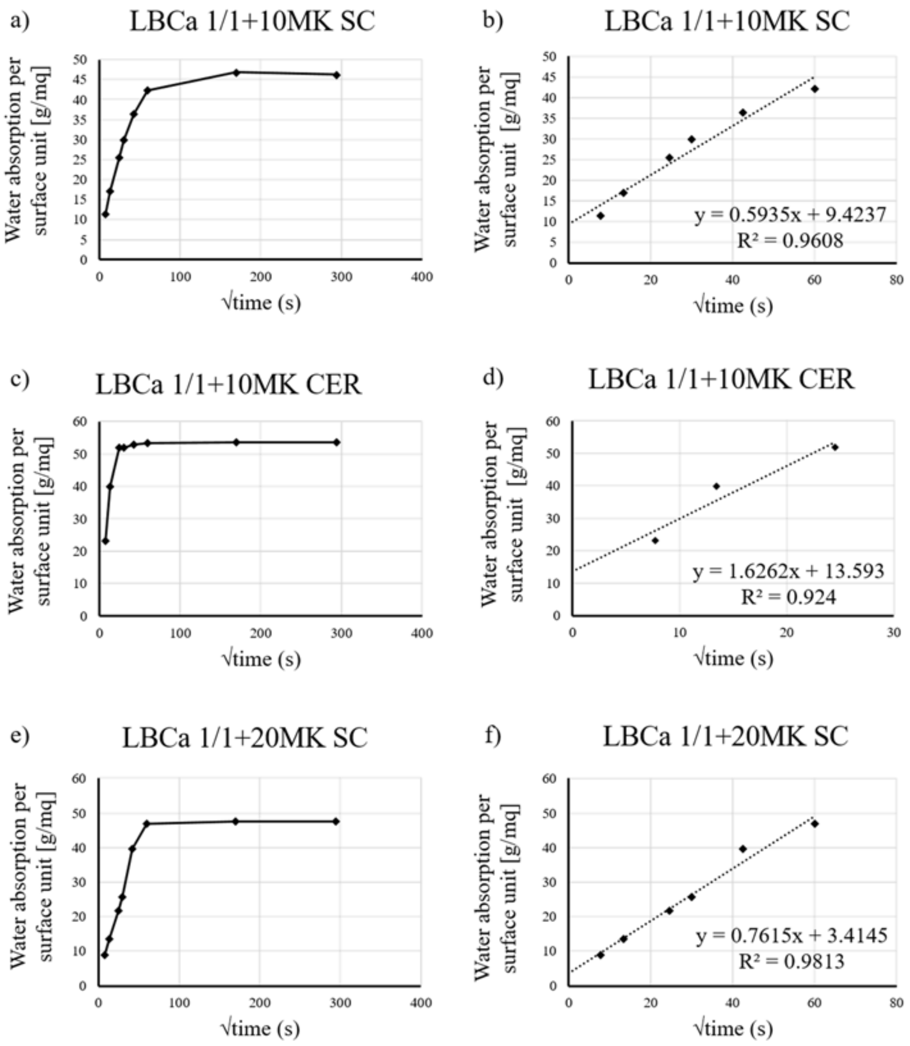

Fig. 6.56 – Part I – Capillary absorption graphs of samples LBCa 1/1+10MK SC, LBCa 1/1+10MK CER and LBCa 1/1+20MK SC. On the left are shown all the absorption steps, on the right the re-elaborated graphs after the elimination of the plateau. The angular coefficient is also indicated.

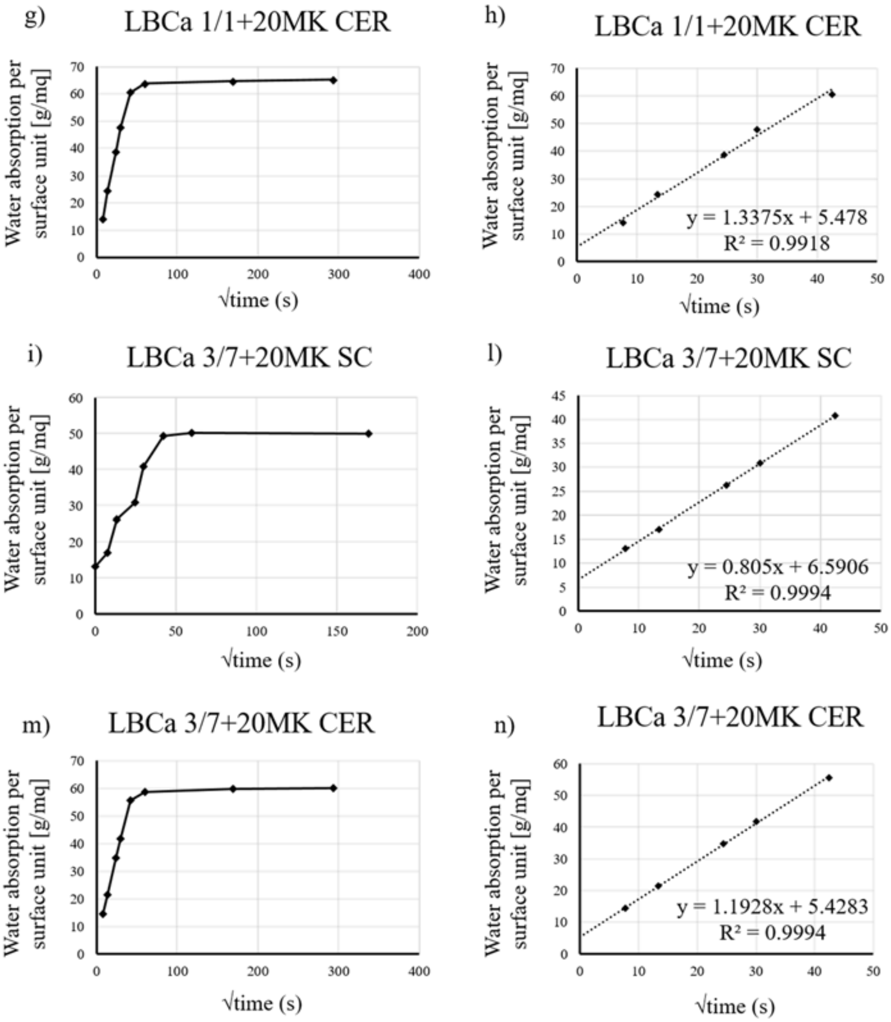

Fig. 6.56 – Part II – Capillary absorption graphs of samples LBCa 1/1+20MK CER, LBCa 3/7+20MK SC and LBCa 3/7+20MK CER. On the left are shown all the absorption steps, on the right the re-elaborated graphs after the elimination of the plateau. The angular coefficient is also indicated.

a) LBCa 1/1+10MK SC

Time [s]	Radq Time [√s]	Water absorption per surface unit [g/mq]	Capillary absorption coefficient [g/mq * √s]
0	0.00		
60	7.75	11.3	
180	13.42	17.0	
600	24.49	25.5	
900	30.00	29.8	0.5935
1800	42.43	36.3	
3600	60.00	42.4	
28800	*169.71*	*46.8*	
86400	*293.94*	*46.3*	

b) LBCa 1/1+10MK CER

Time [s]	Radq Time [√s]	Water absorption per surface unit [g/mq]	Capillary absorption coefficient [g/mq * √s]
0	0.00		1.626
60	7.75	23.2	
180	13.42	39.9	
600	24.49	51.9	
900	*30.00*	*51.92*	
1800	*42.43*	*52.9*	
3600	*60.00*	*53.27*	
28800	*169.71*	*53.6*	
86400	*293.94*	*53.5*	

c) LBCa 1/1+20MK SC

Time [s]	Radq Time [√s]	Water absorption per surface unit [g/mq]	Capillary absorption coefficient [g/mq * √s]
0	0.00		0.7615
60	7.75	8.7	
180	13.42	13.5	
600	24.49	21.6	
900	30.00	25.7	
1800	42.43	39.6	
3600	60.00	46.9	
28800	*169.71*	*47.7*	
86400	*293.94*	*47.7*	

d) LBCa 1/1+20MK CER

Time [s]	Radq Time [√s]	Water absorption per surface unit [g/mq]	Capillary absorption coefficient [g/mq * √s]
0	0.00		1.338
60	7.75	14.1	
180	13.42	24.5	
600	24.49	38.6	
900	30.00	47.6	
1800	42.43	60.6	
3600	*60.00*	*63.7*	
28800	*169.71*	*64.9*	
86400	*293.94*	*65.2*	

e) LBCa 3/7+20MK SC

Time [s]	Radq Time [√s]	Water absorption per surface unit [g/mq]	Capillary absorption coefficient [g/mq * √s]
0	0.00		0.805
60	7.75	13.2	
180	13.42	17.0	
600	24.49	26.2	
900	30.00	30.8	
1800	42.43	40.8	
3600	*60.00*	*49.4*	
28800	*169.71*	*50.2*	
86400	*293.94*	*50.0*	

f) LBCa 3/7+20MK CER

Time [s]	Radq Time [√s]	Water absorption per surface unit [g/mq]	Capillary absorption coefficient [g/mq * √s]
0	0.00		1.193
60	7.75	14.4	
180	13.42	21.5	
600	24.49	34.7	
900	30.00	41.8	
1800	42.43	55.6	
3600	*60.00*	*58.6*	
28800	*169.71*	*59.8*	
86400	*293.94*	*60.1*	

Table 6.11 – Data of the absorption tests on mortars LBCa 1/1+10MK SC a), LBCa 1/1+10MK CER b), LBCa 1/1+20MK SC c), LBCa 1/1+20MK CER d), LBCa 3/7+20MK SC e) and LBCa 3/7+20MK CER f). In italic are indicated the points constituting the plateau.

6.2.5 Colorimetry

The mortars have been analysed in order to quantify their colorimetric parameters and to individuate the differences in colour with respect to the original binder, and to the archaeological references. It is interesting to notice that in the mortars the observed surface layering problem typical of the binders does not occur, hence similar results are measured on both the surfaces of the sample. Here, for the purpose of comparison with the binders, the data obtained on the bottom surface are reported. Nevertheless, all the data are shown in Attachment 6.4.

The colorimetric data of the mortars and the comparison with the original binders and bricks to restore are shown in Tables 6.12 and 6.13 respectively. Histograms showing the total colour variation ΔE and the single parameters' variations (ΔL, ΔC and ΔH) compared to the original binder and to the two reference materials of archaeological interests are reported in Figg. 6.57, 6.58 and 6.59. The colour appearance in order to immediately compare the different mortars obtained are shown in Figg. 6.60 and 6.61.

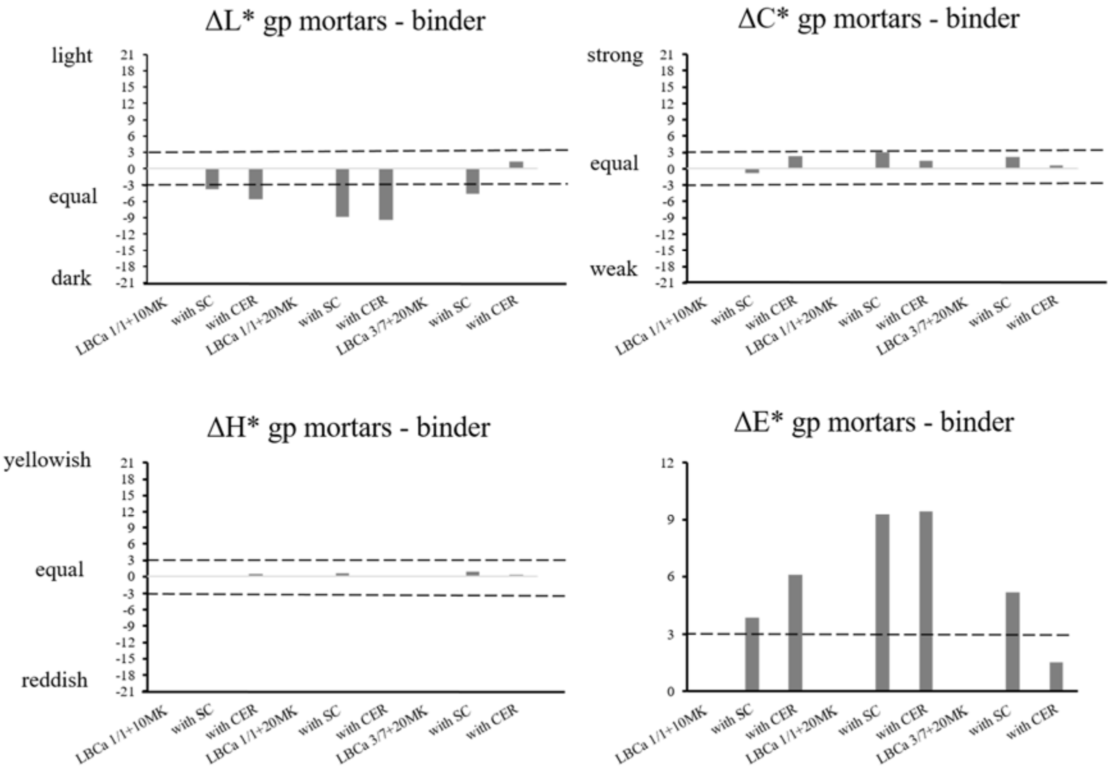

Fig. 6.57 – Partial and total colour differences of the LBCa geopolymeric mortars in respect to the original binder LBCa. In the partial colour differences ΔL, ΔC* and ΔH* the same vertical numeric scales are used to show the relative weight of three chromatic variables on the total colour differences ΔE*. ΔL=lightness variation, ΔC=chroma variation and ΔH=hue variation. The dashed lines indicate the perceptibility limit, which is equal to 3 units (Benavente et al., 2003).*

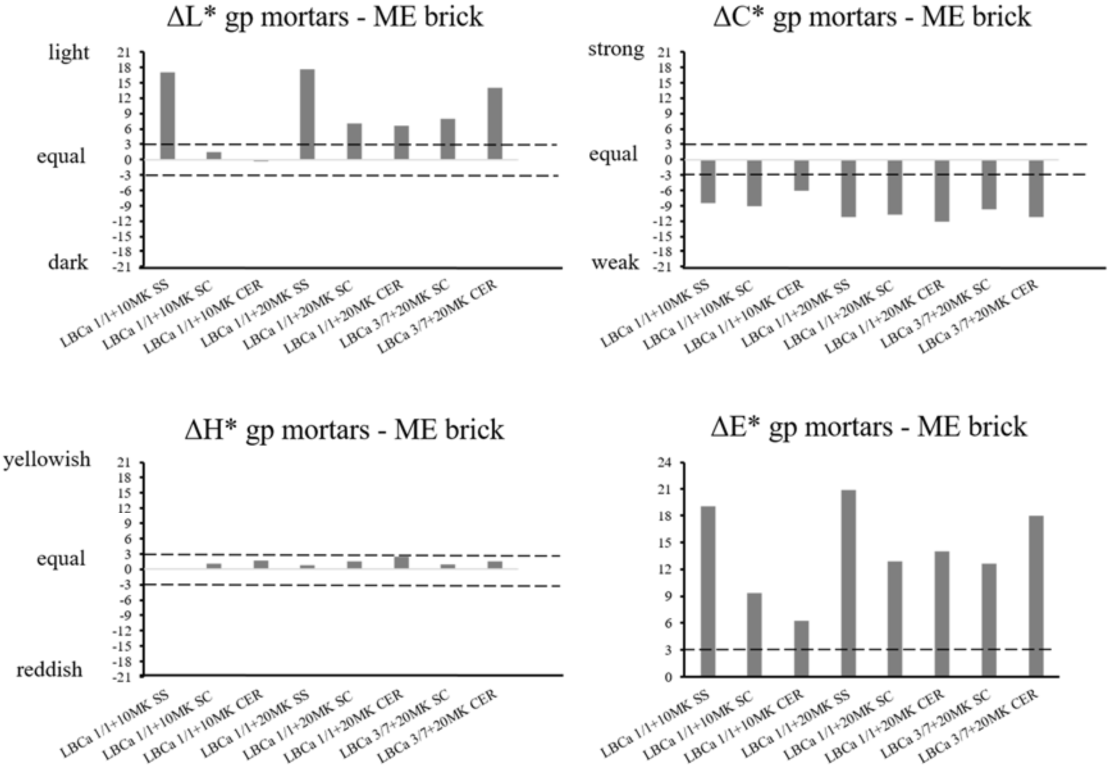

Fig. 6.58 – Partial and total colour differences of the LBCa geopolymeric mortars in respect to the ME brick. In the partial colour differences ΔL, ΔC* and ΔH* the same vertical numeric scales are used to show the relative weight of three chromatic variables on the total colour differences ΔE*. ΔL=lightness variation, ΔC=chroma variation and ΔH=hue variation. The dashed lines indicate the perceptibility limit, which is equal to 3 units (Benavente et al., 2003).*

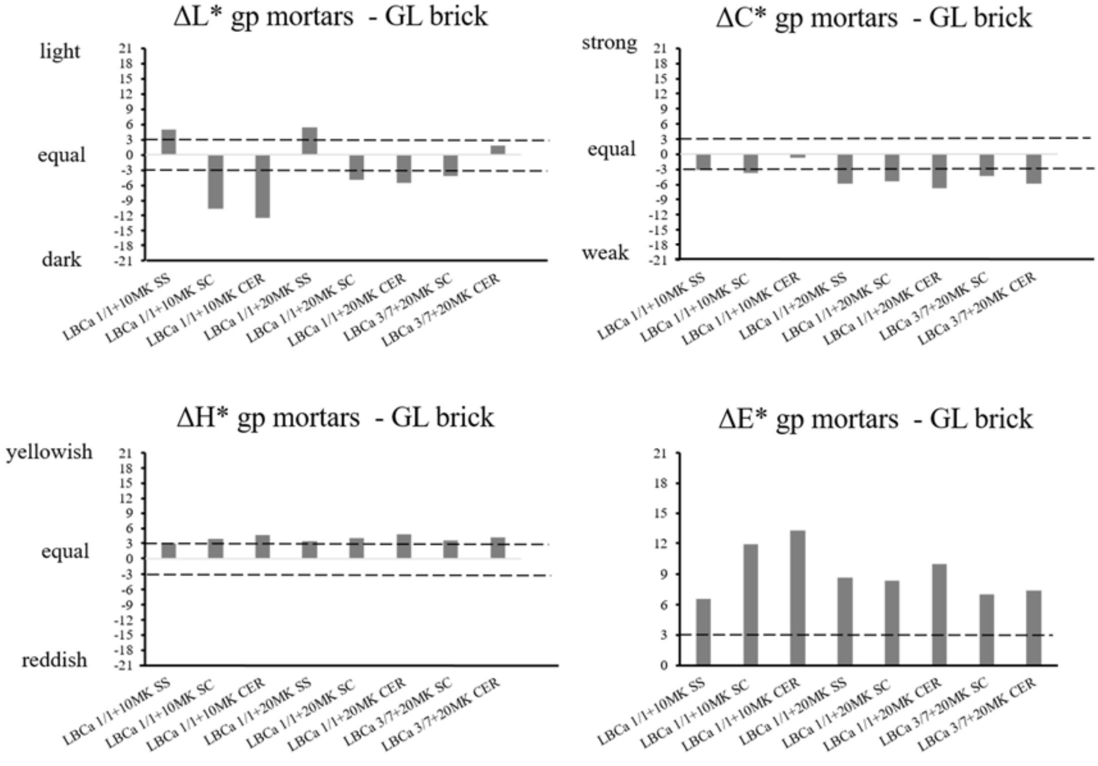

Fig. 6.59 – Partial and total colour differences of the LBCa geopolymeric mortars in respect to the GL brick. In the partial colour differences ΔL, ΔC* and ΔH* the same vertical numeric scales are used to show the relative weight of three chromatic variables on the total colour differences ΔE*. ΔL=lightness variation, ΔC=chroma variation and ΔH=hue variation. The dashed lines indicate the perceptibility limit, which is equal to 3 units (Benavente et al., 2003).*

As expected, it is possible to notice how the addition of aggregates affects the colour parameters. Particularly, regardless to the type of aggregates used, the mortars show lower lightness values with respect to the original binder, with the exception of LBCa 3/7+20MK CER, which however does not show a perceptible colour change. All the ΔE calculated to the original binders are lower than 10, thus indicating the possibility to change the general appearance of the mortars by playing with the aggregates, but maintaining values similar to the original binders already studied. Chroma and hue variations are instead considered irrelevant.

Regarding the differences with the archaeological materials, it is important to note that good results are obtained in all the cases, with ΔE between 5 and 15, indicating a perceivable but not disturbing change in colour with respect to the surface to restore, in line with the restoration requests. The only exceptions are registered between ME brick and the mortars LBCa 3/7+20MK CER as well as those with siliceous sands, whose ΔE falls between 18 and 21. The best results for the purposes of this research are obtained for the mortars LBCa 1/1+10MK with carbonate sand and ceramic aggregates compared to ME brick, and LBCa 3/7+20MK with both type of aggregates compared to GL brick, as desired. These are lighter, while less saturated in respect to the brick on which we want to test them.

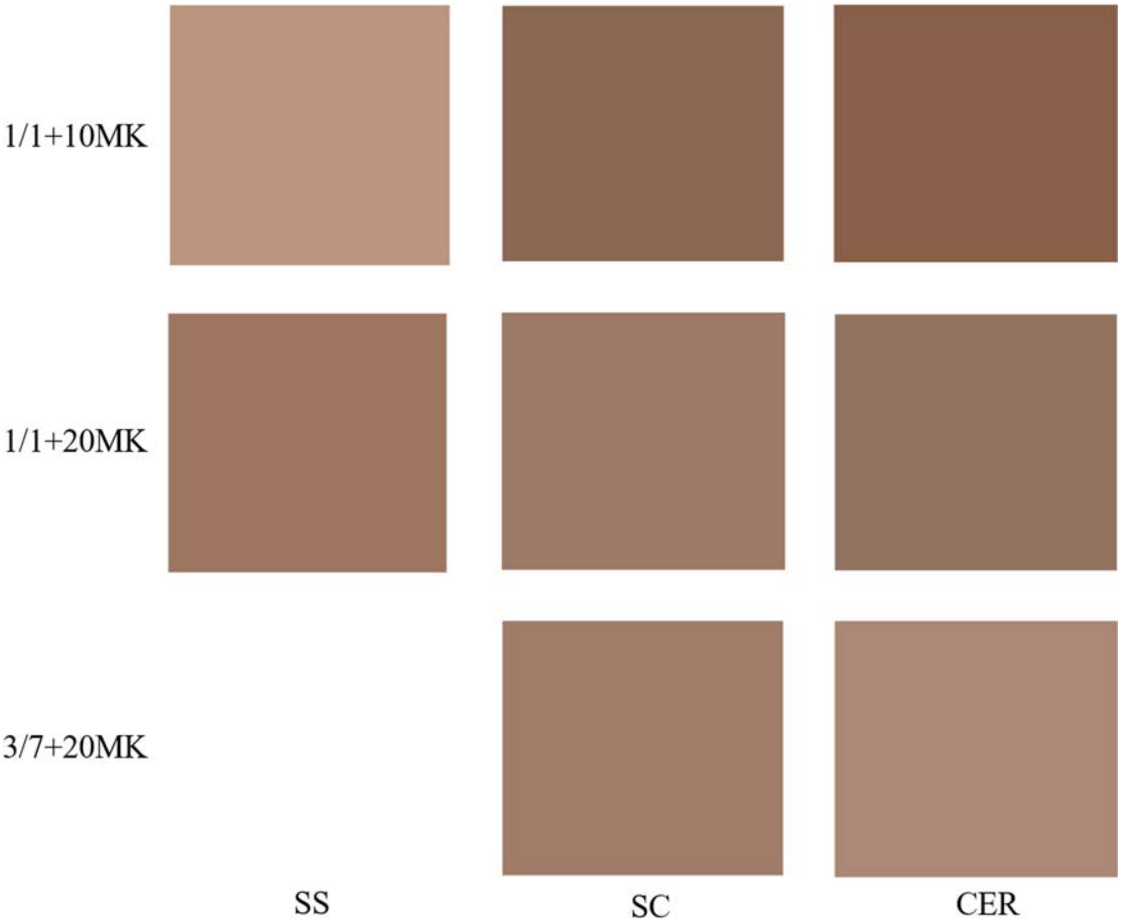

Fig. 6.60 – Pseudo-colours of the LBCa mortars.

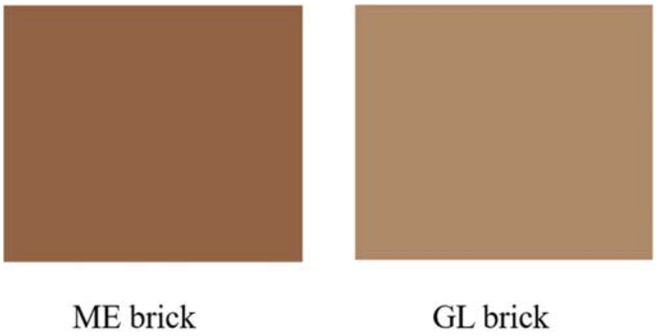

Fig. 6.61 – Pseudo-colours of the reference materials of archaeological interest.

				Comparison with ME brick						Comparison with GL brick					
Sample	L*	a*	b*	ΔL*	Δa*	Δb*	ΔE*	ΔC*	ΔH*	ΔL*	Δa*	Δb*	ΔE*	ΔC*	ΔH*
LBCa 1/1+10MK SS	64	11	18	17	-4	-7	19	-8	0	5	1	-4	7	-3	3
LBCa 1/1+10MK SC	49	11	17	1	-4	-8	9	-9	1	-11	2	-5	12	-4	4
LBCa 1/1+10MK CER	47	14	19	0	-2	-6	6	-6	2	-12	4	-3	13	-1	5
LBCa 1/1+20MK SS	65	10	15	18	-5	-10	21	-11	1	5	0	-7	9	-6	3
LBCa 1/1+20MK SC	54	11	15	7	-5	-10	13	-11	2	-5	1	-7	8	-5	4
LBCa 1/1+20MK CER	54	11	14	7	-5	-11	14	-12	2	-6	1	-8	10	-7	5
LBCa 3/7+20MK SC	55	11	16	8	-5	-9	13	-10	1	-4	1	-6	7	-4	4
LBCa 3/7+20MK CER	61	11	15	14	-5	-10	18	-11	2	2	1	-7	7	-6	4

*Table 6.12 – CIE-L*a*b* chromatic parameters measured on LBCa geopolymeric mortars and comparison with references archaeological bricks (ME brick and GL brick).*

Mortars vs Binders	L*	a*	b*	ΔL*	Δa*	Δb*	ΔE*	ΔC*	ΔH*
LBCa 1/1+10MK	52	12	17						
with SC	49	11	17	-4	0	-1	4	-1	0
with CER	47	14	19	-6	2	2	6	2	1
LBCa 1/1+20MK	63	10	12						
with SC	54	11	15	-9	1	3	9	3	1
with CER	54	11	14	-9	1	1	9	2	0
LBCa 3/7+20MK	60	10	14						
with SC	55	11	16	-5	0	2	5	2	1
with CER	61	11	15	1	0	1	2	1	0

*Table 6.13 – CIE-L*a*b* chromatic parameters measured on LBCa geopolymeric mortars and comparison with references LBCa binders.*

References

Alipour, L., Hamamoto, M., Nakashima, S., Harui, R., Furiki, M., Oku, O., 2016. Infrared Microspectroscopy of Bionanomaterials (Diatoms) with Careful Evaluation of Void Effects. Appl. Spectrosc. 70, 427–442. https://doi.org/10.1177/0003702815626665

Aly, Z., Vance, E.R., Perera, D.S., Hanna, J. V., Griffith, C.S., Davis, J., Durce, D., 2008. Aqueous leachability of metakaolin-based geopolymers with molar ratios of Si/Al = 1.5-4. J. Nucl. Mater. 378, 172–179. https://doi.org/10.1016/j.jnucmat.2008.06.015

Arnoult, M., Perronnet, M., Autef, A., Rossignol, S., 2018. How to control the geopolymer setting time with the alkaline silicate solution. J. Non. Cryst. Solids 495, 59–66. https://doi.org/10.1016/j.jnoncrysol.2018.02.036

Azevedo, A.G. de S., Strecker, K., Lombardi, C.T., 2018. Produção de geopolímeros à base de metacaulim e cerâmica vermelha. Cerâmica 64, 388–396. https://doi.org/10.1590/0366-69132018643712420

Barone, G., Campani, E., Casoli, A., La Russa, M.F., Lo Giudice, A., Mazzoleni, P., Pezzino, A., 2008. The Cathedral of St. Giorgio in Ragusa Ibla (Italy): A case study of the use of protective products. Environ. Geol. 54, 1501–1506. https://doi.org/10.1007/s00254-007-0931-3

Barone, G., Finocchiaro, C., Lancellotti, I., Leonelli, C., Mazzoleni, P., Sgarlata, C., Stroscio, A., 2021. Potentiality of the Use of Pyroclastic Volcanic Residues in the Production of Alkali Activated Material. Waste and Biomass Valorization 12, 1075–1094. https://doi.org/10.1007/s12649-020-01004-6

Barone, G., Mazzoleni, P., Spagnolo, G., Aquilia, E., 2012. The transport amphorae of Gela: A multidisciplinary study on provenance and technological aspects. J. Archaeol. Sci. 39, 11–22. https://doi.org/10.1016/j.jas.2011.06.018

Belver, C., Breen, C., Clegg, F., Fernandes, C.E., Vicente, M.A., 2005. A variable-temperature diffuse reflectance infrared fourier transform spectroscopy study of the binding of water and pyridine to the surface of acid-activated metakaolin. Langmuir 21, 2129–2136. https://doi.org/10.1021/la048323m

Benavente, D., Martínez-Verdú, F., Bernabeu, A., Viqueira, V., Fort, R., García del Cura, M.A., Illueca, C., Ordóñez, S., 2003. Influence of Surface Roughness on Color Changes in Building Stones. Color Res. Appl. 28, 343–351. https://doi.org/10.1002/col.10178

Berns, R.S., 2000. Billmeyer and Saltzman's Principles of Color Technology, 3rd ed. John Wiley, New York.

Caggiani, M.C., Coccato, A., Barone, G., Finocchiaro, C., Fugazzotto, M., Lanzafame, G., Occhipinti, R., Stroscio, A., Mazzoleni, P., 2021. Raman spectroscopy potentiality in the study of geopolymers reaction degree. J. Raman Spectrosc. 1–13. https://doi.org/10.1002/jrs.6167

Clausi, M., Fernández-Jiménez, A.M., Palomo, A., Tarantino, S.C., Zema, M., 2018. Reuse of waste sandstone sludge via alkali activation in matrices of fly ash and metakaolin. Constr. Build. Mater. 172, 212–223. https://doi.org/10.1016/j.conbuildmat.2018.03.221

Clausi, M., Tarantino, S.C., Magnani, L.L., Riccardi, M.P., Tedeschi, C., Zema, M., 2016. Metakaolin as a precursor of materials for applications in Cultural Heritage: Geopolymer-based mortars with ornamental stone aggregates. Appl. Clay Sci. 132–133, 589–599. https://doi.org/10.1016/j.clay.2016.08.009

Criado, M., Palomo, A., Fernández-Jiménez, A., 2005. Alkali activation of fly ashes. Part 1: Effect of curing conditions on the carbonation of the reaction products. Fuel 84, 2048–2054. https://doi.org/10.1016/j.fuel.2005.03.030

D'Elia, A., Pinto, D., Eramo, G., Laviano, R., Palomo, A., Fernández-Jiménez, A., 2020. Effect of alkali concentration on the activation of carbonate-high illite clay. Appl. Sci. 10, 1–14. https://doi.org/10.3390/app10072203

Deere, D.U., Miller, R.P., 1966. Engineering classification and index properties for intact rocks. Technical Report AFNL-TR-65-116. Air Force Weapon Laboratory, New Mexico.

Duxson, P., Fernández-Jiménez, A., Provis, J.L., Lukey, G.C., Palomo, A., Van Deventer, J.S.J., 2007. Geopolymer technology: The current state of the art. J. Mater. Sci. 42, 2917–2933. https://doi.org/10.1007/s10853-006-0637-z

Duxson, P., Provis, J.L., Lukey, G.C., Mallicoat, S.W., Kriven, W.M., Van Deventer, J.S.J.,

2005. Understanding the relationship between geopolymer composition, microstructure and mechanical properties. Colloids Surfaces A Physicochem. Eng. Asp. 269, 47–58. https://doi.org/10.1016/j.colsurfa.2005.06.060

Fernández-Jiménez, A., de la Torre, A.G., Palomo, A., López-Olmo, G., Alonso, M.M., Aranda, M.A.G., 2006. Quantitative determination of phases in the alkaline activation of fly ash. Part II: Degree of reaction. Fuel 85, 1960–1969. https://doi.org/10.1016/j.fuel.2006.04.006

Fernández-Jiménez, A., Palomo, A., 2005. Composition and microstructure of alkali activated fly ash binder: Effect of the activator. Cem. Concr. Res. 35, 1984–1992. https://doi.org/10.1016/j.cemconres.2005.03.003

Froment, F., Tournié, A., Colomban, P., 2008. Raman identification of natural red to yellow pigments: ochre and iron-containing ores. J. Raman Spectrosc. 38, 560–568.

Frost, R.L., Jonansson, U., 1998. Combination bands in the infrared spectroscopy of kaolins - A drift spectroscopic study. Clays Clay Miner. 46, 466–477. https://doi.org/10.1346/CCMN.1998.0460411

García-Lodeiro, I., Fernández-Jiménez, A., Palomo, A., 2013. Variation in hybrid cements over time. Alkaline activation of fly ash-portland cement blends. Cem. Concr. Res. https://doi.org/10.1016/j.cemconres.2013.03.022

García-Lodeiro, I., Maltseva, O., Palomo, Á., Fernández-Jiménez, A., 2012. Hybrid alkaline cements. Part I: Fundamentals. Rev. Rom. Mater. Rom. J. Mater. 42 (4), 330–335.

Garcia-Lodeiro, I., Palomo, A., Fernandez-Jimenez, A., Macphee, D.E., 2011. Compatibility studies between N-A-S-H and C-A-S-H gels. Study in the ternary diagram Na2O–CaO–Al2O3–SiO2–H2O. Cem. Concr. Res. 41, 923–931. https://doi.org/10.1016/j.cemconres.2011.05.006

Granizo, M.L., Blanco-Varela, M.T., Martínez-Ramírez, S., 2007. Alkali activation of metakaolins: Parameters affecting mechanical, structural and microstructural properties. J. Mater. Sci. 42, 2934–2943. https://doi.org/10.1007/s10853-006-0565-y

Hajimohammadi, A., Provis, J.L., Van Deventer, J.S.J., 2011. Time-resolved and spatially-resolved infrared spectroscopic observation of seeded nucleation controlling geopolymer gel formation. J. Colloid Interface Sci. 357, 384–392. https://doi.org/10.1016/j.jcis.2011.02.045

He, J., Zhang, J., Yu, Y., Zhang, G., 2012. The strength and microstructure of two geopolymers derived from metakaolin and red mud-fly ash admixture: A comparative study. Constr. Build. Mater. 30, 80–91. https://doi.org/10.1016/j.conbuildmat.2011.12.011

Jentzsch, P.V., Kampe, B., Ciobotă, V., Rösch, P., Popp, J., 2013. Inorganic salts in atmospheric particulate matter: Raman spectroscopy as an analytical tool. Spectrochim. Acta - Part A Mol. Biomol. Spectrosc. 115, 697–708. https://doi.org/10.1016/j.saa.2013.06.085

Khan, M.I., Azizli, K.A., Sufian, S., Man, Z., Khan, A.S., Ullah, H., Siyal, A.A., 2016. A Short Review of Infra-Red Spectroscopic Studies of Geopolymers. Adv. Mater. Res. 1133, 231–235. https://doi.org/10.4028/www.scientific.net/amr.1133.231

Komnitsas, K., Zaharaki, D., 2007. Geopolymerisation: A review and prospects for the minerals industry. Miner. Eng. 20, 1261–1277. https://doi.org/10.1016/j.mineng.2007.07.011

Komnitsas, K., Zaharaki, D., Vlachou, A., Bartzas, G., Galetakis, M., 2015. Effect of synthesis parameters on the quality of construction and demolition wastes (CDW) geopolymers. Adv. Powder Technol. 26, 368–376. https://doi.org/10.1016/j.apt.2014.11.012

Kosor, T., Nakić-Alfirević, B., Gajović, A., 2016a. Geopolymerization index of fly ash geopolymers. Vib. Spectrosc. 85, 104–111. https://doi.org/10.1016/j.vibspec.2016.04.005

Kosor, T., Nakić-Alfirević, B., Svilović, S., 2016b. Geopolymer depolymerization index. Vib. Spectrosc. 86, 143–148. https://doi.org/10.1016/j.vibspec.2016.07.004

Lancellotti, I., Catauro, M., Ponzoni, C., Bollino, F., Leonelli, C., 2013. Inorganic polymers from alkali activation of metakaolin: Effect of setting and curing on structure. J. Solid State Chem. 200, 341–348. https://doi.org/10.1016/j.jssc.2013.02.003

Lee, W.K.W., Van Deventer, J.S.J., 2004. The interface between natural siliceous aggregates and geopolymers. Cem. Concr. Res. 34, 195–206.

https://doi.org/10.1016/S0008-8846(03)00250-3

Lentini, M.C., Martinelli, M.C., Vanaria, M.G., 2010. Messina - Stratigrafia di una città. Resti dell'antico tessuto urbano in Piazza Duomo (campagna di scavi 2005-2006)., in: Atti Della Accademia Nazionale Dei Lincei. Notizie Degli Scavi Di Antichità. Scienze e Lettere Ediore commerciale, Roma, pp. 359–420.

Leonelli, C., Romagnoli, M., 2013. Geopolimeri: polimeri inorganici attivati chimicamente., 2nd ed. ICerS, Bologna.

Madejová, J., Komadel, P., 2001. Baseline studies of the clay minerals society source clays: Infrared methods. Clays Clay Miner. 49, 410–432. https://doi.org/10.1346/CCMN.2001.0490508

Mierzwiński, D., Łach, M., Hebda, M., Walter, J., Szechyńska-Hebda, M., Mikuła, J., 2019. Thermal phenomena of alkali-activated metakaolin studied with a negative temperature coefficient system. J. Therm. Anal. Calorim. 138, 4167–4175. https://doi.org/10.1007/s10973-019-08471-7

Mladenović, N., Kljajević, L., Nenadović, S., Ivanović, M., Čalija, B., Gulicovski, J., Trivunac, K., 2020. The Applications of New Inorganic Polymer for Adsorption Cadmium from Waste Water. J. Inorg. Organomet. Polym. Mater. 30, 554–563. https://doi.org/10.1007/s10904-019-01215-y

Murad, E., 1997. Identification of minor amounts of anatase in kaolins by Raman spectroscopy. Am. Mineral. 82, 203–206. https://doi.org/10.2138/am-1997-1-222

Norme tecniche per le costruzioni. Decreto del Ministero delle Infrastrutture, 14/01/2008.

Occhipinti, R., Stroscio, A., Finocchiaro, C., Fugazzotto, M., Leonelli, C., Lo Faro, M.J., Megna, B., Barone, G., Mazzoleni, P., 2020. Alkali activated materials using pumice from the Aeolian Islands (Sicily, Italy) and their potentiality for cultural heritage applications: Preliminary study. Constr. Build. Mater. 259, 120391. https://doi.org/10.1016/j.conbuildmat.2020.120391

Pacheco-Torgal, F., Jalali, S., 2010. Reusing ceramic wastes in concrete. Constr. Build. Mater. 24, 832–838. https://doi.org/10.1016/j.conbuildmat.2009.10.023

Pachego-Torgal, F., Labrincha, J.A., Leonelli, C., Palomo, A., Chindaprasirt, P., 2014.

Handbook of Alkali-activated cements, mortars and concretes. Elsevier.

Panizza, M., Natali, M., Garbin, E., Tamburini, S., Secco, M., 2018. Assessment of geopolymers with Construction and Demolition Waste (CDW) aggregates as a building material. Constr. Build. Mater. 181, 119–133. https://doi.org/10.1016/j.conbuildmat.2018.06.018

Pardal, X., Pochard, I., Nonat, A., 2009. Experimental study of Si–Al substitution in calcium-silicate-hydrate (C-S-H) prepared under equilibrium conditions. Cem. Concr. Res. 39, 637–643. https://doi.org/10.1016/j.cemconres.2009.05.001

Pathak, A., Kumar, S., V.K., J., 2014. Development of Building Material from Geopolymerization of Construction and Demolition Waste (CDW). Trans. Indian Ceram. Soc. 73, 133–137. https://doi.org/10.1080/0371750X.2014.922429

Rees, C.A., Provis, J.L., Lukey, G.C., Van Deventer, J.S.J., 2007. Attenuated Total Reflectance Fourier Transform Infrared Analysis of Fly Ash Geopolymer Gel Aging. Langmuir 23, 8170–8179. https://doi.org/10.1021/la700713g

Reig, L., Tashima, M.M., Borrachero, M. V., Monzó, J., Cheeseman, C.R., Payá, J., 2013. Properties and microstructure of alkali-activated red clay brick waste. Constr. Build. Mater. 43, 98–106. https://doi.org/10.1016/j.conbuildmat.2013.01.031

Renaudin, G., Russias, J., Leroux, F., Cau-dit-Coumes, C., Frizon, F., 2009. Structural characterization of C-S-H and C-A-S-H samples-Part II: Local environment investigated by spectroscopic analyses. J. Solid State Chem. 182, 3320–3329. https://doi.org/10.1016/j.jssc.2009.09.024

Rescic, S., Fratini, F., 2013. Geopolimeri e Beni Culturali., in: Leonelli, C., Romagnoli, M. (Eds.), Geopolimeri: Polimeri Inorganici Attivati Chimicamente. ICerS, Bologna, pp. 252–278.

Robayo, R.A., Mulford, A., Munera, J., Mejía de Gutiérrez, R., 2016. Alternative cements based on alkali-activated red clay brick waste. Constr. Build. Mater. 128, 163–169. https://doi.org/10.1016/j.conbuildmat.2016.10.023

Rovnaník, P., Rovnaníková, P., Vyšvařil, M., Grzeszczyk, S., Janowska-Renkas, E., 2018. Rheological properties and microstructure of binary waste red brick powder/metakaolin geopolymer. Constr. Build. Mater. 188, 924–933.

https://doi.org/10.1016/j.conbuildmat.2018.08.150

Rüscher, C.H., Mielcarek, E., Wongpa, J., Jirasit, F., Lutz, W., 2010. New Insights on Geopolymerisation Using Molybdate, Raman, and Infrared Spectroscopy, in: Kriven, W.M., Zhou, Y., Radovic, M., Mathur, S., Ohji, T. (Eds.), Strategic Materials and Computational Design. The American Ceramic Society, Westerville, pp. 17–34.

Steinerová, M., Schweigstillová, J., 2013. Porous microstructure of the interfacial transition zone in geopolymer composites. Ceram. - Silikaty 57 (4), 328–335.

Sun, Z., Cui, H., An, H., Tao, D., Xu, Y., Zhai, J., Li, Q., 2013. Synthesis and thermal behavior of geopolymer-type material from waste ceramic. Constr. Build. Mater. 49, 281–287. https://doi.org/10.1016/j.conbuildmat.2013.08.063

Szechyńska-Hebda, M., Marczyk, J., Ziejewska, C., Hordyńska, N., Mikuła, J., Hebda, M., 2019. Neutral geopolymer foams reinforced with cellulose studied with the FT-Raman spectroscopy. IOP Conf. Ser. Mater. Sci. Eng. 706. https://doi.org/10.1088/1757-899X/706/1/012017

Tuyan, M., Andiç-Çakir, Ö., Ramyar, K., 2018. Effect of alkali activator concentration and curing condition on strength and microstructure of waste clay brick powder-based geopolymer. Compos. Part B Eng. 135, 242–252. https://doi.org/10.1016/j.compositesb.2017.10.013

UNI, 2000. Beni culturali - Materiali lapidei naturali ed artificiali - Determinazione dell'assorbimento d'acqua per capillarità. 10859.

Volz, H., 2001. Industrial color testing. Weinheim.

Walrafen, G.E., 1975. Raman spectra from Si-OH groups in solid optical fibers. J. Chem. Phys. 62, 297–298. https://doi.org/10.1063/1.430224

Wan, Q., Rao, F., Song, S., Zhang, Y., 2019. Immobilization forms of ZnO in the solidification/stabilization (S/S) of a zinc mine tailing through geopolymerization. J. Mater. Res. Technol. 8, 5728–5735. https://doi.org/10.1016/j.jmrt.2019.09.040

Winter, N.B., 2009. Understanig cement. An introduction to cement production, cement hydration and deleterious processes in concrete. WHD Microanalysis Consultants Ltd.

Xu, G., Zhong, J., Shi, X., 2018. Influence of graphene oxide in a chemically activated fly ash. Fuel 226, 644–657. https://doi.org/10.1016/j.fuel.2018.04.033

Yip, C.K., Lukey, G.C., Van Deventer J.S.J., 2005. The coexistence of geopolymeric gel and calcium silicate hydrate at the early stage of alkaline activation. Cem. Concr. Res. 32, 1688–1697. https://doi.org/10.1016/j.cemconres.2004.10.042

Yip, C.K., Lukey, G.C., Provis, J.L., Van Deventer J.S.J., 2008. Effect of calcium silicate sources on geopolymerisation. Cem. Concr. Res. 38, 554–564. https://doi.org/10.1016/j.cemconres.2007.11.001

Chapter 7

Geopolymers from industrial hollow bricks

7.1 Geopolymeric binders

7.1.1 Mineralogical characterization (XRD)

The XRD patterns of the studied binders are reported in Figg. 7.1 (binders from ceramic waste) and 7.2 (binary mixtures). The XRD patterns of the ceramic and MK precursors have been reported for comparison. All the measurements have been carried out after 28 days of curing.

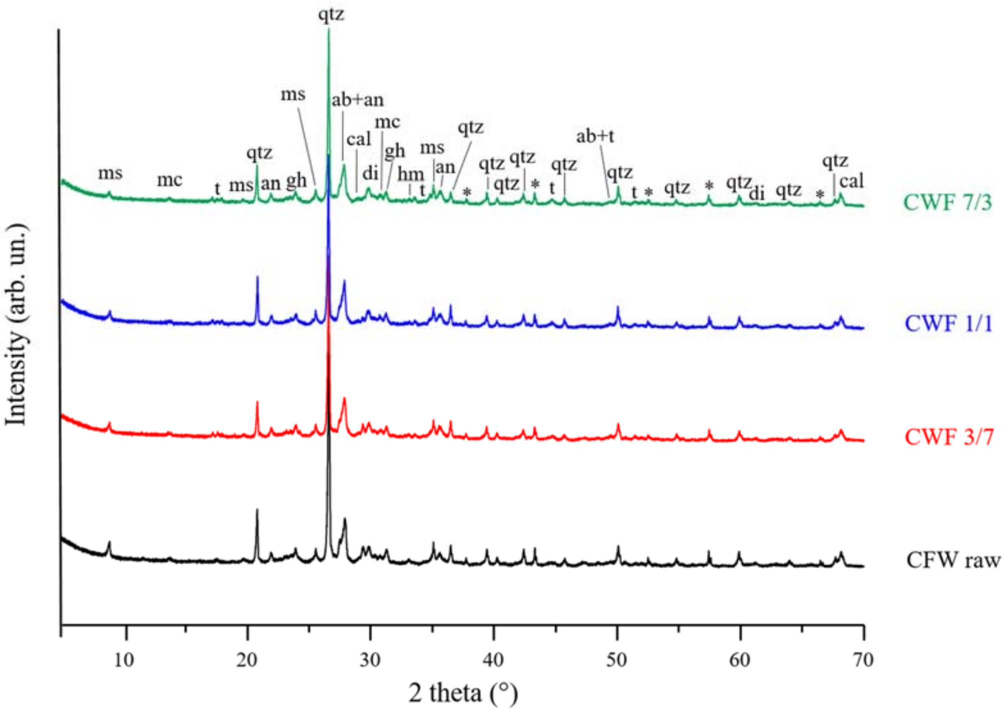

*Fig. 7.1 – Diffraction patterns of CWF 3/7, CWF 1/1, CWF 7/3 and CWF raw; qtz=quartz; di=diopside; gh=gehlenite; hm=haematite; mc=microcline; an=anorthite; ab=albite; cal=calcite; ms=muscovite; t=trona; * indicates corundum, added as internal standard.*

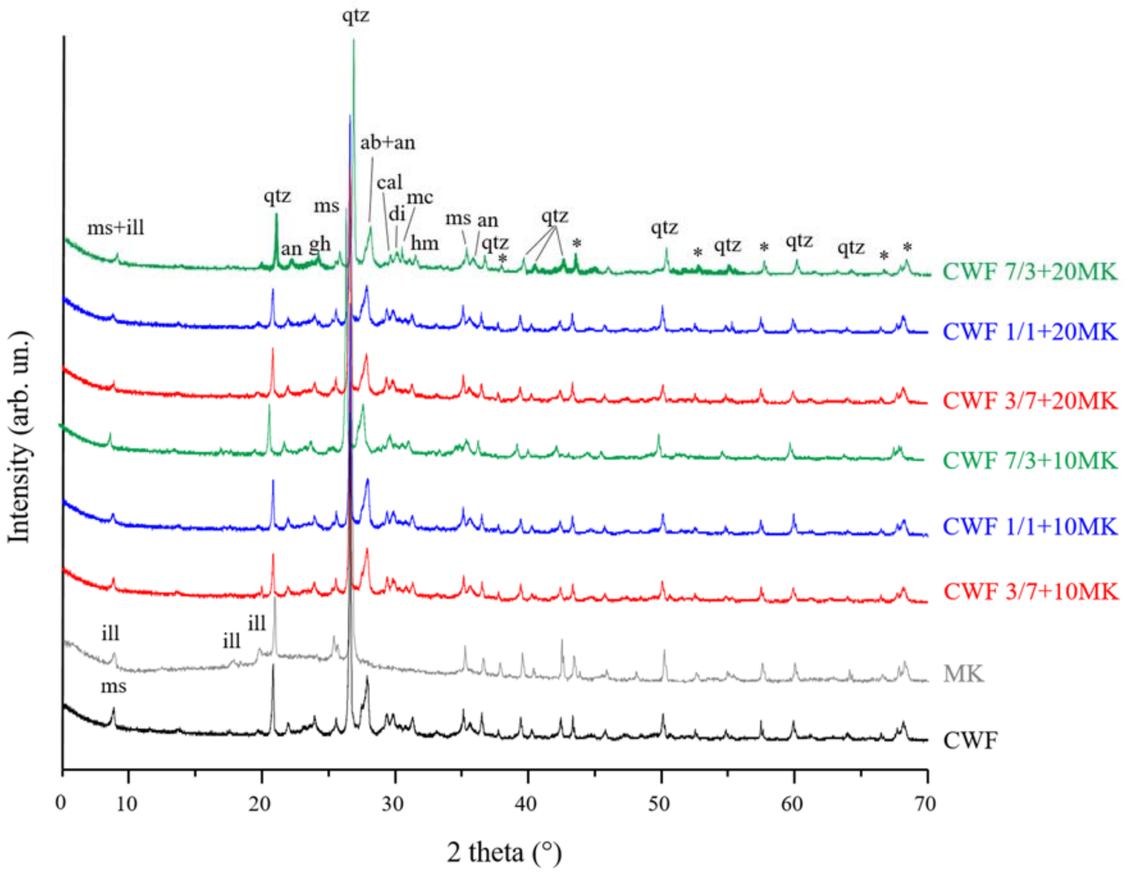

*Fig. 7.2 – Diffraction patterns of 10% MK e 20% MK samples and the relative raw materials CWF and MK; qtz=quartz; di=diopside; gh=gehlenite; hm=haematite; mc=microcline; an=anorthite; ab=albite; cal=calcite; ms=muscovite; ill=illite; * indicates corundum, added as internal standard.*

All diffraction patterns display peaks due to crystalline phases deriving from the precursors, namely quartz, diopside, gehlenite, haematite, feldspars (microcline and plagioclases), calcite and muscovite, with the addition of illite from MK in the binary samples. Furthermore, new phases related to carbonate efflorescences (mainly natron and trona) are individuated. Other new crystalline phases are not evidenced and no significant differences are highlighted between geopolymer series with different alkaline solution ratios. Similar to what observed for LBCa-based geopolymeric binders, no zeolites are individuated, probably because of the synthesis parameters which involve room temperature and too low amounts of reactive alumina (D’Elia et al., 2020).

The Rietveld refinement gave the possibility to study the amorphous content increment between the precursors and the relative geopolymers. The results are summarized in Fig. 7.3, together with the content of efflorescences.

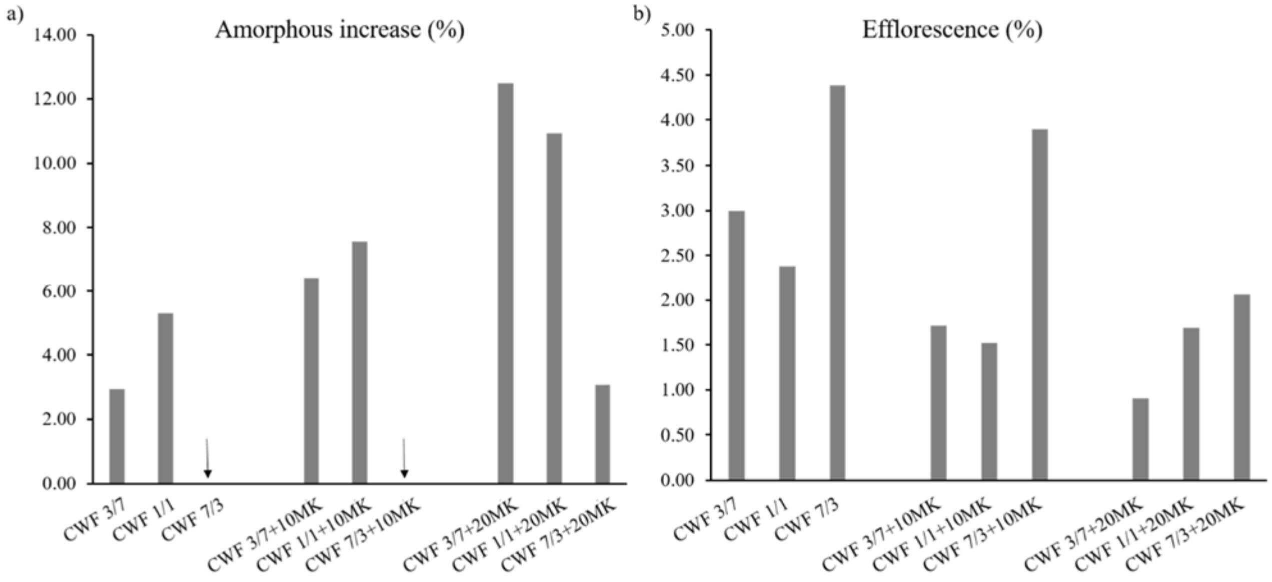

Fig. 7.3 – Histogram of CWF geopolymer series showing the amorphous content increase a) and efflorescence amounts b). The amorphous content has been calculated after the normalization of the data without efflorescence amounts. The black arrows indicate those samples which present negative values.

The amorphous content increases with the increase of MK in the paste, except to sample 7/3+20MK which is comparable to 3/7 sample. Regarding the sodium hydroxide/waterglass, the amorphous content increases going from 3/7 to 1/1, thus suggesting a better geopolymerization with the intermediate values. When exceeding this sodium hydroxide/waterglass ratio, the amorphous content appears instead reduced. The negative values calculated for samples 7/3 and 7/3+10MK have to be attributed to an incorrect corundum addition or inhomogeneous mixing of it.

An opposite pattern is evident, instead, when going from the formulation with 10% of MK towards those with 20%: in particular, the amorphous increases together with the waterglass increase.

Regarding the efflorescences, these are generally low in the series 3/7, increasing in the series 7/3, thus indicating clearly an excess of Na in the 7/3 pastes. In this latter case, the sodium not being taken up in the geopolymer structure remains available for environmental carbonation processes, as already seen in the LBCa geopolymeric series.

Considering the decrease of the single phases, it was possible to individuate the higher contribution (i.e. dissolution) in the geopolymerization process of calcite (c.a. decrease of 80%), microcline and gehlenite (c.a. 40% each).

7.1.2 Microstructural characterization and gel chemical investigation (SEM-EDS, TEM-EDS)

SEM-EDS

As already done for the LBCa series, in order to point out the differences in the microstructure and chemical composition of the products developed from CWF, SEM-EDS analyses at different length scales have been carried out.

The SEM-micrographs will show in sequence the low magnification images of the formulations without MK (Fig. 7.4), the low magnification images of the formulations with 10% (Fig. 7.5) and of those with 20% of MK (Fig. 7.6). The relative spectra acquired on the matrix morphologies are shown in the already mentioned figures. Details at higher magnification of the matrix and/or relict minerals and/or secondary products, with the relative spectra eventually acquired, are shown in the successive images, again in sequence for formulations containing 0% (Fig. 7.7), 10% (Fig. 7.8) and 20% of MK (Fig. 7.9).

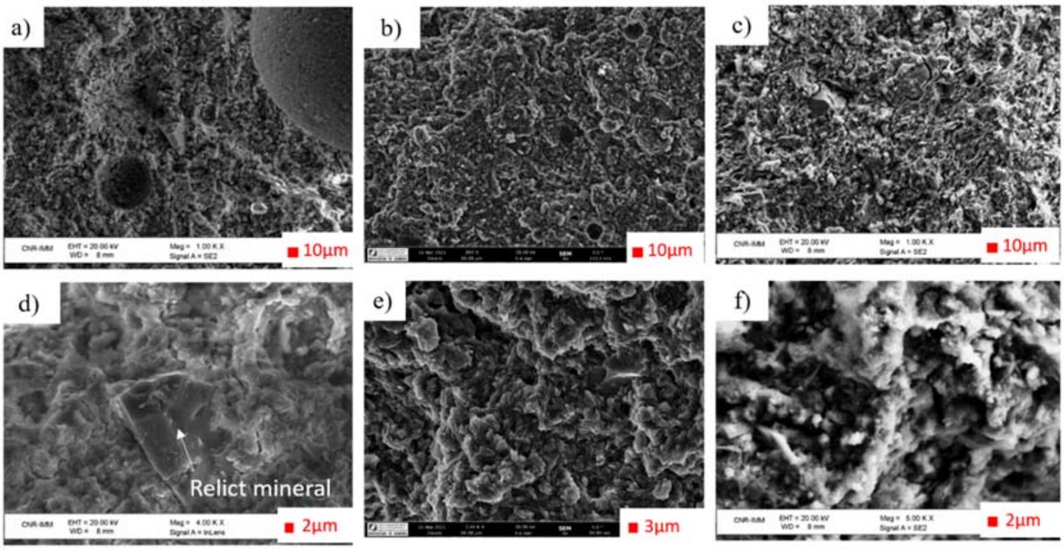

Fig. 7.4 – SEM micrographs at different magnifications of CWF 3/7 a) and d); CWF 1/1 b) and e); and CWF 7/3 c) and f).

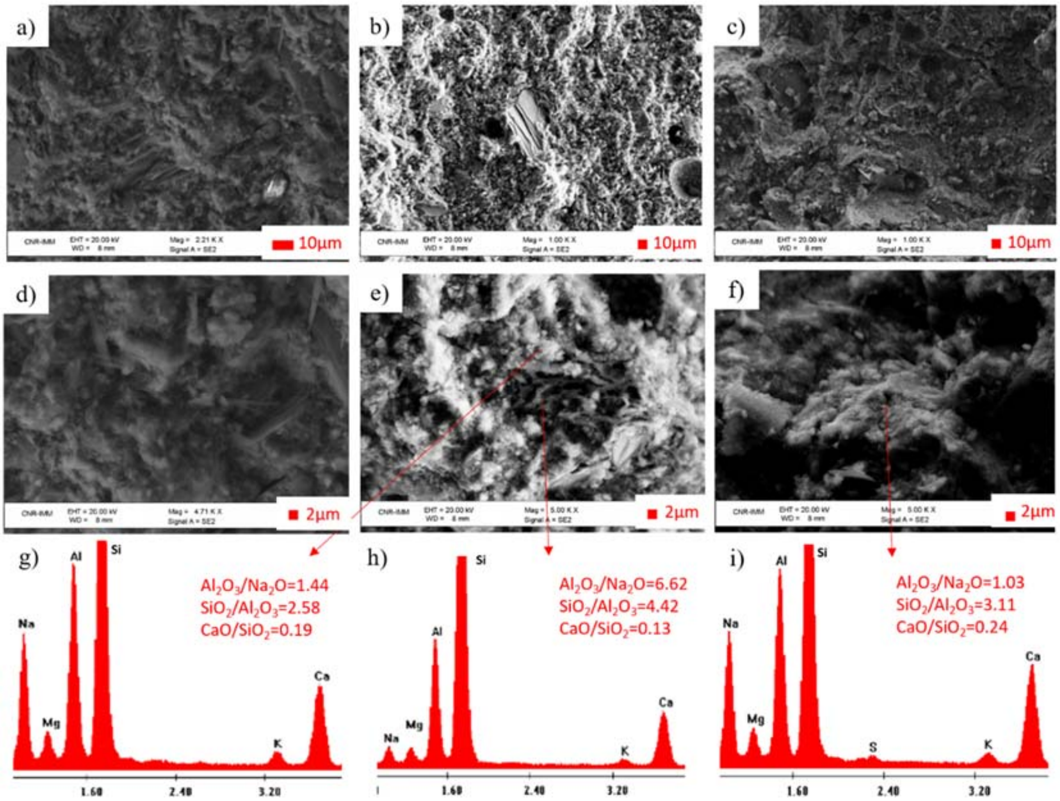

Fig. 7.5 – SEM micrographs at different magnifications of CWF 3/7+10MK a) and d); CWF 1/1+10MK b) and e); and CWF 7/3+10MK c) and f). The representative spectra acquired on the granular morphologies g) and i) and on the net morphology h) are also shown.

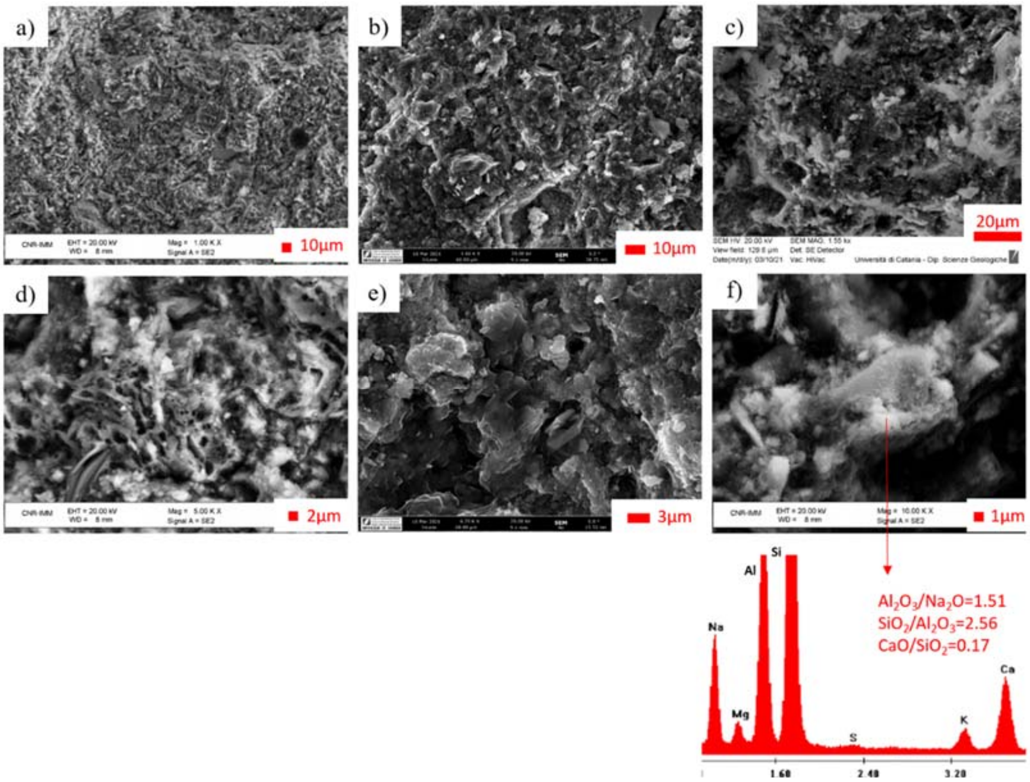

Fig. 7.6 – SEM micrographs at different magnifications of CWF 3/7+20MK a) and d); CWF 1/1+20MK b) and e); and CWF 7/3+20MK c) and f). The representative spectrum acquired on the granular morphologies are also shown.

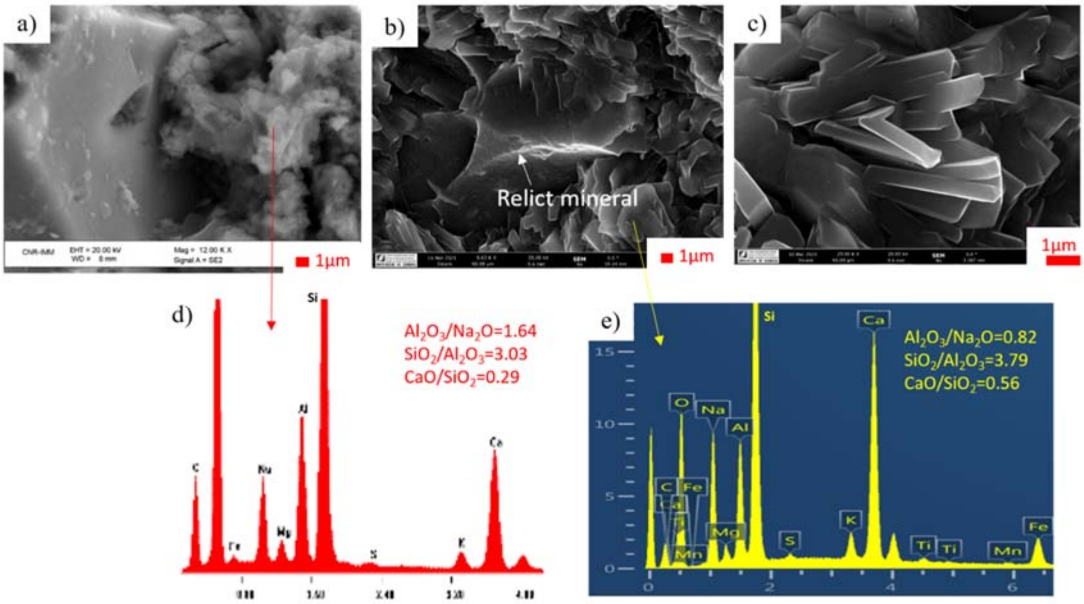

Fig. 7.7 – SEM micrographs of CWF 3/7 a); CWF 1/1 b) and c); and the relative matrices spectra d) and e). The micrographs represent details of granular particles embedding a relict mineral and a detail of the geometrical morphology.

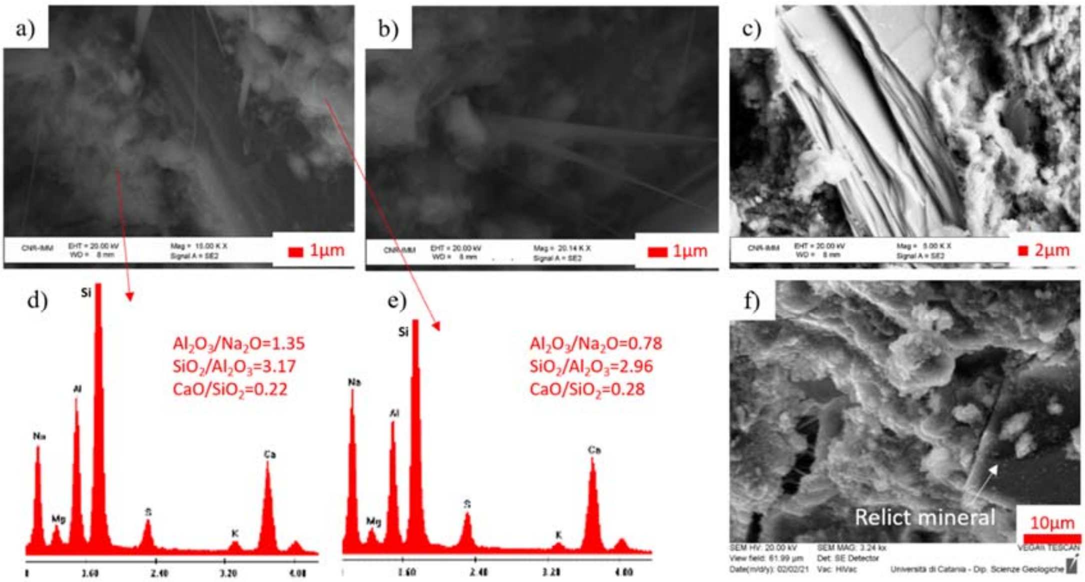

Fig. 7.8 – SEM micrographs details of CWF 3/7+10MK matrix around a relict mineral a) and acicular crystal b); spectra acquired in different points of the matrix of CWF 3/7+10MK d) and e). Details of the matrix embedding a relict mineral in sample CWF 1/1+10MK c) and in sample CWF 7/3+10MK f) are also shown.

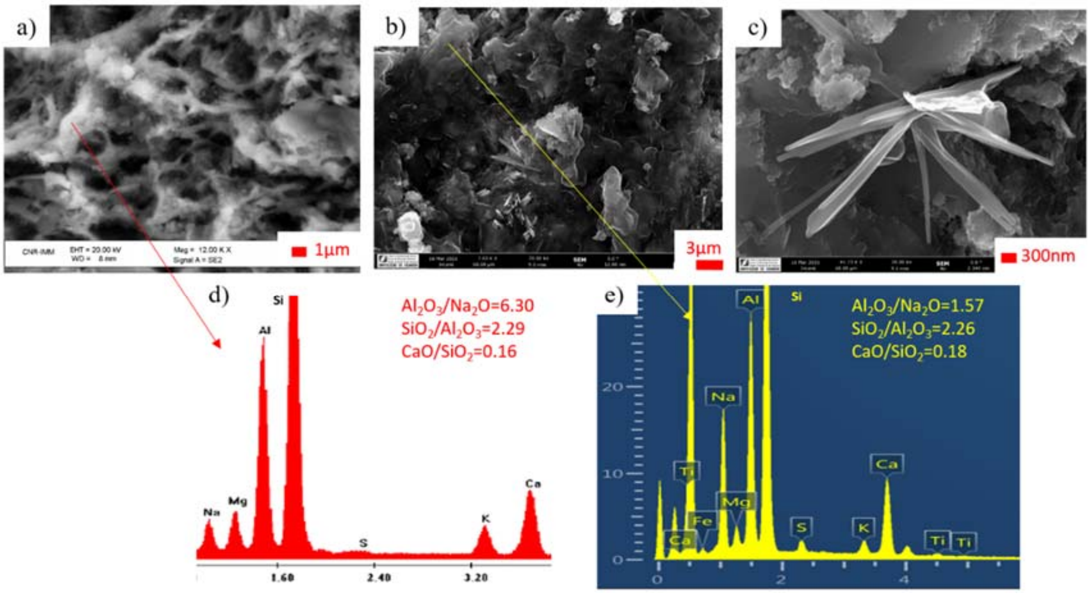

Fig. 7.9 – SEM micrographs of CWF 3/7+20MK a); CWF 1/1+20MK b) and c); spectra of the net/granular morphology d) and of the prismatic one e) are also shown. The micrographs represent details of the granular and net morphologies a), of the smoother one b) and of an acicular crystal c).

At low magnification all the samples show a homogeneous structure, whose morphology is consistent with that of geopolymeric resins (Azevedo et al., 2018; Reig et al., 2013; Robayo et al., 2016; Sun et al., 2013). All matrices appear compact with a dense texture, characterized by granular morphologies more or less "welded" particularly visible on the surfaces (Figg. 7.4, 7.5 and 7.6), consistent with the geopolymeric gel morphology (García-Lodeiro et al., 2012; He et al., 2012). Furthermore, sample 1/1+20MK reveals a glassy-like area, giving clues of a successful reaction (Fig. 7.6e). These observations are analogous to what observed in the LBCa-based geopolymeric binders.

At low magnifications, the presence of heterogeneous porosity spread all over the surfaces is evident (Figg. 7.4, 7.5 and 7.6). As well as on the LBCa geopolymeric series, their shape and dimension allow to attribute them to air bubbles trapped in the matrix during the synthesis (Duxson et al., 2005; Komnitsas et al., 2015; Panizza et al., 2018; Robayo et al., 2016).

Going to higher magnifications, it is possible to identify different kinds of matrix morphologies. Besides the granular amorphous clouds/particles (es. Fig. 7.7a), two further shapes have been detected:

- a particular geometrical morphology (es. Fig. 7.7c) evident in samples 1/1, 3/7+10MK and 1/1+20MK; this morphology could resemble that of zeolites (Fernández-Jiménez et al., 2008; García-Lodeiro et al., 2012; Zhang et al., 2016);
- a net morphology (es. Fig. 7.5e, 7.6d and 7.9a), more superficial, evident in samples 3/7, 7/3, 1/1+10MK and 3/7+20MK; a similar morphology has been found also by Komnitsas et al. (2015), who does not suggest anyway any particular interpretation.

The appearance of a certain morphology rather than another does not seem to follow the increase/decrease of the solid and/or liquid precursors. It is however possible to hypothesize a link with particular stoichiometric conditions. In any case, these observations highlight a complex geopolymeric system. These two morphologies (geometrical and net) do not find any analogy with the observed features characterizing the LBCa-based geopolymeric samples, neither in their shape nor in their distribution point of view.

The chemical composition acquired on different points of the matrices is compatible with a multi-component system of (N,C-)-A-S-H (Figg. 7.5g and i; 7.6f and 7.7d, 7.8d and e), where the net morphology shows a higher Al_2O_3/Na_2O ratio (Figg. 7.5h and 7.9a). On the contrary the "geometrical" areas show a lower Al_2O_3/Na_2O ratio (Figg. 7.7e and 7.9e), thus indicating as the different morphologies are probably determined by a different Al distribution in the geopolymeric gels.

Defects in the gel network are represented by the presence of small crystals, acicular (Fig. 7.8b) or star-like (Fig. 7.9c), which have been found in voids and cracks, probably grown as secondary products. Unfortunately, due to their small dimensions, the EDS analyses have been affected by the surrounding compositions, not giving useful results.

Only few relict minerals are visible (Figg. 7.4d, 7.5b, 7.7a and b, 7.8a, c and f), probably because of a good continuity of the gel matrix; with the exception of the series 3/7 where the gel could be interpreted as less continuous.

In order to better understand the gel composition, semi-quantitative EDS analyses of more than 150 points analysis has been carried out (Fig. 7.10 and 7.11).

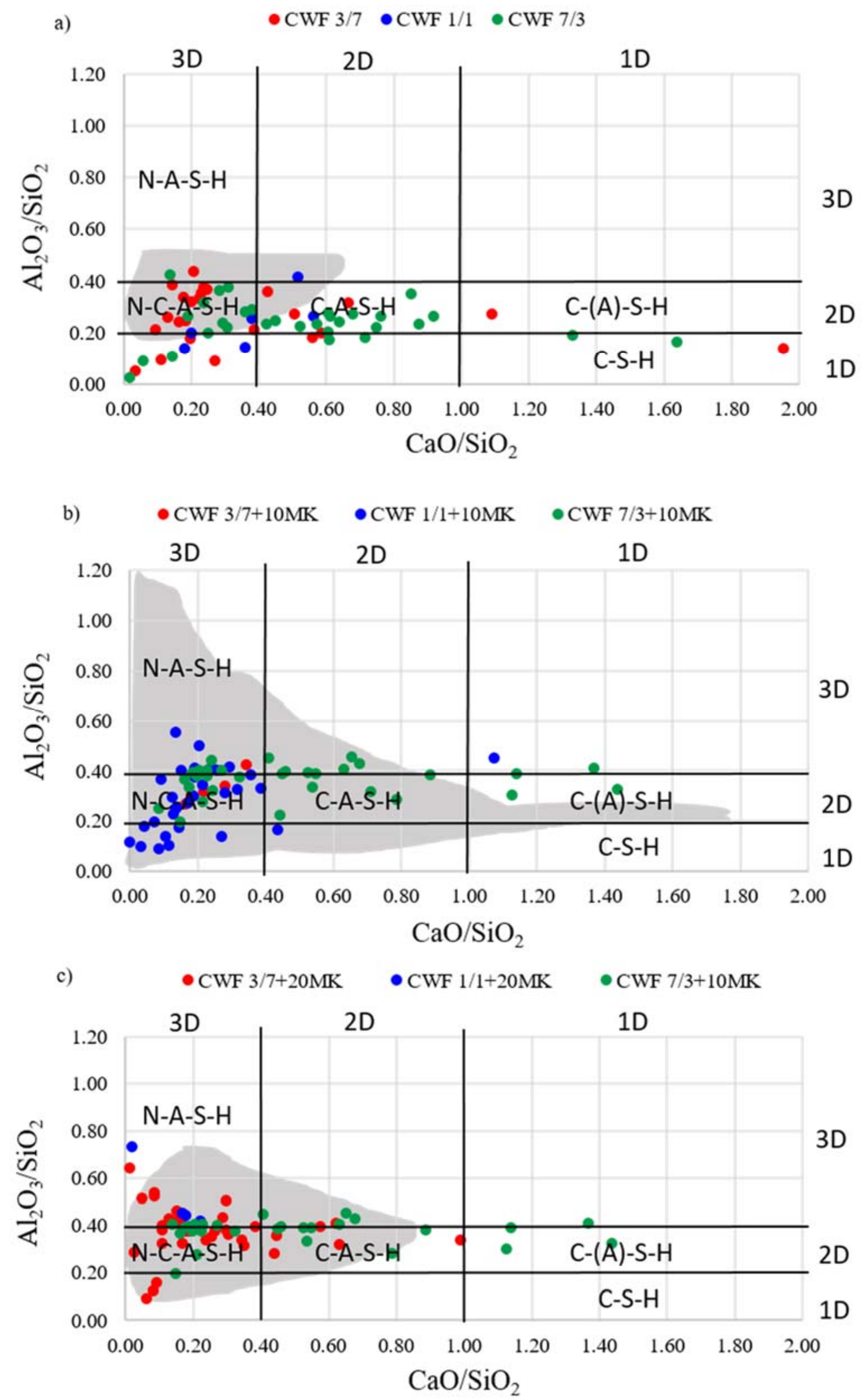

Fig. 7.10 – Al_2O_3/SiO_2 vs. CaO/SiO_2 ratios for gels precipitating in hybrid cements (based on EDS findings); CWF binders without MK; b) CWF binders with 10% of MK; c) CWF binders with 20% of MK. In the graphs, the areas related to the gel identified in the LBCa series are also indicated for comparison (in grey).

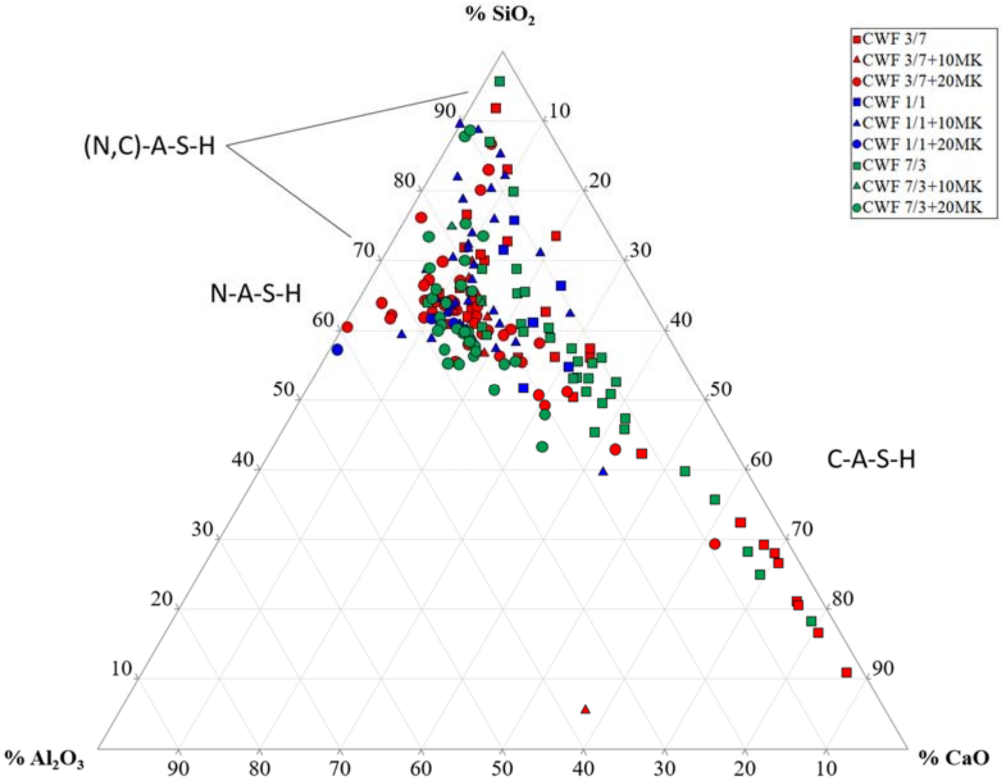

Fig. 7.11 – SiO_2-Al_2O_3-CaO ternary diagram for the gel detected on all the AAMs series developed: CWF 3/7 series, CWF 1/1 series and CWF 7/3 series. The gel ranges indicated are reported from the literature (Garcia-Lodeiro et al., 2013; Pachego-Torgal et al., 2014).

The Al_2O_3/SiO_2 and CaO/SiO_2 ratios have been plotted in Fig. 7.10; the composition ranges which characterize the main types of gels, (C-S-H, C-(A)-S- H, C-A-S-H, N-A-S-H and (N,C)-A-S-H), are also marked on the figure according to literature (Garcia-Lodeiro et al., 2011; Pardal et al., 2009). Overall it is possible to notice that all the samples show a hybrid gel characterized by a (N,C)-A-S-H composition, similarly to the LBCa series, with some points of analysis stretched toward the C-A-S-H area (in all the series) and other points towards pure N-A-S-H area (samples with 20% of MK), in accordance with literature (Pachego-Torgal et al., 2014). This interpretation is confirmed by the visualization of data in the SiO_2-Al_2O_3-CaO ternary diagram for the gel detection reported in Fig. 7.11 and compared with literature data (Pachego-Torgal et al., 2014). Fig. 7.12 summarizes the SEM-EDS results.

Talking in general, the gel composition distribution is similar to that observed in samples from LBCa, with a (N,C)-A-S-H characterizing all the samples. N-A-S-H increases in the samples with MK. Whereas in the LBCa series C-A-S-H gel was mainly detected in samples with 10% of MK, it appears almost in all the CWF-samples.

The complex system shown could be attributed to the precursors characteristics, which in respect to the more straightforward LBCa results, present higher Ca available for the reaction, thus determining, depending on the local stoichiometric conditions, also the formation of CSH and the related form which have been uptake the Al, namely C(A)SH (García-Lodeiro et al., 2013, 2012, 2011; Pachego-Torgal et al., 2014; Yip et al., 2005, 2008). Probably the presence of points of such different chemistry in the same sample could be associated to an ill homogenization of the paste or, otherwise, to a particular dynamic of the reaction processes.

An exhaustive sequence of SEM image collected on all the samples is exposed in Attachment 7.1.

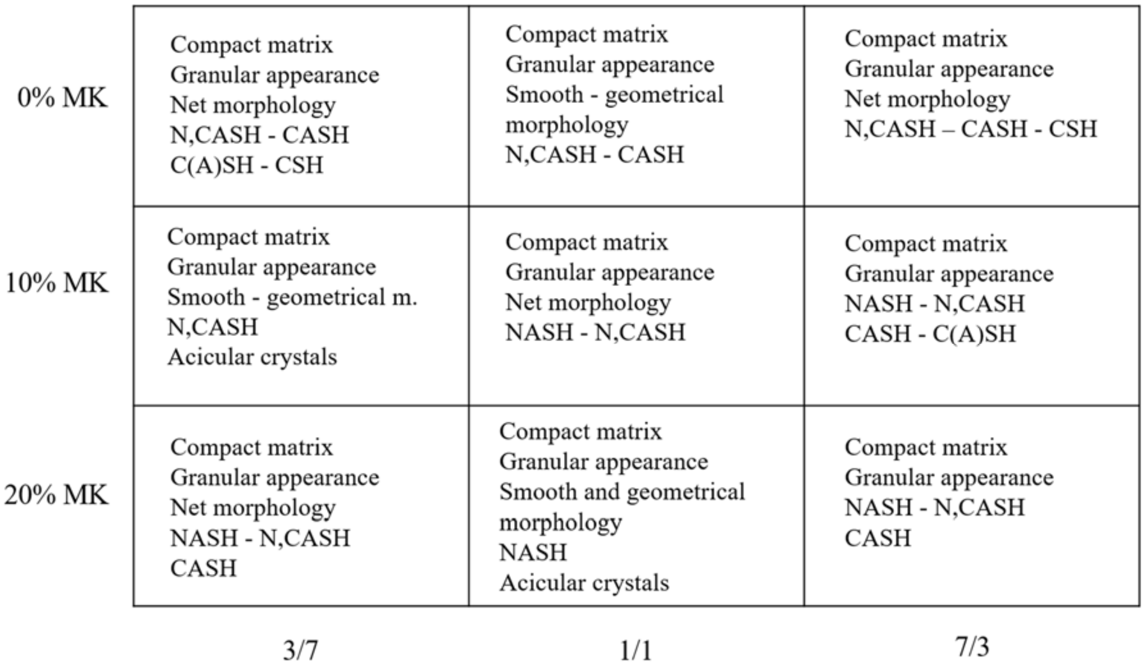

	3/7	1/1	7/3
0% MK	Compact matrix Granular appearance Net morphology N,CASH - CASH C(A)SH - CSH	Compact matrix Granular appearance Smooth - geometrical morphology N,CASH - CASH	Compact matrix Granular appearance Net morphology N,CASH – CASH - CSH
10% MK	Compact matrix Granular appearance Smooth - geometrical m. N,CASH Acicular crystals	Compact matrix Granular appearance Net morphology NASH - N,CASH	Compact matrix Granular appearance NASH - N,CASH CASH - C(A)SH
20% MK	Compact matrix Granular appearance Net morphology NASH - N,CASH CASH	Compact matrix Granular appearance Smooth and geometrical morphology NASH Acicular crystals	Compact matrix Granular appearance NASH - N,CASH CASH

Fig. 7.12 – Gel type chart of CWF binders: schematic summary of the SEM-EDS results.

TEM-EDS

The preliminary TEM investigation carried out on two representative samples have shown interesting results, as in the case of samples from LBCa. The analyzed samples are CWF 1/1 and CWF 1/1+20MK, in order to compare the observations of a pure ceramic geopolymeric binder with a binary mixture. The analyses have been carried out after 28 days of curing.

The formation of a different structure in the two types of geopolymers is evident: CWF 1/1 shows a superimposition of various pseudo-geometrical morphologies, similar to those observed in sample LBCa 1/1; CWF 1/1+20MK shows a cloudier appearance with a distinguishable granular structure (Fig. 7.13). Also for this latter sample, it is possible to notice an analogy with the correspondent of the LBCa series. Looking at the chemical maps, Na and Ca again are spread all over the surface, often overlapping (Fig. 7.14). It could be possible to observe that the Ca-Na phase is surrounded by a richer Na phase, differently to LBCa samples, where a complete interpenetration was assessed.

Diffraction analysis performed in different points allowed to establish amorphous and semi-crystalline phases, consistent with the presence of the amorphous geopolymeric gel. Hence, the simultaneous presence of N-A-S-H and C-A-S-H gel could be assumed, as in the case of the LBCa series.

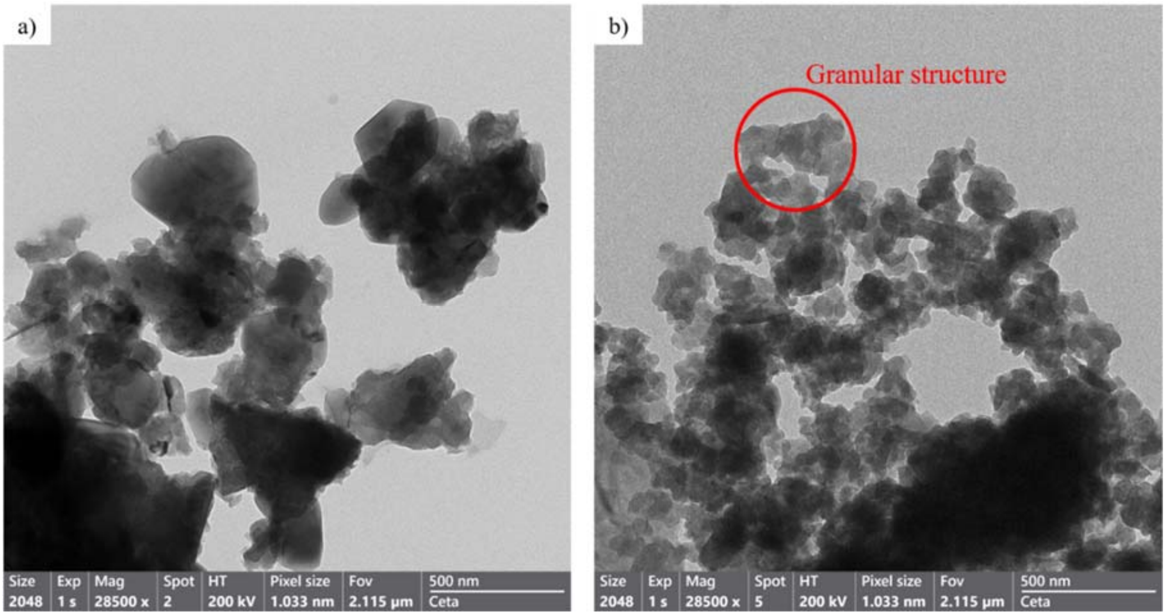

Fig. 7.13 – TEM micrograph of a fragment of samples CWF 1/1 a) and CWF 1/1+20MK b).

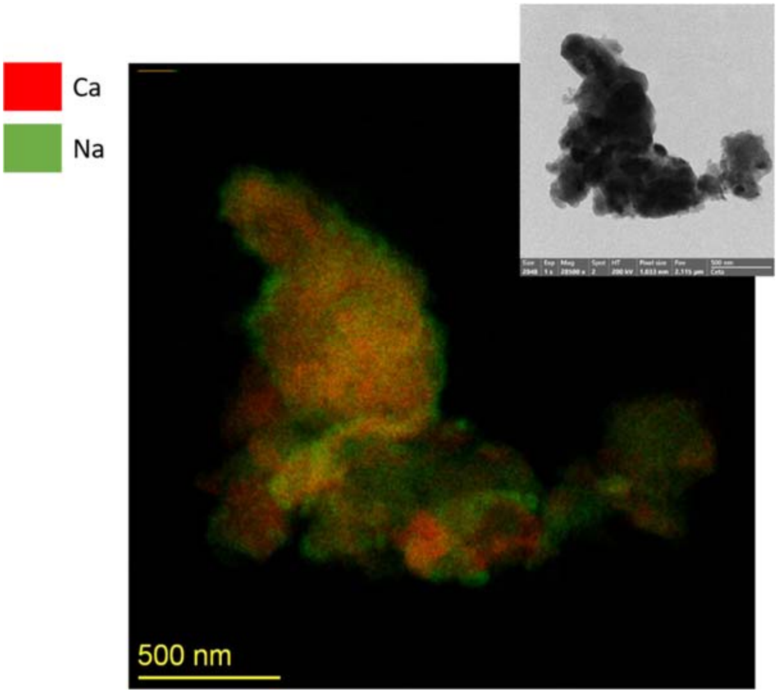

Fig. 7.14 – TEM map visualizing Ca and Na distribution on a fragment of CWF 1/1, whose morphology is shown in the up-right side of the image.

7.1.3 Molecular characterization (FTIR-ATR)

FTIR-ATR

Following the procedure used for LBCa binders, FTIR-ATR analysis has been performed on all the CWF geopolymeric binders at 28 days of curing and the obtained spectra have been compared with those of the raw materials (Fig. 7.15). For the binary geopolymers, dry mixtures with 10 and 20% of MK are again considered for comparison.

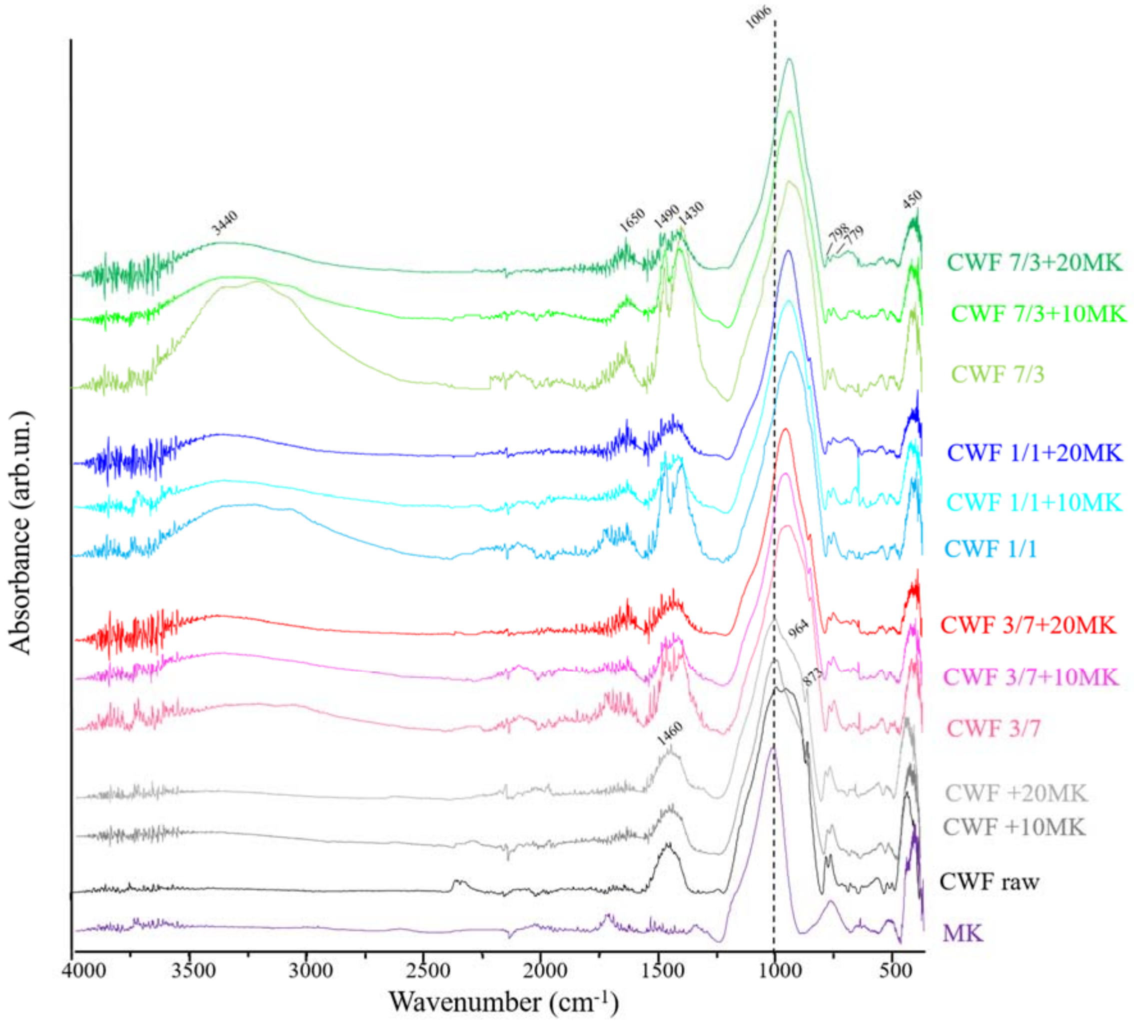

Fig. 7.15 – ATR spectra of CWF 3/7, CWF 1/1 and CWF 7/3 series, together with the raw materials CWF, MK and the dry mixtures CWF+10MK and CWF+20MK. The spectra have been normalized in order to allow direct comparisons. The spectra are stacked for clarity.

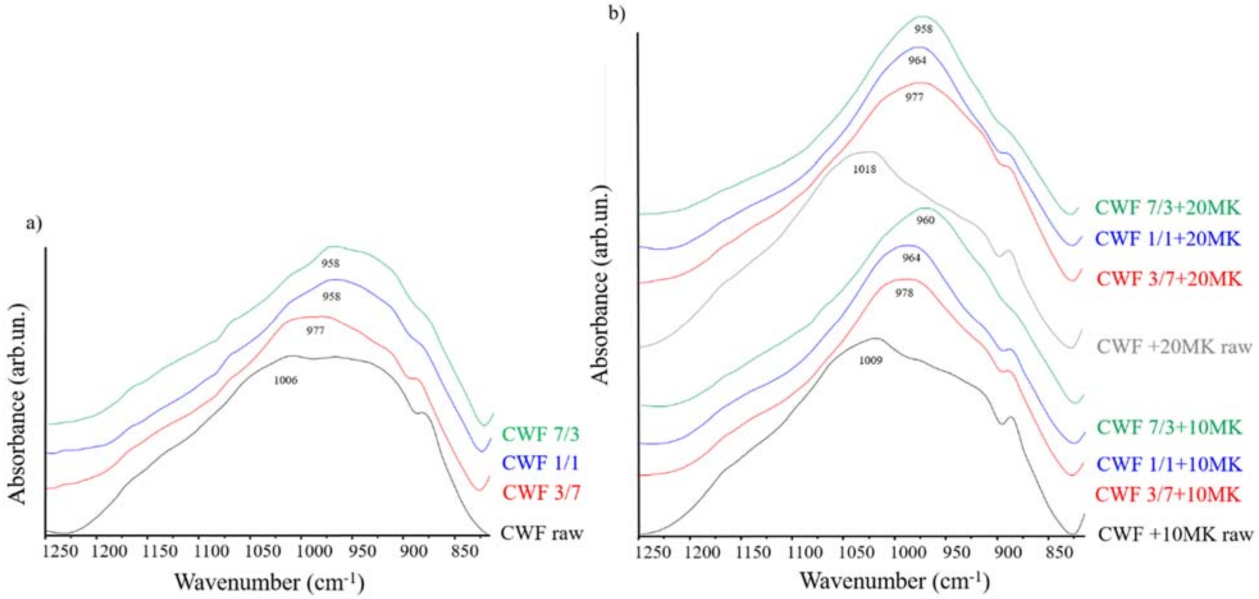

Fig. 7.16 – Zoom of the main band observed in the CWF geopolymeric samples without MK, compared with the ceramic raw material CWF a); zoom of the main band observed in the CWF geopolymeric samples with 10% of MK and 20% ofMK, respectively compared with the dry mixtures of the raw materials CWF with 10% and 20% of MK b). The spectra have been normalized in order to allow direct comparisons and stacked for clarity.

The ceramic raw material ATR spectrum shows a broad main band in the area of the absorption of the alumino-silicate phases, structured in different signals, of which the two more intense ones are located at 1006 cm^{-1} (marked with a black dotted line in figure) and a shoulder at 964 cm^{-1}. The ATR spectrum is strikingly similar to that of LBCa, but with additional bands attributable to carbonates at 1460 and 873 cm^{-1} (Farmer, 1974; Hughes et al., 1995; Rodriguez-Blanco et al., 2011), as expected from the XRD analysis which highlights the presence of calcite. The individuated maximum peak, linked to the Si-O-T stretching vibrations (Khan et al., 2016; Rovnaník et al., 2018; Tuyan et al., 2018), undergoes a shift towards lower wavenumbers in the spectra of the analysed geopolymers. In particular, as shown in Fig 7.16, sample 3/7 shows the maximum for this band at 977 cm^{-1}, while samples 1/1 and 7/3 are characterized by a higher shift, with the maximum located at 958 cm^{-1}. Concerning the samples with MK, it is possible to notice that the maxima of the reference dry mixtures with 10 and 20% of MK are located respectively at 1009 and 1018 cm^{-1}. The behaviour of the shift in the binary geopolymers is the same of the samples without MK, with the maxima for samples 3/7+10MK, 1/1+10MK, 7/3+10MK respectively at 978, 964 and 960 cm^{-1}, and for samples 3/7+20MK, 1/1+20MK, 7/3+20MK respectively at 977, 964 and 958 cm^{-1}. The correlation between the shift and the amount of sodium hydroxide in the slurry appears evident. Furthermore, an interesting difference between the raw materials spectra and those acquired on the geopolymers concerns the carbonate phases. While the band at 873 cm^{-1} progressively disappears with the increase of waterglass and MK in the slurry, the signal at around 1460 cm^{-1} is substituted by two bands at around 1430 and 1490 cm^{-1} indicating that something occurs during the geopolymerization thanks to the carbonate components (Fig. 7.15). This pattern decreases with increasing amounts of MK.

A re-arrangement of the calcium carbonate present in the raw material could be suggested: starting from a partially amorphous calcium carbonate evidenced by the presence of the CO_3^{2-} band at 1460 cm^{-1} in the precursor (Rodriguez-Blanco et al., 2011), calcite re-organizes itself during the geopolymerization process, via the formation of vaterite (Rodriguez-Blanco et al., 2011), identified by the two bands around 1430 and 1490 cm^{-1} (Jones and Jackson, 1993). Although this hypothesis could be considered realistic, a deeper study of the process should be performed in order to better understand it and validate it. Indeed, as confirmed by literature about the kinetic of calcium carbonates and their polymorphs' characterization (Andersen and Brečević, 1991; D'Elia et al., 2020; Fabbri et al., 2014; Rodriguez-Blanco et al., 2011; Shen et al., 2006), it is not easy to define a clear and univocal vibrational assignment for calcium carbonates. Furthermore, in this case we have to keep in mind the possible overlap of bands related to sodium carbonate salts due to efflorescences, which show absorption peaks in the same areas (D'Elia et al., 2020; Jones and Jackson, 1993; Joshi et al., 2013). Trona and natrite, for example, among the most widespread sodium carbonates in geopolymers (Criado et al., 2005; Leonelli, 2013; Lloyd et al., 2010; Najafi Kani et al., 2012; Provis and Van Deventer, 2009; Rowles and O'Connor, 2009; Yip et al., 2008; Zhang et al., 2018), present absorption peaks respectively at 1465 (Jones and Jackson, 1993) and 1450 cm^{-1} (Joshi et al., 2013).

Analogously to the LBCa geopolymer series, a large band at 3440 cm^{-1} together with a band at 1650 cm^{-1}, representing the stretching and bending vibration of the OH bonds linked to the new hydrated mineral phases (Azevedo et al., 2018; Khan et al., 2016; Rovnaník et al., 2018; Tuyan et al., 2018), appear. The band at around 450 cm^{-1} decreases in intensity in geopolymers in respect to raw materials: this could be attributed to the dissolution of Al-O and Si-O species with the subsequent formation of Si-O-Al moieties, as reported by (Azevedo et al., 2018).

Furthermore, looking at the doublet located at 796 and 778 cm^{-1}, which is distinctive of quartz (Reig et al., 2013), it is possible to notice a consistent intensity reduction, compared with its intensity in the spectrum of the raw material, thus indicating its partial reaction (Reig et al., 2013).

Principal component analysis has been performed considering the entire series of CWF binders. The results are shown in Fig. 7.17.

On the basis of PC1 it is possible to distinguish the samples in function of MK; particularly a more evident cluster is formed grouping the samples with 20% of MK, quite independently on the sodium hydroxide/waterglass contribution. The precursors contribution becomes more evident instead for the other clusters, with 10% or without MK. The first three PCs show an explained variance of 94.6%.

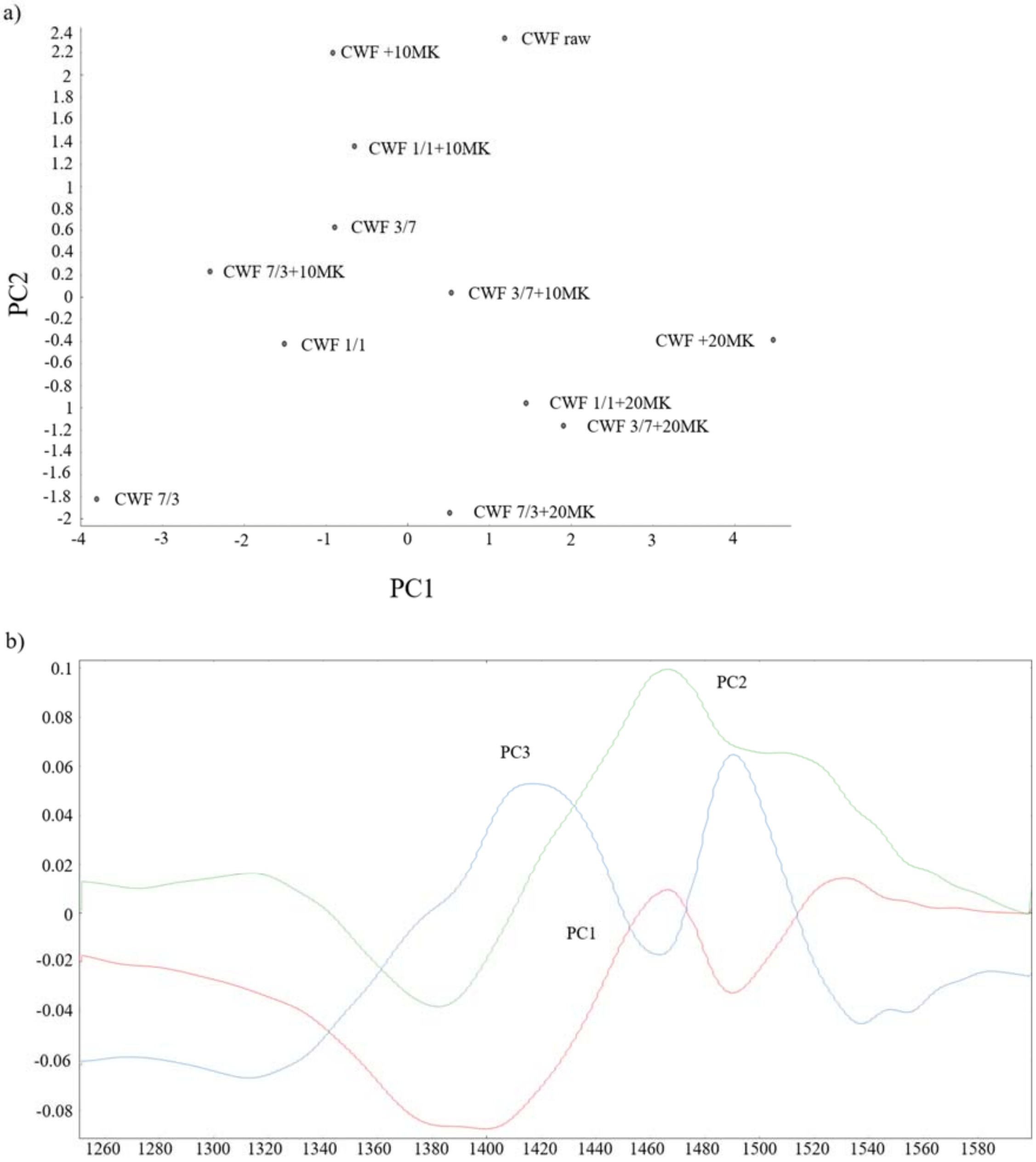

Fig. 7.17 – Score plot (PC1 and PC2) of the 9 ATR spectra with PCA treatment; b) Loadings diagram of the first three principal components.

7.1.4 Mercury Intrusion Porosimetry (MIP)

All the binders have been studied, after 28 days of curing, with Mercury Intrusion Porosimetry in order to investigate their porous structure. The bulk density is also obtained. All the data (bulk density, accessible porosity, total pore volume, average pore diameter, modal pore diameter and incremental volume of the pores) are shown in Table 7.1.

		CWF 7/3	CWF 7/3+10 MK	CWF 7/3+20 MK	CWF 1/1	CWF 1/1+10 MK	CWF 1/1+20 MK	CWF 3/7	CWF 3/7+10 MK	CWF 3/7+20 MK
Bulk density (g/cm^3)		1.86	1.71	1.66	1.86	1.73	1.69	1.86	1.74	1.81
Accessible Porosity (%)		33.07	35.58	34.17	27.73	31.77	32.14	28.86	30.70	29.42
Total Pore Volume (cm^3/g)		0.18	0.21	0.21	0.15	0.18	0.19	0.16	0.18	0.16
Average Pore Diameter (μm)		0.07	0.05	0.07	0.19	0.05	0.05	0.11	0.06	0.04
Modal Pore Diameter (μm)		0.01	0.07	0.12	1.14	0.06	0.05	0.86	0.06	0.04
Incremental Volume (cm^3/g)	100-10 μm	0.02	0.03	0.02	0.02	0.02	0.01	0.03	0.01	0.02
	10-1 μm	3.13	0.12	0.06	1.09	0.03	0.03	0.39	0.05	0.03
	1-0.1 μm	17.12	16.97	19.39	43.96	0.13	0.06	39.27	0.40	0.06
	0.1-0.01 μm	48.54	100.69	92.10	32.32	101.52	103.79	41.85	81.98	78.31
	0.01-0.001 μm	8.09	12.38	10.89	7.74	9.69	9.66	9.10	8.62	8.60

Table 7.1 – Porosimetric data of the CWF geopolymeric slurries.

Figg. 7.18, 7.19 and 7.20 show the pore distribution diagrams by series in order to investigate the possible influence of MK in the porous structure. Furthermore, for a better comparison, the extremes of the series have been observed together, Fig. 7.21. It is possible to notice that for the series with the highest content of sodium hydroxide (series 7/3), the sample without MK is characterized by a broad porosimetric distribution, with a maximum at 0.1 μm in the samples with MK. A different trend is observed for the series 1/1 and 3/7: the samples without MK show a prevalent dimension of the average radius around 1-0.1 μm, while the introduction of MK in the system lowers this value.

Studying the formulations without MK (Fig. 7.22), in order to investigate the effect of the waterglass content on the geopolymer porous structure, it is possible to infer that increasing waterglass in the slurry lowers the pores dimension, even if in a not evident way.

Concerning the open porosity, attested on 27-35%, as already seen for the samples LBCa, no evident variations are visible depending on the percentage of MK or on the sodium hydroxide/waterglass ratio.

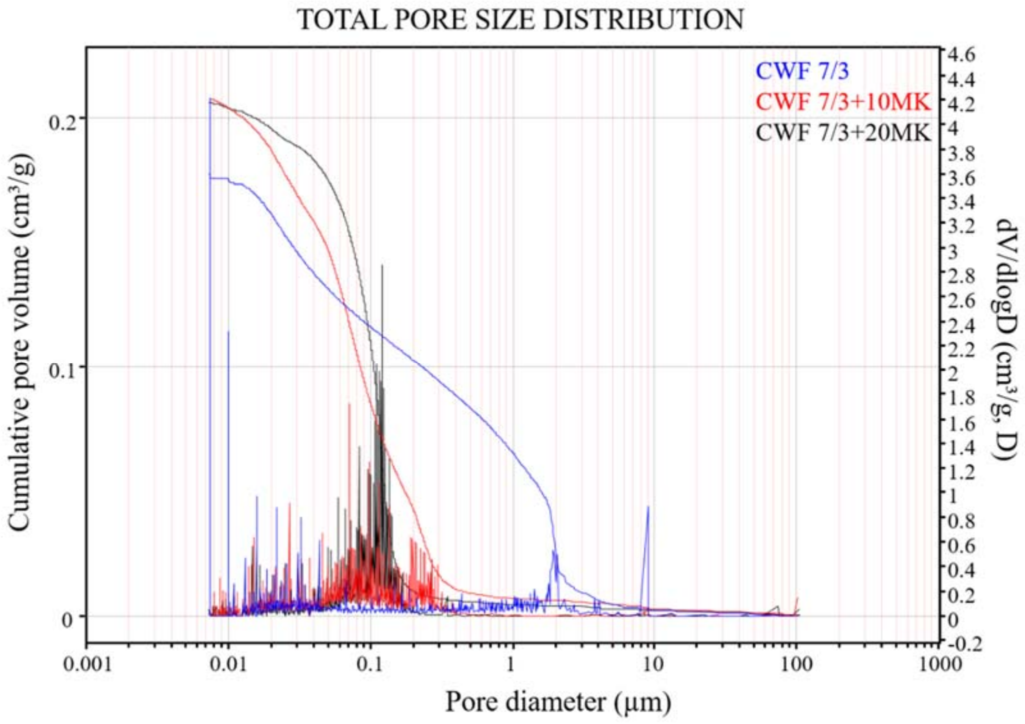

Fig. 7.18 – Total pore size distribution of the 7/3 series.

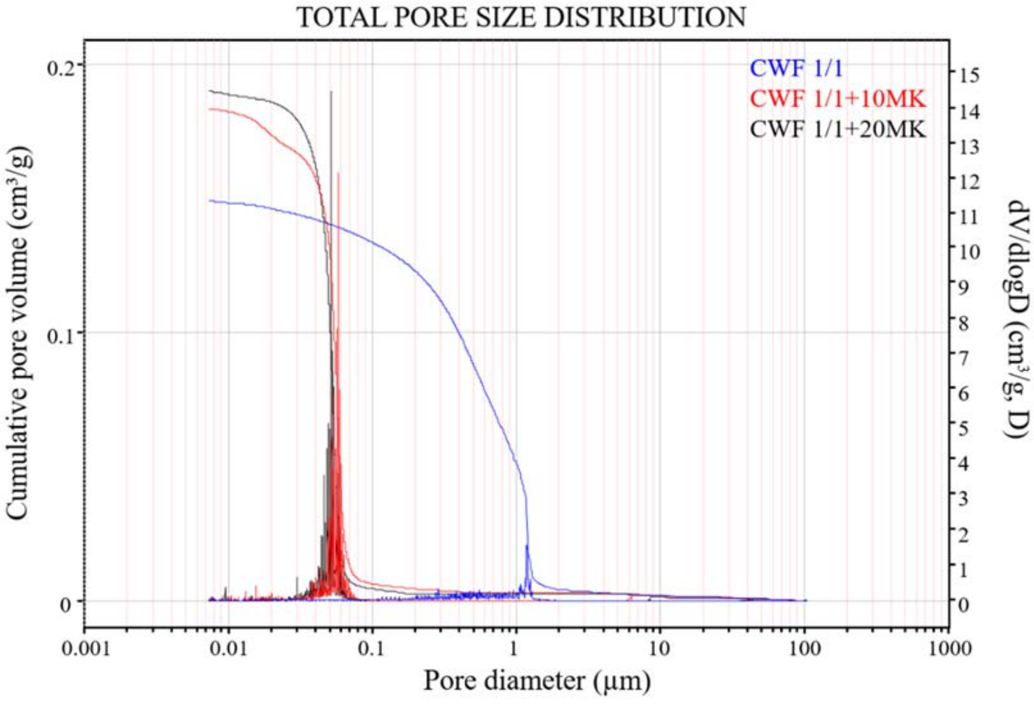

Fig. 7.19 – Total pore size distribution of the 1/1 series.

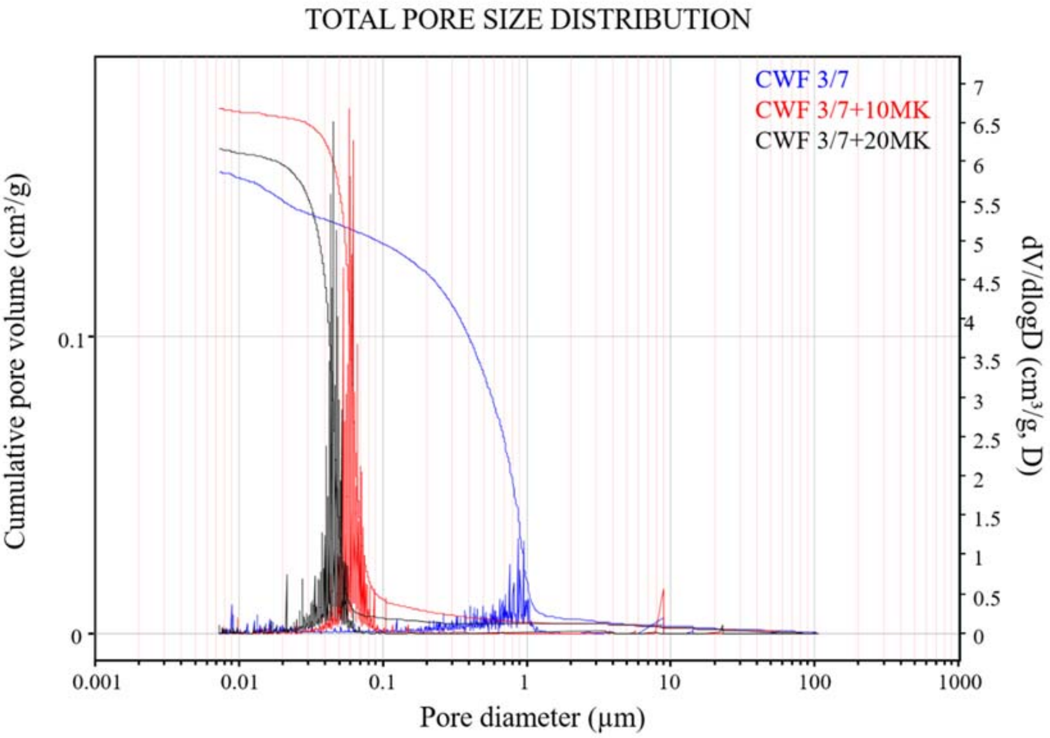

Fig. 7.20 – Total pore size distribution of the 3/7 series.

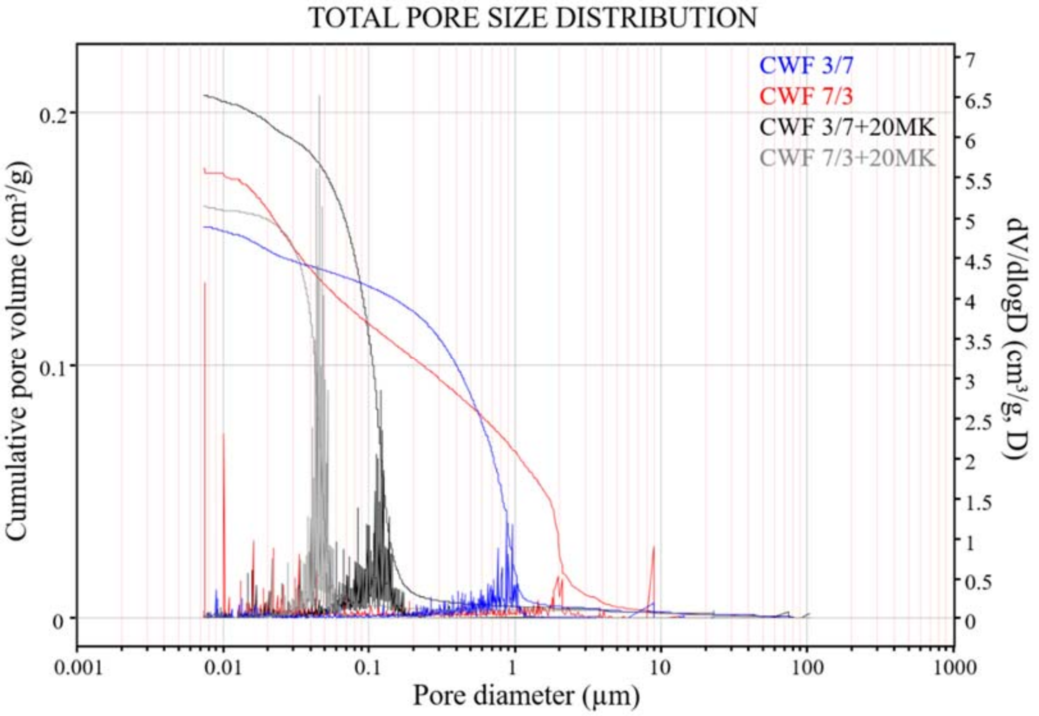

Fig. 7.21 – Comparison of the total pore size distributions characterizing the extremes of the series: CWF 3/7, CWF 3/7+20MK; CWF 7/3 and CWF 7/3+20MK.

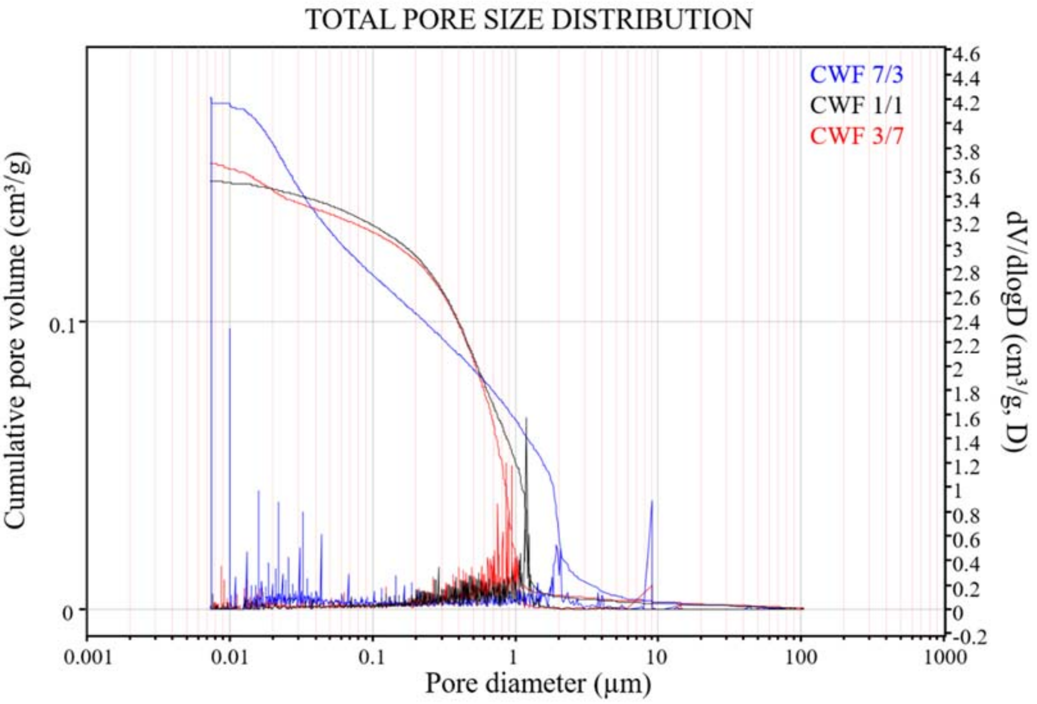

Fig. 7.22 – Comparison of the total pore size distributions characterizing samples without MK, in order to study the waterglass influence on porous structure.

7.1.5 Mechanical characterization – uniaxial compressive test

Ascertained the necessity of at least six specimens in order to have reliable data, as observed for LBCa binders, six samples of 2*2*2 cm for each formulation have been tested, after 28 days of curing. The results obtained are shown in Table 7.2 and Fig. 7.23.

Sample	Resistance (MPa)	Average	St. Dev.	Bottom limit	Up limit	Accepted values	New average	New St. Dev.	Bottom limit	Up limit	Variation coeff.
CWF 3/7_1	17.56	20.04	3.97	16.07	24.01	17.56	20.04	1.80	18.24	21.84	0.09
CWF 3/7_2	22.40					22.40					
CWF 3/7_3	20.88					20.88					
CWF 3/7_4	26.43										
CWF 3/7_5	19.31					19.31					
CWF 3/7_6	13.65										
CWF 1/1_1	41.13	28.40	6.45	21.95	34.85		26.91	2.88	24.02	29.79	0.11
CWF 1/1_2	23.72					23.72					
CWF 1/1_3	31.59					31.59					
CWF 1/1_4	26.27					26.27					
CWF 1/1_5	21.67										
CWF 1/1_6	26.04					26.04					

CWF 7/3_1	14.18	17.97	2.50	15.47	20.48		17.86	1.12	16.74	18.97	0.06
CWF 7/3_2	16.81					16.81					
CWF 7/3_3	16.69					16.69					
CWF 7/3_4	19.16					19.16					
CWF 7/3_5	18.77					18.77					
CWF 7/3_6	22.23										
CWF 3/7+10MK_1	37.81	33.39	4.98	28.41	38.37	37.81	35.14	3.38	31.76	38.52	0.10
CWF 3/7+10MK_2	31.78					31.78					
CWF 3/7+10MK_3	37.72					37.72					
CWF 3/7+10MK_4	24.66										
CWF 3/7+10MK_5	30.30					30.30					
CWF 3/7+10MK_6	38.09					38.09					
CWF 1/1+10MK_1	25.71	26.73	2.63	24.10	29.37	25.71	25.44	0.83	24.61	26.27	0.03
CWF 1/1+10MK_2	30.07										
CWF 1/1+10MK_3	30.42										
CWF 1/1+10MK_4	26.30					26.30					
CWF 1/1+10MK_5	23.59										
CWF 1/1+10MK_6	24.31					24.31					
CWF 7/3+10MK_1	3.01	3.03	0.66	2.37	3.69	3.01	8.69	0.08	8.61	8.77	0.01
CWF 7/3+10MK_2	4.24										
CWF 7/3+10MK_3	2.85					2.85					
CWF 7/3+10MK_4	2.22										
CWF 7/3+10MK_5	2.82					2.82					
CWF 7/3+10MK_6											
CWF 3/7+20MK_1	41.28	37.48	7.85	29.62	45.33	41.28	38.49	2.93	35.56	41.42	0.08
CWF 3/7+20MK_2	41.51					41.51					
CWF 3/7+20MK_3	36.18					36.18					
CWF 3/7+20MK_4	35.00					35.00					

CWF 3/7+20MK_5	22.74										
CWF 3/7+20MK_6	48.17										
CWF 1/1+20MK_1	33.04	32.07	5.77	26.31	37.84	33.04	31.81	3.40	28.40	35.21	0.11
CWF 1/1+20MK_2	41.34										
CWF 1/1+20MK_3	28.24					28.24					
CWF 1/1+20MK_4	29.15					29.15					
CWF 1/1+20MK_5	23.89										
CWF 1/1+20MK_6	36.81					36.81					
CWF 7/3+20MK_1	4.57	6.10	1.00	5.10	7.10		6.22	0.64	5.58	6.87	0.10
CWF 7/3+20MK_2	7.27										
CWF 7/3+20MK_3	7.03					7.03					
CWF 7/3+20MK_4	6.18					6.18					
CWF 7/3+20MK_5	5.46					5.46					
CWF 7/3+20MK_6											

Table 7.2 – Compressive resistance results of CWF-based geopolymers.

With the only exception of the 7/3 series, the compressive strength of the CWF-geopolymers increases with the increase of MK. It is possible to support this trend despite the similar values of 1/1 and 1/1+10MK, if considered the values of the standard deviatons on all the samples.

The same behaviour is observed with the increase of waterglass in the binders.

The 7/3 series instead shows a complete opposite trend. Furthermore, considering the standard deviations, among the samples which show the highest compressive strength (higher than 20 MPa), the more reliable values are registered on sample 1/1+10MK.

As observed for LBCa binders, after the exclusion of the aberrant ones, all the data acquired show CoV well below the threshold (fixed at 0.15) and can be considered of high quality in regard to what foreseen by the technical legislation on concretes (D. Min. Infrastrutture 14/01/2008).

Observing the behaviour of the failure during compression tests, it is possible to distinguish soft samples, which slowly flatten during the test, and resistant samples characterized by an abrupt failure, typical of cement materials (Deere and Miller, 1966; Occhipinti et al., 2020), already individuated on resistant samples of the LBCa series. Also in this case, the final appearance of the sample is of a cube which has lost the external walls, the remainder taking an hourglass shape (Fig. 7.24).

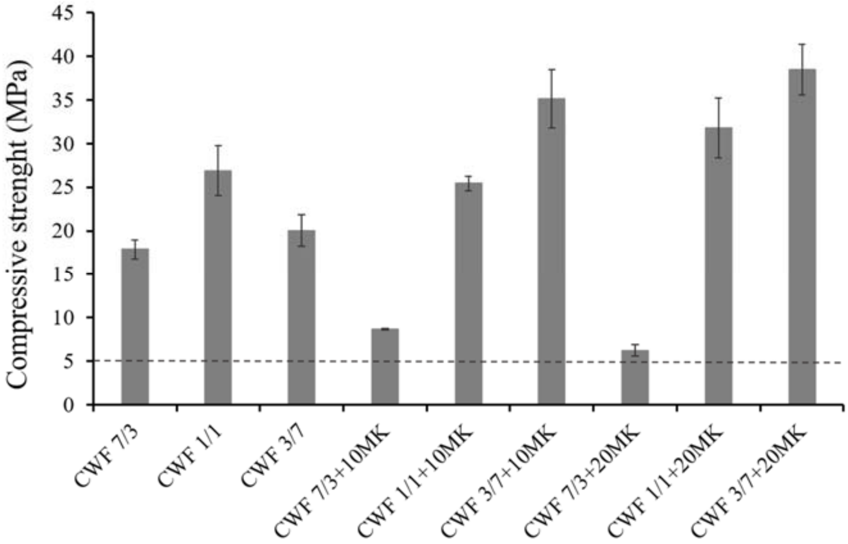

Fig. 7.23 – Compressive strength average, measured on all the experimented geopolymers on six replicates for each formulation. The standard deviation bar is also indicated. The dotted lines indicate the arbitrary threshold of 5 MPa.

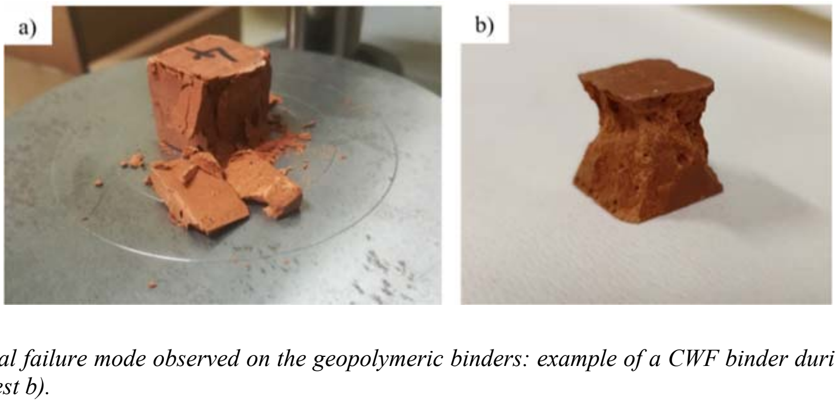

Fig. 7.24 – Typical failure mode observed on the geopolymeric binders: example of a CWF binder during compression a) and after the test b).

7.1.6 Colorimetry

The colour quantification has been collected on both surfaces of the samples, the bottom surface in contact with the plastic used during curing and the upper surface, where a very thin stratification occurred in some samples, probably because of waterglass' surfacing on the top. Thus, the results of the bottom surfaces are reported in detail in Table 7.3, as they are considered more reliable, while all the data are reported in Attachment 7.2. In order to have an immediate perception of the colour relative appearance, a colour chart has been realized, and is shown in Fig. 7.25 including all the binders obtained by CWF raw material with different % of MK and different sodium hydroxide/waterglass proportions.

				Comparison with CWF raw						Comparison with ME brick						Comparison with GL brick					
Sample	L*	a*	b*	ΔL*	Δa*	Δb*	ΔE*	ΔC*	ΔH*	ΔL*	Δa*	Δb*	ΔE*	ΔC*	ΔH*	ΔL*	Δa*	Δb*	ΔE*	ΔC*	ΔH*
CWF 3/7	44	22	30	-15	6	4	16	6	3	-3	7	5	9	8	3	-15	12	8	21	13	6
CWF 1/1	44	23	27	-15	6	1	16	4	4	-3	7	2	8	6	4	-16	13	6	21	12	8
CWF 7/3**	42	21	26	-17	5	0	18	2	4	-6	6	1	8	5	4	-18	11	4	22	10	7
CWF 3/7+10MK	53	18	25	-6	1	-2	6	-1	2	6	2	0	6	1	2	-6	8	3	11	7	5
CWF 1/1+10MK	58	15	22	0	-1	-5	5	-5	1	11	0	-3	12	-3	2	-1	6	0	6	3	5
CWF 7/3+10MK	52	17	21	-6	0	-6	8	-5	3	5	1	-4	7	-2	3	-7	7	-1	10	3	6
CWF 3/7+20MK	51	19	25	-7	2	-1	8	0	2	4	4	0	5	2	3	-8	9	4	13	8	6
CWF 1/1+20MK	51	17	24	-8	1	-3	8	-2	2	4	2	-1	4	0	2	-8	8	2	11	5	6
CWF 7/3+20MK	60	14	18	2	-3	-8	9	-8	3	13	-1	-7	15	-6	3	1	4	-4	6	-1	6

*Table 7.3 – CIE-L*a*b* chromatic parameters measured on CWF geopolymers; colorimetric data results in comparison with references raw material CWF and archaeological bricks (ME brick and GL brick). The sample marked with the asterisk was covered by efflorescences.*

The L*, a* and b* values measured on the binders are then compared with the original raw material CWF, in order to understand possible correlations with the addition of MK in the mixture and with the sodium hydroxide and waterglass proportions (Fig. 7.26). A good correlation between the colorimetric parameters and the MK percentage in the mixtures or the alkaline activators proportions is not evident. What is easily noticed is the lower lightness characterizing the samples without MK, while chroma and hue do not seem to influence the total colour variation. Indeed, the majority of the samples show values of ΔC and ΔH within the range of perceptibility, defined by the limits +3 and -3 (Benavente et al., 2003).

Figg. 7.27 and 7.28 show respectively the comparisons of the colorimetric parameters with the ME and GL brick. Regarding the brick from Messina, a general colour variation is highlighted, perceptible with human eye (above the threshold of 3 units), but so far moderate. The majority of the samples indeed show a ΔE lower than 11, which is considered by some authors still an acceptable value in the field of conservation of Cultural Heritage (Clausi et al., 2016). Only samples 1/1+10MK and 7/3+20MK overcome this value, respectively with ΔE equal to +12 e +15. The colour variation seems to be mainly influenced by the lightness, while chroma and hue could be on the whole considered irrelevant. The only samples which are distinguished based on the chroma are the two extremes of the series, 7/3 and the 3/7+20MK, appearing respectively less and more saturated. For what concerns the comparison with the brick from Gela, a general high colorimetric difference is highlighted, where the samples synthesized only by ceramic waste, without the use of MK, reach values above the 20 units, with a consistent lightness decrease and saturation increase. This time also the hue parameter becomes an influent value, even if the variation is maintained below the 10 units, with positive values. The pattern is analogous for the other samples, but with lower values. It is noteworthy that samples 1/1+10MK and 7/3+20MK deviate from the general pattern, being within the range of not perceptibile colour change for what concerns the lightness and chroma variation, with positive values barely up to the threshold regarding hue and total colour difference.

The large range of colour change' values obtained, between values barely perceptible and well visible colour changes, will allow to select the right formulation for the implementation of suitable mortars according to the colour characteristics of the original material on which to intervene. Archaeological ceramics could indeed be characterized by very different shades of colours.

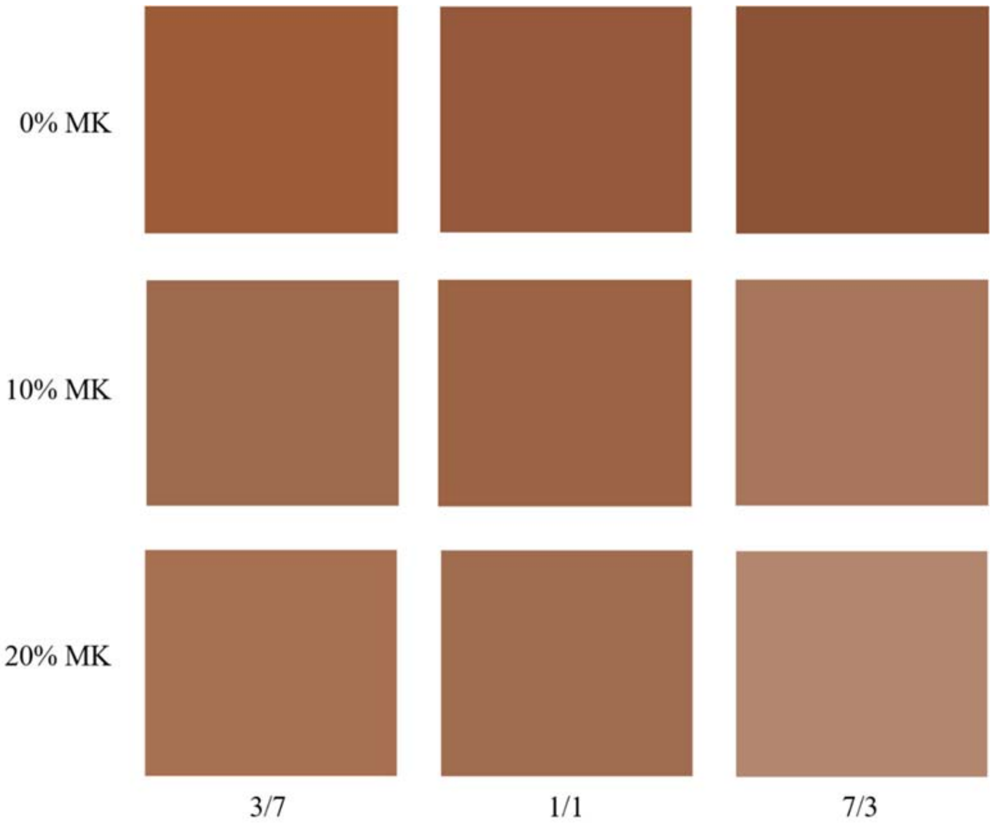

Fig. 7.25 – Pseudo-colours of CWF binders.

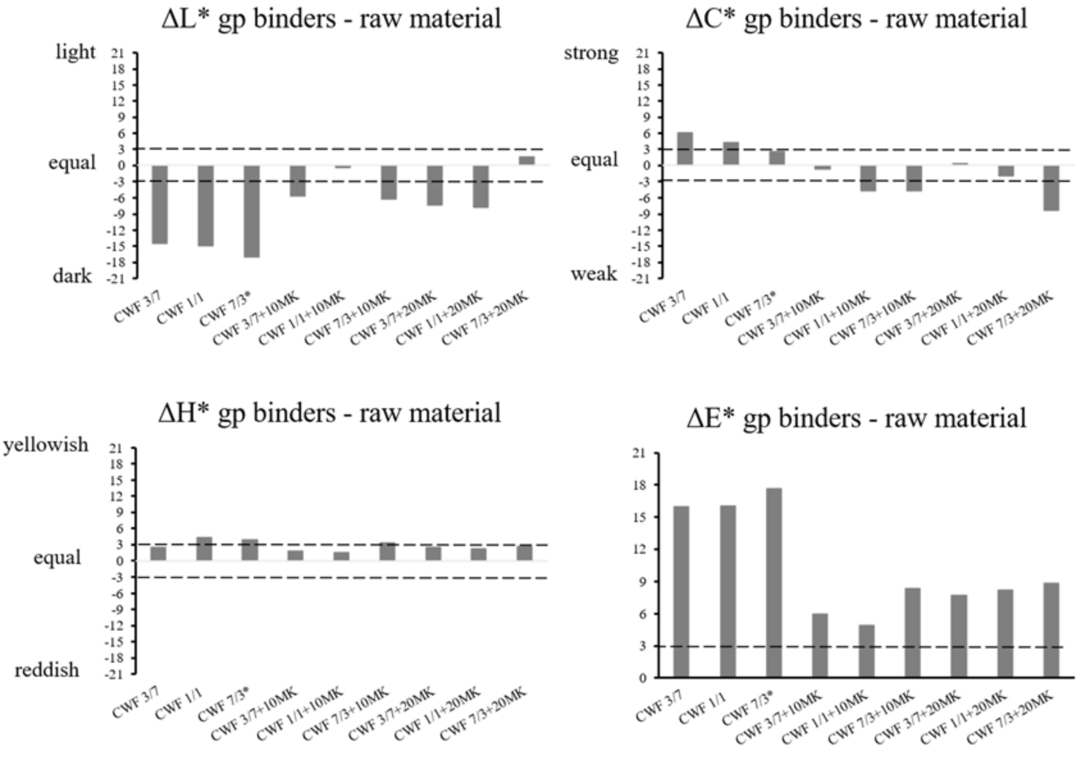

Fig. 7.26 – Partial and total colour differences of the CWF geopolymers in respect to the ceramic precursor. In the partial colour differences ΔL, ΔC* and ΔH* the same vertical numeric scales are used to show the relative weight of three chromatic variables on the total colour differences ΔE*. ΔL=lightness variation, ΔC=chroma variation and ΔH=hue variation. The dashed lines indicate the perceptibility limit, which is equal to 3 units (Benavente et al., 2003).*

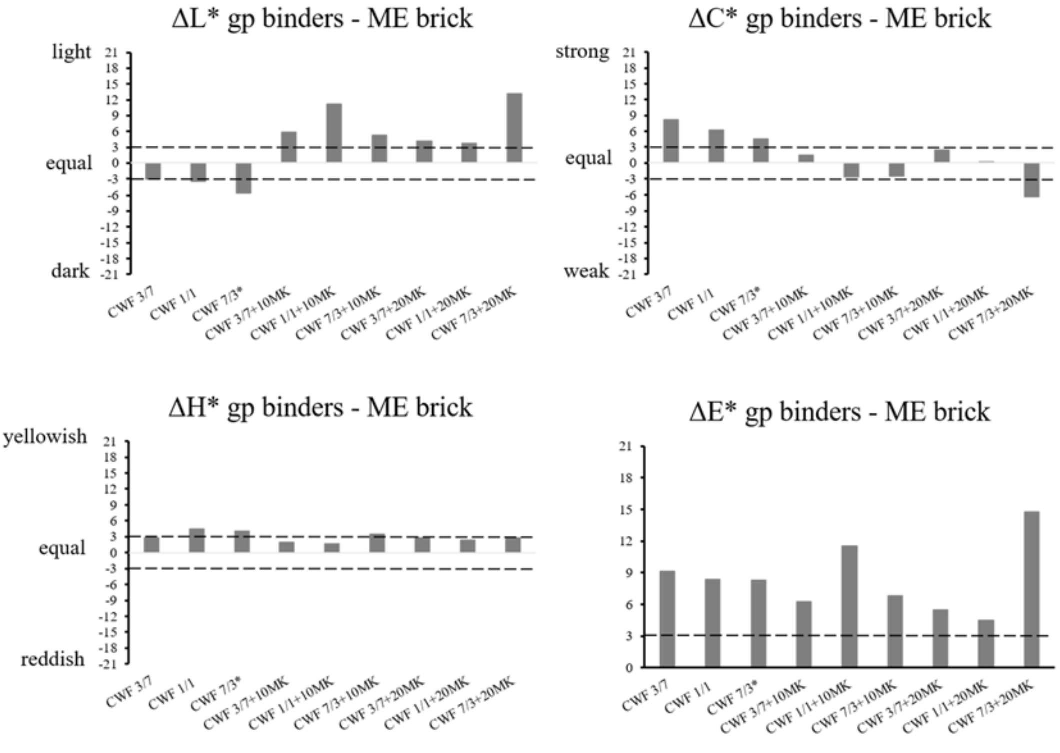
ΔL* gp binders - ME brick

ΔC* gp binders - ME brick

ΔH* gp binders - ME brick

ΔE* gp binders - ME brick

Fig. 7.27 – Partial and total colour differences of the CWF geopolymeric binders in respect to the ME brick. In the partial colour differences ΔL, ΔC* and ΔH* the same vertical numeric scales are used to show the relative weight of three chromatic variables on the total colour differences ΔE*. ΔL=lightness variation, ΔC=chroma variation and ΔH=hue variation. The dashed lines indicate the perceptibility limit, which is equal to 3 units (Benavente et al., 2003).*

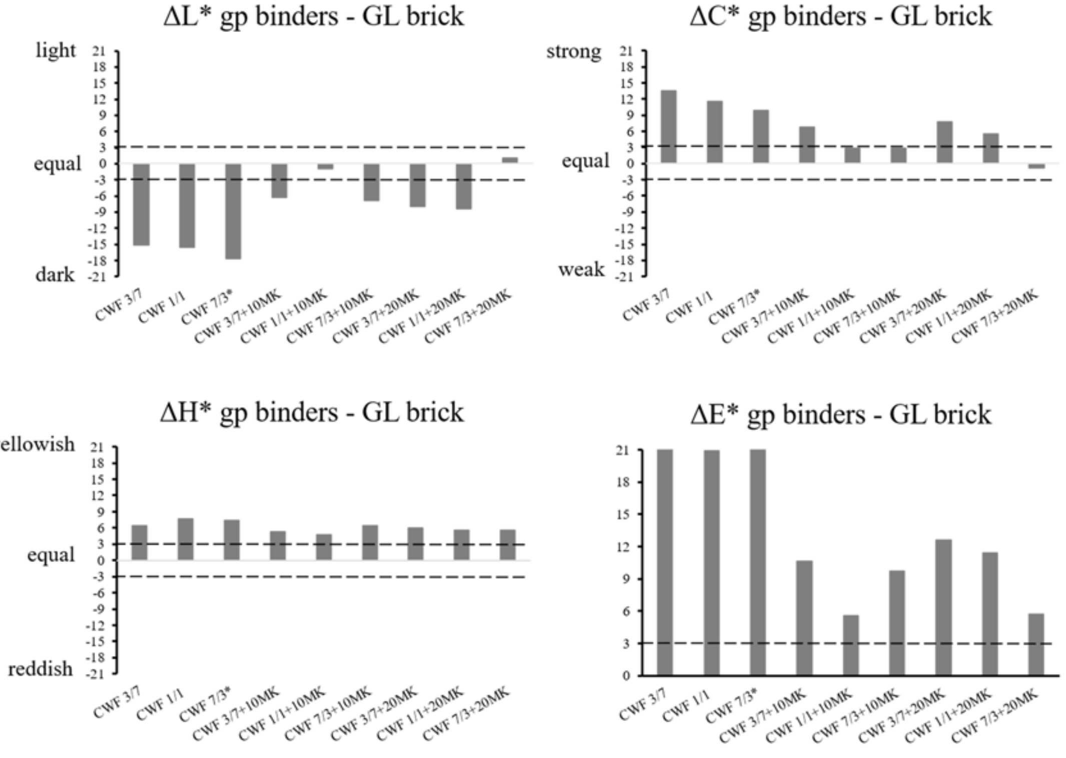
ΔL* gp binders - GL brick

ΔC* gp binders - GL brick

ΔH* gp binders - GL brick

ΔE* gp binders - GL brick

Fig. 7.28 – Partial and total colour differences of the CWF geopolymeric binders in respect to the GL brick. In the partial colour differences ΔL, ΔC* and ΔH* the same vertical numeric scales are used to show the relative weight of three chromatic variables on the total colour differences ΔE*. ΔL=lightness variation, ΔC=chroma variation and ΔH=hue variation. The dashed lines indicate the perceptibility limit, which is equal to 3 units* (Benavente et al., 2003).

7.1.7 Binders evaluation for the development of restoration products

The occurrence of a geopolymeric process is assessed thanks to Rietveld refinement of diffractograms, as well as from TEM and SEM morphological observation of the samples' matrix and by comparing the FTIR-ATR spectra with those of the raw materials. All these approaches confirm the presence of an amorphous hybrid gel. However, the appearance of the net-like and "geometric" morphologies and the incoherent distribution of the different detected gels, make the interpretation of the CWF geopolymer samples not straightforward, as the observed results and patterns are more diversified than in LBCa-based binders.

Nevertheless, regarding those data considered important for the selection of suitable binders to be used as restoration products, one can observe a quite homogeneous behaviour pattern. The compressive strength seems to be consistent with the MK and waterglass increases in the slurry, but this cannot be confirmed for the 7/3 series. This set shows negative results, with a total failure of samples 7/3+10MK and 7/3+20MK. This could be attributed to the large amounts of efflorescences and the simultaneous low value of amorphous content. This linear and logic reasoning is not valid for sample 7/3 (without MK) and the other samples with good mechanical performance nonetheless the other not good results (1/1 and 3/7).

The unexpected good resistance obtained for sample 7/3, which shows high efflorescences and a low amorphous phases increase, could be explained by the presence of a well-developed structure of net-like appearance, which does not appear in the samples which failed the compressive tests. The same is valid for the other samples without MK.

For the rest, the porosity shows homogeneous results, with very low average pore diameter, with the exception of samples 3/7 and 1/1, showing slightly larger pores.

The selection of the most suitable binders for implementing restoration materials follows the same principles used for the series LBCa. The 7/3 series has been excluded because of the excessive amount of efflorescences, but also because of a variable evolution of the amorphous phases. Once assessed the accomplishment of the geopolymerization, the most suitable product - in terms of mechanical performance, porosity and colour appearance - appears to be sample CWF 3/7+20MK. Good results are also shown by samples CWF 3/7+10MK, CWF 1/1+10MK and CWF 1/1+20MK.

Among these formulations, according particularly to workability, CWF 1/1+10MK has been chosen, in particular to implement geopolymeric bricks and decorations, and other pre-casted elements.

The comparison of the relevant information for selecting the formulation to improve as restoration materials are shown in Table 7.4, including also some synthesis parameters useful for this purpose.

Sample	L/S	Theoretic SiO_2/Al_2O_3	Cur. time (gg)	Efflores. (%)	Amorp. (%)*	Amorp. increase (%)*	FTIR shift (cm^{-1})	Compressive strenght (MPa)	Accessible porosity (%)	Average pore diameter (μm)
CWF 3/7	0.36	4.03	7	2.99	43.83	2.94	29	20.04	33.07	0.07
CWF 1/1	0.37	3.92	7	2.38	46.20	5.31	48	26.91	35.58	0.05
CWF 7/3	0.43	7.22	7	4.38	39.33	-	48	17.86	34.17	0.07
CWF 3/7+10MK	0.40	6.51	1	1.71	50.98	6.42	31	35.14	27.73	0.19
CWF 1/1+10MK	0.36	6.24	1	1.52	52.11	7.55	45	25.44	31.77	0.05
CWF 7/3+10MK	0.40	6.07	1	3.90	40.68	-	49	8.69	32.14	0.05
CWF 3/7+20MK	0.40	5.64	1	0.90	60.71	12.49	41	38.49	28.86	0.11
CWF 1/1+20MK	0.41	5.46	1	1.69	59.14	10.92	54	31.81	30.7	0.06
CWF 7/3+20MK	0.41	5.26	1	2.06	51.28	3.05	60	6.22	29.42	0.04

*Table 7.4 – Results comparison chart of CWF geopolymers, including all the information useful for the selection of suitable binders for mortars synthesis (efflorescences and amorphous %, FTIR shift, average compressive strength and porosimetric data) and the synthesis parameters of L/S and theoretical silica/alumina ratios, as well as the curing time. Min. curing time= minimum curing time; Effloresc.=Efflorescence; Amorp.=Amorphous content; Amorp. Increase=Amorphous Increase. Negative data are not indicated as they should be attributed to an incorrect corundum addition or to inhomogeneous mixing of it. *The amorphous amounts are calculated excluding the efflorescence data.*

7.2 Geopolymeric mortars and three-dimensional substitution elements (bricks, tiles, decorative elements)

According to the binders' results, the formulation CWF 1/1+10MK has been chosen for the optimization of restoration materials. Preliminary tests performed following the scheme already used for LBCa mortars, highlighted poor workability when aggregates are added; simultaneously, the faster setting time of geopolymers based on CWF ceramic (evident during the synthesis) allowed the implementation of a pourable mortar, increasing the L/S ratio. Since the binder is characterized by a L/S ratio = 0.36, it is here increased until 0.48

by adding water to the liquid component. The objective is the creation of pourable mortars for moulding decorative elements, bricks or tiles for substitution intervention of missing or compromised parts of built Cultural Heritage.

The good results obtained on LBCa mortars with carbonate sand, as well as fruitful discussions with restorers, determined the selection of carbonate sand as aggregate for this kind of restoration products, mixed with commercial fine-powdered marble. The latter has been supplied by the restorers involved in the case-studies shown in the following Chapter. The granulometry of the sand aggregates instead has been defined according to the type of final product to obtain: specifically, 1 mm aggregates were used for bricks, tiles, and other structural elements, while a finer granulometry is preferable for decorative elements, especially if details of small size need to be reproduced (as for example in decorated gateways). The new mortar is thus obtained by a binder/aggregates ratio = 1/1, without a specific granulometric curve (which is instead required for bedding mortars, as shown in Chapter 6). In this case two granulometric fractions are used, optimizing their dimensions according to the final product desired. The aggregate's granulometry indeed should be defined case by case, according in particular, to homogeneity and porosity of the substrate to restore; generally preferring fine aggregates for fine textures, while compact materials and coarser aggregates (with a wider granulometry distribution) for materials of rougher texture and porosity (Lazzarini and Laurenzi Tabasso, 1986).

Considering the primary objective of this research, focused on brick masonry, CWF mortar characterization has been carried out on samples with the coarses granulometry. The obtained mortar is labelled CWF 1/1+10MK SCM (where SCM indicates the aggregates Carbonate Sand and Marble).

7.2.1 Mechanical characterization (compressive and flexural tests)

Uniaxial compressive test

The uniaxial compressive test has been performed on six replicates of 2*2*2 cm, after 28 days of curing. The results are reported in Table 7.5 and compared with the resistance obtained on the original binder (Table 7.6).

Sample	Resistance (MPa)	Average	St. Dev.	Bottom limit	Up limit	Accepted values	New average	New St. Dev.	Bottom limit	Up limit	Variation coeff
CWF 1/1+10MK SCM_1	failed	10.68	0.97	9.71	11.64		10.51	0.50	10.01	10.51	0.05
CWF 1/1+10MK SCM_2	9.573										
CWF 1/1+10MK SCM_3	10.213					10.213					
CWF 1/1+10MK SCM_4	10.096					10.096					
CWF 1/1+10MK SCM_5	11.208					11.208					
CWF 1/1+10MK SCM_6	12.294										

Table 7.5 – Compressive resistance results of CWF geopolymeric mortar.

Sample	Resistance average (MPa)	St. Dev.	Bottom limit	Up limit	Variation coeff.
CWF1/1+10MK	25.44	0.83	24.61	26.27	0.03
CWF 1/1+10MK SCM	10.51	0.50	10.01	10.51	0.05

Table 7.6 – Comparison between the compressive resistance results of CWF geopolymeric mortar and the original binder.

It is possible to notice as the original binder is characterized by a higher resistance, probably due to a more compact structure. As we noticed for the mortars obtained from LBCa raw material, the addition of aggregates to the mixture affects the resistance of the final product. Contrary to what observed in the mortars from LBCa with carbonate sand, in this case a decrease in resistance is registered. This incongruity could be attributed to the different granulometry used, less heterogeneous, to the presence of marble powder, or to the increase in liquid component in order to make the mortar pourable.

Nevertheless, the resistance obtained could be considered acceptable for the substitution of bricks and of three-dimensional parts in ancient or compromised structures, in order to preserve them.

Three points flexural test

The flexural test has been performed on three replicates of 2*2*8 cm, after 28 days of curing. Table 7.7 shows the measured flexural resistances, with an average value of 3 MPa. Even though lower than some values reached by mortars from LBCa, this resistance could be still considerd a value in the norm for this kind of materials (Rovnaník et al., 2018).

Sample	Flexural resistance (MPa)	Average	Dev.St.
CWF 1/1+10MK SCM_1	2.95	3.02	0.51
CWF 1/1+10MK SCM_2	2.433		
CWF 1/1+10MK SCM_3	3.666		

Table 7.7 – Flexural resistance results of CWF mortar.

7.2.2. Capillary water absorption test

With the same procedure adopted for LBCa mortar samples, six replicates of 2*2*2 cm of CWF 1/1+10MK SCM formulation have been studied. Also in this case, it was not possible to perform the porosimetric investigation.

Fig. 7.29a shows the average values of water absorption per surface unit in function of time. The plateau created by the last two points demonstrates that the saturation level has been reached. The same data, without the two points of the plateau, allows to individuate the capillary absorption coefficient, represented by the angular coefficient of the marked regression line (Fig. 7.29 b). The data acquired are shown in Table 7.8.

Thanks to the comparison with the other data obtained, it is possible to affirm that this is a potentially absorbent material.

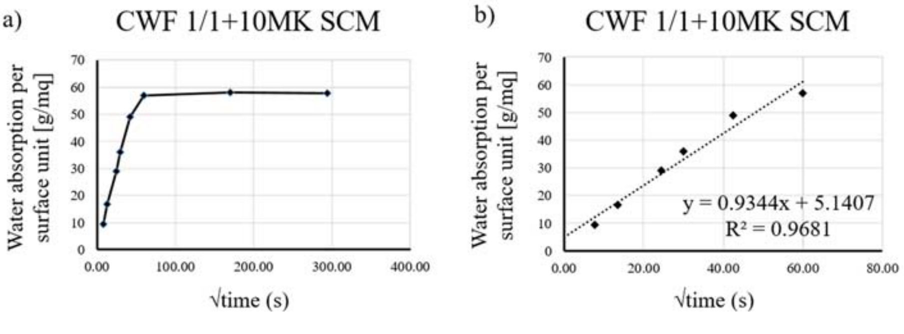

Fig. 7.29 – Capillary absorption graphs of the geopolymeric mortar sample CWF 1/1+10MK SCM. On the left are shown all the absorption steps, on the right the re-elaborated graph after the elimination of the plateau. The angular coefficient is also indicated.

CWF 1/1+10MK SCM

Time [s]	Radq Time [$\sqrt{s}$]	Water absorption per surface unit [g/mq]	Capillary absorption coefficient [g/mq * $\sqrt{s}$]
0	0.00		
60	7.75	9.6	
180	13.42	16.7	
600	24.49	28.9	
900	30.00	36.1	0.9344
1800	42.43	49.0	
3600	60.00	57.0	
28800	*169.71*	*58.1*	
86400	*293.94*	*57.8*	

Table 7.8 – Data of the absorption tests on the mortar CWF 1/1+10MK SCM. The data in italic represent the measurements constituting the plateau.

7.2.3. Colorimetry

In order to define the colour of the obtained mortar, and the differences in colour parameters compared to the original binder as well as to the archaeological references used in this study, colorimetric analysis has been performed. The data are indicated in Table 7.9.

	L*	a*	b*	ΔL*	Δa*	Δb*	ΔE*	ΔC*	ΔH*
CWF 1/1+10MK SCM	57	17	25						
Comparison with CWF 1/1+10MK binder				-1	2	3	4	3	0
Comparison with ME brick				10	2	0	10	1	2
Comparison with GL brick				-2	7	3	8	6	5

*Table 7.9 – CIE-L*a*b* chromatic parameters measured on CWF geopolymeric mortars; colorimetric data results in comparison with reference binder and archaeological bricks (ME brick and GL brick).*

As it is possible to notice, the introduction of aggregates in the system does not determine a perceptible variation in the colour parameters L*, a* and b*, neither on hue and chroma. Only the total colour variation shows a value considered up to the threshold, being ΔE=4, but we can still consider it irrelevant. In respect to the brick from Messina, this mortar shows instead a perceptible increase in lightness, and a total colour variation equal to 10, which is still considered acceptable. Concerning the brick from Gela, again a general perceptible but acceptable colour variation is evidenced, with the highest values of difference regarding ΔC and ΔH, while the lightness variation, with negative value, is not perceived by human eye.

In order to have an immediate perception of the colour appearance, the pseudo-colour is shown in Fig. 7.30.

Fig. 7.30 – Pseudo-colour of CWF 1/1+10MK SCM.

References

Andersen, F.A., Brečević, L., 1991. Infrared spectra of amorphous and crystalline calcium carbonate. Acta Chem. Scand. https://doi.org/10.3891/acta.chem.scand.45-1018

Azevedo, A.G. de S., Strecker, K., Lombardi, C.T., 2018. Produção de geopolímeros à base de metacaulim e cerâmica vermelha. Cerâmica 64, 388–396. https://doi.org/10.1590/0366-69132018643712420

Benavente, D., Martínez-Verdú, F., Bernabeu, A., Viqueira, V., Fort, R., García del Cura, M.A., Illueca, C., Ordóñez, S., 2003. Influence of Surface Roughness on Color Changes in Building Stones. Color Res. Appl. 28, 343–351. https://doi.org/10.1002/col.10178

Clausi, M., Tarantino, S.C., Magnani, L.L., Riccardi, M.P., Tedeschi, C., Zema, M., 2016. Metakaolin as a precursor of materials for applications in Cultural Heritage: Geopolymer-based mortars with ornamental stone aggregates. Appl. Clay Sci. 132–133, 589–599. https://doi.org/10.1016/j.clay.2016.08.009

Criado, M., Palomo, A., Fernández-Jiménez, A., 2005. Alkali activation of fly ashes. Part 1: Effect of curing conditions on the carbonation of the reaction products. Fuel 84, 2048–2054. https://doi.org/10.1016/j.fuel.2005.03.030

D'Elia, A., Pinto, D., Eramo, G., Laviano, R., Palomo, A., Fernández-Jiménez, A., 2020. Effect of alkali concentration on the activation of carbonate-high illite clay. Appl. Sci. 10, 1–14. https://doi.org/10.3390/app10072203

Deere, D.U., Miller, R.P., 1966. Engineering classification and index properties for intact rocks. Technical Report AFNL-TR-65-116. Air Force Weapon Laboratory, New Mexico.

Duxson, P., Provis, J.L., Lukey, G.C., Mallicoat, S.W., Kriven, W.M., Van Deventer, J.S.J., 2005. Understanding the relationship between geopolymer composition, microstructure and mechanical properties. Colloids Surfaces A Physicochem. Eng. Asp. 269, 47–58. https://doi.org/10.1016/j.colsurfa.2005.06.060

Fabbri, B., Gualtieri, S., Shoval, S., 2014. The presence of calcite in archeological ceramics. J. Eur. Ceram. Soc. 34, 1899–1911.

https://doi.org/10.1016/j.jeurceramsoc.2014.01.007

Farmer, V.C., 1974. The infrared spectra of minerals. Mineralogical Society, London.

Fernández-Jiménez, A., Monzó, M., Vicent, M., Barba, A., Palomo, A., 2008. Alkaline activation of metakaolin-fly ash mixtures: Obtain of Zeoceramics and Zeocements. Microporous Mesoporous Mater. 108, 41–49. https://doi.org/10.1016/j.micromeso.2007.03.024

García-Lodeiro, I., Fernández-Jiménez, A., Palomo, A., 2013. Variation in hybrid cements over time. Alkaline activation of fly ash-portland cement blends. Cem. Concr. Res. https://doi.org/10.1016/j.cemconres.2013.03.022

García-Lodeiro, I., Maltseva, O., Palomo, Á., Fernández-Jiménez, A., 2012. Hybrid alkaline cements. Part I: Fundamentals. Rev. Rom. Mater. Rom. J. Mater. 42, 330–335.

Garcia-Lodeiro, I., Palomo, A., Fernandez-Jimenez, A., Macphee, D.E., 2011. Compatibility studies between N-A-S-H and C-A-S-H gels. Study in the ternary diagram Na2O–CaO–Al2O3–SiO2–H2O. Cem. Concr. Res. 41, 923–931. http://doi.org/10.1016/j.cemconres.2011.05.006

He, J., Zhang, J., Yu, Y., Zhang, G., 2012. The strength and microstructure of two geopolymers derived from metakaolin and red mud-fly ash admixture: A comparative study. Constr. Build. Mater. 30, 80–91. https://doi.org/10.1016/j.conbuildmat.2011.12.011

Hughes, T.L., Methven, C.M., Jones, T.G.J., Pelham, S.E., Fletcher, P., Hall, C., 1995. Determining cement composition by Fourier transform infrared spectroscopy. Adv. Cem. Based Mater. 2, 91–104. https://doi.org/10.1016/1065-7355(94)00031-X

Jones, G.C., Jackson, B., 1993. Infrared Transmission Spectra of Carbonate Minerals Infrared Transmission Spectra of Carbonate Minerals. Springer, Dordrecht.

Joshi, S., Kalyanasundaram, S., Balasubramanian, V., 2013. Quantitative analysis of sodium carbonate and sodium bicarbonate in solid mixtures using Fourier Transform Infrared Spectroscopy (FT-IR). Appl. Spectrosc. 67, 841–845. https://doi.org/10.1366/12-06915

Khan, M.I., Azizli, K.A., Sufian, S., Man, Z., Khan, A.S., Ullah, H., Siyal, A.A., 2016. A Short Review of Infra-Red Spectroscopic Studies of Geopolymers. Adv. Mater. Res. 1133, 231–235. https://doi.org/10.4028/www.scientific.net/amr.1133.231

Komnitsas, K., Zaharaki, D., Vlachou, A., Bartzas, G., Galetakis, M., 2015. Effect of synthesis parameters on the quality of construction and demolition wastes (CDW) geopolymers. Adv. Powder Technol. 26, 368–376. https://doi.org/10.1016/j.apt.2014.11.012

Lazzarini, L., Laurenzi Tabasso, M., 1986. Il restauro della pietra. CEDAM, Padova.

Leonelli, C., 2013. Definizione, preparazione, proprietà ed applicazioni., in: Leonelli, C., Romagnoli, M. (Eds.), Geopolimeri: Polimeri Inorganici Attivati Chimicamente. ICerS, Bologna, pp. 1–22.

Lloyd, R.R., Provis, J.L., Van Deventer, J.S.J., 2010. Pore solution composition and alkali diffusion in inorganic polymer cement. Cem. Concr. Res. 40, 1386–1392. https://doi.org/10.1016/j.cemconres.2010.04.008

Najafi Kani, E., Allahverdi, A., Provis, J.L., 2012. Efflorescence control in geopolymer binders based on natural pozzolan. Cem. Concr. Compos. 34, 25–33. https://doi.org/10.1016/j.cemconcomp.2011.07.007

Norme tecniche per le costruzioni. Decreto del Ministero delle Infrastrutture, 14/01/2008.

Occhipinti, R., Stroscio, A., Finocchiaro, C., Fugazzotto, M., Leonelli, C., Lo Faro, M.J., Megna, B., Barone, G., Mazzoleni, P., 2020. Alkali activated materials using pumice from the Aeolian Islands (Sicily, Italy) and their potentiality for cultural heritage applications: Preliminary study. Constr. Build. Mater. 259, 120391. https://doi.org/10.1016/j.conbuildmat.2020.120391

Pachego-Torgal, F., Labrincha, J.A., Leonelli, C., Palomo, A., Chindaprasirt, P., 2014. Handbook of Alkali-activated cements, mortars and concretes. Elsevier.

Panizza, M., Natali, M., Garbin, E., Tamburini, S., Secco, M., 2018. Assessment of geopolymers with Construction and Demolition Waste (CDW) aggregates as a building material. Constr. Build. Mater. 181, 119–133. https://doi.org/10.1016/j.conbuildmat.2018.06.018

Pardal, X., Pochard, I., Nonat, A., 2009. Experimental study of Si–Al substitution in calcium-silicate-hydrate (C-S-H) prepared under equilibrium conditions. Cem. Concr. Res. 39, 637–643. https://doi.org/10.1016/j.cemconres.2009.05.001

Provis, J.L., Van Deventer, J.S.J., 2009. Geopolymers. Structure, processing, properties and industrial applications. Woodhead Publishing Limited, Cambridge.

Reig, L., Tashima, M.M., Borrachero, M. V., Monzó, J., Cheeseman, C.R., Payá, J., 2013. Properties and microstructure of alkali-activated red clay brick waste. Constr. Build. Mater. 43, 98–106. https://doi.org/10.1016/j.conbuildmat.2013.01.031

Robayo, R.A., Mulford, A., Munera, J., Mejía de Gutiérrez, R., 2016. Alternative cements based on alkali-activated red clay brick waste. Constr. Build. Mater. 128, 163–169. https://doi.org/10.1016/j.conbuildmat.2016.10.023

Rodriguez-Blanco, J.D., Shaw, S., Benning, L.G., 2011. The kinetics and mechanisms of amorphous calcium carbonate (ACC) crystallization to calcite, via vaterite. Nanoscale 3, 265–271. https://doi.org/10.1039/c0nr00589d

Rovnaník, P., Rovnaníková, P., Vyšvařil, M., Grzeszczyk, S., Janowska-Renkas, E., 2018. Rheological properties and microstructure of binary waste red brick powder/metakaolin geopolymer. Constr. Build. Mater. 188, 924–933. https://doi.org/10.1016/j.conbuildmat.2018.08.150

Rowles, M.R., O'Connor, B.H., 2009. Chemical and structural microanalysis of aluminosilicate geopolymers synthesized by sodium silicate activation of metakaolinite. J. Am. Ceram. Soc. 92, 2354–2361. https://doi.org/10.1111/j.1551-2916.2009.03191.x

Shen, Q., Wei, H., Zhou, Y., Huang, Y., Yang, H., Wang, D., Xu, D., 2006. Properties of amorphous calcium carbonate and the template action of vaterite spheres. J. Phys. Chem. B 110, 2994–3000. https://doi.org/10.1021/jp055063o

Sun, Z., Cui, H., An, H., Tao, D., Xu, Y., Zhai, J., Li, Q., 2013. Synthesis and thermal behavior of geopolymer-type material from waste ceramic. Constr. Build. Mater. 49, 281–287. https://doi.org/10.1016/j.conbuildmat.2013.08.063

Tuyan, M., Andiç-Çakir, Ö., Ramyar, K., 2018. Effect of alkali activator concentration and curing condition on strength and microstructure of waste clay brick powder-based geopolymer. Compos. Part B Eng. 135, 242–252. https://doi.org/10.1016/j.compositesb.2017.10.013

Yip, C.K., Lukey, G.C., Van Deventer J.S.J., 2005. The coexistence of geopolymeric gel and calcium silicate hydrate at the early stage of alkaline activation. Cem. Concr. Res. 32, 1688–1697. https://doi.org/10.1016/j.cemconres.2004.10.042

Yip, C.K., Lukey, G.C., Provis, J.L., Van Deventer J.S.J., 2008. Effect of calcium silicate sources on geopolymerisation. Cem. Concr. Res. 38, 554–564. https://doi.org/10.1016/j.cemconres.2007.11.001

Zhang, Z., Provis, J.L., Ma, X., Reid, A., Wang, H., 2018. Efflorescence and subflorescence induced microstructural and mechanical evolution in fly ash-based geopolymers. Cem. Concr. Compos. 92, 165–177. https://doi.org/10.1016/j.cemconcomp.2018.06.010

Zhang, Z.H., Zhu, H.J., Zhou, C.H., Wang, H., 2016. Geopolymer from kaolin in China: An overview. Appl. Clay Sci. 119, 31–41. https://doi.org/10.1016/j.clay.2015.04.023

Chapter 8

Chemical, physico-mechanical and aesthetic compatibility of geopolymeric mortars in the field of restoration: case-studies

The discussion of the obtained results on the geopolymeric binders from LBCa and CWF has allowed to develop and test optimized products of good suitability for applications in the field of restoration of stone and ceramic Cultural Heritage. We have seen indeed how both the technical (e.g. compressive strength, open porosity and pore size distribution) and aesthetic properties (colour parameters) are similar to those measured on reference samples.

The obtained results are in agreement with the Venice charter (Icomos, 1964) regarding the process of restoration, which states:

- (…) *Its aim is to preserve and reveal the aesthetic and historic value of the monument and is based on respect for original material and authentic documents. (...)* – art. 9

- *Replacements of missing parts must integrate harmoniously with the whole, but at the same time must be distinguishable from the original so that restoration does not falsify the artistic or historic evidence* – art. 12

Even if the importance of these concepts is universally recognized, archaeological sites frequently undergo incorrect intervention actions and are, unfortunately, negatively affected by poor selection of materials, wrong intervention practices and questionable policy decisions. Hence during time, many items of cultural interest have been definitively lost (Rodrigues and Grossi, 2007).

As already assessed in the introductory chapters, the cultural heritage conservation field, and specifically that of restoration, is a very complex field. Many variables come in to play, often very difficult to predict. For this reason, it is not possible to indicate specific guidelines, as on the contrary is usual to do for building materials. Certainly, common ethical lines could be outlined, to be taken into account when defining, case by case, the set of requirements for the restoration product to apply and the intervention typology itself.

First of all, it must be paid attention to the compatibility issue.

Compatibility is one of the most complex concepts in conservation and the word in itself is certainly one of the most frequently used in the conservation practice. Considered generally in parallel with other traditional concepts, such as minimum intervention, reversibility or harmfulness, it does not find a simple and generic definition. As a multifaceted concept, it can be decomposed in simpler categories, namely physical, chemical, mechanical, operational and so on.. (Pecchioni et al., 2008; Rodrigues and Grossi, 2007).

In the following paragraphs the matters concerning compatibility will be exposed, focussing on the type of products realized in this PhD thesis, thus restoration mortars (bedding, repointing, etc.) and artificial stone-like pre-casted elements. Practical examples of application of the formulations tested to some case-studies will be then exposed, highlighting once again the versatility of these products, which, created for the restoration of historical and archaeological masonries, if suitably optimized, can also find a wide field of application in the restoration of other ceramic materials of museological interest, such as pottery.

8.1 Chemical compatibility

Restoration mortars must be analogous to the substrate from the chemical-mineralogical point of view, in order to ensure a good adhesion without interruptions. A certain reactivity of the applied product toward the substrate is thus requested (Leonelli and Romagnoli, 2013).

It is also important that the mortar or substitutional material does not contain soluble salts, which in case of rising damp or water infiltration, or simply heavy rain, could migrate inside the masonry structure or the materials (Charola and Bläuer, 2015), with the consequent damages exposed in Chapter 1.

Another fundamental requirement is that the product is resistant to chemical attack, for example in respect to acid rains, a significant external impacting factor (Charola and Lazzarini, 1986).

Besides the risk to be affected by salts crystallization, geopolymers exhibit a very good chemical resistance and compatibility with stones, particularly towards ceramic materials (both are indeed strictly alumino-silicatic materials). The mineralogical and chemical analogies, as well as the reactivity with the substrate, thus a good adhesion, is theoretically stated and confirmed by the results here shown.

However, chemical compatibility is an unavoidable requirement in case of consolidation treatment, where the reaction between the restoration product and the substrate ensures a higher durability with respect to the traditional materials of organic nature (polymeric resins).

8.2 Physico-mechanical compatibility

The first element to consider for a good physico-mechanical compatibility is porosity. Actually, this must be such as not to make the mortar (or pre-casted object) susceptible to frost or salt crystallization. Hence, the pores should have sizes close to 1 μm. The restoration material may have a total porosity similar to that of the material on which it should be applied, but with smaller pores, in such a way to preferentially attract the water molecules by means of capillary phenomena. In this way the restoration material will be eventually damaged, maintaining the original substrate preserved (Leonelli and Romagnoli, 2013).

It is clear that this is a general indication, as the desired requirements could be different in case of mortars with specific functions. For example, dehumidifying plasters should have a macro porosity in order to facilitate the evaporation process (Pinto Guerra, 2008).

On the contrary, water vapour permeability must be less than that of the materials to be restored, in such a way that the original substrate could allow eventual absorbed water (still in the liquid phase) to move into the restoration product, thus transporting any solubilized salts out and avoiding their internal crystallization (Leonelli and Romagnoli, 2013; Pecchioni et al., 2008). The restoration material should allow to the masonry to “breathe” (Clausi et al., 2016).

Furthermore, in order to face the issues derived from thermal cycles, it is suggested that the restoration material has a thermal expansion coefficient as similar as possible to the substrate to restore (Leonelli and Romagnoli, 2013; Sassoni et al., 2016); the same is valid for the imbibition coefficient (Leonelli and Romagnoli, 2013).

Concerning instead the mechanical properties, for preventing damage on the original materials, the restoration materials (mortars, stuccoes, substitutional pieces and so on…) should not be stronger than the materials on which they have to be applied. Lower mechanical strengths are preferable (Leonelli and Romagnoli, 2013; Matteini and Moles, 2007; Pecchioni et al., 2008; Sassoni et al., 2016).

In the end, the shrinkage of the new materials must be as low as possible, in such a way to allow, together with the chemical properties, a good adhesion to the substrate.

On the whole, the studied materials satisfy the requirements that determine a good physico-mechanical compatibility towards natural and artificial stone materials, with particular regard to the ceramic ones. In detail, the desired porosimetric parameters, as similar total porosity and simultaneously smaller pores dimensions, were assessed on the geopolymeric binders and mortars studied, as well as the properties linked with water absorption. Indeed, all the mortars are characterized by a relatively high absorption coefficient, which is linked to the pores structure of the samples. Nevertheless, because of a large variability of the porosimetric parameters of ancient materials, it is highlighted the necessity to thoroughly investigate the porosimetric properties case by case in each intervention project.

Concerning the mechanical properties, all the tested materials show enough resistance for conservation issues, but not so high to compromise the original structure. Furthermore, also in this case there is the possibility of optimizing the mixing design to adjust the strength values as desired.

8.3 Aesthetic compatibility

While in the past interventions on Cultural Heritage often determined a complete alteration of the initial appearance of the work of art, for propaganda needs or in order to follow beauty standards across different époques, a higher sensitivity to the preservation of the originals developed with time. The awareness of conservation needs cames to the already mentioned concept of the minimum intervention, concerning both technical aspects and aesthetical ones.

So, the actual ethic of responsible restoration practices has been established, in favour of actions which should be as little as invasive as possible, not altering the overall aspect of the work of art/monument.

Hence, as it is a consolidant/protective intervention or an integration or partial substitution, it must foresee the maintenance of the original colour appearance.

Integration materials, in particular, must be as similar as possible to the object to reintegrate, both from the chromatic and textural points of view, taking into account the porous structure and/or the presence of aggregates. A commonly adopted practice in restoration indeed regards the surface finishing of mortars, bricks and other three-dimensional products, by polishing or abrading the surface according to the specific intervention. For example, the texture appearance of a mortar can be adjusted by brushing and/or tapping the surface after its initial setting (Grimmer, 1984; Rescic and Fratini, 2013).

Nevertheless, as already mentioned, attention must be paid in order to avoid the production of fakes, making the intervention recognizable. For this reason, colours with lower intensity are suggested for example, or lowered surfaces.

Also, from the aesthetic point of view, the results obtained on the experimental geopolymers are highly promising.

In agreement with the pioneers of conservation science in Italy, first of all Cesare Brandi and Antonio Paolucci, the protection of cultural object results in the conservation of its physical integrity and its symbolic value, thus of the entire system of relations which link the single parts together (Fiori et al., 2003).

Considering all the described issues, absolute compatibility appears thus more as a wishful thinking than an achievable objective (Rodrigues and Grossi, 2007).

Actually, most conservation interventions foresee a certain level of risk, frequently even because of non technical and economic feasibility; it is not realistic to consider acceptable only interventions without risk. Therefore, the best achievable aim is not to find a perfectly compatible product or intervention, but rather to find those that minimise the level of incompatibility (Rodrigues and Grossi, 2007).

According to all these concerns, the general criteria to follow would be that the restoration material should receive the degradation: it must be considered as a sacrificial material (Leonelli and Romagnoli, 2013; Pecchioni et al., 2008). A restoration intervention cannot avoid at all the decays, but only slow down the degradation mechanisms.

In order to avoid (or slow down) eventual long-term negative consequences, it will be anyway necessary to foresee the answer of the system to the restoration intervention (Leonelli and Romagnoli, 2013).

A responsible restoration project needs to always consider that higher does not necessarily mean better. A higher mechanical resistance in a repointing mortar with respect to the masonry units will determine a differential decay at the expenses of the original materials, which would be more vulnerable.

In the end, for a restoration intervention to be considered suitable and compatible, it needs to be reversible (Fiori et al., 2003; Matteini and Moles, 2007). Reversibility is one of the fundamental requirements in Cultural Heritage restoration field, born from the recognition that the progress of sciences could make some old restoration interventions or materials obsolete, particularly in comparison with innovative products which could also be more efficient (Fiori et al., 2003).

When it is not possible to guarantee it by mechanical actions, reversibility should at least be possible by using chemical agents, as solubilizing products, and eventually with the help of heat or ultrasounds. It is obvious that when the reversibility cannot be achieved, compatibility becomes a critical issue (Matteini and Moles, 2007).

Compatibility and re-treatability should require certain tolerance limits, but currently these have not been fixed (Rodrigues and Grossi, 2007). Due to the lack of a specific codification, it is necessary to be confident in the sensibility of the restoration designer and of the restorers (Lazzarini and Laurenzi Tabasso, 1986).

Regarding geopolymers, assessed their general good compatibility in the three dimensions of chemical, physical and aesthetic issues, reversibility is still a property to better investigate. Their reactivity towards the substrate and the high chemical affinity determine for sure a certain reaction at the interfaces, which ensures good adhesion, but at the same time could determine difficulties in the chemical removing. Some tests, however, demonstrate the possibility of a mechanical removal, even when the reaction with the substrate occurred properly, with the help of chemicals (e.g. hydrochloric acid based products).

With all these premises, observed the high complexity and abundance of variables which can determine a good restoration intervention, having access to versatile products as the studied geopolymers must be considered absolutely convenient.

8.4 Case-studies

8.4.1 Odéon (Catania)

Fig. 8.1 – Decay morphologies on the restoration bricks of the Odéon, Catania.

The Odéon of Catania has been selected as a first case-study for the application test of the geopolymers implemented. It is a monument of fundamental importance for the history of ancient Catania. It is dated back to the II century A.D. and it is situated in the historical center, behind the more recent roman theatre. The two monuments are interconnected and belong to the Parco Archeologico e Paesaggistico of Catania.

The Odéon is constituted by eighteen walls which create long and narrow covered areas. The structural integrity of the entire monument was, during time, compromised, imposing substantial restoration interventions during the XX century. These interventions particularly regarded the brick elements constituting the walls and have entailed the substitution of entire pillars. Unfortunately, the restoration materials, both the bricks and the mortars, did not show good durability, being today severely affected by decays, such as disintegration and scaling (Fig. 8.1).

The importance and uniqueness of the archaeological site determined the preliminary application, in the contest of this PhD thesis, of geopolymeric mortars on the already damaged restoration bricks. The tests have been performed with the collaboration of the restorers of a prominent restoration company, Piacenti Spa.

Two tests have been performed, applying both an LBCa- and CWF-based mortars on two different pillars, one partially sheltered being on the side of the pillar (area 1), the other directly exposed to the atmospheric agents (area 2) (Fig. 8.2).

Fig. 8.2 – Areas selected for the geopolymeric mortars application tests.

The selected mortars are LBCa 1/1+10MK SC (which was applied in area 1 – Figg. 8.3 and 8.4) and the respective formulation starting from CWF ceramic, CWF 1/1+10MK SC (applied in area 2 – Fig. 8.5).

The fruitful discussion with the restorers was a very important milestone of the entire research; it was indeed a productive moment for individuating the best application modes, the requirements for the optimization of the workability - to be performed on site, as well as for treating the surface of a test application in order to create a finishing similar to the substrate.

It was useful to re-consider the mortars based on the impossibility to synthesize them according to stoichiometric procedures while being on site, that meant overcoming the weighting of the solid and liquid components of the mortar: the new versions of the optimized mortars have indeed foreseen the approximation of the weight of each single component, obtaining a recipe in parts instead of weights.

After the mixing of the solid components with the liquid ones, the slurries have been mixed manually and applied upon previous wetting of the surface by means of waterglass spread by brush (Fig. 8.3). This trick has been used in order to avoid the preferential absorption of the liquid components of the mortars by the porous substrate. This procedure had already given good results in the lab, but here it became even more relevant, because we do not have the possibility to cover the surface of the fresh mortar, thus the drying would occur inevitably faster.

Observed the natural tendency of this kind of materials to fall when applied on vertical surfaces, it was decided to spread one thin layer after another with a spatula, with pauses of more or less ten to fifteen minutes between layers, in order to give the layer anough time to set and receive the new layer without collapsing.

The surface of the CWF mortar was furthermore finished by abrading it with the spatula, exposing the aggregates, in order to test the possibility of giving an antique-looking appearance (Fig. 8.5).

Fig. 8.3 – Geopolymeric mortar application in area 1.

Fig. 8.4 – Geopolymeric mortar applied in area 1 – detail at time zero.

Fig. 8.5 – Geopolymeric mortar application in area 2.

The applications have been then monitored for three months (Fig. 8.6). The results, as visible from the images, are very satisfying. Both mortars are well adherent to the substrate and do not show any efflorescences or shrinkage; no cracks are also visible, with the exception of a very thin fissure on the surface of LBCa mortar. This was present already at time zero after the setting, so probably could be ascribed to the application procedure.

Fig. 8.6 – Monitoring over time of the two geopolymeric mortars in situ.

For what concerns the colour appearance, CWF mortar reached a high degree of similarity to the substrate, but probably this kind of intervention would not be considered ethic in terms of recognizability of the intervention. In cases like this, the creation of lowered surfaces would be preferable. The LBCa test instead shows more recognizable appearance, with a colour that does not alter the whole aesthetical appearance. The lightness seems to be lower, maintaining the same hue. Colorimetric analyses would be needed to confirm the suitability of this kind of material in respect to the substrate.

Fig. 8.7 shows an overview of the monument with the applied interventions, demonstrating how the interventions are not visible at a first sight, but could be recognized looking better.

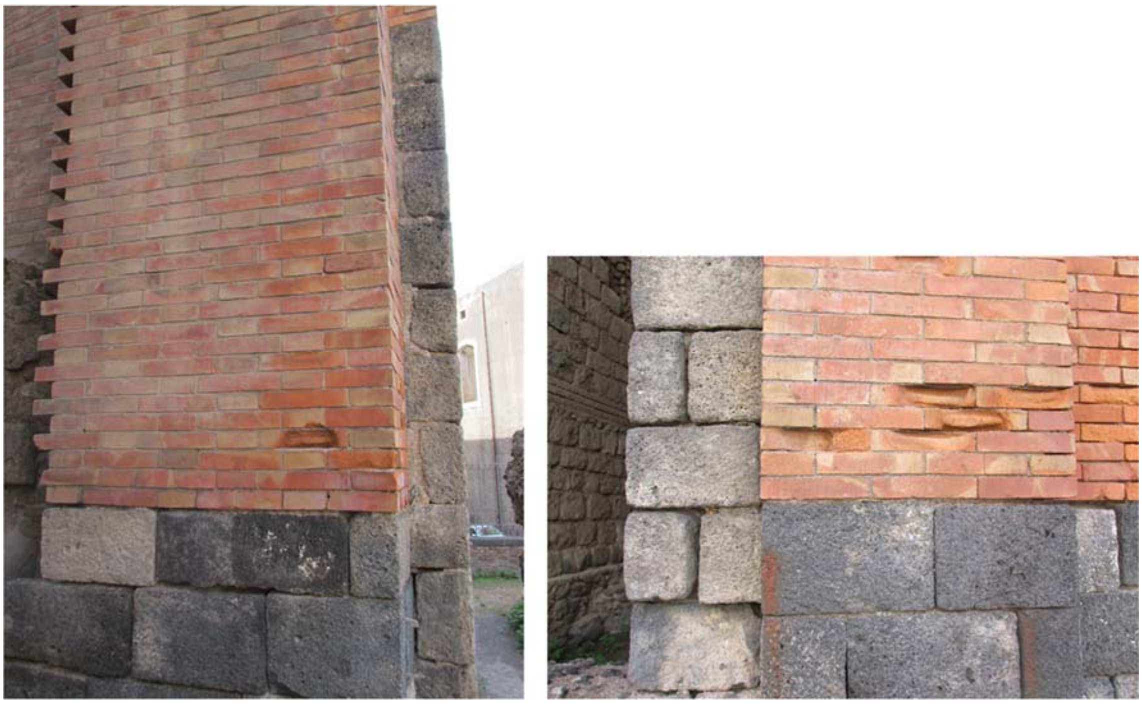

Fig. 8.7 – Final general appearance of the waste ceramic based-geopolymeric mortars applied on brick masonries: test 1 with LBCa formulation - on the left; test 2 with CWF formulation and treated texture - on the right..

We need to consider that these are preliminary tests, made mainly to understand the potential critical aspects linked with the on site productions and the effectiveness of these products in this context. The good results nevertheless, did not just allow to optimize the formulation in order to obtain good workability on site, but also showed good adhesion, and in general good efficiency and compatibility. Then, we should also consider that tests must be done exactly on the material on which to intervene. For that, as these first tests allowed to obtain very promising results, further tests on the original bricks can be planned.

Summarizing, the efficiency in this context was assessed for both tests: the absence of efflorescence, despite the very harsh climate of Catania (humidity and temperature cycles during the summer, succession of rainy and sunny days during the autumn), is in the end one of the most important outcomes, considering that the problem of efflorescences is one of the strictest limits in the application of this kind of materials. In the end, the good results obtained with the new recipes were also a very relevant achievement. This way of preparing the solids and liquids overcomes the necessity of precisely weighting them on site, which is a time-consuming task. This aspect could be able, in itself, to allow the restorers to make a practical choice.

Furthermore, the realization of a small masonry is foreseen, completely made of geopolymeric materials. The LBCa 1/1+10MK SC formulation has been selected in order to create the pre-casted bricks of standard dimensions (25*5*12,5 cm).

The bedding mortars will also be realized in the same material, applied by a trowel. This small mock-up masonry will be then positioned on a base constituted by geopolymeric pre-casted bricks mimicking the lava stone, as to replicate the pillars of the Odéon. Starting from the same formulation, thus, by means of small adjustments, there will be the possibility to obtain materials with very different functions (bricks and mortar joints).

8.4.2 Staircase of Santa Maria del Monte (Caltagirone)

Fig. 8.8 – Staircase of Santa Maria del Monte in Caltagirone.

The famous staircase of Caltagirone, namely Santa Maria del Monte, has been chosen as case-study, particularly for evaluating the suitability of geopolymeric products as replicas of three-dimensional objects, as ceramic materials. Thus, it would be interesting to replicate a typical tile of the famous “Ceramica di Caltagirone” (Fig. 8.8), and to try to glaze it.

With the aim to promote a real circular economy, a formulation based on LBCa waste has been used for this test: new "ceramic" tiles made by geopolymeric binders are realized in Caltagirone, starting from the recycling of the ceramic waste of a local industry, involving the company itself in a productive system reconversion.

The already studied LBCa 1/1+10MK binder has been used and its L/S ratio adjusted in order to pour the paste in molds with the real dimensions of a typical tile of the Caltagirone staircase.

The geopolymeric paste has also been tested for the glazing, and as it is possible to see from Fig. 8.9, good results are obtained by glazing the surface with the same procedure used by the company for its artistic products.

Fig. 8.9 – Glazing test performed by La Bottega Calatina on different kinds of geopolymeric samples.

.

8.4.3 Villa Zingali Tetto (Catania)

The pavement of Villa Zingali Tetto in Catania has also been chosen as further case study. The pavement is realized by traditional *cementine*, a very important local technology used in historical architecture during the late XIX and early XX century. Finding a way to restore them, to eventually reconstruct the overall decoration of an historical/artistic pavement would be likewise important. *Cementine* are cement tiles decorated on the surface. Being the geopolymeric material an intermediate material between ceramics and cements, it would be interesting to test its application also in this context. Thus, replicas of *cementine* tiles have been realized by using the LBCa 1/1+10MK formulation, again at La Bottega Calatina. Figg. 8.10 and Fig. 8.11 show some operative steps and the final product, before the finishing of the surface.

Fig. 8.10 – Geopolymeric tiles realized at La Bottega Calatina.

Fig. 8.11– Geopolymeric tiles realization process at La Bottega Calatina.

The collaboration with the company was fundamental in order to understand the requirements of an industrial system, and the suitability of these products for the industrial scale-up. Clearly these are only preliminary tests, but very promising.

In this case, the glazing will be made by painting, in order to more faithfully reproduce to the original, which, contrarily to a glazed ceramic, has an opaque and porous appearance.

8.4.4 Pottery

Even if it was not a direct objective of this thesis, I had the opportunity to test the implemented geopolymeric mortars for the restoration of museum materials, particularly for the reintegration of pottery as dishware, pitchers, amphorae and other potsherds.

The study was conducted at the restoration laboratory of the Parco Archeologico e Paesaggistico of Catania, in the historical building of Manifattura Tabacchi, with the collaboration of the restorers Daniela Carella and Marco Patrì. Traditional materials have been compared with these new ones. The study has been particularly interesting and also it proved more complex than expected. Traditionally, for this kind of restoration the employed materials, as gypsum and clays, are easily commercially available, and ready to be used. They tend to maintain their plasticity over time, thus giving the restorers the possibility to work in different moments towards the restoration interventions, modifying the surface even the day after. They seem to be, theoretically, very good restoration materials for museum collections. However, even if the indoor museum environment should be controlled, with limited climatic variations, the reality is very different. Generally, museums are humid environments and, often for economic reasons especially for small museums, a not efficient or not active environmental conditioning is in place: the temperature and humidity variations indoor follow seasonal variations. Moreover, the microclimate of the cases could sometimes have a negative effect on the stored materials (Del Curto, 2010; Realini, 2016). In this context, the traditional materials could face degradation problems that, even if not as bad as those observed outdoors, can anyway compromise the integrity and stability of the museum objects.

Three original objects have been selected for the test: a *terra sigillata* dish, a vessel and an amphora retrieved in the excavation of Via Crociferi, in Catania. The first two fragmentary remains have been previously recomposed according to the available fragments, and than used for phase I. The amphora was used instead, after the preliminary recomposition, for the final test (phase III).

According to the results exposed in the previous chapters and paying attention to the colour appearance, LBCa 1/1+10MK SC and CWF 1/1+10MK SC mortars have been selected for this application test. This case-study has been conducted in three steps: the first step has seen the application of the products as such, in order to define their efficiency and pitfalls in this specific case (Figg. 8.12 and 8.13); the second phase was a laboratory work aiming at improving the formulations in order to achieve better mortars for the specific case (Fig.8.14); the third step was the application of the final products on the original remains (Fig. 8.15).

Phase I

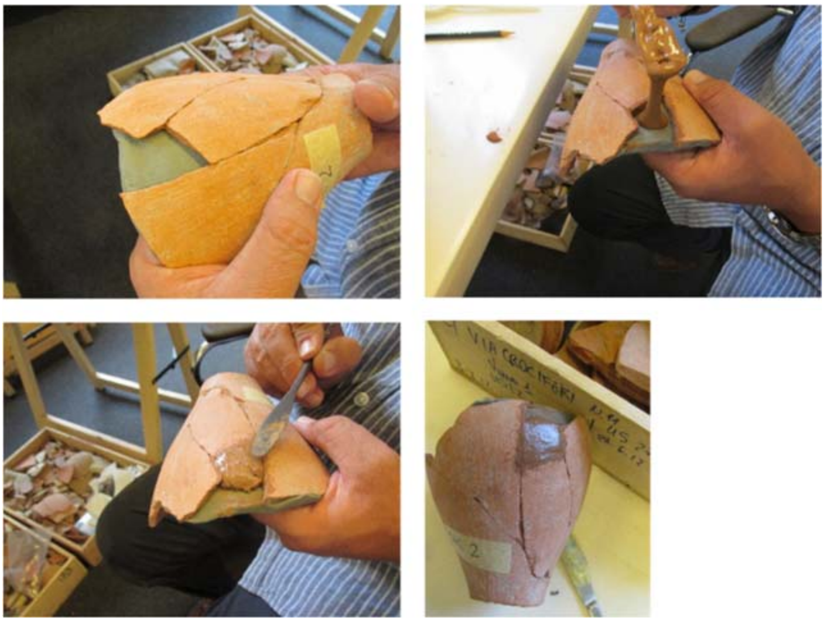

Fig. 8.12 – Application of LBCa geopolymeric mortar on ceramic archaeological remains.

Fig. 8.13 – Application of CWF geopolymeric mortar on ceramic archaeological remains.

The first phase allowed to understand some issues and specific requirements of the product to use: the typical thixotropic behavior of the geopolymeric materials needs to be in some way attenuated. The product indeed tends to remain attached to the spatula, and it is difficult to work for three-dimensional surfaces, as for example a small plinth of a dish. In order to replicate decorations, small molding, etc. the product should be workable for a certain time (at least 30 minutes), it needs to maintain the shape but, in order to receive eventual modification during the application, not to dry too fast. A more plastic material is thus desired. After one day of curing at room conditions, the materials applied are completely dried and very hard, thus it is difficult to work on them, not even for surface leveling by abrasive papers. A certain visible shrinkage is also present. Instead, the colour appearance is really good. The hardened mortars where then removed by mechanical action with the help, in some instances, of hydrochloric acid.

Phase II

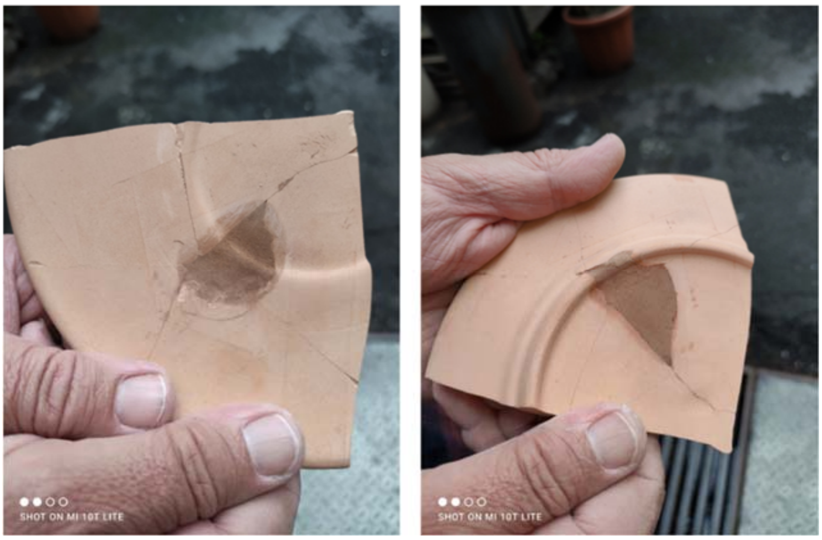

Fig. 8.14 – Optimization of the LBCa geopolymeric mortar and application on modern ceramic.

In order to obtain a more plastic and workable product, to lower the shrinkage and improve the adhesion, many attempts have been performed. The tests have foreseen:

A) the addition of a calcium additive (Prompt) in 10 and 20% in weight to the original formulations;

B) the modification of the original formulation by excluding waterglass;

C) the addition of a calcium additive (Prompt) in 10 and 20% in weight to the modified original formulation where R=3 waterglass was substituted with a less concentrated one (R=2);

D) all the previous tests have been replicated with the addition of powdered marble in 4/1 binder/aggregate ratio.

With the aim to reduce the shrinkage due to water evaporation, the mortars were cured inside a sealed plastic bag. These tests were performed on modern ceramic fragments.

It was possible to notice as both the tricks of using calcium-rich additives, or reducing the waterglass in the mixture (by reducing the concentration or excluding it from the formulation) gave better workability properties. However, when waterglass is excluded, efflorescences start to appear, while these are not individuated in the test with less concentrated waterglass. At the same time, test A shows a very hard consolidated product after few hours, that makes it difficult to work on it over time. The best solution appears to be a compromise of the first two attempts (case C), by using both Prompt and reducing the concentration of the waterglass (Fig. 8.14). The 20% weight of Prompt showed improved workability. The best results are furthermore obtained when aggregates are added. This allowed moreover to control the shrinkage (Pecchioni et al., 2008).

These observations are valid for both LBCa and CWF mortars, even if the workability appears to be better for LBCa-based products.

Phase III

Fig. 8.15 – Application of the optimized geopolymeric mortars on original archaeological support.

After one-month monitoring of the applied products, having not seen efflorescence crystallization and good adhesion (no shrinkage), they were applied on the ancient amphora (Fig. 8.15).

The good results obtained in all the case-studies exposed are obtained thanks to the optimization of the products in function of the specific requests, through the definition of the best application mode case by case. Indeed, while for the Odéon case-study it was important to apply the product layer by layer, paying attention in having a good adhesion between the different layers, in order to avoid the typical tendency of the product to collapse under the force of gravity (Matteini and Moles, 2007); in the case of the three-dimensional tiles for the Caltagirone and Villa Zingali Tetto case studies it was important to make the mortars more fluid, in order to pour them easily and faster, as well as to obtain materials which could receive glazing or other decoration. In the last case-study, instead, it was very important to obtain a more plastic material which had to be applied in excess, in order to properly adhere to the interfaces without discontinuities, and then flattened by abrasive papers once consolidated. This is a usual technique in the restoration field, due to the fact that liquid components tend to create a meniscus, determining difficulties to obtain planar surfaces (Matteini and Moles, 2007). The high versatility of the formulations studied are those confirmed!

References

Charola, A.E., Bläuer, C., 2015. Salts in Masonry: An Overview of the Problem. Restor. Build. Monum. 21, 119–135. https://doi.org/10.1515/rbm-2015-1005

Charola, A.E., Lazzarini, L., 1986. Deterioration of Brick Masonry Caused By Acid Rain. ACS Symp. Ser. 250–258. https://doi.org/10.1021/bk-1986-0318.ch017

Clausi, M., Tarantino, S.C., Magnani, L.L., Riccardi, M.P., Tedeschi, C., Zema, M., 2016. Metakaolin as a precursor of materials for applications in Cultural Heritage: Geopolymer-based mortars with ornamental stone aggregates. Appl. Clay Sci. 132–133, 589–599. https://doi.org/10.1016/j.clay.2016.08.009

Del Curto, D., 2010. Indoor environment and preservation. Climate control in museums and historic buildings. Nardini Editore, Milano.

Fiori, C., Lorusso, S., Pentrella, R., 2003. Restauro, manutenzione, conservazione dei Beni Culturali: materiali, prodotti, tecniche, I Beni Culturali e l'Ambiente. Pitagora Editrice, Bologna.

Grimmer, A.E., 1984. A glossary of historic masonry deterioration problems and preservation treatments. Government Printing Office, Washington D.C.

Icomos, 1964. International Charter for the conservation and restoration of monuments and sites (The Venice Charter 1964). IInd Int. Congr. Archit. Tech. Hist. Monum. 1–4.

Lazzarini, L., Laurenzi Tabasso, M., 1986. Il restauro della pietra. CEDAM, Padova.

Leonelli, C., Romagnoli, M., 2013. Geopolimeri: polimeri inorganici attivati chimicamente., 2nd ed. ICerS, Bologna.

Matteini, M., Moles, A., 2007. La chimica nel restauro. I materiali dell'arte pittorica. Nardini Editore, Firenze.

Pecchioni, E., Fratini, F., Cantisani, E., 2008. Le malte antiche e moderne tra tradizione ed innovazione. Pàtron Editore, Bologna.

Pinto Guerra, E., 2008. Risanamento di murature umide e degradate : manuale, guida progettuale, soluzioni. Dario Flaccovio Editore, Palermo.

Realini, M., 2016. La Scienza delle Vetrine. Analisi dei rischi della conservazione. CNR

Press, Roma.

Rescic, S., Fratini, F., 2013. Geopolimeri e Beni Culturali., in: Leonelli, C., Romagnoli, M. (Eds.), Geopolimeri: Polimeri Inorganici Attivati Chimicamente. ICerS, Bologna, pp. 252–278.

Rodrigues, J.D., Grossi, A., 2007. Indicators and ratings for the compatibility assessment of conservation actions. J. Cult. Herit. 8, 32–43. https://doi.org/10.1016/j.culher.2006.04.007

Sassoni, E., Pahlavan, P., Franzoni, E., Bignozzi, M.C., 2016. Valorization of brick waste by alkali-activation: A study on the possible use for masonry repointing. Ceram. Int. 42, 14685–14694. https://doi.org/10.1016/j.ceramint.2016.06.093

Conclusions

The experimental study exposed in this PhD thesis led to a series of important outputs for the scientific development in the field of green restoration of ceramic materials, with particular interest towards bricks and brick masonries of archaeological interest. Furthermore, interesting discussion points could be put forward for the improvement of the comprehension of geopolymerization mechanisms in ceramic waste alkali activation, a research topic still little investigated.

Good physical and mechanical performative materials of geopolymeric nature have been obtained by alkali activating ceramic waste supplied by a local industry, without pre-treatment and with curing at environmental temperature. This is the most important outcome obtained by this study, together with the assessment of the great versatility of the products experimented, allowing to evaluate the suitability of these materials for on site restoration campaigns, and for encouraging a circular economy while simultaneously reducing production costs.

In detail:

- Amorphous hybrid geopolymeric gel ((N,C)-A-S-H, C-A-S-H and N-A-S-H) has been detected in all the series experimented, starting from two ceramic waste of low reactivity (tiles and bricks).

  Good results have been obtained without prompting the synthesis conditions, thus allowing to assess the possibility of valorizing this kind of waste.

  From these good results it would be possible to foresee even better results starting from other more reactive ceramic waste raw materials studied.

- All the geopolymeric series studied are characterized by good adhesion, moderate mechanical strength, similar overall porosity and pore dimensions slightly lower than that of archaeological substrates, relatively high absorption properties, less bright appearance and perceptible but moderate colour variation with respect to the archaeological fragments. The few exceptions found could anyway find an explanation in the synthesis parameters used.

- The case-studies allowed to confirm the high versatility of this products. Starting from a specific formulation, by changing the L/S ratio and/or the type and granulometry of the aggregates and/or by adding some eventual additives and/or treating the surfaces, it is possible to tailor the mortar to a specific intervention. Equilibrating these parameters would allow indeed to adjust workability, setting velocity and colour or texture appearance.
- The monitoring over time of the applications as case-studies, as well as the stability tests carried out, furthermore, allowed to hypothesize a good durability, even if specific tests are needed to confirm it.

  Not less important, the great problem of geopolymers, efflorescences, has been overcome in these formulations.

In this way, restoration mortars suitable both for outdoor monuments and for museums objects, tiles, bricks and decorative pre-casted elements have been realized.

In the end, it is necessary to point out that those binders' formulations that have been experimented, but that have not been chosen for the realization of the restoration products, according to the scientific characterization here exposed should not be considered as "bad" formulations, but only not adequate for the applicative aims of this work.

Further outcomes that need to be mentioned are the assessing of the usefulness of spectroscopic techniques not usually applied for the characterization of geopolymeric materials, namely DRIFT and Raman.

To conclude, the results obtained highlight the complexity of these systems and the difficulties in understanding the mechanisms, which vary according to the raw materials used, modifying the type of gel formed and therefore the performance of the final products. On the other hand, comparing the analytical results obtained by different complementary techniques allowed us to infer or hypothesize the cause of a particular or unexpected behaviour.

From all of that the suggestion comes to systematically study a corpus of formulations by changing the parameters one by one, and to investigate them with a plethora of techniques.

A scheme (SWOT analysis) identifying strengths and weaknesses coming from this research, followed by the related opportunities, together with the proposed action for facing the weak points is here shown.

Strength	Weakness
✓ Good degree of sustainability ✓ Possibility to be prepared at room temperature ✓ No needs of thermic treatments ✓ Recycling of waste ceramic ✓ Porous structure suitable for restoration products ✓ Mechanical strength suitable for restoration products ✓ Versatility – possibility to modify the formulation ad hoc for each intervention ✓ Possibility to prepare the materials in situ	▪ Complex and heterogeneous systems that need more investigations to be understood ▪ Not recognizable morphologies in the gel microstructure which could be a clue of an incomplete reaction or of secondary products

Opportunities	Solutions and further challenges
✓ Applications in the restoration field, for different kind of interventions ✓ Promoting green restoration ✓ Promoting re-conversion of the production systems for re-integrating the waste – circular economy	▪ Further investigation by means of higher magnification SEM and TEM observations, linked with chemical mapping and punctual analysis. ▪ Further study of the formulations by a stoichiometric approach

Geopolymers offer a great opportunity for the growth of innovative and eco-sustainable restoration practices, but these need to be studied case by case, starting from an already established formulation.

Differently to how we usually think about restoration materials, the geopolymerization process should not be considered as the universal solutios to create new materials adapted to each and every conservation problem, but a tool for tailoring the characteristics of the restoration product, by adjusting the mix design in order to optimize the properties as desired.

Acknowledgements

The end of a PhD research project is a crucial moment, it is the end of an important journey in scientific training and the starting point towards a successful career in the academic field. In the past three years I have been able to tackle a complex thematic, and if results have been promising and satisfying, it is, really, also thanks to the great support of some people, whom I would like to sincerely thank below.

I would like to express my sincere gratitude to Prof. Germana Barone, my PhD tutor and point of inspiration to always do better and not give up, notwithstanding the difficulties that could hamper the path. Thank you for having believed in me.

I am deeply grateful to Prof. Paolo Mazzoleni, my Phd co-tutor and precious and unique role model for scientific discussions. Thank you for having dedicated your time to me and particularly, for your insightful suggestions.

I would like to extend my sincere thanks to Prof. Giuseppe Cultrone, my PhD co-tutor of the University of Granada, for his unwavering support and availability. Thank you for the opportunity to collaborate with the Department of Mineralogy and Petrology, despite the difficulties due to the pandemic.

Thanks to all the Professors and researchers that allowed the development of scientific analysis in different Universities, all cited in the text.

I would also like to offer my special thanks to Dr. Gioconda Lamagna of the Parco archeologico e paesaggistico of Catania, that allowed me to work on the unique site of Odèon and on archeological pottery. For that, I also want to give thanks to the restorers Marcello Patrì, Daniela Carella of the Parco and Girolamo Nucatolo of the Piacenti Spa for the precious exchange of knowledge.

A particular thanks goes to Nico Parrinello of La Bottega Calatina and to Laquattro Srl, who supplied the raw materials, believing in this research project.

Thanks to the PhD Course Coordinator, Prof. Pietro Militello, a constant presence for all us PhD Students.

Last but not least, a special thanks goes to my colleagues of the Department of Biological, Geological and Environmental Sciences, Antonio Stroscio, Roberta Occhipinti, Cristina Caggiani, Alessia Coccato, Claudio Finocchiaro and Gabriele Lanzafame, with whom, needless to say, I shared everything. It has been a great opportunity for me to be part of this research group.

Attachments

Attachment 5.1 – Results of uniaxial compressive strength tests performed on samples of geopolymers cured at room temperature and at 65 °C for 24h.

Sample	Dimensions (mm)			Compressive resistance (MPa)	Mean (MPa)
	x	y	z		
LBCa 5_1	21.9	18	20	13.15	
LBCa 5_2	21.9	18.5	20.9	12.04	11.03
LBCa 5_3	20.1	18.5	20	7.89	
LBCa 5A_1	26	21.5	23.9	6.74	
LBCa 5A_2	23.9	23.6	26	6.02	6.44
LBCa 5A_3	26	22.6	24	6.57	
LBCa 5+10MK_1	21	20	20	14.45	
LBCa 5+10MK_2	20.8	21.5	17.9	13.56	14.27
LBCa 5+10MK_3	21.1	19.3	20.6	14.79	
LBCa 5+10MKA_1	26.4	22.1	24	10.1	
LBCa 5+10MKA_2	26.4	23.7	23.9	9.69	9.79
LBCa 5+10MKA_3	26.6	23.7	23.9	9.59	
LBCa 12_1	21	20.9	17	3.17	
LBCa 12_2	21	21	16.3	4.11	3.5
LBCa 12_3	20.9	20.9	16.3	3.22	
LBCa 12A_1	27.5	23.6	29	2.54	
LBCa 12A_2	23.5	23	26	2.41	2.25
LBCa 12A_3	26.6	24.7	23	1.8	

Attachment 5.2 – Porosimetric data of geopolymeric samples cured at room temperature and at 65 °C for 24h.

Sample	Bulk Density (g/cm^3)	Acces. Porosity (%)	Total pore volume (mm^3/ g)	Average pore diameter (μm)	Modal pore diameter (μm)
LBCa 5	1.77	22.65	128.22	0.20	1.03
LBCa 5A	1.69	26.02	154.05	0.16	0.67
LBCa 5+10MK	1.78	23.07	129.95	0.09	0.59
LBCa_5+10MK-A	1.79	29.09	162.09	0.10	0.18
LBCa 12	1.72	29.01	168.38	0.20	0.66
LBCa 12A	1.64	37.05	225.35	0.18	0.50

Attachment 6.1 – SEM micrographs of the geopolymeric binders based on LBCa ceramic waste precursor.

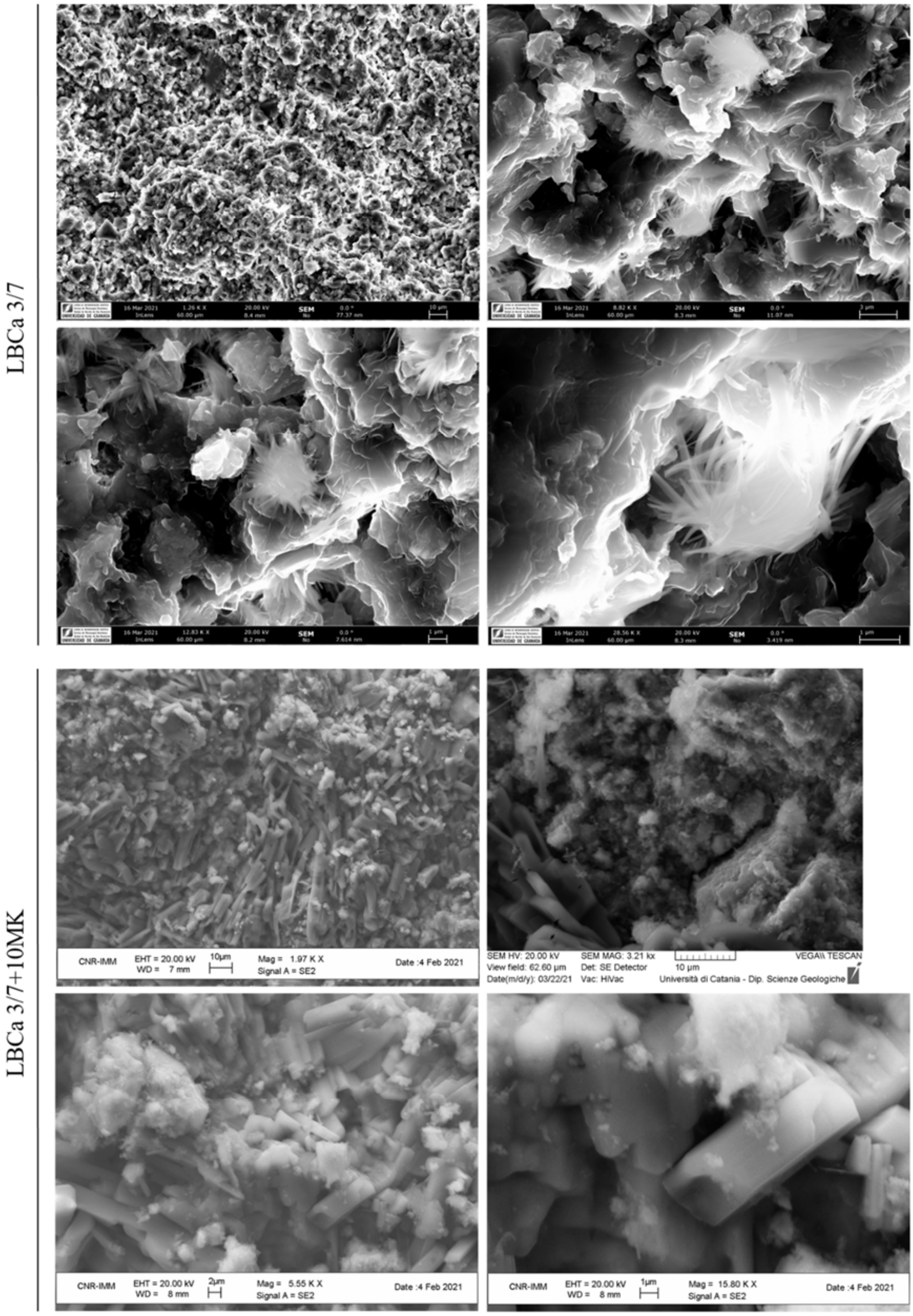

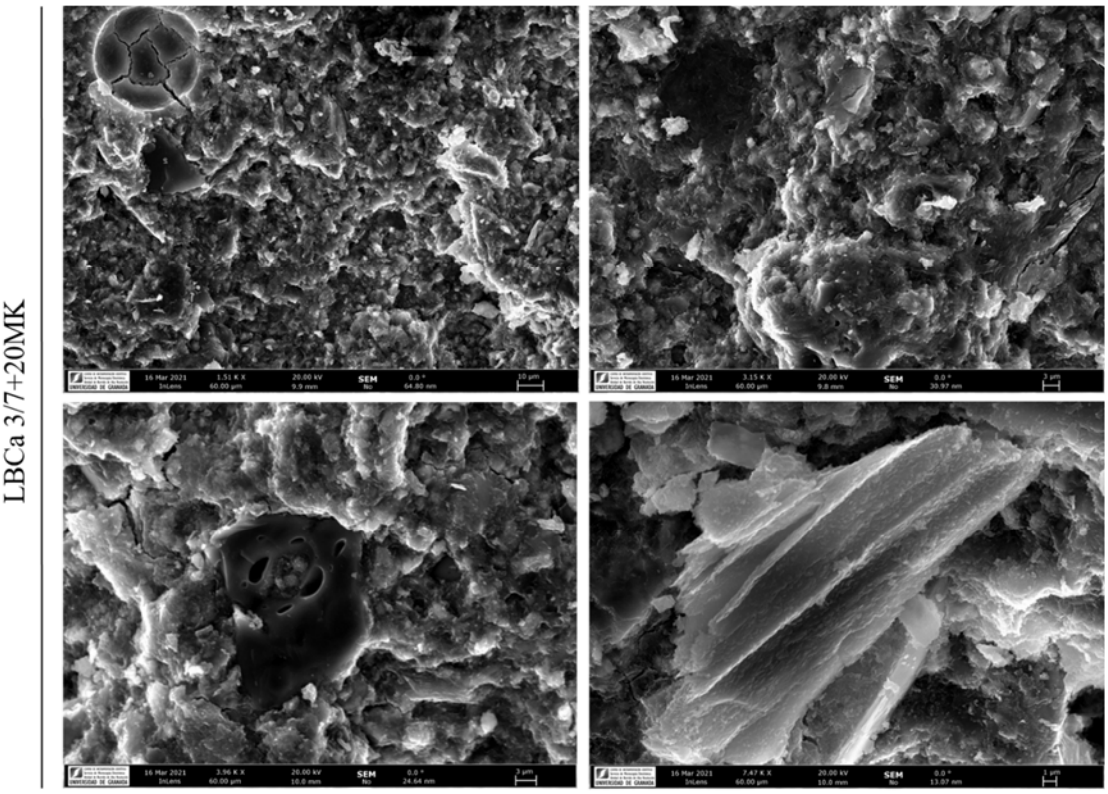
LBCa 3/7+20MK

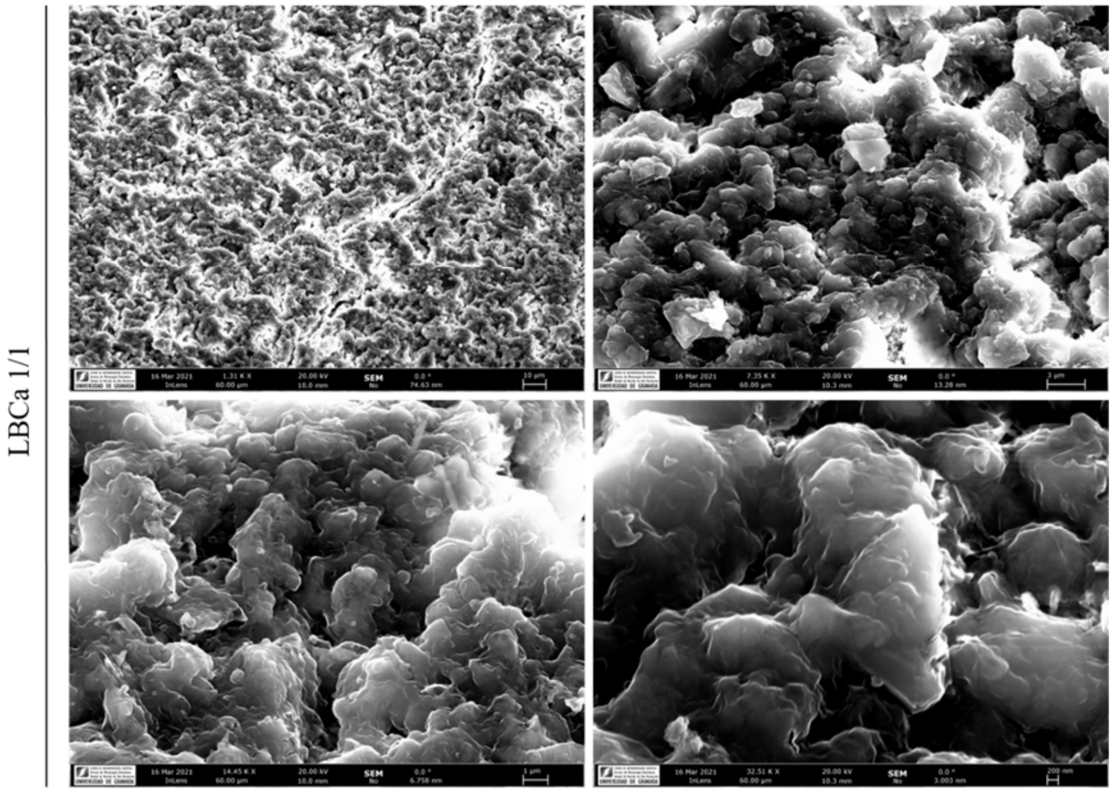
LBCa 1/1
16 Mar 2021 1.31 K X 20.00 kV SEM 0.0 ° 10 µm
InLens 60.00 µm 10.0 mm No 74.63 nm
16 Mar 2021 7.35 K X 20.00 kV SEM 0.0 ° 2 µm
InLens 60.00 µm 10.3 mm No 13.28 nm
16 Mar 2021 14.45 K X 20.00 kV SEM 0.0 ° 1 µm
InLens 60.00 µm 10.0 mm No 6.758 nm
16 Mar 2021 32.51 K X 20.00 kV SEM 0.0 ° 200 nm
InLens 60.00 µm 10.3 mm No 3.003 nm
UNIVERSIDAD DE GRANADA

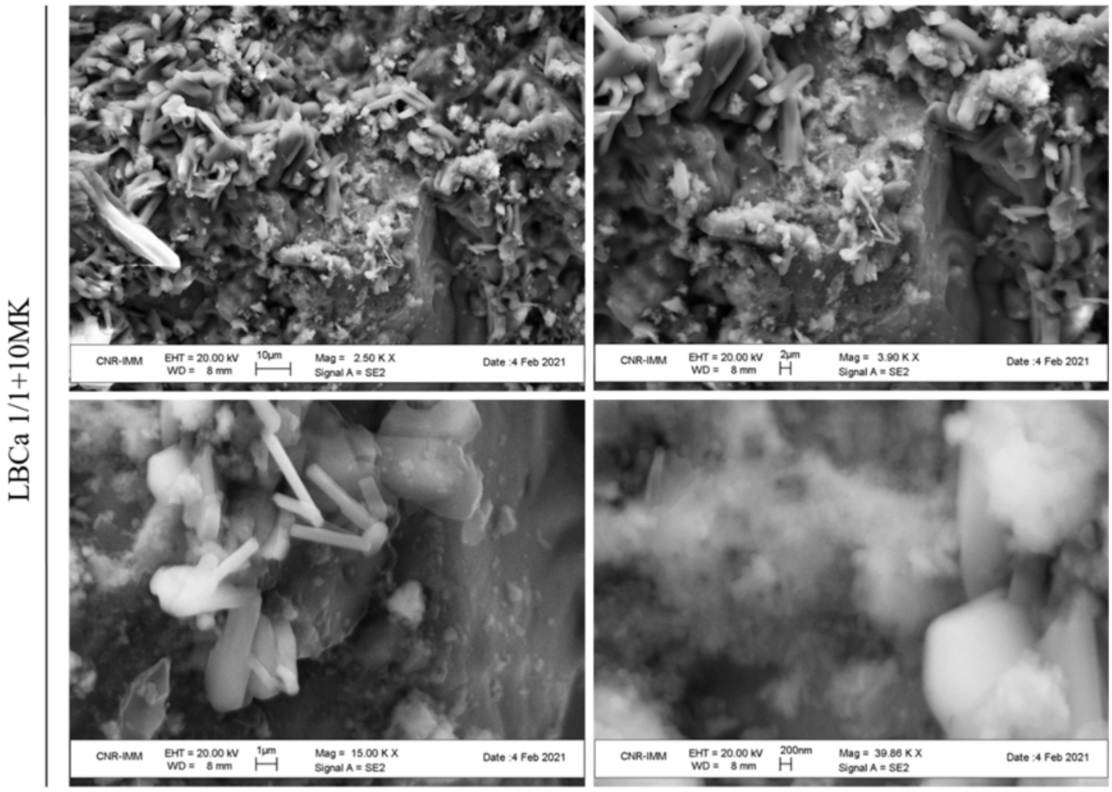
LBCa 1/1+10MK
CNR-IMM EHT = 20.00 kV WD = 8 mm 10µm Mag = 2.50 K X Signal A = SE2 Date :4 Feb 2021
CNR-IMM EHT = 20.00 kV WD = 8 mm 2µm Mag = 3.90 K X Signal A = SE2 Date :4 Feb 2021
CNR-IMM EHT = 20.00 kV WD = 8 mm 1µm Mag = 15.00 K X Signal A = SE2 Date :4 Feb 2021
CNR-IMM EHT = 20.00 kV WD = 8 mm 200nm Mag = 39.86 K X Signal A = SE2 Date :4 Feb 2021

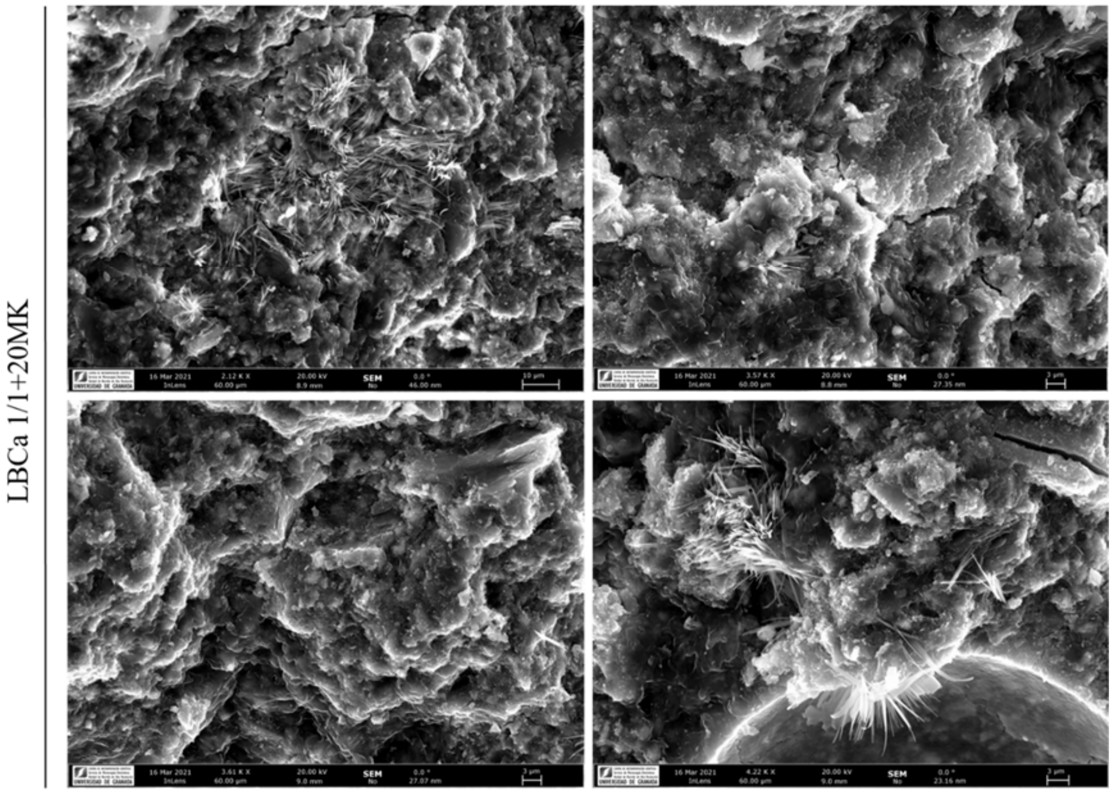
LBCa 1/1+20MK

LBCa 7/3

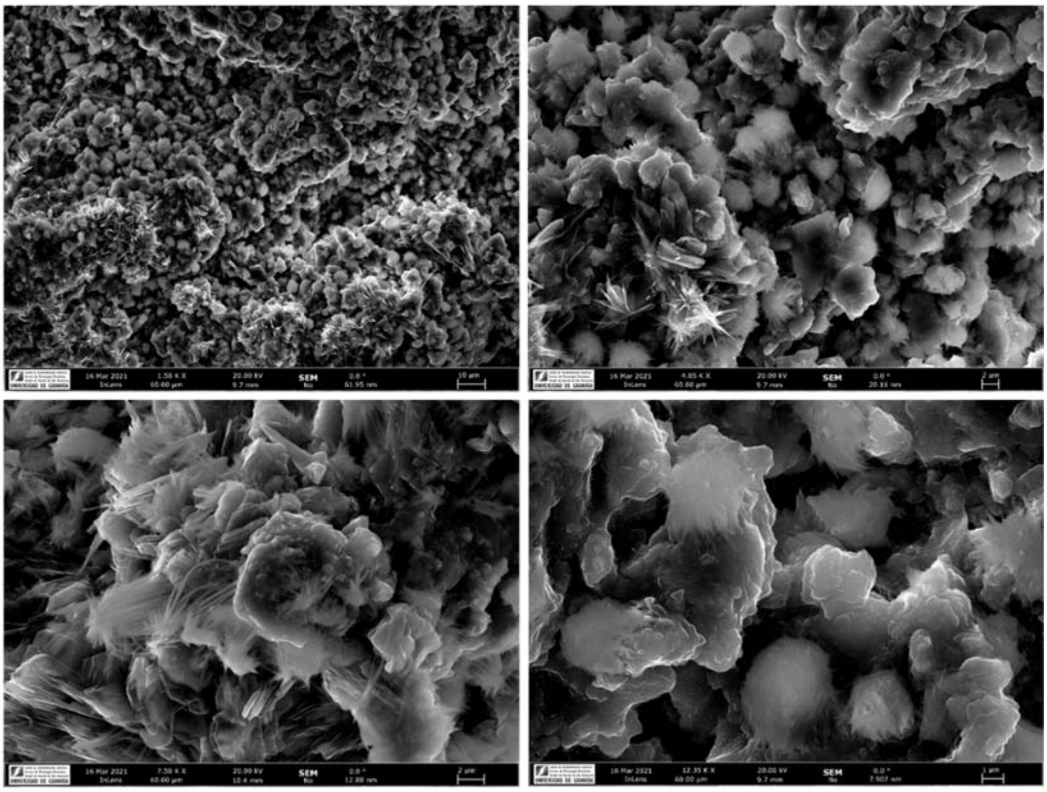

LBCa 7/3+10MK

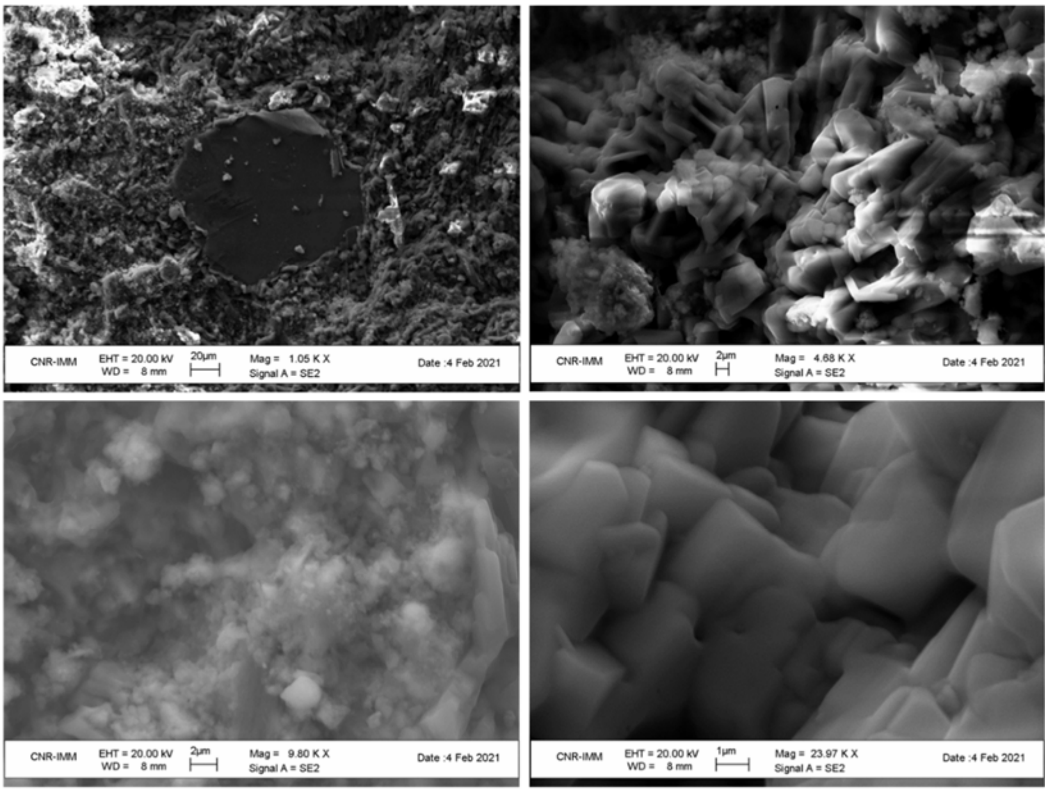

LBCa 7/3+20MK

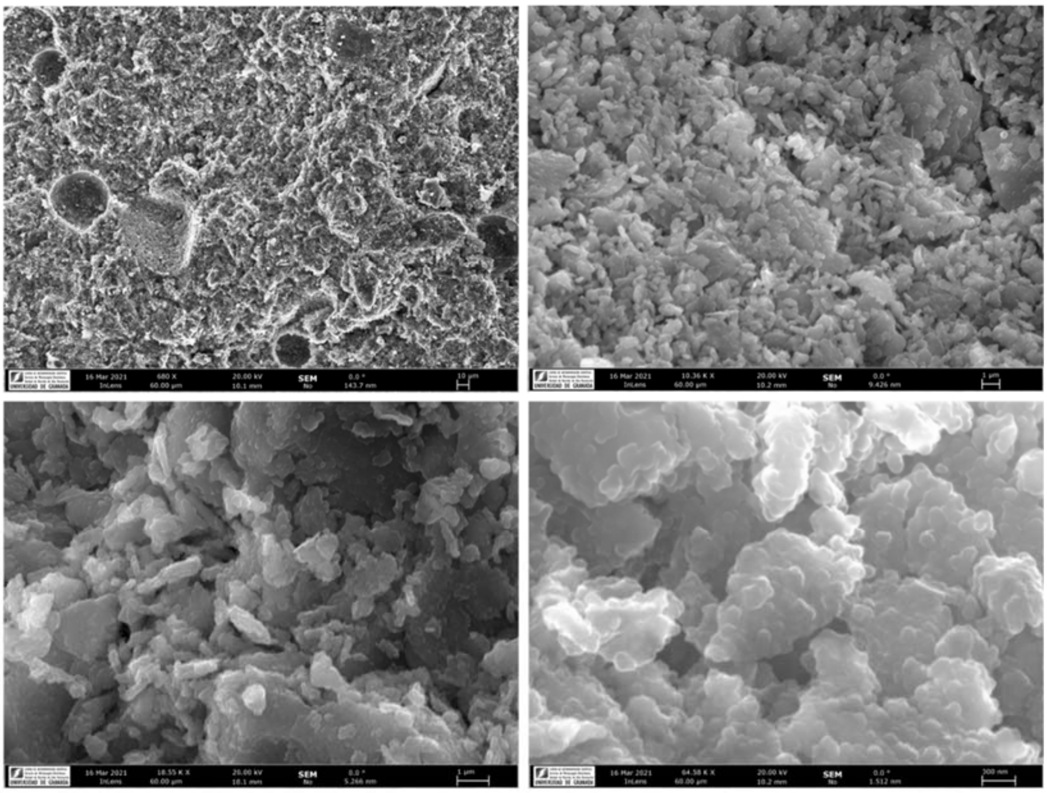
16 Mar 2021
680 X
20.00 kV
SEM
10 µm
16 Mar 2021
10.36 K X
20.00 kV
SEM
1 µm
16 Mar 2021
18.55 K X
20.00 kV
SEM
1 µm
16 Mar 2021
64.58 K X
20.00 kV
SEM
300 nm

Attachment 6.2 – Colorimetric data collected on the upper and bottom surfaces of all the LBCa binders. The colour parameters variations are also calculated in respect to LBCa raw material and to the two archaeological references (ME brick and GL brick).

Samples		L*	a*	b*	ΔL*	Δa*	Δb*	ΔE*	ΔC*	ΔH*	ΔL*	Δa*	Δb*	ΔE*	ΔC*	ΔH*	ΔL*	Δa*	Δb*	ΔE*	ΔC*	ΔH*
LBCa 7/3	bottom	40.31	14.89	20.37	-17	2	-1	17	0	2	-7	-1	-5	8	-4	2	-19	5	-1	20	1	5
	up	40.58	14.71	20.05	-17	2	-1	17	0	2	-7	-1	-5	8	-4	2	-19	5	-2	19	1	5
LBCa 1/1	bottom	39.07	15.16	20.44	-18	2	-1	19	1	3	-8	0	-4	9	-4	2	-20	5	-1	21	2	5
	up	44.56	15.16	21.78	-13	2	0	13	2	2	-3	0	-3	4	-3	1	-15	5	0	16	3	5
LBCa 3/7	bottom	45.20	15.10	20.65	-12	2	-1	13	1	2	-2	0	-4	5	-4	2	-14	5	-1	15	2	5
	up	47.17	15.14	22.35	-10	2	1	11	2	1	0	0	-3	3	-2	1	-12	5	1	13	3	4
LBCa 7/3+10MK	bottom	62.90	10.55	17.70	5	-2	-4	7	-4	0	16	-5	-7	18	-9	0	4	1	-4	5	-3	2
	up	44.63	15.21	20.29	-13	2	-1	13	0	3	-3	0	-5	5	-4	2	-15	5	-1	16	1	5
LBCa 1/1+10MK	bottom	52.43	11.77	17.26	-5	-1	-4	7	-4	1	5	-4	-8	10	-8	1	-7	2	-4	8	-3	4
	up	44.97	14.38	19.80	-12	2	-2	13	0	2	-2	-1	-5	6	-5	2	-14	5	-2	15	1	5
LBCa 3/7+10MK	bottom	53.15	10.51	15.22	-4	-2	-6	8	-6	1	6	-5	-10	12	-11	1	-6	1	-7	9	-5	4
	up	52.33	13.64	20.51	-5	1	-1	5	0	1	5	-2	-4	7	-5	1	-7	4	-1	8	1	4
LBCa 7/3+20MK	bottom	68.62	8.88	13.64	11	-4	-8	14	-9	1	21	-7	-11	25	-13	0	9	-1	-8	12	-8	3
	up	70.75	7.32	12.32	13	-5	-9	17	-11	0	24	-8	-13	28	-15	0	11	-3	-9	15	-10	2
LBCa 1/1+20MK	bottom	63.05	9.58	12.31	6	-3	-9	11	-9	2	16	-6	-13	21	-14	2	4	0	-9	10	-8	5
	up	60.26	10.64	13.96	3	-2	-7	8	-7	2	13	-5	-11	18	-12	2	1	1	-8	8	-6	5
LBCa 3/7+20MK	bottom	59.81	10.42	13.94	2	-2	-7	8	-7	2	13	-5	-11	17	-12	2	1	1	-8	8	-6	4
	up	60.71	11.46	15.73	3	-1	-6	7	-5	2	14	-4	-9	17	-10	2	1	2	-6	6	-4	4

Reference samples				
ME brick	average	47.17	15.39	24.87
GL brick	average	59.29	9.86	21.75
LBCa raw	average	57.46	12.75	21.38

Attachment 6.3 – Weight of geopolymeric mortars measured at intervals of time during the water absorption tests.

	Measures (weight g)										
Sample	dry	1min	3min	10min	15min	30min	1h	8h	24h	Area (cm^2)	Area (m^2)
	0s	60s	180s	600s	900s	1800s	3600 s	28800s	86400s		
	t0	t1	t3	t10	t15	t30	t60	t480	t1440		
LBCa 1-1+10MK SC_1	16.00	16.39	16.59	16.87	17.02	17.25	17.58	17.86	17.83	3.61	0.04
LBCa 1-1+10MK SC_2	16.69	17.24	17.50	17.91	18.10	18.35	18.48	18.58	18.54	4.41	0.04
LBCa 1-1+10MK SC_3	16.31	16.75	16.96	17.29	17.46	17.73	17.97	18.16	18.13	3.61	0.04
LBCa 1-1+10MK SC_4	15.99	16.36	16.55	16.83	16.98	17.25	17.56	17.81	17.79	4	0.04
LBCa 1-1+10MK SC_5	15.78	16.24	16.47	16.78	16.96	17.22	17.43	17.53	17.53	4	0.04
LBCa 1-1+10MK SC_6	16.32	16.77	17.03	17.44	17.62	17.86	18.04	18.16	18.16	4	0.04
LBCa 1/1+10MK CER_1	14.35	15.35	15.87	16.35	16.35	16.38	16.40	16.42	16.42	4	0.04
LBCa 1/1+10MK CER_2	13.63	14.69	15.12	15.54	15.55	15.59	15.60	15.60	15.62	4	0.04
LBCa 1/1+10MK CER_3	14.45	14.48	16.03	16.44	16.45	16.47	16.48	16.51	16.49	3.99	0.04
LBCa 1/1+10MK CER_4	13.11	14.13	14.56	14.93	14.92	14.97	14.99	14.99	14.99	3.61	0.04
LBCa 1/1+10MK CER_5	13.89	14.94	15.41	15.85	15.85	15.88	15.89	15.91	15.91	3.42	0.03
LBCa 1/1+10MK CER_6	13.91	14.86	15.29	15.82	15.83	15.87	15.88	15.88	15.88	3.42	0.03
LBCa 1-1+20MK SC_1	16.60	16.94	17.13	17.49	17.67	18.25	18.51	18.52	18.51	4	0.04
LBCa 1-1+20MK SC_2	16.69	17.05	17.25	17.59	17.75	18.31	18.59	18.62	18.62	4	0.04
LBCa 1-1+20MK SC_3	16.52	16.88	17.08	17.43	17.60	18.17	18.44	18.49	18.49	4	0.04
LBCa 1-1+20MK SC_4	16.48	16.81	17.00	17.30	17.47	18.03	18.36	18.38	18.39	4	0.04
LBCa 1-1+20MK SC_5	16.82	17.16	17.34	17.63	17.79	18.33	18.71	18.76	18.75	4	0.04
LBCa 1-1+20MK SC_6	15.59	15.95	16.12	16.42	16.58	17.09	17.34	17.37	17.37	4	0.04
LBCa 3-7+20MK SC_1	15.47	15.87	16.06	16.40	16.57	16.92	17.31	17.32	17.32	3.61	0.04
LBCa 3-7+20MK SC_2	16.27	16.78	17.00	17.34	17.52	17.91	18.21	18.28	18.24	4	0.04
LBCa 3-7+20MK SC_3	16.46	16.99	17.16	17.51	17.70	18.09	18.40	18.42	18.42	3.8025	0.04
LBCa 3-7+20MK SC_4	15.73	16.28	16.39	16.72	16.89	17.25	17.61	17.63	17.64	4	0.04
LBCa 3-7+20MK SC_5	15.45	15.96	16.06	16.42	16.59	16.97	17.27	17.30	17.30	3.61	0.04
LBCa 3-7+20MK SC_6	16.18	16.71	16.81	17.19	17.38	17.79	18.11	18.14	18.14	4	0.04
LBCa 3-7+20MK CER_1	14.09	14.62	14.94	15.49	15.78	16.32	16.42	16.47	16.48	4	0.04
LBCa 3-7+20MK CER_2	13.58	14.14	14.44	14.96	15.23	15.75	15.85	15.89	15.90	4	0.04
LBCa 3-7+20MK CER_3	14.25	14.82	15.10	15.63	15.91	16.49	16.61	16.66	16.67	4	0.04
LBCa 3-7+20MK CER_4	14.34	14.91	15.19	15.71	16.00	16.55	16.72	16.77	16.78	4	0.04

LBCa 3-7+20MK CER_5	13.54	14.13	14.38	14.87	15.14	15.66	15.78	15.83	15.85	3.57	0.04
LBCa 3-7+20MK CER_6	13.39	13.94	14.20	14.69	14.96	15.50	15.60	15.64	15.66	4	0.04
LBCa 1/1+20MK CER_1	14.02	14.52	14.90	15.44	15.80	16.33	16.48	16.54	16.55	3.6	0.04
LBCa 1/1+20MK CER_2	13.85	14.43	14.85	15.44	15.82	16.25	16.32	16.35	16.38	4.2	0.04
LBCa 1/1+20MK CER_3	13.93	14.52	14.95	15.51	15.87	16.34	16.40	16.43	16.43	3.6	0.04
LBCa 1/1+20MK CER_4	14.27	14.80	15.21	15.74	16.11	16.64	16.79	16.85	16.87	4	0.04
LBCa 1/1+20MK CER_5	14.15	14.68	15.08	15.60	15.93	16.50	16.64	16.67	16.67	4	0.04
LBCa 1/1+20MK CER_6	12.89	13.40	13.74	14.25	14.51	14.96	15.12	15.16	15.17	3.61	0.04

Attachment 6.4 – Colorimetric data collected on the upper and bottom surfaces of all LBCa mortars. The colour parameters variations are also calculated in respect to the two archaeological references (ME brick and GL brick).

Samples		L*	a*	b*	ΔL*	Δa*	Δb*	ΔE*	ΔC*	ΔH*	ΔL*	Δa*	Δb*	ΔE*	ΔC*	ΔH*
LBCa 1/1+10MK SS	bottom	64.27	11.10	17.62	17	-4	-7	19	-8	0	5	1	-4	7	-3	3
	up	53.82	11.87	16.71	7	-4	-8	11	-9	2	-5	2	-5	8	-3	4
LBCa 1-1+10MK SC	bottom	48.66	11.40	16.58	1	-4	-8	9	-9	1	-11	2	-5	12	-4	4
	up	47.27	12.11	17.39	0	-3	-7	8	-8	1	-12	2	-4	13	-3	4
LBCa 1-1+10MK CER	bottom	46.84	13.54	18.90	0	-2	-6	6	-6	2	-12	4	-3	13	-1	5
	up	52.99	13.11	18.03	6	-2	-7	9	-7	2	-6	3	-4	8	-2	5
LBCa 1/1+20MK SS	bottom	64.75	10.05	15.00	18	-5	-10	21	-11	1	5	0	-7	9	-6	3
	up	56.04	12.74	16.52	9	-3	-8	12	-8	3	-3	3	-5	7	-3	5
LBCa 1-1+20MK SC	bottom	54.28	10.81	15.09	7	-5	-10	13	-11	2	-5	1	-7	8	-5	4
	up	45.49	11.75	16.01	-2	-4	-9	10	-9	2	-14	2	-6	15	-4	5
LBCa 1-1+20MK CER	bottom	53.72	10.51	13.52	7	-5	-11	14	-12	2	-6	1	-8	10	-7	5
	up	56.99	11.27	14.87	10	-4	-10	15	-11	2	-2	1	-7	7	-5	5
LBCa 3-7+20MK SC	bottom	55.16	10.89	16.22	8	-5	-9	13	-10	1	-4	1	-6	7	-4	4
	up	45.13	12.01	16.59	-2	-3	-8	9	-9	2	-14	2	-5	15	-3	4
LBCa 3-7+20MK CER	bottom	61.15	10.55	14.63	14	-5	-10	18	-11	2	2	1	-7	7	-6	4
	up	48.37	12.23	15.43	1	-3	-9	10	-10	3	-11	2	-6	13	-4	5

Reference samples				
ME brick	average	47.17	15.39	24.87
GL brick	average	59.29	9.86	21.75

Attachment 7.1 - SEM micrographs of the geopolymeric binders based on CWF ceramic waste precursor.

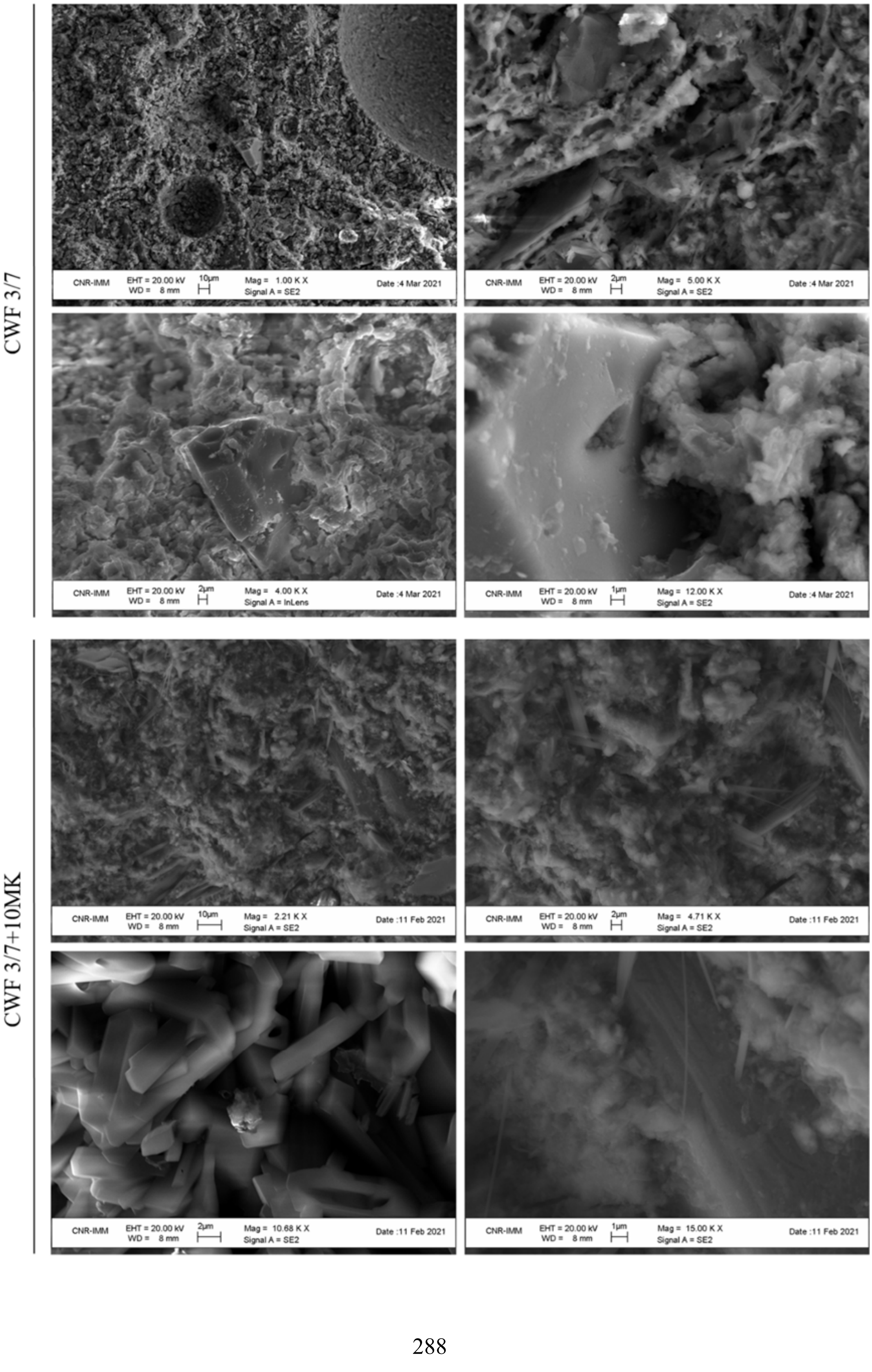

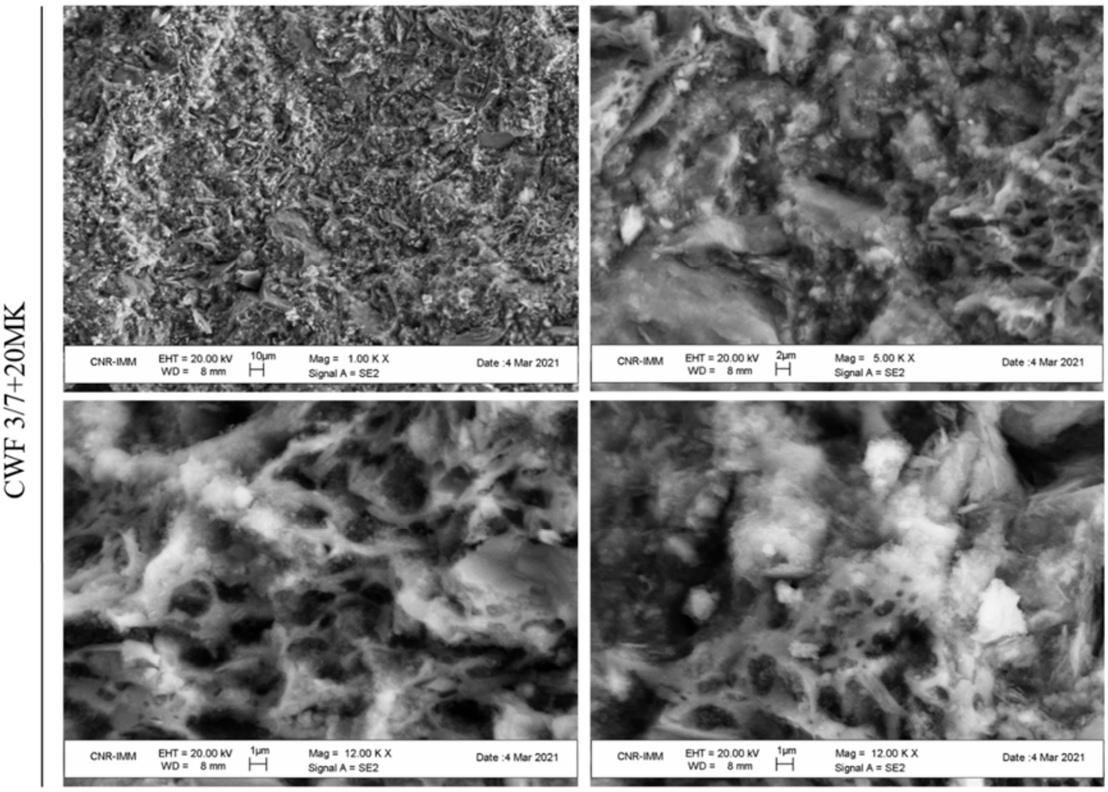
CWF 3/7+20MK
CNR-IMM EHT = 20.00 kV WD = 8 mm 10µm Mag = 1.00 K X Signal A = SE2 Date :4 Mar 2021
CNR-IMM EHT = 20.00 kV WD = 8 mm 2µm Mag = 5.00 K X Signal A = SE2 Date :4 Mar 2021
CNR-IMM EHT = 20.00 kV WD = 8 mm 1µm Mag = 12.00 K X Signal A = SE2 Date :4 Mar 2021
CNR-IMM EHT = 20.00 kV WD = 8 mm 1µm Mag = 12.00 K X Signal A = SE2 Date :4 Mar 2021

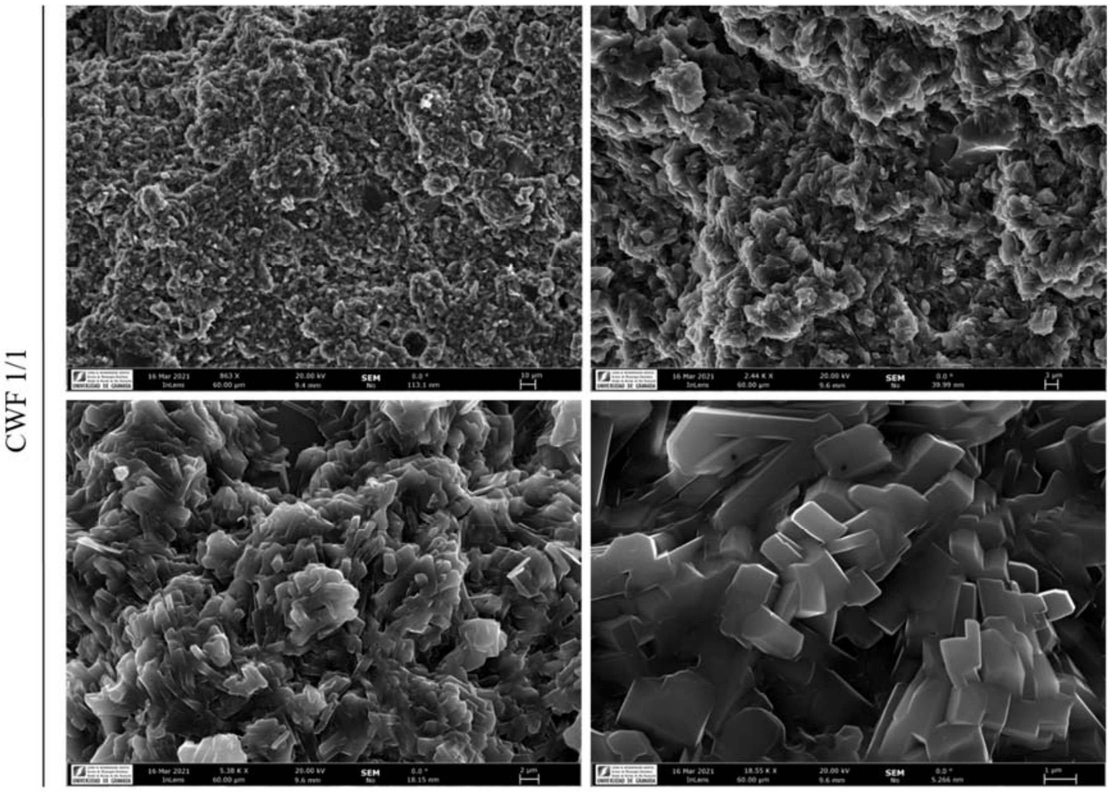
CWF 1/1
16 Mar 2021 863 X InLens 60.00 µm 20.00 kV 9.4 mm SEM No 0.0 ° 113.1 nm 10 µm
16 Mar 2021 2.44 K X InLens 60.00 µm 20.00 kV 9.6 mm SEM No 0.0 ° 39.99 nm 2 µm
16 Mar 2021 5.38 K X InLens 60.00 µm 20.00 kV 9.6 mm SEM No 0.0 ° 18.15 nm 2 µm
16 Mar 2021 18.55 K X InLens 60.00 µm 20.00 kV 9.6 mm SEM No 0.0 ° 5.266 nm 1 µm

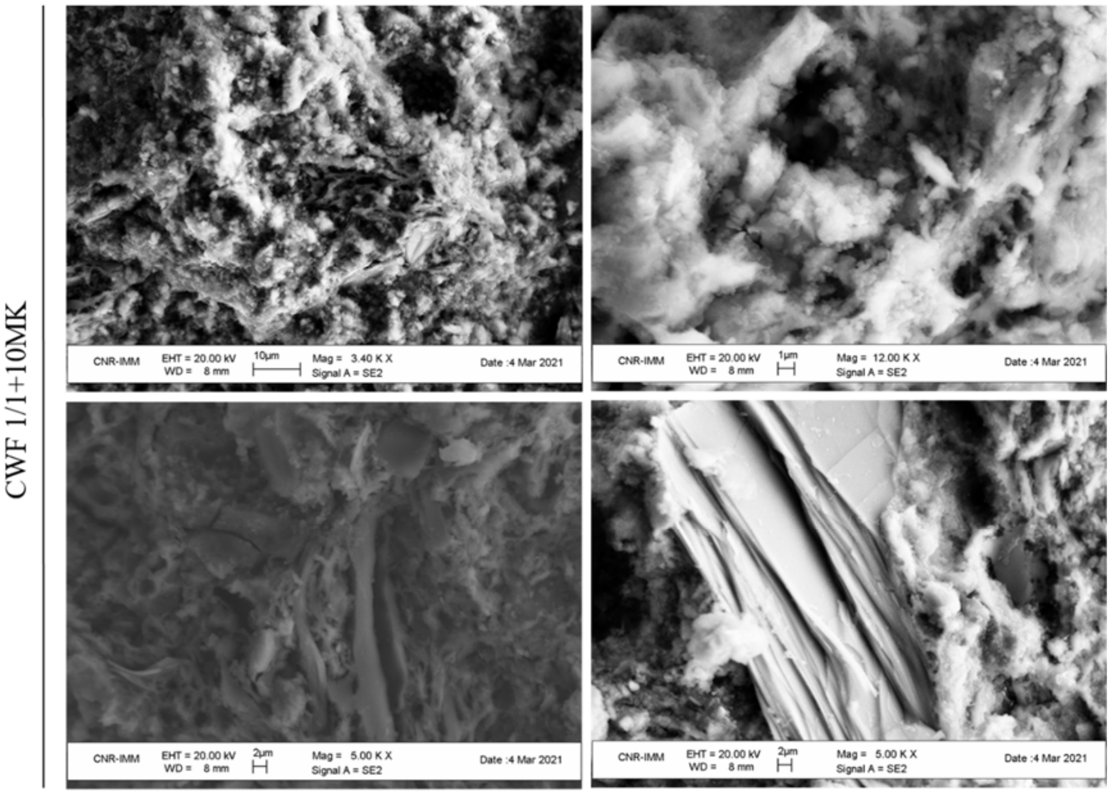
CWF 1/1+10MK
CNR-IMM EHT = 20.00 kV WD = 8 mm 10µm Mag = 3.40 K X Signal A = SE2 Date :4 Mar 2021
CNR-IMM EHT = 20.00 kV WD = 8 mm 1µm Mag = 12.00 K X Signal A = SE2 Date :4 Mar 2021
CNR-IMM EHT = 20.00 kV WD = 8 mm 2µm Mag = 5.00 K X Signal A = SE2 Date :4 Mar 2021
CNR-IMM EHT = 20.00 kV WD = 8 mm 2µm Mag = 5.00 K X Signal A = SE2 Date :4 Mar 2021

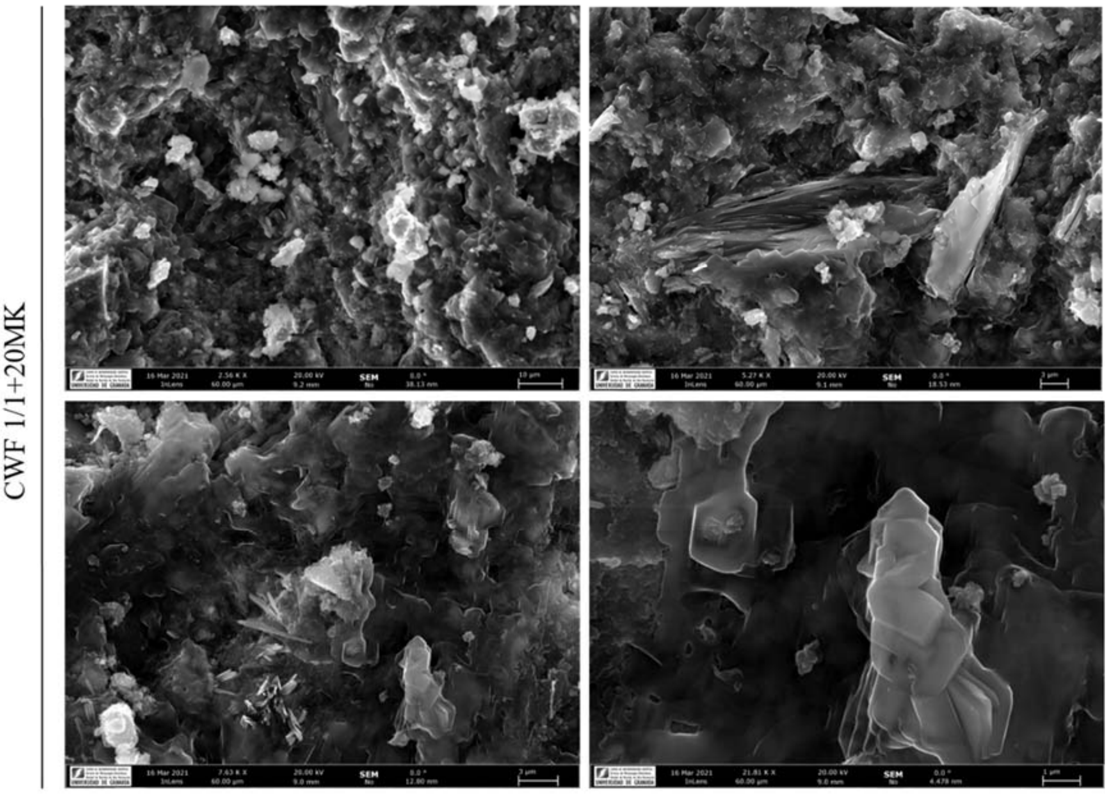
CWF 1/1+20MK
16 Mar 2021
InLens
2.56 K X
60.00 µm
20.00 kV
9.2 mm
SEM
No
0.0 °
38.13 nm
10 µm
16 Mar 2021
InLens
5.27 K X
60.00 µm
20.00 kV
9.1 mm
SEM
No
0.0 °
18.53 nm
2 µm
16 Mar 2021
InLens
7.63 K X
60.00 µm
20.00 kV
9.0 mm
SEM
No
0.0 °
12.80 nm
2 µm
16 Mar 2021
InLens
21.81 K X
60.00 µm
20.00 kV
9.0 mm
SEM
No
0.0 °
4.478 nm
1 µm
UNIVERSIDAD DE GRANADA

CWF 7/3

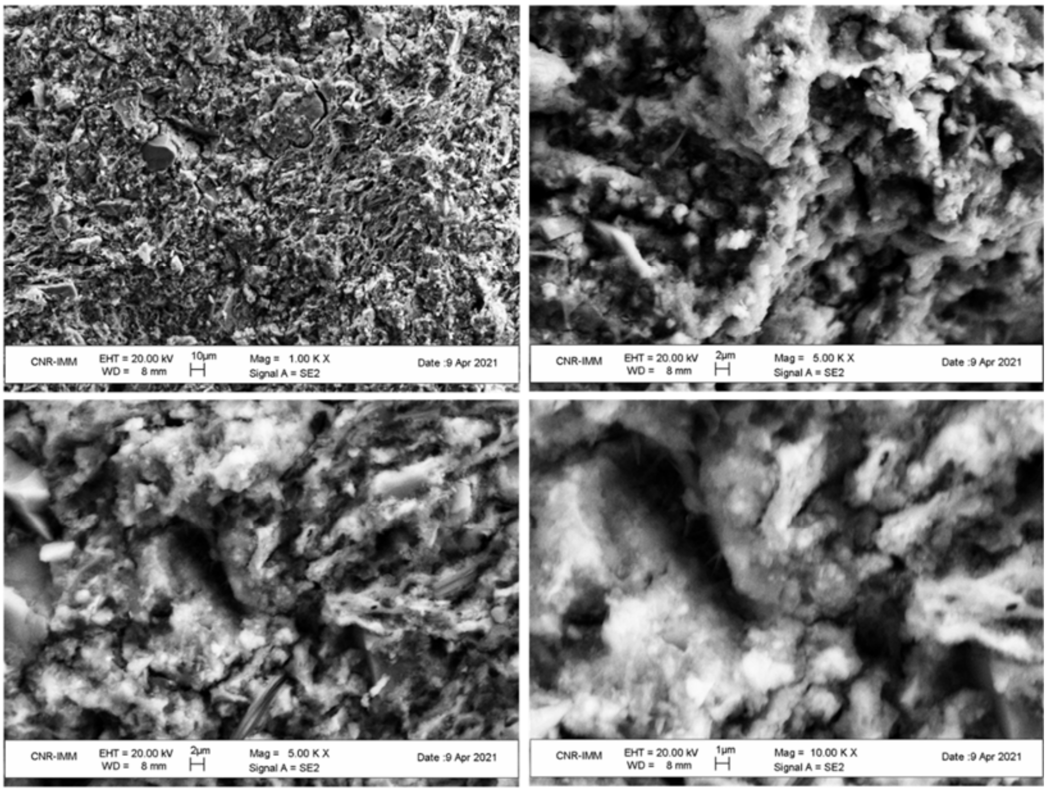

CWF 7/3+10MK

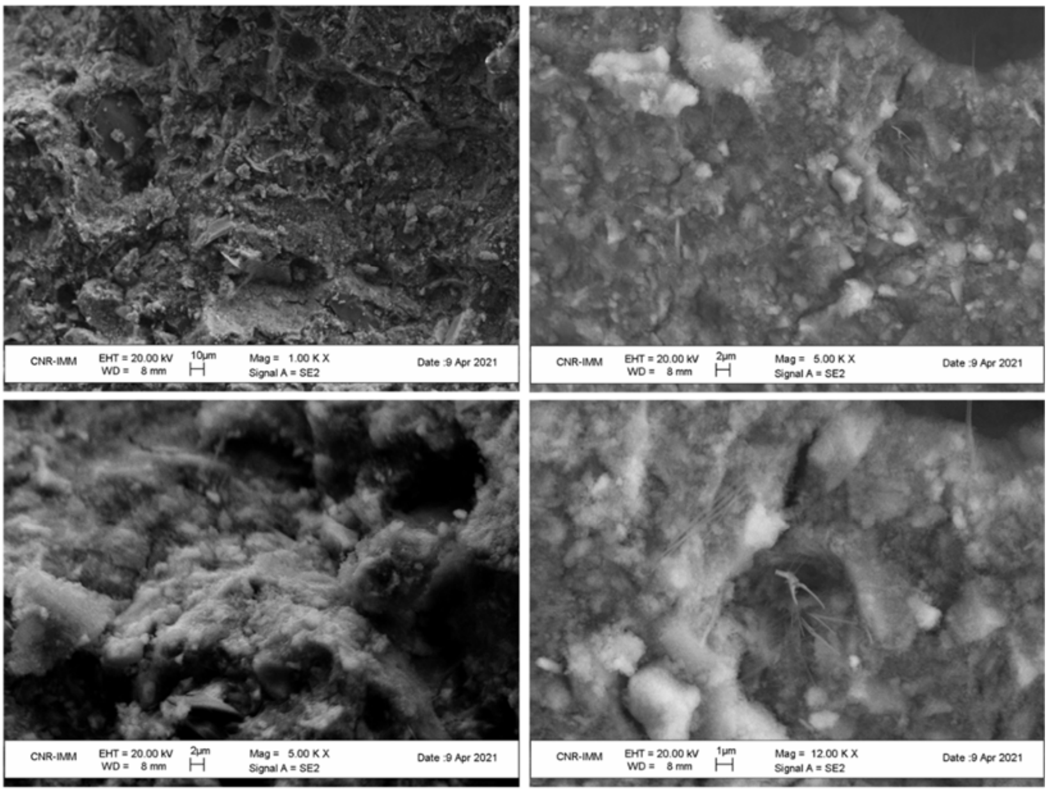

CWF 7/3+20MK

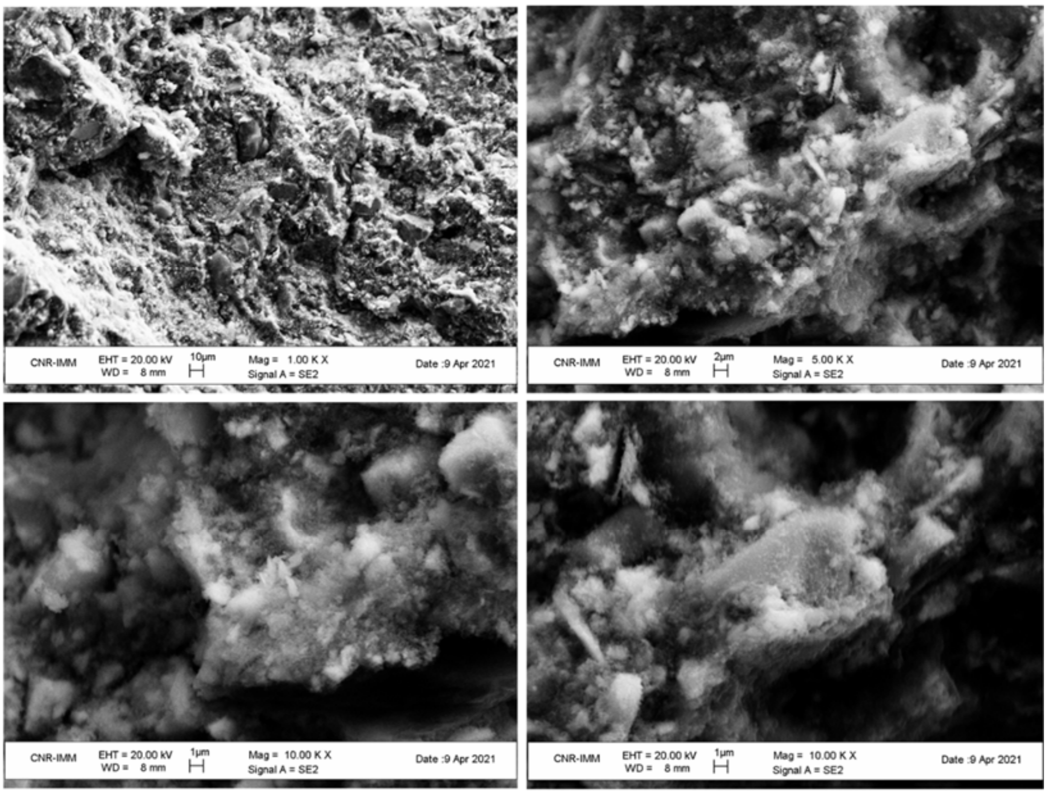
CNR-IMM
EHT = 20.00 kV
WD = 8 mm
10µm
Mag = 1.00 K X
Signal A = SE2
Date :9 Apr 2021
CNR-IMM
EHT = 20.00 kV
WD = 8 mm
2µm
Mag = 5.00 K X
Signal A = SE2
Date :9 Apr 2021
CNR-IMM
EHT = 20.00 kV
WD = 8 mm
1µm
Mag = 10.00 K X
Signal A = SE2
Date :9 Apr 2021
CNR-IMM
EHT = 20.00 kV
WD = 8 mm
1µm
Mag = 10.00 K X
Signal A = SE2
Date :9 Apr 2021

Attachment 7.2 – Colorimetric data collected on the upper and bottom surfaces of all the CWF binders. The colour parameters variations are also calculated in respect to CWF raw material and to the two archaeological references (ME brick and GL brick).

Samples		L*	a*	b*	ΔL*	Δa*	Δb*	ΔE*	ΔC*	ΔH*	ΔL*	Δa*	Δb*	ΔE*	ΔC*	ΔH*	ΔL*	Δa*	Δb*	ΔE*	ΔC*	ΔH*
CWF 3/7	bottom	44.12	22.26	30.03	-15	6	4	16	6	3	-3	7	5	9	8	3	-15	12	8	21	13	6
	up	45.46	21.31	27.36	-13	5	1	14	3	3	-2	6	2	7	5	3	-14	11	6	19	11	7
CWF 1/1	bottom	43.73	22.61	27.36	-15	6	1	16	4	4	-3	7	2	8	6	4	-16	13	6	21	12	8
	up	39.12	20.30	21.09	-20	4	-5	21	-2	6	-8	5	-4	10	0	6	-20	10	-1	23	5	9
CWF 7/3 (covered of efflorescence)	bottom	41.61	21.36	26.21	-17	5	0	18	2	4	-6	6	1	8	5	4	-18	11	4	22	10	7
	up	41.32	19.59	19.74	-17	3	-7	19	-4	6	-6	4	-5	9	-1	6	-18	10	-2	21	4	9
CWF 3/7+10MK	bottom	52.98	17.79	24.94	-6	1	-2	6	-1	2	6	2	0	6	1	2	-6	8	3	11	7	5
	up	50.74	19.72	26.54	-8	3	0	8	2	2	4	4	2	6	4	3	-9	10	5	14	9	6
CWF 1/1+10MK	bottom	58.30	15.38	21.80	0	-1	-5	5	-5	1	11	0	-3	12	-3	2	-1	6	0	6	3	5
	up	49.24	19.67	25.68	-9	3	-1	10	1	3	2	4	1	5	3	3	-10	10	4	15	8	6
CWF 7/3+10MK	bottom	52.48	16.78	20.86	-6	0	-6	8	-5	3	5	1	-4	7	-2	3	-7	7	-1	10	3	6
	up	49.72	11.95	9.88	-9	-5	-17	19	-16	7	3	-3	-15	16	-14	7	-10	2	-12	15	-8	9
CWF 3/7+20MK	bottom	51.31	18.97	25.30	-7	2	-1	8	0	2	4	4	0	5	2	3	-8	9	4	13	8	6
	up	50.61	20.51	25.98	-8	4	0	9	2	3	3	5	1	6	4	4	-9	11	4	14	9	7
CWF 1/1+20MK	bottom	50.95	17.42	23.63	-8	1	-3	8	-2	2	4	2	-1	4	0	2	-8	8	2	11	5	6
	up	50.79	20.14	25.52	-8	3	-1	9	1	3	4	5	1	6	3	4	-8	10	4	14	9	7
CWF 7/3+20MK	bottom	60.27	14.18	18.16	2	-3	-8	9	-8	3	13	-1	-7	15	-6	3	1	4	-4	6	-1	6
	up	48.75	15.56	18.16	-10	-1	-8	13	-7	4	2	0	-7	7	-5	4	-11	6	-4	13	0	7

Reference samples				
ME brick	average	47.17	15.39	24.87
GL brick	average	59.29	9.86	21.75
CWF raw	average	58.63	16.75	26.47